

THE UNIVERSITY OF YAOUNDE I

\*\*\*\*\*

CENTRE FOR RESEARCH AND TRAINING IN  
GRADUATE STUDIES IN LIFE, HEALTH AND  
ENVIRONMENTAL SCIENCES

\*\*\*\*\*

RESEARCH AND DOCTORATE TRAINING  
UNIT IN LIFE SCIENCES



UNIVERSITE DE YAOUNDE I

\*\*\*\*\*

CENTRE DE RECHERCHE ET DE FORMATION  
DOCTORALE EN SCIENCES DE LA VIE ET EN  
VIRONNEMENT

\*\*\*\*\*

UNITE DE RECHERCHE ET DE FORMATION  
DOCTORALE EN SCIENCES DE LA VIE

**LABORATORY FOR PHYTOBIOCHEMISTRY AND MEDICINAL PLANTS STUDY**  
LABORATOIRE DE PHYTOBIOCHIMIE ET D'ETUDE DES PLANTES MEDICINALES  
**ANTIMICROBIAL AND BIOCONTROL AGENTS UNIT**  
UNITE DES AGENTS ANTIMICROBIENS ET DE BIOCONTROLE

# Investigation of gold and silver nano- particles from *Terminalia mantaly* (combretaceae) for their potential against bacteria and cancer cells

Thesis presented in partial fulfilment of the requirements  
for the award of a Doctorat/Ph.D in Biochemistry

By

**Majoumouo Michele Stella**  
Registration N° 08R0454  
M.sc in Biochemistry



**Supervisors:**

**Mervin Meyer**

**Professor**

**University of the Western Cape**

**Fabrice Fekam Boyom**

**Professor**

**University of Yaounde I**

**Academic year (2021-2022)**

UNIVERSITE DE YAOUNDE I

CENTRE DE RECHERCHE ET DE  
FORMATION DOCTORALE EN SCIENCE DE  
LA VIE, SANTE ET ENVIRONNEMENT

UNITE DE RECHERCHE ET DE FORMATION  
DOCTORALE EN SCIENCE DE LA VIE

DEPARTEMENT DE BIOCHIMIE



THE UNIVERSITY OF YAOUNDE I

CENTRE FOR RESEARCH AND TRAINING  
IN GRADUATE STUDIES IN LIFE, HEALTH  
AND ENVIRONMENTAL SCIENCES

RESEARCH DOCTORATE TRAINING UNIT  
IN LIFE SCIENCES

DEPARTMENT OF BIOCHEMISTRY

## ATTESTATION DE CORRECTION

Nous soussignés, Pr. MOUNDIPA Fewou Paul et Pr. PIEME Constant Anatole respectivement Examineur et Président du jury de Thèse de Doctorat/PhD en Biochimie, spécialité Pharmacologie Moléculaire, soutenue par Mme MAJOUMOUO Michele Stella (matricule: **08R0454**) le 27 Janvier 2022 à 11h dans la salle multimedia de la Faculté de Sciences de l'Université de Yaoundé I sur le thème intitulée «**Investigation of gold and silver nanoparticles from *Terminalia mantaly* (Combretaceae) for their potential against bacteria and cancer**» attestons que la candidate a effectué les corrections conformément aux exigences du jury.

En foi de quoi la présente attestation lui est délivrée pour servir et valoir ce que de droit.

Fait à Yaoundé, le **04 MARS 2022**.....

Examineur

Pr. PIEME Constant Anatole  
Maître de Conférences de Biochimie

FMSB UYI

Président du Jury

Moundipa Fewou Paul  
Professeur  
Enzymologie - Toxicologie

Le Chef de Département





# Made with Scan Hero

A powerful tool to create and edit  
multi-paged PDF documents

[Download for iOS](#)



[Download for Android](#)





**LIST OF PERMANENT TEACHING STAFF**  
**ACADEMIC YEAR 2021/2022**

(By Department and by Grade)

**UPDATE: 22, September 2021**

**ADMINISTRATION**

**Dean:** TCHOUANKEU Jean- Claude, Associate professor

**VICE-Dean / DPSAA :** ATCHADE Alex de Théodore, Associate professor

**VICE-Dean/ DSSE :** NYEGUE Maximilienne Ascension, Professor

**VICE-Dean/ DRC :** ABOSSOLO Monique, Associate professor

**Head of Division of Academic affairs, Research and corporation:** NDOYE FOE Florentine Marie Chantal, Associate professor

**Head of Administrative and Financial Division:** AJEAGAH Gideon AGHAINDUM, Professor

**1- DEPARTMENT OF BIOCHIMISTRY (BCH) (40)**

N°	NAME AND SURNAME	GRADE	OBSERVATIONS
1	BIGOGA DAIGA Jude	Professor	In duty
2	FEKAM BOYOM Fabrice	Professor	In duty
3	FOKOU Elie	Professor	In duty
4	KANSCI Germain	Professor	In duty
5	MBACHAM FON Wilfried	Professor	In duty
6	MOUNDIPA FEWOU Paul	Professor	<b>Head of Department</b>
7	NINTCHOM PENLAP V. épse BENG	Professor	In duty
8	OBEN Julius ENYONG	Professor	In duty
9	ACHU Merci BIH	Associate Professor	In duty
10	ATOGHO Barbara Mma	Associate Professor	In duty
11	AZANTSA KINGUE GABIN BORIS	Associate Professor	In duty
12	BELINGA née NDOYE FOE F. M. C.	Associate Professor	<b>Head DAF / FS</b>
13	BOUDJEKO Thaddée	Associate Professor	In duty
14	DJUIDJE NGOUNOUE Marceline	Associate Professor	In duty
15	EFFA ONOMO Pierre	Associate Professor	In duty
16	EWANE Cécile Annie	Associate Professor	In duty
17	MOFOR née TEUGWA Clotilde	Associate Professor	<b>Insp. Serv. MINESUP</b>

18	NANA Louise épouse WAKAM	Associate Professor	In duty
19	NGONDI Judith Laure	Associate Professor	In duty
20	NGUEFACK Julienne	Associate Professor	In duty
21	NJAYOU Frédéric Nico	Associate Professor	In duty
22	TCHANA KOUATCHOUA Angèle	Associate Professor	In duty
23	AKINDEH MBUH NJI	Senior Lecturer	In duty
24	BEBEE Fadimatou	Senior Lecturer	In duty
25	BEBOY EDJENGUELE Sara Nathalie	Senior Lecturer	In duty
26	DAKOLE DABOY Charles	Senior Lecturer	In duty
27	DJUIKWO NKONGA Ruth Viviane	Senior Lecturer	In duty
28	DONGMO LEKAGNE Joseph Blaise	Senior Lecturer	In duty
29	FONKOUA Martin	Senior Lecturer	In duty
30	KOTUE TAPTUE Charles	Senior Lecturer	In duty
31	LUNGA Paul KEILAH	Senior Lecturer	In duty
32	MANANGA Marlyse Joséphine	Senior Lecturer	In duty
33	MBONG ANGIE M. Mary Anne	Senior Lecturer	In duty
34	Palmer MASUMBE NETONGO	Senior Lecturer	In duty
35	PECHANGOU NSANGOU Sylvain	Senior Lecturer	In duty
36	FOUPOUAPOUOGNIGNI Yacouba	Assist. Lecturer	In duty
37	KOUOH ELOMBO Ferdinand	Assist. Lecturer	In duty
38	MBOUCHE FANMOE Marceline Joëlle	Assist. Lecturer	In duty
39	OWONA AYISSI Vincent Brice	Assist. Lecturer	In duty
40	WILFRIED ANGIE Abia	Assist. Lecturer	In duty

## 2- DEPARTMENT OF ANIMAL BIOLOGY AND PHYSIOLOGY (A. B. P.) (51)

1	AJEAGAH Gideon AGHAINDUM	Professor	<b>DAARS/FS</b>
2	BILONG BILONG Charles-Félix	Professor	<b>Head of Department</b>
3	DIMO Théophile	Professor	In duty
4	DJIETO LORDON Champlain	Professor	In duty
5	DZEUFIET DJOMENI Paul Désiré	Professor	In duty
6	ESSOMBA née NTSAMA MBALA	Professor	<b>Vice Dean/FMSB/UIYI</b>
7	FOMENA Abraham	Professor	In duty
8	KAMTCHOING Pierre	Professor	In duty
9	KEKEUNOU Sévilor	Professor	In duty
10	NJAMEN Dieudonné	Professor	In duty
11	NJIOKOU Flobert	Professor	In duty
12	NOLA Moïse	Professor	In duty
13	TAN Paul VERNYUY	Professor	In duty

14	TCHUEM TCHUENTE Louis Albert	Professor	<b>Insp. Serv. Coord. Progr. in HEALTH</b>
15	ZEBAZE TOGOUET Serge Hubert	Professor	In duty
16	BILANDA Danielle Claude	Associate Professor	In duty
17	DJIOGUE Séfirin	Associate Professor	In duty
18	JATSA BOUKENG Hermine épouse MEGAPTCHE	Associate Professor	In duty
19	LEKEUFACK FOLEFACK Guy B.	Associate Professor	In duty
20	MEGNEKOU Rosette	Associate Professor	In duty
21	MONY Ruth épouse NTONE	Associate Professor	In duty
22	NGUEGUIM TSOFAK Florence	Associate Professor	In duty
23	TOMBI Jeannette	Associate Professor	In duty
24	ALENE Désirée Chantal	Senior Lecturer	In duty
25	ATSAMO Albert Donatien	Senior Lecturer	In duty
26	BELLET EDIMO Oscar Roger	Senior Lecturer	In duty
27	DONFACK Mireille	Senior Lecturer	In duty
28	ETEME ENAMA Serge	Senior Lecturer	In duty
29	GOUNOUE KAMKUMO Raceline	Senior Lecturer	In duty
30	KANDEDA KAVAYE Antoine	Senior Lecturer	In duty
31	MAHOB Raymond Joseph	Senior Lecturer	In duty
32	MBENOUN MASSE Paul Serge	Senior Lecturer	In duty
33	MOUNGANG Luciane Marlyse	Senior Lecturer	In duty
34	MVEYO NDANKEU Yves Patrick	Senior Lecturer	In duty
35	NGOULATEU KENFACK Omer Bébé	Senior Lecturer	In duty
36	NGUEMBOK	Senior Lecturer	In duty
37	NJUA Clarisse Yafi	Senior Lecturer	<b>Chief Div. UBA</b>
38	NOAH EWOTI Olive Vivien	Senior Lecturer	In duty
39	TADU Zephyrin	Senior Lecturer	In duty
40	TAMSA ARFAO Antoine	Senior Lecturer	In duty
41	YEDE	Senior Lecturer	In duty
42	AMPON NSANGOU Indou	Assist. Lecturer	In duty
43	BASSOCK BAYIHA Etienne Didier	Assist. Lecturer	In duty
44	ESSAMA MBIDA Désirée Sandrine	Assist. Lecturer	In duty
45	FEUGANG YOUMSSI François	Assist. Lecturer	In duty
46	FOKAM Alvine Christelle Epse KEGNE	Assist. Lecturer	In duty
47	GONWOUO NONO Legrand	Assist. Lecturer	In duty
48	KOGA MANG DOBARA	Assist. Lecturer	In duty
49	LEME BANOCK Lucie	Assist. Lecturer	In duty
50	NWANE Philippe Bienvenu	Assist. Lecturer	In duty
51	YOUNOUSSA LAME	Assist. Lecturer	In duty

**3- DEPARTMENT OF PLANT BIOLOGY AND PHYSIOLOGY (P. B. P.) (31)**

1	AMBANG Zachée	Professor	<b>Chief of Division/UYII</b>
2	BELL Joseph Martin	Professor	In duty
3	DJOCGOUE Pierre François	Professor	In duty
4	MBOLO Marie	Professor	In duty
5	MOSSEBO Dominique Claude	Professor	In duty
6	YOUMBI Emmanuel	Professor	<b>Head of Department</b>
7	ZAPFACK Louis	Professor	In duty
8	ANGONI Hyacinthe	Associate Professor	In duty
9	BIYE Elvire Hortense	Associate Professor	In duty
10	MALA Armand William	Associate Professor	In duty
11	MBARGA BINDZI Marie Alain	Associate Professor	CT/ MINESUP
12	NDONGO BEKOLO	Associate Professor	CE / MINRESI
13	NGODO MELINGUI Jean Baptiste	Associate Professor	In duty
14	NGONKEU MAGAPTCHE Eddy L.	Associate Professor	In duty
15	TONFACK Libert Brice	Associate Professor	In duty
16	TSOATA Esaïe	Associate Professor	In duty
17	DJEUANI Astride Carole	Senior Lecturer	In duty
18	GOMANDJE Christelle	Senior Lecturer	In duty
19	MAFFO MAFFO Nicole Liliane	Senior Lecturer	In duty
20	MAHBOU SOMO TOUKAM. Gabriel	Senior Lecturer	In duty
21	NGALLE Hermine BILLE	Senior Lecturer	In duty
22	NNANGA MEBENGA Ruth Laure	Senior Lecturer	In duty
23	NOUKEU KOUAKAM Armelle	Senior Lecturer	In duty
24	ONANA JEAN MICHEL	Senior Lecturer	In duty
25	GODSWILL NTSOMBOH NTSE-FONG	Assist. Lecturer	In duty
26	KABELONG BANAHOU Louis-Paul-Roger	Assist. Lecturer	In duty
27	KONO Léon Dieudonné	Assist. Lecturer	In duty
28	LIBALAH Moses BAKONCK	Assist. Lecturer	In duty
29	LIKENG-LI-NGUE Benoit C	Assist. Lecturer	In duty
30	TAEDOUNG Evariste Hermann	Assist. Lecturer	In duty
31	TEMEGNE NONO Carine	Assist. Lecturer	In duty

**4- DEPARTMENT OF INORGANIC CHEMISTRY (I. C.) (32)**

1	AGWARA ONDOH Moïse	Professor	<b>Head of Department</b>
2	DJOUFAC WOUMFO Emmanuel	Professor	In duty
3	Florence UFI CHINJE épouse ME-LO	Professor	<b>Rector Univ. Ngaoundere</b>
4	GHOGOMU Paul MINGO	Professor	<b>Minister in charge of mission. P.R.</b>
5	NANSEU Njiki Charles Péguy	Professor	In duty

6	NDIFON Peter TEKE	Professor	<i>CT MINRESI</i>
7	NDIKONTAR Maurice KOR	Professor	<b>Vice-Dean Un. Bamenda</b>
8	NENWA Justin	Professor	In duty
9	NGAMENI Emmanuel	Professor	<b>Dean F.S. U. Ds</b>
10	NGOMO Horace MANGA	Professor	<b>Vice Chancellor/UB</b>
11	ACAYANKA Elie	Associate Professor	In duty
12	EMADACK Alphonse	Associate Professor	In duty
13	KAMGANG YOUBI Georges	Associate Professor	In duty
14	KEMMEGNE MBOUGUEM Jean C.	Associate Professor	In duty
15	KONG SAKEO	Associate Professor	In duty
16	NDI NSAMI Julius	Associate Professor	In duty
17	NJIOMOU C. épse DJANGANG	Associate Professor	In duty
18	NJOYA Dayirou	Associate Professor	In duty
19	TCHAKOUTE KOUAMO Hervé	Associate Professor	In duty
20	BELIBI BELIBI Placide Désiré	Senior Lecturer	CS/ ENS Bertoua
21	CHEUMANI YONA Arnaud M.	Senior Lecturer	In duty
22	KENNE DEDZO GUSTAVE	Senior Lecturer	In duty
23	KOUOTOU DAOUDA	Senior Lecturer	In duty
24	MAKON Thomas Beauregard	Senior Lecturer	In duty
25	MBEY Jean Aime	Senior Lecturer	In duty
26	NCHIMI NONO KATIA	Senior Lecturer	In duty
27	NEBAH Née NDOSIRI Bridget NDOYE	Senior Lecturer	CT/ MINPROFF
28	NYAMEN Linda Dyorisse	Senior Lecturer	In duty
29	PABOUDAM GBAMBIE A.	Senior Lecturer	In duty
30	NJANKWA NJABONG N. Eric	Assist. Lecturer	In duty
31	PATOUOSSA ISSOFA	Assist. Lecturer	In duty
32	SIEWE Jean Mermoz	Assist. Lecturer	In duty

#### 5- DEPARTMENT OF ORGANIC CHIMISTRY (O. C.) (40)

1	DONGO Etienne	Professor	<b>Vice Dean/CSA/ F. SED</b>
2	GHOGOMU TIH Robert Ralph	Professor	<b>Director B. A. I Fouban</b>
3	NGOUELA Silvère Augustin	Professor	<b>Head of Department UDs</b>
4	NYASSE Barthélemy	Professor	<b>In duty</b>
5	PEGNYEMB Dieudonné Emmanuel	Professor	<b>Director/ MINESUP/ Head of Department</b>
6	WANDJI Jean	Professor	In duty
7	Alex de Théodore ATCHADE	Associate Professor	Vice-Dean / DPSAA
8	AMBASSA Pantaléon	Associate Professor	In duty
9	EYONG Kenneth OBEN	Associate Professor	In duty
10	FOLEFOC Gabriel NGOSONG	Associate Professor	In duty
11	FOTSO WABO Ghislain	Associate Professor	In duty
12	KEUMEDJIO Félix	Associate Professor	In duty
13	KENMOGNE Marguerite	Associate Professor	In duty



14	KOUAM Jacques	Associate Professor	In duty
15	MBAZOA née DJAMA Céline	Associate Professor	Associate Professor
16	MKOUNGA Pierre	Associate Professor	In duty
17	MVOT AKAK CARINE	Associate Professor	In duty
18	NGO MBING Joséphine	Associate Professor	<b>Sous/Direct. MINERESI</b>
19	NGONO BIKOBO Dominique Serge	Associate Professor	<b>C.E/ MINESUP</b>
20	NOTE LOUGBOT Olivier Placide	Associate Professor	<b>C.S/ MINESUP</b>
21	NOUNGOUE TCHAMO Diderot	Associate Professor	In duty
22	TABOPDA KUATE Turibio	Associate Professor	In duty
23	TAGATSING FOTSING Maurice	Associate Professor	In duty
24	TCHOUANKEU Jean-Claude	Associate Professor	<b>Dean /FS/ UYI</b>
25	TIH née NGO BILONG E. Anastasie	Associate Professor	In duty
26	YANKEP Emmanuel	Associate Professor	In duty
27	ZONDEGOUNBA Ernestine	Associate Professor	In duty
28	KAMTO Eutrophe Le Doux	Senior Lecturer	In duty
29	NGNINTEDO Dominique	Senior Lecturer	In duty
30	NGOMO Orléans	Senior Lecturer	In duty
31	OUAHOUE WACHE Blandine M.	Senior Lecturer	In duty
32	SIELINOUE TEDJON Valérie	Senior Lecturer	In duty
33	MESSI Angélique Nicolas	Assist. Lecturer	In duty
34	MUNVERA MFIFEN Aristide	Assist. Lecturer	In duty
35	NONO NONO Éric Carly	Assist. Lecturer	In duty
36	OUETE NANTCHOUANG Judith Laure	Assist. Lecturer	In duty
37	TCHAMGOUE Joseph	Assist. Lecturer	In duty
38	TSAFFACK Maurice	Assist. Lecturer	In duty
39	TSAMO TONTSA Armelle	Assist. Lecturer	In duty
40	TSEMEUGNE Joseph	Assist. Lecturer	In duty

#### 6- DEPARTMENT OF COMPUTER SCIENCE (C. S.) (25)

1	ATSA ETOUNDI Roger	Professor	<b>Chief Div.MINESUP</b>
2	FOUDA NDJODO Marcel Laurent	Professor	<b>Chief Dpt ENS/Chief IGA.MINESUP</b>
3	NDOUNDAM René	Associate Professor	In duty
4	ABESSOLO ALO'O Gislain	Senior Lecturer	In duty
5	AMINOUE Halidou	Senior Lecturer	<b>Head of Department</b>
6	DJAM Xaviera YOUH - KIMBI	Senior Lecturer	In duty
7	DOMGA KOMGUEM Rodrigue	Senior Lecturer	In duty
8	EBELE Serge Alain	Senior Lecturer	In duty
9	KOUOKAM KOUOKAM E. A.	Senior Lecturer	In duty
10	MELATAGIA YONTA Paulin	Senior Lecturer	In duty
11	MONTHÉ DJIADEU Valéry M.	Senior Lecturer	In duty
12	MOTO MPONG Serge Alain	Senior Lecturer	In duty

13	OLLE OLLE Daniel Claude De- lort	Senior Lecturer	<b>C/D Enset. Ebolowa</b>
14	TAPAMO Hyppolite	Senior Lecturer	In duty
15	TINDO Gilbert	Senior Lecturer	In duty
16	TSOPZE Norbert	Senior Lecturer	In duty
17	WAKU KOUAMOU Jules	Senior Lecturer	In duty
18	BAYEM Jacques Narcisse	Assist. Lecturer	In duty
19	EKODECK Stéphane Gaël Ray- mond	Assist. Lecturer	In duty
20	HAMZA Adamou	Assist. Lecturer	In duty
21	JIOMEKONG AZANZI Fidel	Assist. Lecturer	In duty
22	MAKEMBE. S . Oswald	Assist. Lecturer	In duty
23	MESSI NGUELE Thomas	Assist. Lecturer	In duty
24	MEYEMDOU Nadège Sylvianne	Assist. Lecturer	In duty
25	NKONDOCK. MI. BAH- NACK.N.	Assist. Lecturer	In duty

**7- DEPARTMENT OF MATHEMATICS (MAT) (35)**

1	AYISSI Raoult Domingo	Professor	<b>Head of Department</b>
2	EMVUDU WONO Yves S.	Professor	<b>CD Info/Inspector MINESUP</b>
3	KIANPI Maurice	Associate Professor	In duty
4	MBANG Joseph	Associate Professor	In duty
5	MBEHOU Mohamed	Associate Pro fessor	In duty
6	MBELE BIDIMA Martin Ledoux	Associate Professor	In duty
7	NKUIMI JUGNIA Célestin	Associate Professor	In duty
8	NOUNDJEU Pierre	Associate Professor	<b>Chief serv. certif. prog. /FS/UYI</b>
9	TCHAPNDA NJABO Sophonie B.	Associate Professor	<b>Director/AIMS Rwanda</b>
10	TCHOUNDJA Edgar Landry	Associate Professor	In duty
11	BOGSO ANTOINE MARIE	Senior Lecturer	In duty
12	AGHOUKENG JIOFACK Jean Gérard	Senior Lecturer	<b>Chief Cell MINPLAMAT</b>
13	CHENDJOU Gilbert	Senior Lecturer	In duty
14	DJIADEU NGAHA Michel	Senior Lecturer	In duty
15	DOUANLA YONTA Herman	Senior Lecturer	In duty
16	FOMEKONG Christophe	Senior Lecturer	In duty
17	KIKI Maxime Armand	Senior Lecturer	In duty
18	MBAKOP Guy Merlin	Senior Lecturer	In duty
19	MENGUE MENGUE David Joe	Senior Lecturer	In duty
20	NGUEFACK Bernard	Senior Lecturer	In duty
21	NIMPA PEFOUKEU Romain	Senior Lecturer	In duty
22	POLA DOUNDOU Emmanuel	Senior Lecturer	In duty
23	TAKAM SOH Patrice	Senior Lecturer	In duty
24	TCHANGANG Roger Duclos	Senior Lecturer	In duty
25	TETSADJIO TCHILEPECK M. E.	Senior Lecturer	In duty

26	TIAYA TSAGUE N. Anne-Marie	Senior Lecturer	In duty
27	BITYE MVONDO Esther Claudine	Assistante	In duty
28	FOKAM Jean Marcel	Assistant	In duty
29	LOUMNGAM KAMGA Victor	Assistant	In duty
30	MBATAKOU Salomon Joseph	Assistant	In duty
31	MBIAKOP Hilaire George	Assistant	In duty
32	MEFENZA NOUNTU Thiery	Assistant	In duty
33	OGADOA AMASSAYOGA	Assistant	In duty
34	TCHEUTIA Daniel Duviol	Assistant	In duty

### 8- DEPARTEMENT OF MICROBIOLOGY (MIB) (21)

1	ESSIA NGANG Jean Justin	Professor	<b>Head of Department</b>
2	NYEGUE Maximilienne Ascension	Professor	<b>VICE-DEAN / DSSE</b>
3	NWAGA Dieudonné M.	Professor	En poste
4	ASSAM ASSAM Jean Paul	Associate Professor	In duty
5	BOYOMO ONANA	Associate Professor	In duty
6	KOUITCHEU MABEKU Epse KOUAM Laure Brigitte	Associate Professor	In duty
7	RIWOM Sara Honorine	Associate Professor	In duty
8	SADO KAMDEM Sylvain Leroy	Associate Professor	In duty
4	ASSAM ASSAM Jean Paul	Associate Professor	In duty
5	BOYOMO ONANA	Associate Professor	In duty
6	KOUITCHEU MABEKU Epse KOUAM Laure Brigitte	Associate Professor	In duty
7	RIWOM Sara Honorine	Associate Professor	In duty
8	SADO KAMDEM Sylvain Leroy	Associate Professor	In duty
9	BODA Maurice	Senior Lecturer	In duty
10	BOUGNOM Blaise Pascal	Senior Lecturer	In duty
11	ESSONO OBOUGOU Germain G.	Senior Lecturer	In duty
12	NJIKI BIKOÏ Jacky	Senior Lecturer	In duty
13	TCHIKOUA Roger	Senior Lecturer	In duty
14	ESSONO Damien Marie	Assist. Lecturer	In duty
15	LAMYE Glory MOH	Assist. Lecturer	In duty
16	MEYIN A EBONG Solange	Assist. Lecturer	In duty
17	MONI NDEDI Esther Del Florence	Assist. Lecturer	In duty
18	NKOUDOU ZE Nardis	Assist. Lecturer	In duty
19	SAKE NGANE Carole Stéphanie	Assist. Lecturer	In duty
20	TAMATCHO KWEYANG Blaindine Pulchérie	Assist. Lecturer	In duty
21	TOBOLBAÏ Richard	Assist. Lecturer	In duty

\

**9. DEPARTMENT OF PHYSICS (PHY) (44)**

1	BEN- BOLIE Germain Hubert	Professor	In duty
2	DJUIDJE KENMOE épouse ALOYEM	Professor	In duty
3	EKOBENA FOU DA Henri Paul	Professor	<b>Vice-Rector. UN</b>
4	ESSIMBI ZOBO Bernard	Professor	In duty
5	KOFANE Timoléon Crépin	Professor	In duty
6	NANA ENGO Serge Guy	Professor	In duty
7	NANA NBENDJO Blaise	Professor	In duty
8	NDJAKA Jean Marie Bienvenu	Professor	<b>Head of Department</b>
9	NJANDJOCK NOUCK Philippe	Professor	In duty
10	NOUAYOU Robert	Professor	In duty
11	PEMHA Elkana	Professor	In duty
12	TABOD Charles TABOD	Professor	Dean FS Univ/Bda
13	TCHAWOUA Clément	Professor	In duty
14	WOAFO Paul	Professor	In duty
15	ZEKENG Serge Sylvain	Professor	In duty
16	BIYA MOTTO Frédéric	Associate Professor	<b>DG/HYDRO Mekin</b>
17	BODO Bertrand	Associate Professor	In duty
18	ENYEGUE A NYAM épse BELINGA	Associate Professor	In duty
19	EYEBE FOU DA Jean sire	Associate Professor	In duty
20	FEWO Serge Ibraïd	Associate Professor	In duty
21	HONA Jacques	Associate Professor	In duty
22	MBANE BIOUELE César	Associate Professor	In duty
23	MBINACK Clément	Associate Professor	In duty
24	NDOP Joseph	Associate Professor	In duty
25	SAIDOU	Associate Professor	<b>Chief of centre/IRGM/MINRESI</b>
26	SIEWE SIEWE Martin	Associate Professor	In duty
27	SIMO Elie	Associate Professor	In duty
28	VONDOU Derbetini Appolinaire	Associate Professor	In duty
29	WAKATA née BEYA Annie	Associate Professor	<i>Director/ENS/UYI</i>
30	ABDOURAHIMI	Senior Lecturer	In duty
31	CHAMANI Roméo	Senior Lecturer	In duty
32	EDONGUE HERVAIS	Senior Lecturer	In duty
33	FOUEDJIO David	Senior Lecturer	Chief Cell. MINADER
34	MBONO SAMBA Yves Christian U.	Senior Lecturer	In duty
35	MELI'I Joelle Larissa	Senior Lecturer	In duty
36	MVOGO ALAIN	Senior Lecturer	In duty
37	OBOUNOU Marcel	Assist. Lecturer	DA/Univ Inter Etat/Sangmalima
38	WOULACHE Rosalie Laure	Assist. Lecturer	In duty
39	AYISSI EYEBE Guy François Valérie	Assist. Lecturer	In duty
40	DJIOTANG TCHOTCHOU Lucie	Assist. Lecturer	In duty

	Angennes		
41	LAMARA Maurice	Assist. Lecturer	In duty
42	OTTOU ABE Martin Thierry	Assist. Lecturer	In duty
43	TEYOU NGOUPOU Ariel	Assist. Lecturer	In duty

### 10-DEPARTMENT OF EARTH SCIENCES (E. S.) (42)

1	BITOM Dieudonné	Professor	<b>Dean / FASA / UDs</b>
2	FOUATEU Rose épouse YONGUE	Professor	In duty
3	NDAM NGOUPAYOU Jules-Remy	Professor	In duty
4	NDJIGUI Paul Désiré	Professor	<b>Head of Department</b>
5	NGOS III Simon	Professor	In duty
6	NKOUMBOU Charles	Professor	In duty
7	NZENTI Jean-Paul	Professor	In duty
8	ABOSSOLO née ANGUE Monique	Associate Professor	<b>Vice-Dean / DRC</b>
9	BISSO Dieudonné	Associate Professor	<b>Director/Project Bar- rage Memve'ele</b>
10	EKOMANE Emile	Associate Professor	In duty
11	GANNO Sylvestre	Associate Professor	In duty
12	GHOLOMU Richard TANWI	Associate Professor	CD/Uma
13	MOUNDI Amidou	Associate Professor	<b>CT/ MINIMDT</b>
14	NGUEUTCHOUA Gabriel	Associate Professor	<b>CEA/MINRESI</b>
15	NJILAH Isaac KONFOR	Associate Professor	In duty
16	NYECK Bruno	Associate Professor	In duty
17	ONANA Vincent Laurent	Associate Professor	<b>Chief serv. Mater. Maint /UYII</b>
18	TCHAKOUNTE J. épouse NUMBEM	Associate Professor	<b>Chief. cell / MINRESI</b>
19	TCHOUANKOUE Jean-Pierre	Associate Professor	Associate Professor
20	TEMDJIM Robert	Associate Professor	Associate Professor
21	YENE ATANGANA Joseph Q.	Associate Professor	<b>Chief Div. /MINTP</b>
22	ZO'O ZAME Philémon	Associate Professor	<b>DG/ART</b>
23	ANABA ONANA Achille Basile	Senior Lecturer	In duty
24	BEKOA Etienne	Senior Lecturer	In duty
25	ELISE SABABA	Senior Lecturer	In duty
26	ESSONO Jean	Senior Lecturer	In duty
27	EYONG JOHN TAKEM	Senior Lecturer	In duty
28	FUH Calistus Gentry	Senior Lecturer	<b>Sec. D'Etat/MINMIDT</b>
29	LAMILEN BILLA Daniel	Senior Lecturer	In duty
30	MBESSE CECILE OLIVE	Senior Lecturer	In duty
31	MBIDA YEM	Senior Lecturer	In duty
32	METANG Victor	Senior Lecturer	In duty
33	MINYEM Dieudonné-Lucien	Senior Lecturer	<b>CD/Uma</b>
34	NGO BELNOUN Rose Noël	Senior Lecturer	In duty
35	NGO BIDJECK Louise Marie	Senior Lecturer	In duty
36	NOMO NEGUE Emmanuel	Senior Lecturer	In duty
37	NTSAMA ATANGANA Jacqueline	Senior Lecturer	In duty
38	TCHAPTCHET TCHATO De P.	Senior Lecturer	In duty

39	TEHNA Nathanaël	Senior Lecturer	In duty
40	TEMGA Jean Pierre	Senior Lecturer	In duty
41	FEUMBA Roger	Assist. Lecturer	In duty
42	MBANGA NYOBE Jules	Assist. Lecturer	In duty
41	FEUMBA Roger	Assist. Lecturer	In duty

**DISTRIBUTION OF PERMANENT LECTURERS IN THE FACULTY OF  
SCIENCE ACCORDING TO DEPARTMENTS**

**NUMBER OF LECTURERS**

Department	Professor	Associate Professor	Senior Lecturer	Assist. Lecturer	Total
BCH	8 (01)	14 (10)	13 (05)	05 (02)	<b>40 (18)</b>
BPA	15 (01)	8 (06)	18 (05)	10 (03)	<b>51 (15)</b>
BPV	07 (01)	9 (01)	8 (06)	07 (01)	<b>31 (9)</b>
CI	10 (01)	09 (02)	10 (02)	03 (0)	<b>32 (5)</b>
CO	6 (0)	21 (05)	05 (02)	08 (02)	<b>40 (9)</b>
IN	2 (0)	1 (0)	14 (01)	08 (01)	<b>25 (2)</b>
MAT	2 (0)	8 (0)	15 (01)	09 (02)	<b>34 (7)</b>
MIB	3 (0)	5 (03)	06 (01)	06 (02)	<b>20 (6)</b>
PHY	15 (0)	14 (02)	09 (03)	08 (03)	<b>46 (8)</b>
ST	7 (1)	15 (01)	18 (05)	02 (0)	<b>42 (7)</b>
<b>Total</b>	<b>75 (5)</b>	<b>104 (30)</b>	<b>116 (31)</b>	<b>66 (16)</b>	<b>361 (86)</b>

<b>A total of:</b>	<b>361 (86)</b> including:
Professor	<b>75 (5)</b>
Associate professor	<b>104 (30)</b>
Senior Lecturer	<b>116 (31)</b>
Assist. Lecturer	<b>66 (16)</b>
( ) = Nombre de Femmes	<b>86</b>

**The Dean of the Faculty of Science**  
Prof. TCHOUANKEU Jean-Claude



*I dedicate my thesis to my*

*Parents:*

*Joseph Ngangoun Mouafo*

*Pauline Majum*



## ACKNOWLEDGMENT

*All honor and glory to the almighty God of creation, to Gods of my ancestors, and to my beloved father, without which I would have not made. It was not easy but with your grace, I have been able to reach the end of the chapter.*

*I would like to express my sincere gratitude to all the people and institutions that made this project possible.*

*With the utmost degree of sincerity, I will be forever grateful for the amazing opportunity to work under the supervision of the brilliant and incomparable minds: **Prof Fabrice Boyom** and **Prof Mervin Meyer**. I have learned a lot from you and have become a better researcher through your mentorship. Thank you very much for your patience and support, it has got me through some difficult phases of this work. May this thesis be a symbol of my sincere and profound gratitude.*

*My sincere gratitude goes to **Prof Moundipa Fewou Paul**, Head of Department of Biochemistry, Faculty of Science, University of Yaoundé I, Cameroon, for the relentless efforts towards my achievement of these studies so far and also for the facilities placed at my disposal to enable me to carry out the studies. I would like to acknowledge the entire staff members of the Department of Biochemistry, for the knowledge and encouragement during the research.*

*I found no theoretical gems in the ocean of words to express my heartfelt sense of gratitude to my research menthor **Dr. Marius Tincho** of the Department of Medical Pathology, Division of Medical Virology, University of Cape Town, South Africa, your support and encouragement is highly appreciated and I also thank **Dr. Morris** of Department of Medical Bioscience, University of the Western Cape, South Africa for your moral support.*

*I would like to express special thanks to **Prof Paulo Oliveira**, Ph.D. Principal Investigator, "MitoXT - Mitochondrial Toxicology and Experimental Therapeutics Laboratory" Mitochondria, Metabolism and Disease Group that designed my project in cancer research and guide me to be awarded the Coimbra Group Short Stay Scholarship Programme for young*



researchers from Sub-Saharan Africa, 2015, CNC - Center for Neuroscience and Cell Biology UC Biotech Building, Portugal.

I place on record my esteem regard and sincere thanks to my first co-supervisor **Prof Chitra Mandal** who gave me the opportunity to start my Ph.D. in the cancer research field and the technician **Mrs. Asish** who guide me for tissue culture, and both of them are from Cancer Biology and Inflammatory Disorder Division, Council of Scientific and Industrial Research-Indian Institute of Chemical Biology, West Bengal, India.

I feel highly obliged and gratified while offering gratitude to **INAM S&T, Centre Research Training Fellowship for Developing Country Scientists (RTF-DCS)**, and **CSIR-IICB**, West Bengal, Kolkata, India.

My esteemed gratitude to the Organization for Women in Science for the **Developing World (OWSD)** for sponsoring my Ph.D. studies (2017-2019), this work would not have been possible without the support from fellowship findings.

I'm grateful to **DST/Mintek Nanotechnology Innovation Centre** and **Chemical Industries Education & Training Authority (CHIETA)** for funding this project.

I would like to extend my heartfelt gratitude to all my former and present colleagues of Cancer Biology and Inflammatory Disorder Division, Council of Scientific and Industrial Research-Indian Institute of Chemical Biology, Kolkata, West Bengal, India especially **Mr. Prasun** for your assistance, **Dr. Dewatidii**, **Dr. Shalini Nath** and **Dr. Samanpa Maiti** for your friendship, **Dr. Susmita Monday** for troubleshooting in flow cytometry techniques.

I also extend my heartfelt gratitude to all my former and present colleagues in the NIC Bio labels groups and the Biotechnology Department, Lab life of the University of the Western Cape. **Dr. Jyoti Sharma**, **Dr. Nicole Sibuyi** for your stress environment that helps me to be strong, **Dr. Elbagory Abdouraman** your support, and encouragement are highly appreciated, **Dr. Phumizile**, **Mr. Mohammed**, **Miss. Yonela**, **Miss. Buetomelo**, **Mr. Martin Riziki**, **Miss. Caroline**, **Miss. Tahirah**, **Miss. Tina**, and **Miss. Toni** for your friendship.

I wish to address a special thanks to **Herman Kwemi Djanda** for his support and assistance, thanks you make the end of thesis journey wonderful.

*I am particularly grateful to my friends and collaborators, Dr. Rufin Toghueo, Dr. Elisabeth Memkem, Dr. Eké Pierre, Dr. Marguerite Simo, Dr. Christelle Mabou, Mr. Fred Djague, Miss. Michèle Inès Mbekou Kankou for their assistance.*

*Academic life without friends is beyond imagination, I am grateful to Almighty God of creation who has blessed me with such wonderful friends. My special thanks to place a gratitude to all my group members Dr. Taffou, Dr. Tsouh Fokou, Dr. Hounda Fokou, Dr. Issakou Bakarnga-Via, Dr. Tchokouaha Yamthe, Dr. Ngoutane Mfopa, Dr. Ngo Mback, Dr. Bedine Boat, Mr. Jiatsa Mbouna, Mrs. Mireille Chouegouong, Mr. Rodrigue Keumoe, Mr. Cyrille Njanpa, Miss Darline Dize. All senior researchers and students in the Laboratory of Phytobiochemistry and Medicinal Plants Studies, for their constructive ideas, advice, assistance, and contribution in this work.*

*Saving the best for last: MY Family, my life, and my all! BLOOD bonds are by far the strongest and unbreakable and have realized the value of having family support through this trying period. You guys are my world, the best treasure any human being can ask for. You are my pride and joy, the very best part of me! I'm practically nothing without you by my side. You've been patient and supportive throughout my studies, with you by my side I know I can laugh at the face of whatever the world throws at me. You all are my anchor, my strength, with you lot I can fly higher than an eagle.*

*I love you to the moon and back forevermore!*

*Words fail to express my deep gratitude from the depth of my heart to my lovely mother Pauline Majum, my father Joseph Mouafo, my brother Junior Kamdoun, and my first sister Carole Guelo and her husband Mr. Pierre Njontu, whose prayers and financial support kept me going. Last but not least I thank every supportive hand that has not been mentioned by name but has given invaluable help in their way directly or indirectly with this study and soliciting good wishes for my future.*

## TABLE OF CONTENTS

DEDICACE.....	xii
ACKNOWLEDGMENT .....	i
TABLE OF CONTENTS .....	iv
LIST OF FIGURES.....	vii
LIST OF TABLES .....	x
LIST OF APPENDICES .....	x
LIST OF ABBREVIATIONS & ACRONYMS .....	xii
ABSTRACT .....	xvi
RESUME.....	xviii
INTRODUCTION.....	1
CHAPTER I: LITTERATURE REVIEW .....	4
I.1 Nano .....	4
I.1.1. Classification Of Nanomaterials.....	4
I.1.2 Physical And Chemical Synthesis Methods Of Metallic Nanoparticles .....	8
I.1.3 Green Synthesis Methods .....	16
I.2 Broad Applications Of Metallic Nanoparticles & Biologically Inspired Templates .....	21
I.2.1 Biological And Medical Application Of Silver Nanoparticles.....	22
I.2.2 Biological And Medical Application Of Gold Nanoparticles .....	23
I.2.3 Nanomedicine For Cancer Applications.....	23
I.3 Challenge And Advance In Nanotechnology .....	36
I.3.1 Safety And Environmental Impact Of Nanoparticles.....	36
I.3.2 Significance Progress In Green Nanotechnology .....	37
CHAPITRE II: MATERIAL AND METHODS .....	52
II.1 MATERIALS.....	52



II.1.1 Chemicals Reagents And Their Suppliers.....	52
II.1.2 Instruments .....	52
II.1.3 Bacteria Strains .....	52
II.1.4 Cancer Cells Maintaining.....	53
II.1.5 <i>Terminalia mantaly</i> Harvest And Identification .....	54
II.2 METHODS .....	54
II.2.1 Green synthesis And Characterization Of Gold And Silver Nanoparticles .....	54
II.2.1.1 TM Samples Preparation And Extraction.....	54
II.2.1.2 Phytochemical Screening Of Crude Extracts .....	54
II.2.1.3 Synthesis Of Biogenic Gold And Silver Nanoparticles.....	56
II.2.1.3.1 Measurement Of Nanoparticles Concentrations .....	56
II.2.1.3.2 Characterisation Of Synthesized TM-AgNPs And TM-AuNPs .....	56
II.2.2 Evaluate <i>in vitro</i> Antibacterial Screening And MIC Determination Of The Bio-active Crude Extracts, Gold And Silver Nanoparticles.....	58
II.2.3 Assesment The Anproliferative Potential Of Extracts, More Stable Gold And Silver Nanoparticles On Four Resistant Models Cells Line .....	60
II.2.4 Statistical Analysis .....	65
CHAPTER III: RESULTS AND DISCUSSION .....	54
III.1 Results Of Green synthesis And Characterization Of Gold And Silver Nanoparticles	54
III.1.1 Phytochemicals Composition.....	54
III.1.2 Physical Formation Of TM-AgNPs And TM-AuNPs.....	55
III.1.3 HRTEM, SAED, EDX Analyses And FTIR Analyses Of Bio-Active TM-AgNPs and TM-AuNPs.....	62
III.2. Antibacterial Activity Of TM extracts, And Derived TM-AuNPs And TM-AgNPs ..	73
III.2.1. Preliminary Antibacterial Screening: Evaluation Of spectra Of Activity.....	73



III.2.2 Determination Of The Minimal Inhibitory Concentration (MIC) Of The More Active TM Extracts And TM-AgNPs .....	77
III.2.3. Growth Inhibitory Kinetics Of TM-AgNPs .....	78
III.3 Potential Antiproliferative Effect Of Extracts, And The More Stable Gold And Silver Nanoparticles Against A Panel Of Three Resistant Cancer Cells Line And Study Of Mechanism Of Cell Death .....	81
III.3.1 Effect Of TM Crude Extract, Stable TM Gold And Silver Nanoparticles On Cell Proliferation Of Cancer Cells.....	81
III.3.2 Effect Of The Selective Crude Extract, More Stable Gold And Silver Nanoparticles On A Normal Fibroblast Cells Line (KMST-6).....	86
III.3.3 Therapeutic Potential Of Targeted Nanotherapy: Investigation Into The Mode Of Cell Death Induced By Bio-active Crude Extracts, AuNPs, And AgNPs .....	88
CHAPTER IV: CONCLUSION AND PERSPECTIVES.....	105
IV-1-CONCLUSION.....	105
IV-2 PERSPECTIVES .....	106
REFERENCES.....	107
APPENDICES.....	a
ARTICLE PUBLISHED .....	p



## LIST OF FIGURES

<b>Figure 1:</b> Lycurgus Cup courtesy of the British Museum. The light source is (A) in the cup or (B) outside the cup. Black circles indicate the positions of extracted colours.....	4
<b>Figure 2:</b> Basic structure of inorganic nanoparticles figure reprinted with permission from Elsevier .....	6
<b>Figure 3:</b> Structure and energetics of gold and silver nanoparticles .....	6
<b>Figure 4:</b> Schematic illustration for the deduced process of gold nanoparticles formation. Reduction and nucleation.....	8
<b>Figure 5:</b> Schematic representation of the synthesis of colloidal silver nanoparticles using the chemical reduction process. ....	8
<b>Figure 6:</b> Schematic representation of different methods of metallic nanoparticles (AuNPs and AgNPs) synthesis .....	9
<b>Figure 7:</b> UV-visible Spectroscopy Analysis. (A): UV-Visible Instruments, (B): Surface Plasmon Resonance of gold nanoparticle .....	11
<b>Figure 8:</b> Dynamic Light Scattering Analysis. (A): Zetasizer Malvern Instruments, (B): Z-Average size distribution, (C): Zeta potential	13
<b>Figure 9:</b> TEM images of gold nanoprisms (A, B) and nanorods (C, D) obtained at 20-200 KeV .....	14
<b>Figure 10:</b> Microanalysis HRTEM techniques of gold nanoparticles: (A): HRTEM microscope instrument; (B): X-ray energy dispersive spectra; (C): gold facet, (D): Spherical shapes; (E): Selected Area electron diffraction pattern with crystalline effect .....	15
<b>Figure 11:</b> Advantages of green synthesis of AuNPs and AgNPs by plant extracts.....	18
<b>Figure 12:</b> Critical biophysical parameters that can influence the production of monodisperse, stable, high-yield nanoparticles.....	20
<b>Figure 13:</b> General applications of nanoparticles.....	21
<b>Figure 15:</b> Diagram represent the different mechanisms of action of NPs including silver nanoparticles in bacterial cells .....	22
<b>Figure 14:</b> Three models for the cytosolic escape of mitochondrial proteins in response to apoptotic stimuli .....	30
<b>Figure 15:</b> Apoptotic changes in the plasma membrane. ....	31



<b>Figure 16:</b> Schematic diagram describing the mechanisms implicated in NP-induced ROS production .....	33
<b>Figure 17:</b> Schematic diagram describing the mechanisms implicated in NP on cell cycle arrest (A): Effect of gold nanoparticles (Kumar <i>et al.</i> , 2015) and silver nanoparticles (B) on cell cycle arrest.....	35
<b>Figure 18:</b> Representative cell cycle histogram of Caco-2 cells analyzed by flow cytometry. ....	36
<b>Figure 20:</b> One-step synthesis of TM-AgNPs and TM-AuNPs by reduction of gold and silver ions with TM phytochemicals. Colour change denoted the presence of AuNPs and AgNPs. ....	56
Note: Aqueous and methanolic TM extracts were used to reduce AgNO <sub>3</sub> into AgNPs, and AuCL <sub>4</sub> into AuNPs, colour change indicates NP formation. ....	56
<b>Figure 21:</b> UV–vis spectral profiles of TM-AuNPs synthesized at 25 °C and 70 °C.....	58
<b>Figure 22:</b> UV–vis spectral profiles of TM-AgNPs synthesized at 25 °C and 70 °C. ....	59
<b>Figure 23:</b> HRTEM micrographs and SAED patterns of selected TM-AgNPs. ....	63
<b>Figure 24:</b> Particles size distribution of more stable and bioactive TM-AgNPs.....	64
<b>Figure 25.</b> EDX spectra of AgNPs synthesized from a TML and aTMSB AgNPs.....	65
<b>Figure 26:</b> HRTEM images of TM-AuNPs synthesized at 25 °C and 70 °C. The arrows point at different NP shapes. The scale bar at 10, 20, and 50 nm.....	68
<b>Figure 27:</b> The particle size distribution of more stable and bio-active TM-AuNPs.....	69
<b>Figure 28:</b> SAED patterns of TM-AuNPs showing single facets of NPs in TEM micrographs .....	58
<b>Figure 29:</b> EDX spectra of bioactive TM-AuNPs.....	59
<b>Figure 30:</b> Screening of the antibacterial effects of TM extracts and AgNPs against a panel of eight bacterial strains. ....	74
<b>Figure 33:</b> Growth inhibitory activities of TML-AgNPs-25 °C against selected bacterial strains .....	79
<b>Figure 31:</b> Growth inhibitory activities of TMSB-AgNPs-70 °C against selected bacterial strains. ....	80
<b>Figure 32:</b> Effects of increasing concentrations of silver nanoparticles on the viability of Caco-2, HepG2 and MCF-7 cells.....	85



**Figure 33:** Cytotoxicity evaluation of bio-active TM extracts and TM-AuNPs at various concentrations against KMST-6 fibroblast normal cells..... 88





## LIST OF TABLES

<b>Table I:</b> A summary of the various types of chemotherapeutics available for cancer therapy. .....	24
<b>Table II:</b> Nanoparticles therapeutics undergoing clinical investigations .	26
<b>Table III:</b> List of some <i>Terminalia</i> species, their parts used, and the biomolecules obtained from the plants responsible for the green synthesis of AgNPs and AuNPs.....	38
<b>Table IV:</b> List of bacterial strains used for antibacterial activity.....	53
<b>Table V:</b> List of cancer and non-cancerous cells line.....	53
<b>Table VI:</b> Phytochemical composition of TM extracts. ....	55
<b>Table VII:</b> SPR and DLS analysis of TM-AgNPs and TM-AuNPs synthesized at 25 °C and 70 °C. ....	62
<b>Table VIII:</b> Comparison FTIR spectra of TM extracts and their respective most active TM- AgNPs.....	67
<b>Table IX:</b> Comparison FTIR spectra of TM extracts and their respective TM-AuNPs.....	73
<b>Table X:</b> Comparison of the bacterial susceptibility to TM extracts and TM-AgNPs.....	76
<b>Table XI</b> MIC for crude TM extracts and derivate TM-AgNPs on selected bacteria strains..	77
<b>Table XII:</b> Cytotoxicity responses of TM extracts and the more stable TM-AuNPs and TM- AgNPs against, Caco-2, HepG2 and MCF-7, cell lines.....	84
<b>Table XIII:</b> Cytotoxicity evaluation of most promising crude extracts, AuNPs, and AgNPs against non-cancerous fibroblast KMST-6 cells.....	87
<b>Table XIV:</b> Apoptotic effects of more potent extracts, TM-AuNPs and TM-AgNPs against Caco-2, HePG2 and MCF-7 cells .....	92
<b>Table XV:</b> Effects of more potent extracts, TM-AuNPs and TM-AgNPs on ROS generated by MCF-7, HePG2 and Caco-2 cells .....	95
<b>Table XVI:</b> Apoptotic effects of more potent extracts, TM-AuNPs and TM-AgNPs against MCF-7, HePG2 and Caco-2 cells. ....	99



## LIST OF APPENDICES

<b>Appendix 1:</b> Measurement of nanoparticles concentrations higher concentration of nanoparticles.....	a
<b>Appendix 2:</b> Schematic representation of the AgNP synthesis from TM plant extracts .....	b
<b>Appendix 3:</b> One-step synthesis of TM-AuNPs by reduction of gold ions with TM phytochemicals. Colour change denoted to the presence of AuNPs.....	c
<b>Appendix 4:</b> Fourier-transform infrared spectra of (A) extract from (aTMSB) of <i>Terminalia mantaly</i> (B) AuNPs- aTMSB prepared at 25 °C and (C) AuNPs-aTMSB synthesized at 70 °C.....	l
<b>Appendix 5:</b> HRTEM images of AuNPs synthesized at 25 °C and 70 °C. The arrows point at different NP shapes. The scale bar at 10, 20 and 50 nm. ....	m
<b>Appendix 6:</b> SAED patterns of TM-AuNPs showing single facets of NPs in TEM micrographs .....	n
<b>Appendix 7:</b> EDX spectra of TM-AuNPs synthesized at 25 °C and 70 °C .....	o
<b>Appendix 8:</b> Core sizes of TM-AuNPs were analyzed by HRTEM .....	p
<b>Appendix 9:</b> FTIR analysis of TM-AuNPs. ....	p
<b>Appendix 10:</b> FTIR spectra of selected TM-AgNPs compared to their respective TM extracts. ....	q
<b>Appendix 11:</b> Apoptotic effect of more active crude extracts, gold, and the silver nanoparticle from <i>Terminalia mantaly</i> on MCF-7 cells. ....	r
<b>Appendix 12:</b> Apoptotic effect of more active crude extracts, two active gold and silver nanoparticles from <i>Terminalia mantaly</i> on HepG2 cells for 24 hrs.....	s
<b>Appendix 13:</b> Apoptotic effect of more active crude extracts, two active gold and silver nanoparticles from <i>Terminalia mantaly</i> on Caco-2 cells for 24 hrs.....	t
<b>Appendix 14:</b> ROS activity in response to various treatments. MCF-7 cells were treated with mTMSB, mTMR, mTMR-AuNPs-25 °C, mTMSB-AuNPs-70 °C, aTML-AgNPs-25 °C, and aTMSB-AgNPs-70 °C at their specific IC50 values, 0.1% H2O2 was used as positive control values for 24 hrs.....	u
<b>Appendix 15:</b> ROS activity in response to various treatment. HepG2 cells were treated with with mTMSB, mTMR, mTMR-AuNPs-25 °C, mTMSB-AuNPs-70 °C, aTML-AgNPs-25 °C, and aTMSB-AgNPs-70 °C at their specific IC50 values, 0.1% H2O2 was used as positive control for 24 hrs.....	v
<b>Appendix 16:</b> ROS activity in response to various treatments. Caco-2 cells were treated with with mTMSB, mTMR, mTMR-AuNPs-25 °C, mTMSB-AuNPs-70 °C, aTML-AgNPs-25 °C, and aTMSB-AgNPs-70 °C at their specific IC50 values, 0.1% H2O2 was used as positive control for 24 hrs.....	w

**Appendix17:** Cell cycle analysis after treatment with active mTMR-AuNPs-25 °C, mTMSB-AuNPs-70 °C, aTML-AgNPs-25 °C, aTMSB-AgNPs-70 °C, mTMSB and mTMR in MCF-7 cells at their specific IC50 values, cisplatin 10 µM was used at positive control after 24 hrs ..... x

**Appendix18:** Cell cycle analysis after treatment with active mTMR-AuNPs-25 °C, mTMSB-AuNPs-70 °C, aTML-AgNPs-25 °C, aTMSB-AgNPs-70 °C, mTMSB and mTMR in HepG2 cells at their specific IC50 values, cisplatin 10 µM was used as positive control after 24 hrs ..... y

**Appendix19:** Cell cycle analysis after treatment with active mTMR-AuNPs-25 °C, mTMSB-AuNPs-70 °C, aTML-AgNPs-25 °C, aTMSB-AgNPs-70 °C, mTMSB and mTMR in Caco-2 cells after 24 hrs ..... z

**Appendix 20:** Preparation of solutions and reagents..... m



## LIST OF ABBREVIATIONS & ACRONYMS

<b>Ag<sup>+</sup></b>	Silver ions
<b>AgNO<sub>3</sub></b>	Silver nitrate
<b>AgNPs</b>	Silver nanoparticles
<b>AIF</b>	Apoptosis-inducing factor
<b>APAF-1</b>	Apoptotic protease activating factor 1
<b>ANOVA</b>	Analysis of variance
<b>Anx</b>	Annexin
<b>Au<sup>+</sup></b>	Gold ions
<b>AuCl<sub>4</sub></b>	Tetrachloroaurate.
<b>AuNPs</b>	Gold nanoparticles
<b>ATCC</b>	American Type Culture Collection
<b>ATP</b>	Adenosine triphosphate
<b><sup>a</sup>TML</b>	Aqueous leaf extract
<b><sup>a</sup>TMSB</b>	Aqueous stem bark extract
<b><sup>a</sup>TMR</b>	Aqueous root extract
<b><sup>a</sup>TML-AgNPs</b>	Silver nanoparticles from the aqueous leaf extract
<b><sup>a</sup>TMSB-AgNPs</b>	Silver nanoparticles from the aqueous stem bark extract
<b><sup>a</sup>TMR-AgNPs</b>	Silver nanoparticles from the aqueous root extract
<b><sup>a</sup>TML-AuNPs</b>	Gold nanoparticles from the leaf extract
<b><sup>a</sup>TMSB-AuNPs</b>	Gold nanoparticles from the aqueous stem bark extract
<b><sup>a</sup>TMSB-AuNPs</b>	Gold nanoparticles from the aqueous stem bark extract
<b>Bax</b>	Bcl-2 homologous antagonist killer
<b>Bax</b>	Bcl-2 associated protein-X
<b>Bcl-2</b>	B-cell lymphoma 2
<b>°C</b>	Degree centigrade
<b>Caco-2</b>	Human Colorectal adenocarcinoma
<b>Caspases</b>	Cysteine aspartate-specific proteases
<b>CC<sub>50</sub></b>	Half maximum cytotoxicity concentration
<b>CDKs</b>	Cyclin-dependent kinases
<b>CLSI</b>	Clinical Laboratory Standard Institute
<b>Cys</b>	Cisplatin
<b>CM-H<sub>2</sub>DCFDA</b>	5-(and-6)-chloromethyl-2',7'-dichlorodihydrofluorescein diacetate acetyl ester
<b>CTAB</b>	Cetyl Ctrimonium bromide
<b>Ctrl</b>	Control
<b>Cyt-C</b>	Cytochrome C
<b>DISC</b>	Death-inducing signal complex
<b>DLS</b>	Dynamic Light Scattering
<b>DMEM</b>	Dulbecco's modified Eagle's medium
<b>DMSO</b>	Dimethyl sulphoxide
<b>DNA</b>	Deoxyribonucleic acid
<b>EDTA</b>	Ethylene Diamine Tetra acetic Acid-Na <sub>2</sub>
<b>EDS</b>	Energy Dispersion Spectroscopy
<b>e.g.</b>	For example

<b>FCC</b>	Face centered cubic
<b>FACS</b>	Fluorescence-activated cell sorting
<b>FADD</b>	FAS-associated DEATH domain protein
<b>FAS-L</b>	Fas Cell Surface Death Receptor ligand
<b>FBS</b>	Fetal bovine serum
<b>FDA</b>	Food and Drug Administration
<b>FTIC</b>	Fluorescein Isothiocyanate
<b>FTIR</b>	Fourier Transform Infrared
<b>GADD45</b>	Growth Arrest and DNA Damage-inducible protein
<b>IC<sub>50</sub></b>	50% Inhibitory Concentration (IC <sub>50</sub> )
<b>INK4</b>	Inhibitor of Cyclin-Dependent Kinase 4
<b>IARC</b>	International Agency for Research on Cancer
<b>H<sub>2</sub>O<sub>d</sub></b>	Double distilled water
<b>HePG2</b>	Human hepatocellular liver carcinoma
<b>Hrs</b>	Hours
<b>HRTEM</b>	High-Resolution Transmission Electron Microscopy
<b>KBr</b>	Potassium Bromide
<b>KMST-6</b>	non-cancerous human skin fibroblast cell line
<b>KH<sub>2</sub>PO<sub>4</sub></b>	Potassium dihydrogen phosphate
<b>MeOH</b>	Methanol
<b>MCF 7</b>	Human breast adenocarcinoma cells
<b>MIC</b>	Minimal Inhibitory Concentration
<b>MHA</b>	Muller Hinton Agar
<b>MHB</b>	Muller Hinton Broth
<b>Mg</b>	Milligram
<b>mg/l</b>	Milligram per Liter
<b>min</b>	Minutes
<b>mV</b>	Mili volt
<b>mTML</b>	Methanolic leaf extract
<b>mTMSB</b>	Methanolic stem bark extract
<b>mTMR</b>	Methanolic root extract
<b>mTML-AgNPs</b>	Silver nanoparticles from the methanolic leaf extract
<b>mTMSB-AgNPs</b>	Silver nanoparticles from the methanolic stem bark extract
<b>mTMR-AgNPs</b>	Silver nanoparticles from the methanolic root extract
<b>mTML-AuNPs</b>	Gold nanoparticles from the methanolic leaf extract
<b>mTMSB-AuNPs</b>	Gold nanoparticles from the methanolic stem bark extract
<b>mTMR-AuNPs</b>	Gold from the methanolic root extract
<b>MTT</b>	3-[4,5-dimethylthiazol-2yl]-2,5-diphenyl-tetrazolium bromide
<b>NCI</b>	National Cancer Institute
<b>Nm</b>	Nano-Meter
<b>NP(s)</b>	Nanoparticle(s)
<b>OD</b>	Optical density
<b>PBS</b>	Phosphate Buffered Saline
<b>PE</b>	Phycoerythrin
<b>PS</b>	Phosphatidylserine
<b>PI</b>	Propidium iodide
<b>Rb</b>	Retinoblastoma protein
<b>RNA</b>	Ribonucleic acid

<b>ROS</b>	Reactive oxygen species
<b>RT</b>	Room temperature
<b>rpm</b>	Rotation Per Minute
<b>SAED</b>	Surface Area Electron Diffraction
<b>SD</b>	Standard Deviation
<b>SI</b>	Selective index
<b>SMAC</b>	second mitochondria-derived activator of caspases
<b>SPR</b>	Surface Plasmon Resonance
<b>TRADD</b>	TNF receptor-1 associated death domain protein
<b>µg</b>	Microgram
<b>µL</b>	Micro Liter
<b>UV-Vis</b>	Ultra-Violet Visible
<b>WST</b>	Water Tetrazolium Solution
<b>WHO</b>	World Health Organization



## ABSTRACT

Nanotechnology is considered to be one of the most important technological advancements in recent years, due to its new, profitable, and wide-spread applications in cancer therapy and bacterial infections. However, the gold (AuNPs) and silver (AgNPs) nanoparticles using plant-derived phytochemicals as both reducing and capping agents have emerged eco-friendly horizons to develop effective and less harmful treatment strategies. This study aimed at investigating the synthesis and characterization of AuNPs and AgNPs, and to evaluate their effects on cancer cells and bacteria strains. The aqueous (<sub>a</sub>TM) and methanolic extracts (<sub>m</sub>TM) of leaf (<sub>a,m</sub>TML), stem bark (<sub>a,m</sub>TMSB, ), and root (<sub>a,m</sub>TMR) from *Terminalia mantaly* were obtained by the maceration procedure. The AuNPs and AgNPs were synthesized and followed by the characterization using the UV-Visible Spectroscopy, Dynamic Light Scattering (DLS), High-Resolution Transmission Electron Microscopy (HRTEM), Energy-Dispersive X-ray Spectroscopy (EDX), Selected Area Electron Diffraction (SAED), and Fourier Transform Infrared (FTIR) analysis. The anti-bacterial screening of the *Terminalia mantaly* extracts and derived gold and silver nanoparticles were evaluated on eight bacterial strains using the broth microdilution assay as described by the CLSI. The growth-inhibitory kinetics of the bio-active silver nanoparticles was assessed on susceptible strains for a period of 8 hrs. The anticancer activity was performed with extracts from *Terminalia mantaly* and derived more stable gold and silver nanoparticles against cancer cells line (Caco-2, HepG2, and MCF-7), and on non-cancerous fibroblast cell line (KMST-6) using MTT assay as described by Sibuyi. (2015). The most promising extracts, gold, and silver nanoparticles were used to study the cell death mechanism of action (apoptosis) using Annexin V-Cy3TM detection kit (APOAC), the intracellular Reactive Oxygen Species (ROS) generation in cells using the 5-(and-6)-chloromethyl-2',7'-dichlorodihydrofluorescein diacetate acetyl ester (CM-H2DCFDA), and Propidium iodide (PI) DNA stained cell cycle analysis using flow cytometry. The production of nanoparticles was visually observed as a colour change of the gold salt from yellow to red wine or red for gold nanoparticles (AuNPs), and colour of silver salt from colourless to yellow, brown, or green for silver nanoparticles (AgNPs). The Surface Plasmon Resonance (SPR) values ranged from 535 to 560 nm, and 438 to 480 nm and thereby confirming the production of AuNPs and AgNPs respectively. The HRTEM confirmed that nanoparticles were crystalline in nature and revealed the formation of different sizes and shapes. Most of the AuNPs and AgNPs were spherical with a mean diameter of 9.3, 6.2, 21 and 28 nm obtained for <sub>a</sub>TML-AgNPs-25 °C, <sub>a</sub>TMSB-AgNPs-70 °C, <sub>m</sub>TMR-AuNPs-25 °C, and <sub>m</sub>TMSB-AuNPs-70 °C respectively. The

EDX spectra of bio-active AuNPs and AgNPs confirmed the presence of gold and silver ions in all the nanoparticles. The FTIR revealed some functional chemical groups such as hydroxyl and aldehyde groups in the *Terminalia mantaly* active metabolites. In this study, the <sup>a</sup>TML-AgNPs-25 °C, and <sup>a</sup>TMSB-AgNPs-70 °C, showed significant antibacterial activity against all the tested bacterial strains and had MIC values of 3.125 and 125.000 µg/mL respectively. The bactericidal effect of <sup>a</sup>TML-AgNPs-25 °C was higher against *Streptococcus pneumonia* and *Haemophilus influenzae*. In general, for the anticancer activity, the IC<sub>50</sub> values ranged from 0.006 to 93.730 µg/ml. The IC<sub>50</sub> values of the TM-AuNPs, and TM-AgNPs were higher than that of the TM extracts. However, MCF-7 cells, in particular, were highly susceptible to the effects of <sup>m</sup>TMR and <sup>m</sup>TMSB extracts, with IC<sub>50</sub> values 2.73 and 19.73 µg/mL, respectively. TM-AgNPs were the most promising on the three tested cells line. For example, <sup>a</sup>TML-AgNPs-25 °C and <sup>a</sup>TMSB-AgNPs-70 °C showed IC<sub>50</sub> of 0.006 and 0.008 µg/mL on HepG2 cells respectively. Similarly, <sup>m</sup>TMR-AuNPs-25 °C displayed cytotoxicity with IC<sub>50</sub> values of 0.18 and 6.56 µg/mL on HepG2 and MCF-7 cells. The Annexin results confirmed the reduction of more than 50% of viable cells after the treatment with bioactive extracts and nanoparticles. The percentage of 70.23 and 78.01 % were obtained for <sup>m</sup>TMSB on HepG2 and Caco-2 cells, respectively. Similarly, the <sup>m</sup>TMR-AuNPs-25 °C and <sup>a</sup>TMSB-AgNPs-70 °C revealed a higher apoptotic effect with the percentage of 63.75, 73.610, and 82.290 % on MCF-7, HepG2, and Caco-2 cells respectively. The <sup>m</sup>TMSB-AuNPs-70 °C and <sup>a</sup>TML-AgNPs-25 °C induced significant ROS production of 62.83 and 63.26 % with Caco-2 and MCF-7 cells respectively. The bioactive extracts and AgNPs mostly induced the cell arrest in G0/G1 phase while the bioactive AuNPs also induced the cell arrest in G2/M phase. The current research highlighted the reducing and the capping potential of biomolecules present in extracts from *Terminalia mantaly* plant that displayed the rapid formation of multiples nanostructures and also demonstrated they're selective and enhance capacities to eradicate cancer cells using apoptosis through DNA fragmentation making it helpful to explore newer approaches in the treatment of cancer disease and associated infections.

**Keywords:** Nanotechnology, *Terminalia mantaly*, Green synthesis, Nanoparticles, Cancer, Proliferation, Apoptosis, Flow cytometry



## RESUME

La nanotechnologie est considérée comme l'avancée technologique la plus importante en raison de ses nouvelles applications répandues et rentables dans le traitement du cancer et des infections bactériennes. Cependant, les nanoparticules d'or (AuNPs) et d'argent (AgNPs) utilisant des composés phytochimiques d'origine végétale comme agents réducteurs et coiffants ont émergé comme alternative pour le développement des stratégies de traitement efficaces et biocompatibles. Ainsi, cette étude vise à réaliser la biosynthèse de nouvelles nanoparticules d'or et d'argent et évaluer leur capacité à éradiquer les cellules cancéreuses et à inhiber les infections bactériennes associées. Les extraits aqueux et méthanolique de feuilles, des écorces de tige, et de racines de *Terminalia mantaly* ont été obtenus par macération. Les nanoparticules d'or et d'argent ont été synthétisées, suivi d'une première caractérisation à l'aide de l'analyse par spectroscopie UV-visible et la diffusion dynamique de la lumière (DLS), la microscopie électronique à transmission à haute résolution (HRTEM), la spectroscopie à rayons X à dispersion d'énergie (EDX), la diffraction électronique en zone sélectionnée (SAED), et l'infrarouge à transformée de Fourier (FTIR). Le screening préliminaire d'activité antibactérien des extraits et des nanoparticules d'or et d'argent dérivant a été évalué sur huit souches bactériennes à l'aide du test de microdilution en milieu liquide comme décrit par le CLSI. La cinétique inhibitrice de croissance des nanoparticules d'argent bioactives a été évaluée sur des souches sensibles pendant une période de 8 heures. L'activité anticancéreuse a été réalisée avec des extraits, les nanoparticules d'or et d'argent les plus stables contre trois lignées cellulaires (Caco-2, MCF-7 et HepG2) et sur la lignée cellulaire fibroblaste non cancéreuse (KMST-6) en utilisant le test de MTT. Les extraits, les nanoparticules d'or et d'argent les plus actives ont été sélectionnés pour étudier les mécanismes de mort cellulaire (Apoptose) en utilisant le kit de détection d'apoptose Annexin V-Cy3<sup>TM</sup> (APOAC), la génération intracellulaire des espèces réactives de l'oxygène (ROS) au niveau des cellules utilisant le 5- (et-6) -chlorométhyl-2', 7'-dichlorodihydrofluorescéine diacétate acétyl ester (CM-H2DCFDA) et une analyse du cycle cellulaire par la méthode colorée de l'ADN à l'iodure de propidium (PI) en utilisant la cytométrie de flux. La formation de nanoparticules a été observée visuellement par un virage de couleur de la solution jaune à celle similaire vin rouge/rouge pour les nanoparticules d'or et le changement de couleur incolore au jaune, marron ou vert pour les nanoparticules d'argent. Les valeurs de résonance plasmonique de surface (SPR) variant de 535 à 560 nm et de 438 à 480 nm respectivement pour les nanoparticules d'or et d'argent fournissent ainsi des preuves de la formation des nanoparticules. La forme sphérique a été majoritai-

rement obtenue avec les nanoparticules de nature cristalline, et un diamètre moyen de 9.3, 6.2, 21 et de 28 nm a été respectivement obtenu avec des nanoparticules d'argent de l'extrait aqueux de feuille à 25 °C et l'extrait aqueux des écorces de tige à 70 °C, et les nanoparticules d'or de l'extrait méthanolique de racines à 25 °C et l'extrait méthanolique des écorces de tige à 70 °C. La caractérisation infrarouge à transformée de Fourier a révélé que certains groupes chimiques fonctionnels tels que les groupes hydroxyle (OH) et aldéhyde (C=O) des métabolites actifs de la plante *Terminalia mantaly*. Les nanoparticules biogéniques d'argent synthétisées à partir de l'extrait aqueux de feuilles à 25 °C et de l'extrait aqueux d'écorce de tige à 70 °C ont montré une activité antibactérienne importante contre toutes les souches bactériennes testées avec des valeurs respectives de CMI de 3.125 et 125. 000 µg/mL. L'effet bactéricide des nanoparticules d'argent synthétisées à partir de l'extrait aqueux de feuilles à 25 °C était particulièrement élevé contre *Streptococcus pneumoniae* et *Haemophilus influenzae*. Les valeurs des CI<sub>50</sub> ont varié de 0.006 à 93.730 µg/mL. Les valeurs des CI<sub>50</sub> des nanoparticules étaient plus importante que celles des extraits. Cependant, les extraits méthanoliques des écorces de tige et de racines ont été les plus actifs avec des CI<sub>50</sub> de 19.73, et de 2.730 µg / mL respectivement sur les cellules MCF-7. Les nanoparticules d'argent stables étaient les plus prometteuses sur les trois cellules testées avec des valeurs de CI<sub>50</sub> de 0.006 et de 0.008 µg/ml sur la cellule HepG2. De plus, les nanoparticules d'or de l'extrait aqueux des racines à 25 °C ont également montré une bonne activité avec des valeurs CI<sub>50</sub> de 0.18 et de 6.56 µg/mL sur les cellules HepG2 et MCF-7. Les extraits bioactifs et les nanoparticules d'or n'ont montré aucun effet significatif sur la cellule normale KMST-6. Les résultats Annexin ont confirmé la réduction de plus de 50 % de cellules viables après traitement avec les extraits et les nanoparticules actives. Les pourcentages apoptotiques de 70.23 and 78.01 % ont été obtenus avec l'extrait méthanolique d'écorce de tige respectivement sur les lignées cellulaires Caco-2 et HepG2 cells. Les nanoparticules d'or provenant d'extrait méthanolique d'écorces de tige à 70 °C et les nanoparticules d'argent d'extrait aqueux de feuilles à 25 °C et, traités respectives avec les cellules Caco-2 et MCF-7 ont induit une production importante d'espèces réactives de l'oxygène respectives de 62.83 % et de 63.26 %. Les extraits et les nanoparticules d'argent bioactifs ont principalement provoqué l'arrêt du cycle cellulaire en phase G0/G1, tandis que les nanoparticules d'or bioactives ont également induit l'arrêt du cycle cellulaire en phase G2/M. Les résultats de cette étude ont mis en évidence la capacité de réductrice et potentielle des biomolécules présentes dans les extraits de *Terminalia mantaly* à produire des nanoparticules d'or et d'argent de petites tailles avec divers motifs structuraux et leurs capacités sélectives d'éradiquer les cellules cancéreuses via des mécanismes d'action tels que l'apoptose à

travers la fragmentation de l'ADN confirmant ainsi l'utilisation traditionnelle de la plante *Terminalia mantaly* pour la prévention, le traitement du cancer et les infections bactériennes associées.

**Mots-clés:** Nanotechnologie, Nanoparticules, *Terminalia mantaly*, Synthèse verte, Cancer, Prolifération, Apoptose, Cytométrie de flux.





# *Introduction*

## INTRODUCTION

Nanotechnology can be termed as the fabrication, characterization, exploration, and application of nanosized (1-100 nm) materials for the development of science that offers an infinite possibility of advancement and innovation in many fields including those in cancer therapeutics, medical imaging, and diagnostics (Adisheshaiah *et al.*, 2016; Ahmed *et al.*, 2017; Enayati *et al.*, 2018). Cancer is increasingly recognized as a critical public health problem and the leading cause of death globally with an estimated 18.1 million new cancer cases and 9.6 million cancer deaths worldwide in 2018 (Bray *et al.*, 2018; Siegel *et al.*, 2019). The different types of cancer that afflict humans are lung, brain, and breast, colorectal, cervical, and pancreatic cancer (Rajkumar *et al.* 2011). Colon cancer is the third most commonly diagnosed and estimated 1.36 million new cases (42 %) and 774,000 deaths every year all over the world (Siegel *et al.*, 2019). Breast cancer is the first most common cancer found in women and approximately 2.1 million cases are estimated in 2018. Liver cancer is the fifth most common cause of cancer death in men and it is the seventh most common cause of cancer death among women and estimated 31,780 deaths (Siegel *et al.*, 2019). In Africa, 715,000 new cases of cancer and 542,000 new deaths were recorded in a year (Parkin *et al.* 2008; Ferlay *et al.* 2015). The incidence and mortality of these cancers have been continuously rising in the central African country including Cameroon with an estimation of 3273 (20.8 %), 871 (5.5 %), and 955 (6.1 %) new cases of breast, colorectum, and liver cancer respectively in 2018 (Enow *et al.*, 2012; Stimpfel and Virant-Klun, 2016).

Cancer progression impairs the normal biological process of healthy cells which is achieved by the invasion of nearby tissues and metastasize to distant tissues. These genetic alterations can be induced by several risk factors including exposure to ionizing radiation, smoking, hormonal, dietary, lifestyle, infection, genetic factors as well as age, race, ethnicity, gender, and family history (Zhang *et al.*, 2018). However, infections are estimated to contribute to 20 % of all human tumours and it has been shown that in 2008 around 2 million cancer cases were caused by infectious agents globally, which was around 16.1 % of the total estimated cancer incidence of that year. (Van and Neefjes, 2018). Recently, infections with specific types of viruses and bacteria were established as risk factors for developing cancer in humans (Mansoori *et al.*, 2017). Chronic *Salmonella typhi* infections are linked to gallbladder carcinoma (Scanu *et al.*, 2015), and *Salmonella enteritidis* infections with colon carcinoma (Mughini *et al.*, 2018). It is speculated that pathogenic bacterias' toxin-mediated assault strategies may contribute to carcinogenesis (El-Serag, 2012; Mughini *et al.*, 2018).

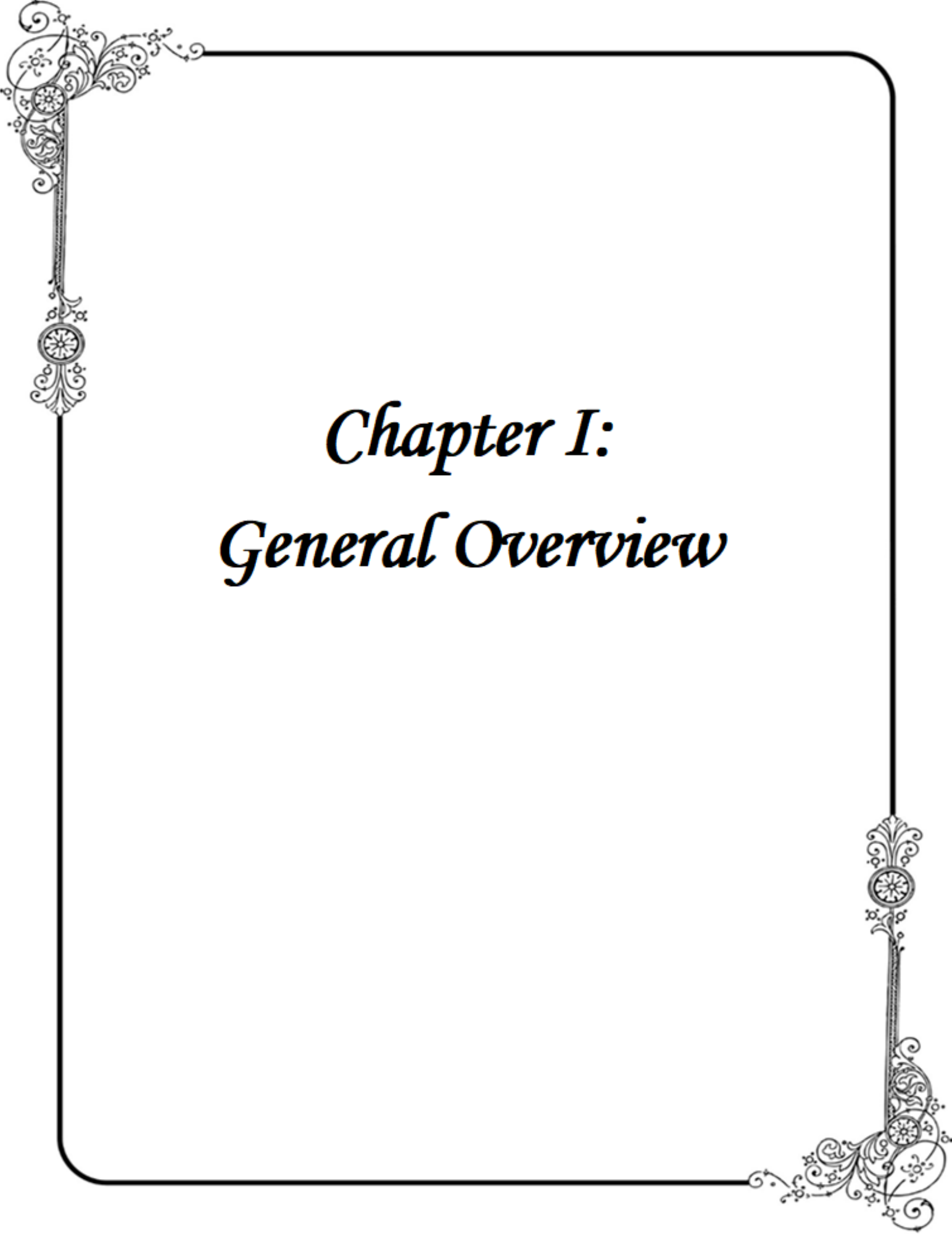
Today, despite these advances, the favoured option for cancer treatment is chemotherapy, and the overall mortality suggesting the contribution of research to the alleviation of the disease were minimal (**Zhou et al., 2016**). Current treatment regimens are no-specific and reduced efficacy as well as inadequate drug delivery at the site of the tumours and adversely implicate healthy tissues and organs causing adverse effects. These include appetite and nausea, cardiotoxicity, nephrotoxicity, ototoxicity, neurotoxicity, leading to the death of cancer patients (**Akindele et al. 2015; Kumari et al., 2016**).

These facts clearly evidence the need for advanced technology for cancer treatment (**Gmeiner and Ghosh, 2015**). Nanoparticle therapy were shown to be promising as alternatives for current treatment regimens, and are effective toward tackling the issue of the development of drug resistance and improving life quality (**Das et al., 2013; Loos et al., 2014; Cruz et al., 2019**). Moreover, the United States Food and Drug Administration (FDA)-approved materials may be selected as nano-scale drug carriers that were proven to be non-inflammatory and non-toxic while enabling the delivery of highly localized concentrations of both hydrophilic and hydrophobic agents (**Danhier et al., 2012**). Amongst nanomaterials, metal nanoparticles especially gold and silver have attracted a great deal of attention and the interest of the scientific community. This is due to their fascinating proprieties making them depend on sizes, shapes with excellent, and diversified resources for cancer therapy (**Mahmoudi et al., 2011, Gräfe et al., 2016, Suvarna et al., 2017; Khatoon et al., 2018**). A variety of physical and chemical protocols for the synthesis of different geometric shapes and sizes of AgNPs and AuNPs are reported (**Elbagory et al. 2016; Aljabali et al., 2018, Assadi et al., 2018**). However, most of the protocols involve the use of toxic chemicals as reducing and capping agents which are likely to produce toxic byproducts. The green synthesis of nanomaterials has generated great interest as it produces simple, cost-effective, readily scalable, and eco-friendly products with minimal toxicity towards human beings. (**Singh et al., 2015**). The natural products are used extensively as reducing and capping agents to prevent agglomeration and increase the stability of the synthesized NPs (**Kharissova et al., 2013; Daniel et al., 2014; Makarov et al., 2014; Rajan et al., 2015**). Biogenic nanoparticles are suggested to induce their toxicity through oxidative stress by generating reactive oxygen species (ROS) involved in a variety of different cellular processes ranging from apoptosis and necrosis to cell proliferation and carcinogenesis (**Al-Sheddi et al., 2018**). Apoptosis is a biological cell-active death process, and it is an important mechanism that the multicellular organism's body regulates and maintains homeostasis. The study conducted by **Ashokkumar et al. (2014)** on the biosynthesis of AuNPs using the seed coat of *Cajanus cajan* showed that spherical shapes of

AuNPs having the size of 9 to 41 nm in diameter induced the HepG2 cell apoptosis. Apoptosis can be triggered by increased intracellular ROS levels, which are also strong evidence involved in the induction of apoptosis (Li *et al.*, 2014). Importantly, the ROS leads to the activation of caspase-3 which is responsible for cell apoptosis by arresting the cell cycle at the G2/M phase (Rai *et al.*, 2016).

The extracts from *Terminalia* species (Combretaceae) such as *Terminalia catappa*, *Terminalia bellerica*, *Terminalia bentazoe*, *Terminalia mellueri*, *Terminalia arjuna*, and *Terminalia cheduba* are widely used by traditional healers to treat diseases such as cancer, dysentery, diabetes, mycosis, malaria, and bacterial infections. (Therese *et al.*, 2006; El-Rafie *et al.*, 2014, Mbouna *et al.*, 2018). The synthesis of silver and gold NPs from *Terminalia* species are reported. Higher stable gold nanoparticles (10-35 nm) were produced using leaf extracts of *Terminalia catappa* (TC) (Ankamwar, 2010; Zakir *et al.*, 2014). Edison and Sethuraman. (2012) used an aqueous extract of *Terminalia chebula* to produce gold nanoparticles with sizes ranging from 6 nm to 60 nm. Bupesh *et al.* (2016) showed the anticancer activity of AgNPs nanoparticles from *Terminalia cheduba* against colon cancer cells (HT-29). Thus the current study aimed to carry out the green synthesis and characterization of gold and silver nanoparticles from *Terminalia mantaly* (Combretaceae) and investigate their potentials effect on bacteria and cancer cells. It is in light of this background that the study was designed specifically to perform:

- ✚ The green synthesis and characterization of gold and silver nanoparticles using the aqueous and methanolic extracts from *Terminalia mantaly* plant;
- ✚ The *in vitro* antibacterial screening: MIC determination and the growth-inhibitory kinetics of the bio-active crude extracts, gold and silver nanoparticles;
- ✚ The potential antiproliferative effect of extracts, more stable gold and silver nanoparticles against a panel of four cells line, and study of the mode of cell death.



*Chapter I:*  
*General Overview*



## CHAPTER I: LITTERATURE REVIEW

### I.1 Nano

The term “NPs” is used to describe particles with a small size of less than 100 nm. One nanometer (nm) is equal to one billionth of a meter ( $1 \text{ nm} = 10^{-9} \text{ m}$ ) at least for one dimension. These particles are made in a nanometer-scale for manipulation of physical, chemical, or biologic processes, and therefore regarded as nanoparticles and were already present in ancient objects such as Lycurgus Cup, with similar features to currently engineered nanostructures, so-called nanoarchaeology (**Bobrovnikova-Marjon, 2014**). Gold and silver colloids were used by Romans were for colouring purposes in ceramics (**Figure 1**).



**Figure 1:** Lycurgus Cup courtesy of the British Museum. The light source is (A) in the cup or (B) outside the cup. Black circles indicate the positions of extracted colours (**Bobrovnikova-Marjon, 2014**).

#### I.1.1. Classification Of Nanomaterials

Nanomaterials can be classified into different types according to the size, morphology, physical and chemical properties (**Figure 2**). Some of them are carbon-based nanoparticles, ceramic nanoparticles, metal nanoparticles, semiconductor nanoparticles, polymeric nanoparticles, and lipid-based nanoparticles (**Buzea et al., 2007; Jeevanandam et al., 2018; Khan et al., 2019**).

### **I.1.1.1 Carbon-Based Nanoparticles**

Carbon-based nanoparticles include two main materials: carbon nanotubes (CNTs) and fullerenes. CNTs can be classified into single-walled carbon nanotubes (SWCNTs) and multi-walled carbon nanotubes (MWCNTs). Fullerenes are the allotropes of carbon having a structure of a hollow cage of sixty or more carbon atoms (Jeevanandam *et al.*, 2018).

### **I.1.1.2 Ceramic Nanoparticles**

Ceramic nanoparticles are inorganic solids made up of oxides, carbides, carbonates, and phosphates. They have applications in photocatalysis, photodegradation of dyes, drug delivery, and imaging. These nanoparticles were used effectively as a drug delivery system for some bacterial infections, glaucoma, cancer, etc.

### **I.1.1.3 Semiconductor Nanoparticles**

The Semiconductor nanoparticles are found in the periodic table in groups II-VI, III-V, or IV-VI. These particles were bandgaps, which on tuning show different properties, metals, and non-metals. Semiconductor nanoparticles are GaN, GaP, InP, InAs from group III-V, ZnO, ZnS, CdS, CdSe, CdTe are II-VI semiconductors and silicon and germanium are from group IV.

### **I.1.1.4 Polymeric Nanoparticles**

A nanosphere particle has a matrix-like structure whereas the nanocapsules particle has core-shell morphology. Polymeric nanoparticles are organic-based nanoparticles. The drug deliveries with polymeric nanoparticles are highly biodegradable and biocompatible (Buzea *et al.*, 2007; Jeevanandam *et al.*, 2018).

### **I.1.1.5 Lipid-Based Nanoparticles**

Lipid nanoparticles are generally spherical with a diameter ranging from 10 to 100 nm. The external core of these nanoparticles is stabilized by surfactants and emulsifiers. These nanoparticles have many applications in the biomedical field as a drug carrier and delivery and RNA release in cancer therapy.

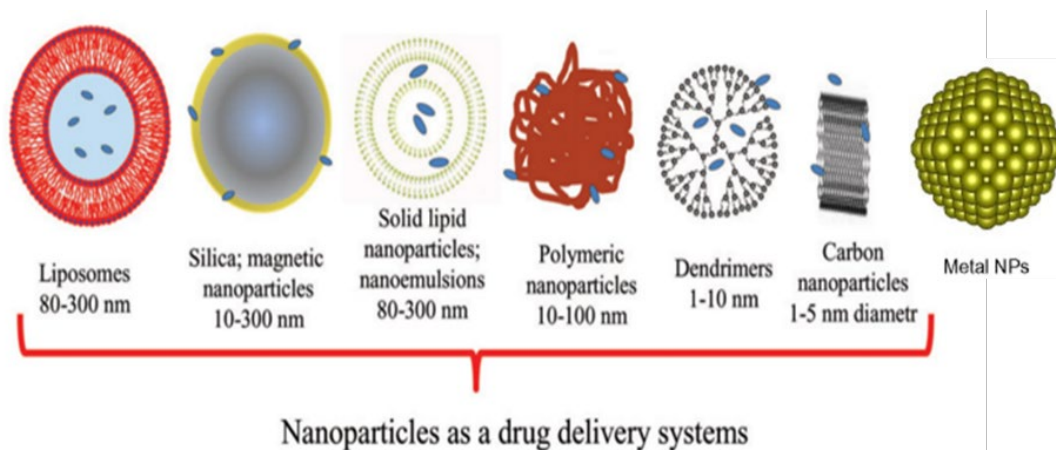


**Figure 2:** Basic structure of inorganic nanoparticles figure reprinted with permission from Elsevier. (Xing *et al.*, 2014).

### I.1.1.6 Metal Nanoparticles

Metal nanoparticles are prepared from metal precursors. These nanoparticles can be synthesized by chemical, electrochemical, or photochemical methods (Jeevanandam *et al.*, 2018). These days, metal nanoparticles (Figure 3) have attracted a great scientific interest due to their unique optoelectronic and physicochemical properties, and particularly Ag, Au, Pd, and Pt are most effectively studied. These properties strongly depend on size, shape, crystallinity, and structure. (Castro *et al.*, 2014).

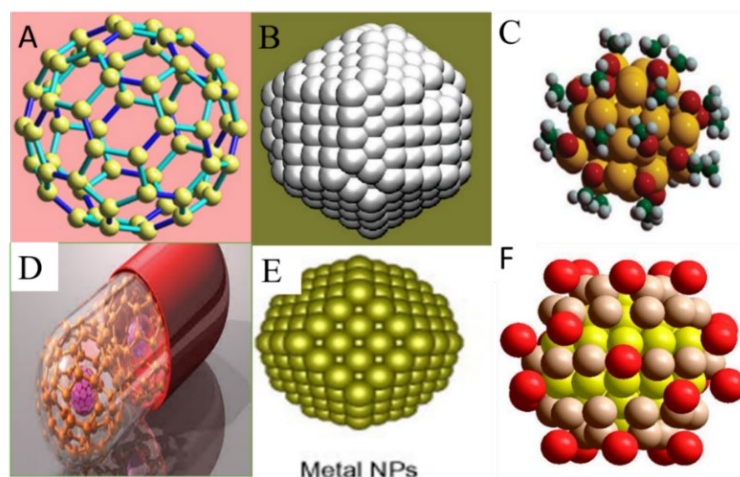


**Figure 3:** Structure and energetics of gold and silver nanoparticles (Wang *et al.*, 2011).

Note: A=Bulky ball, B, C, and E=metallic nanoparticles; D= metallic nanoparticles as drugs delivery systems (Figure reprinted with permission from Elsevier).

Moreover, the metallic nanomaterials especially gold and silver nanoparticles exhibit wholly innovative and improved characteristics compared to the voluminous particles of the bulk

materials with specific characteristics, such as high surface area, high reactivity unique size distribution, and required morphology (Siddiqui *et al.*, 2015; Sekhar *et al.*, 2018). Despite several advantages of a biological synthesis approach for nanoparticles, the polydispersity, stability of the nanoparticles formed remains a challenge. (Hansen *et al.* 2007).

### I.1.1.6.1 Gold (AuNPs) Nanoparticles

(AuNPs) are a focus of intense scientific research owing to their fascinating chemical, electronic, and optical properties and potential applications in biomedicine, sensing, and catalysis owing to its shape, size, and crystal structures arrangement (Leonard *et al.*, 2011). Their synthesis is based on the method developed by Turkevich in 1985 through reduction (Figure 4) of gold aurate by citrate (KimLing *et al.*, 2006). The chemical synthesis of gold nanoparticles has been reported to exhibit a red wine, dark purple colour (Figure 4) in the aqueous solution that is related to their intensity and size owing to its SPR (Mulvaney, 1996). The AuNPs can be stabilized by the addition of proteins such as bovine serum albumin (BSA) on their surface and can be used to attach targeting peptides and prevent their aggregation and precipitation that occurs at their isoelectric point (Liu and Franzen, 2008). AuNPs are a promising candidate for biomedical engineering and drug delivery applications owing to their unique dimensions, nontoxicity, surface functionalities, and capacity for controlled drug release (Datar and Richard, 2010).

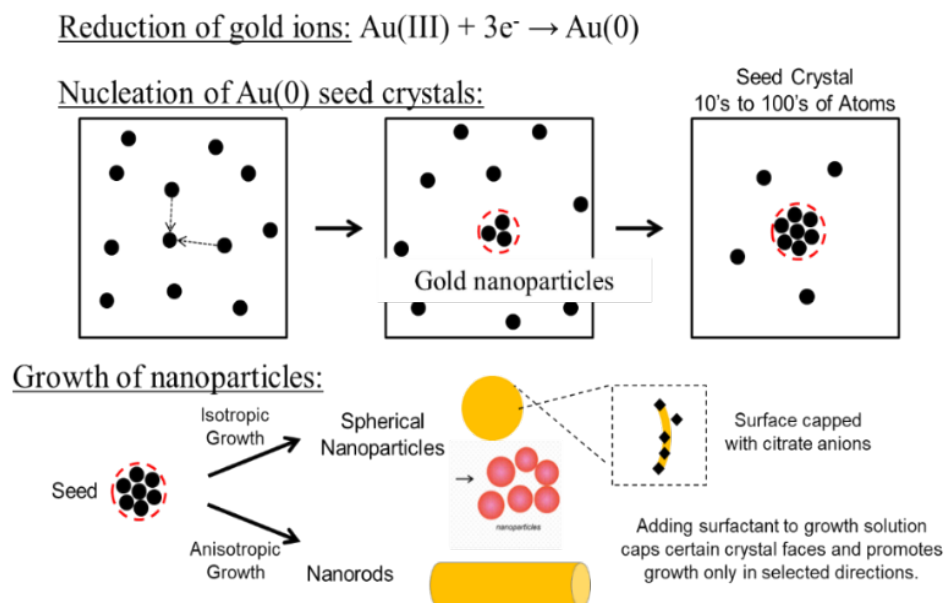


**Figure 4:** Schematic illustration for the deduced process of gold nanoparticles formation. Reduction and nucleation (Polte *et al.*, 2010).

### I.1.1.6.2 Silver (AgNPs) Nanoparticles

AgNPs are one of the most attractive inorganic materials because of their environment free nature (Britto and Sebastian, 2011). Indeed, Silver ions ( $\text{Ag}^+$ ) were subjected to chemical reduction to form silver atoms ( $\text{Ag}^0$ ) (Figure 5). These atoms undergo nucleation to form primary AgNPs that further coalesce with each other to form final AgNPs. Silver nanoparticles formation displays a yellowish to the brown colour in aqueous solution (Figure 5). The importance of silver nanoparticles has played a pivotal role in inhibiting various infectious diseases caused by microbes and helping in the burn wounds healing process, by preventing the infections in the wounds. Furthermore, silver nanoparticles are also known for their anti-inflammatory and antiviral activity (Haider and Kang, 2015).

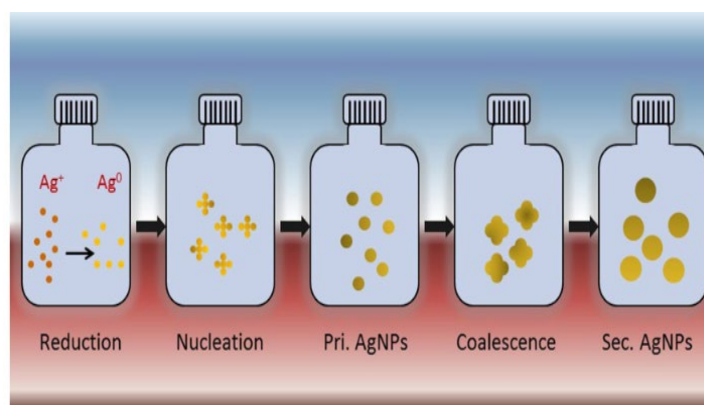


**Figure 5:** Schematic representation of the synthesis of colloidal silver nanoparticles using the chemical reduction process (Salazar *et al.*, 2018).

### I.1.2 Physical And Chemical Synthesis Methods Of Metallic Nanoparticles

The synthesis of NPs is a milestone in nanotechnology. The two different approaches to nanotechnology are graphically termed “top-down and bottom-up” (Kotnala *et al.*, 2015). Whereas “bottom-up” or molecular nanotechnology (figure 6), applies to build organic and inorganic structures atom-by-atom, or molecule-by-molecule (Meyers *et al.*, 2006). Several physical and chemical approaches are explored for the synthesis and stabilization of nanoparticles (Chen *et al.*, 2010). The physical method involves laser ablation and evaporation condensation methods (Jung *et al.*, 2006) whereas chemical methods utilize chemical reductants (citrate,

NaBH<sub>4</sub>, ethylene glycol, etc.), technique and multiple purifications, use of explosive solvents, high consumption for processes such as sonication, high-priced equipment and harmful effects of by-products formed during the process. However, these chemical methods deliver at the cost of expensive reducing and capping agents and toxic solvents along with tedious process control (**Kumar, 2012**).

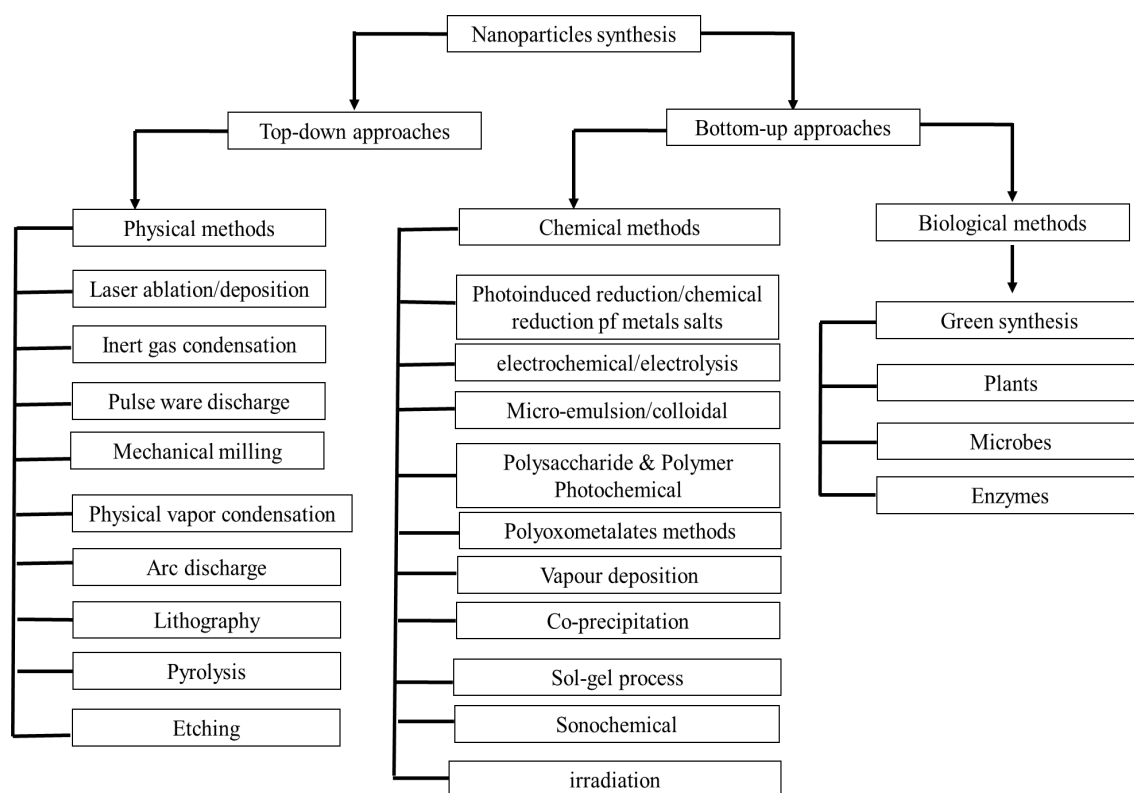


**Figure 6:** Schematic representation of different methods of metallic nanoparticles (AuNPs and AgNPs) synthesis (Krishnaswamy, 2015).

### I.1.2.1 Nanoparticle Characterization Techniques

The characterization of nanoparticles is an important process in understanding the reaction mechanisms and subsequent applications. The microscopy-based techniques such as atomic force microscopy (AFM), transmission electron microscopy (TEM), scanning electron microscopy (SEM), Energy Filtered Transmission Electron Microscopy (EFTEM), are considered direct methods of obtaining data from images taken of the nanoparticles. In particular, both SEM and TEM described here have been extensively used to determine the size and morphological features of nanoparticles (Poinern, 2014). Spectroscopy based techniques such as UV-vis, dynamic light scattering (DLS), powder X-ray diffraction (XRD), energy dispersive spectroscopy (EDS), Selection Area Electron Diffraction (SAED), Fourier transform infrared spectroscopy (FTIR), and, X-Ray photoelectron spectroscopy (XPS), Mossbauer spectroscopy, Thermo gravimetric analysis(TGA), SQUID/FC-ZFC, IR-/Raman are considered indirect methods of determining data related to composition, structure, crystal phase, and properties of nanoparticles (Pérez *et al.*, 2014; Cayado *et al.*, 2015)

### I.1.2.1.1 UV-visible Spectroscopy Analysis

This technique is based on the light absorption or reflectance spectroscopy in the ultraviolet-visible electromagnetic spectral regions in which molecules and other chemical compounds undergo electronic transitions. The principle of localized surface plasmon resonance (LSPR) states that when light interacts with conductive nanoparticles (i.e., AgNPs and AuNPs) which are smaller than the incident wavelength, the resultant electric field excites electrons and generates plasmon oscillations which are dependent on the composition, size, geometry, dielectric environment, and separation distance of NPs (Salazar *et al.*, 2018). For silver and gold nanoparticles, the resonance frequency of this SPR is strongly dependent on different proprieties of nanoparticles such as their sizes, shapes, inter particles interaction, dielectric properties, and the local environment. The absorption affects the identification of colour in the visible range (Sharma *et al.*, 2019). Wavelengths between 300 and 800 nm are generally used for characterizing metallic nanoparticles ranging in size from 2 nm up to around 100 nm (Poinern, 2014). The absorption measurements of silver (Ag) nanoparticles are usually between 400 and 450 nm (Devika *et al.*, 2013; Poinern *et al.*, 2013), while gold nanoparticles have strong absorption in the visible region with the maximum in the range of 500–600 nm (Figure 7) due to the SPR phenomenon (Mishra *et al.*, 2012; Kelly *et al.*, 2003). This is attributed to the collective oscillation of free conduction electrons induced by an interacting electromagnetic field with the concerned metallic nanoparticles. The appearance of extract colour in red, purple, violet, or pink-ruby red due to excitation of SPR vibration in the above-mentioned wavelength confirms the production of gold nanoparticles. The appearance of extract colour in yellowish, brown, and dark brown is related to the formation of silver nanoparticles.



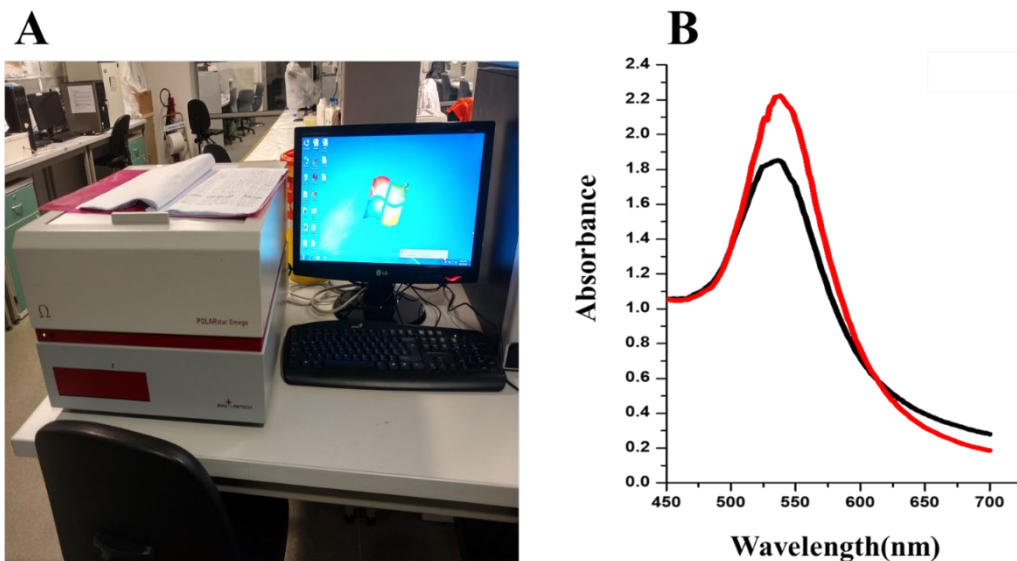


**Figure 7:** UV-visible Spectroscopy Analysis. (A): UV-Visible Instruments, (B): Surface Plasmon Resonance of gold nanoparticle (Photographed by Majoumouo, 2017).

### I.1.2.1.2 Dynamic Light Scattering Analysis

The size distribution, charge, surface chemistry of NPs are particularly important since they strongly influence the mobility and bioavailability of NPs within physiological conditions; and can be used to predict their state in solution (Pavlin and Vladimir, 2012). Dynamic light scattering (DLS) spectroscopy can be used to measure the hydrodynamic diameter, quantify the surface charge of nanoparticles suspended in a liquid (zeta potential), and polydispersity index (Pdi) of the surface charge of nanoparticles suspended in a liquid (Poinern, 2014).

#### I.1.2.1.2.1 Hydrodynamic Diameter Of Nanoparticles

The DLS instrument measures the size distribution by intensity. It is important to note that the size obtained corresponds to the size of the sphere that diffuses the same way as the particle measured. The calculated size is thus a hydrodynamic diameter which for AuNPs or AgNPs corresponds to the size of the core plus the size of the corona (Figure 8). Another limitation is that the method considers a so-called solvation layer around the particle to be a part of it. A solvation layer is a shell around a suspended particle, consisting of the molecules of the solvent. (Berne and Pecora, 2000).

#### I.1.2.1.2.2 Zeta Potential Parameters

Zeta Potential analysis is a technique for determining the surface charge of nanoparticles in solution (colloids). Nanoparticles have a surface charge that attracts a thin layer of ions of

opposite charge to the nanoparticle surface. **(Figure 8)**. Dispersions with a low zeta potential value will eventually aggregate due to Van Der Waal inter-particle attraction **(Clayton *et al.*, 2016)**. The NPs with a Zeta potential of within  $\pm 30$  range are more stable in solution **(Cooper, 2015)**, values may be positive or negative and within this range favor good quality and stable NPs which can be stored for a longer period in suspension. The TM-AuNPs had Zeta potential values that ranged from  $-10$  to  $-37$  mV. This indicates that the NPs repel each other and there is no tendency for them to aggregate as they provide the necessary repulsive forces to remain stable when in solution **(Grabinski, 2015)**. Zeta potential strongly depends on the pH of the solution. For instance, at a fixed temperature ( $25$  °C) at pH 6, zeta potential is  $9.62$  mV that exhibits poor quality, unstable gold nanoparticles. At pH 7 zeta potential value is  $25.7$  mV, whereas at pH 10 zeta potential value is  $-32$  mV, which exhibits good quality and comparatively better stability of gold nanoparticles **(Tripathi *et al.*, 2016)**.

#### **I.1.2.1.2.3 Polydispersity Index (Pdi) Parameters**

The polydispersity index is essential in nanoparticle applications, as it is difficult to control the sample's uniformity with surface conjugation chemistry, and often aggregation of the NPs can occur. Pdi describes the uniformity of the sample. The higher the index, the less uniform the sample is. In general, samples with Pdi below  $0.5$  are considered monodisperse and vice versa, samples with pdi above  $0.5$  are referred to as polydisperse. According to the International Organization for Standardization (ISO), Pdi values  $> 0.5$  indicate that the samples with the size distribution, while Pdi values  $= 0.5$  are more monodispersive **(Elbagory *et al.*, 2019)**.

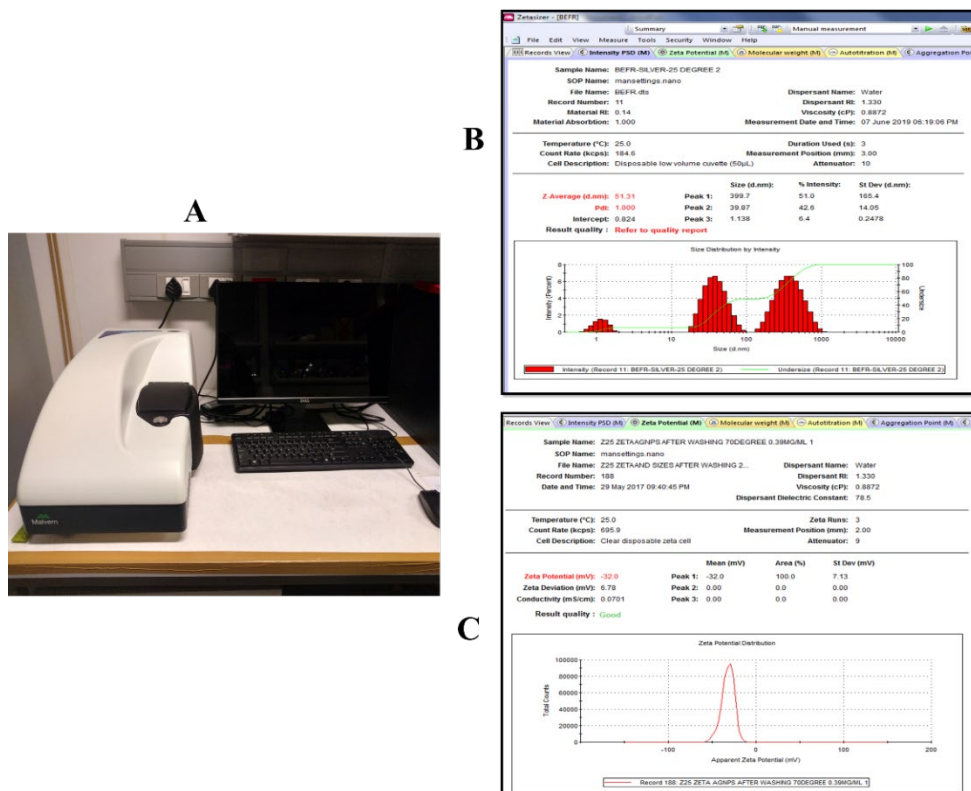


**Figure 8:** Dynamic Light Scattering Analysis. (A): Zetasizer Malvern Instruments, (B): Z-Average size distribution, (C): Zeta potential (Photographed by Majoumou, 2017).

### I.1.2.1.3 Transmission Electron Microscope Analysis

The transmission Electron Microscope (TEM) is one of the most important tools of nanotechnology for imaging nanomaterials with sub-nanometer resolution (High-Resolution TEM) that study some proprieties of nanoparticles such shapes, sizes and which operates on the same basic principles as the light microscope but uses electrons instead of light (Egerton, 2005). In these techniques, a thin specimen is imaged by an electron beam, which is irritated through the sample at uniform current density (Reimer, 1989). Figure 9 illustrates the different kinds of nanoparticle shapes.

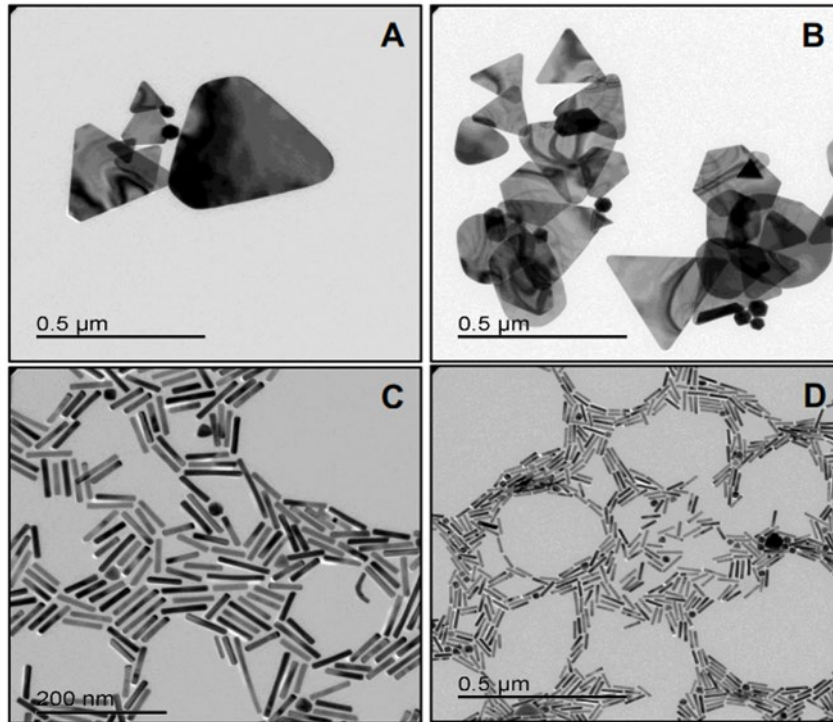


**Figure 9:** TEM images of gold nanoprisms (A, B) and nanorods (C, D) obtained at 20-200 KeV (Patel, 2017).

HRTEM is also used to differentiate microanalysis techniques including selected area electron diffraction (SAED), and X-ray energy dispersive spectrometer (EDX) (Tripathi *et al.*, 2016).

- ✚ Selected area electron diffraction, abbreviated as SAED is used primarily in material science and solids state physics, and, in combination with TEM is one of the most commonly used experimental techniques in those fields (Figure 10). Indeed, SAED is a crystallographic experimental technique that can be implemented with a TEM to identify crystalline phases and examine crystal defects (Reimer, 1989).
- ✚ The energy dispersive spectrum that aims to identify the elemental compositions in the synthesized nanoparticles is a method that records the energy and intensity distribution of x-rays generated by the impact of the electron beams on the surface of the samples (Hawkes, 2006).

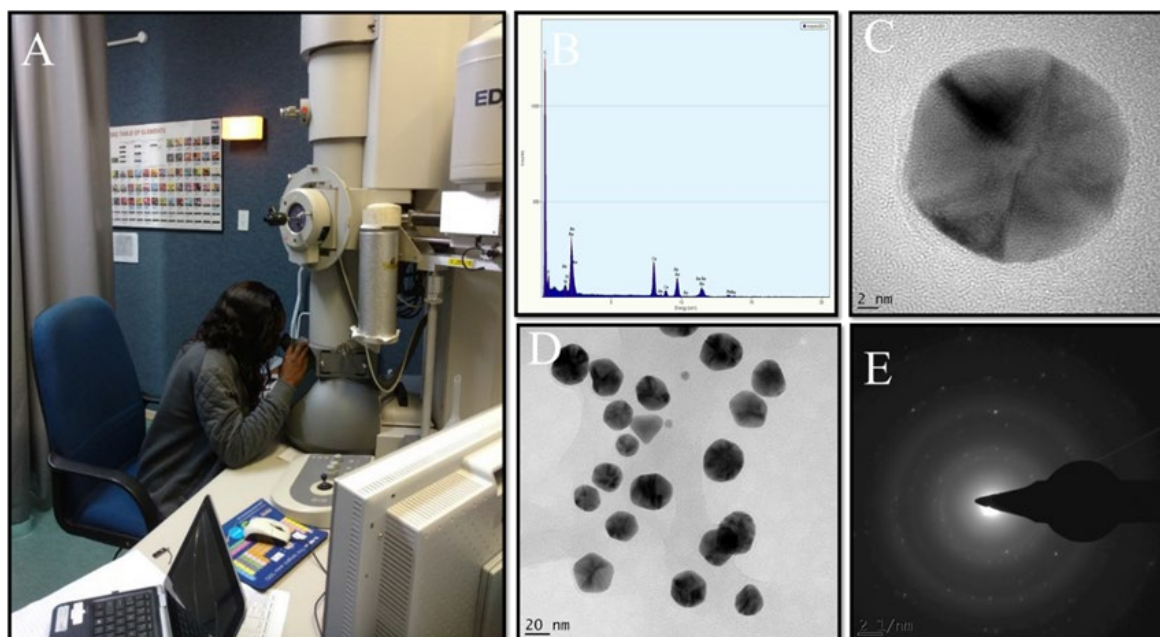


**Figure 10:** Microanalysis HRTEM techniques of gold nanoparticles: (A): HRTEM microscope instrument; (B): X-ray energy dispersive spectra; (C): gold facet, (D): Spherical shapes; (E): Selected Area electron diffraction pattern with crystalline effect (Photographed by **Majoumouo, 2017**).

#### **I.1.2.1.4 Fourier Transform Infrared Spectroscopy Analysis**

The FTIR spectroscopy is used to investigate surface chemistry and identify surface residues such as functional groups like carbonyls and hydroxyls moieties that attach to the surface during nanoparticle synthesis (**Poinern, 2014**). Each chemical bond exhibits a natural vibration frequency when absorbing light and thus shows a characteristic peak on the absorbance spectrum. Base on wavenumber, infrared light can be considered as far-infrared ( $4\text{--}400\text{ cm}^{-1}$ ), mid-infrared ( $400\text{--}4000\text{ cm}^{-1}$ ), and near-infrared ( $4000\text{--}14,000\text{ cm}^{-1}$ ). Several studies compared the FTIR spectrum during the fabrication of gold and silver nanoparticles and produced information about reducing and capping agents such as proteins, polysaccharides, flavonoids, terpenoids, and phenols.

#### **I.1.2.2 Limitations of Physical And Chemical Synthesis Methods**

The chemical and physical synthesis methods of nanoparticles are not only eco-friendly but also cost-effective and can be easily modified for large-scale synthesis (**Geethalakshmi and Sarada, 2012**). Although in the chemical synthesis of NPs, the generation of hazardous by-products is produced highlighted as environmental contaminants. Certain chemicals are expensive and may lead to the presence of noxious chemical species tangled on the surface of NPs, which may have detrimental effects on the environment (**Mittal *et al.*, 2014**). The toxicity represents the most critical and fundamental problem associated with the use of gold and

silver nanoparticles or any other nanoparticles from the chemical process in human disease treatment. **Wan *et al.* (2015)** reported that CTAB-coated gold nanorods (CTAB-AuNPs) are toxic to both tumours and non-malignant transformed cells at nanomolar concentrations. CTAB-AuNPs aggregate on the cell membrane and cause damage to the membrane (**Vijayakumar *et al.*, 2012**). CTAB-AuNPs also increased lysosomal membrane permeation and decreased mitochondrial membrane potential, which subsequently induced cell death (**Freese *et al.*, 2012**) demonstrated that the higher amount of citrate on the surface of AuNPs increases cytotoxicity and decreases the proliferation rate of human dermal microvascular endothelial cells (HDMEC) and the human cerebral microvascular endothelial cell lines (hCMEC/D3). The citrate-stabilized AuNPs (citrate-AuNPs) increased cytotoxicity compared to starch- and gum arabic-stabilized AuNPs (**Vijayakumar *et al.*, 2012**). The AgNPs-induced toxicity depends on nanoparticle size, concentration, and duration of the treatment and to a large extent is associated with the generation of ROS, free radicals, and consequently build-up of oxidative stress (**Figure 11**) (**Ahamed *et al.*, 2010**).

Considering all the above demerits of physical and chemical methods of NPs synthesis, there was a need to find new favorable techniques. Biological synthesis of nanoparticles using plant extracts, plant products, bacteria, yeast, and fungi suggested a valuable alternative tool toward traditional chemical synthesis methods with lower toxicity (**Murawala *et al.*, 2009**; **Wang *et al.*, 2009**).

### **I.1.3 Green Synthesis Methods**

Nanotechnology is currently a flourishing field providing a novel way to fabricate nanoparticles from biological sources. Also, the biological synthesis of nanoparticles using green technology is, nontoxic and provides a cost-effective, simple, and safe approach to synthesize nanoparticles (**Patra and Baek, 2015**). Green nanotechnology involves objectives of several goals:

- ✚ Advancing the development of clean technologies that use nanotechnology;
- ✚ Minimizing potential environmental and human health risks associated with the manufacturing and use of nanotechnology products and encouraging the replacement of existing products with new nanoproducts that are more environmentally friendly (**Castro *et al.*, 2014**).



In a green synthesis of nanoparticles, three important rules of green chemistry should be considered: (i) choice of the green solvents used in the synthesis, ii) choice of an eco-friendly benign reducing agent, and (iii) choice of a nontoxic material as a stabilizer (Salata, 2004).

The biological molecules undergo highly controlled assembly for making them suitable for metal nanoparticle synthesis which was found to be reliable and eco-friendly (Rajoriya *et al.*, 2017). NPs are obtained from bacteria, fungi, algae, and plants, Kalishwaralal & co-workers synthesized gold nanocubes, ranging from 10 to 100 nm, from the bacterium *Bacillus licheniformis* after incubation with gold salt for 48 h (Kalishwaralal *et al.*, 2009). Shankar *et al.* (2003) synthesized spherical AuNPs from an endophytic fungus (*Colletotrichum* sp.) after 96 hrs of incubation. The use of plants is more attractive, compared to the other biological systems, as they are readily available, safer, and contain a wide variety of reducing phytochemicals. The microbial-derived and the plant-derived phytochemicals require shorter incubation periods with gold salt to synthesize AuNPs (Nath and Banerjee, 2013). The plants provide a better platform for nanoparticles synthesis as they are free from toxic chemicals and provide natural capping agents.

### **I.1.3.1 Nanoparticles Plant Extracts**

It is known that plants with the potential to hyper-accumulate and biologically reduce metallic ions. Amongst several biological methods of nanoparticle synthesis, natural plant extracts are used extensively as reducing agents as well as capping agents to inhibit the agglomeration and stability of the synthesized nanoparticles (Kharissova *et al.*, 2013; Malarkodi *et al.*, 2014; Sekhar *et al.*, 2018).

Plant extracts, which are rich in bioactive compounds such as aroma, latex, flavonoids, phenols, alcohols, and proteins can produce NPs from the silver or gold salts. The mechanism of biosynthesis of nanoparticles in plants may be associated with the phytoremediation concept in plants (Shah *et al.*, 2011).

#### **I.1.3.1.1 Advantages of Green Synthesis Of Nanoparticles Using Plant Extracts**

Nanoparticles synthesized using plant extract as biological sources, possess distinct physicochemical properties, such as broad optical properties, low-cost nano synthesis, surface functionalization, and high surface-to-volume ratio which offered a novel opportunity in cancer treatment (Figure 12) (Mittal *et al.*, 2013; Khatami *et al.*, 2015; Singh *et al.*, 2015). Moreover, utilizing plant extracts as reducing agents in synthesizing gold and silver nanoparticles

due to its simplicity, large-scale production, decreased production time and cost were under a great deal of interest as reported in **Makarov. (2014)**. Green nanoparticles advantage of possessing enhanced biological activities for human medical applications due to the availability of active functional groups at the nanoparticle surface is exploited for the attachment of various biological molecules.

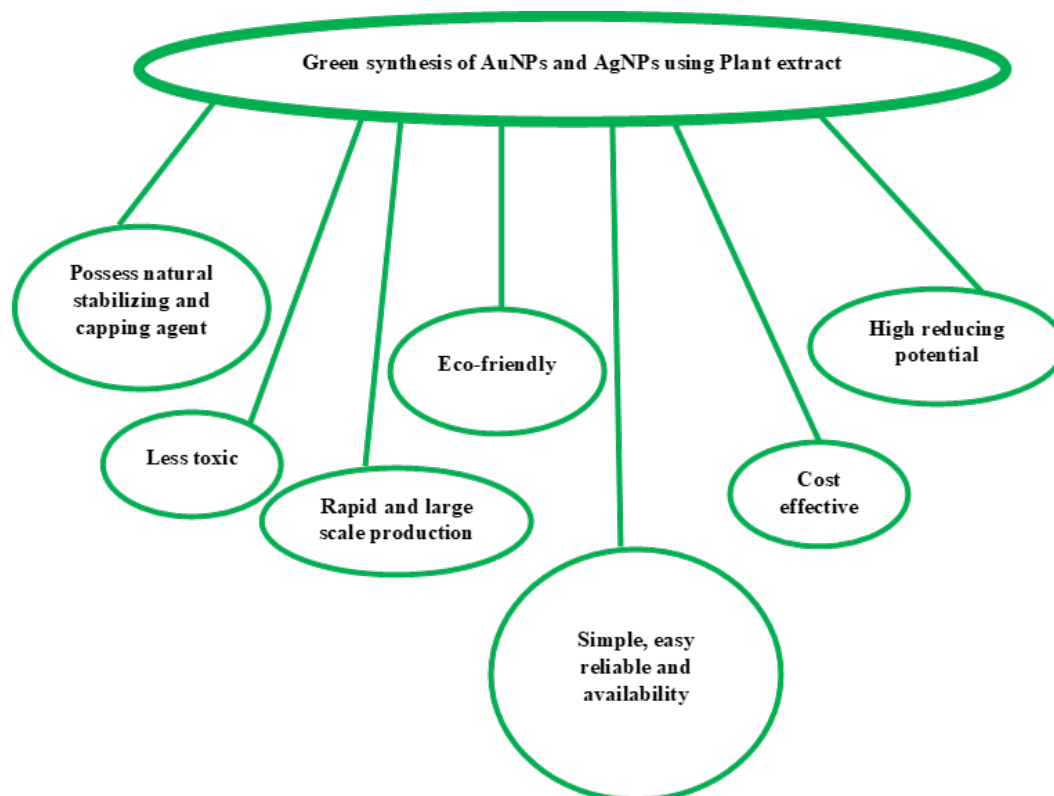


**Figure 11:** Advantages of green synthesis of AuNPs and AgNPs by plant extracts (**Majoumouo 2019**).

### **I.1.3.2 Critical Biophysical Parameters Affecting Biological Synthesis Of Gold And Silver Nanoparticles**

These factors controlling the biological synthesis of metallic nanoparticles, subsequent formation of stabilized nanoparticles include pH, reactant concentrations, reaction time, and temperature (**Figure 13**).

#### **I.1.3.2.1 pH**

The pH value of the reaction medium plays a significant role during the formation of nanoparticles (**Gardea-Torresdey *et al.*, 2010**). The pH variation of the reaction medium tends to produce variability in the shape and size of nanoparticles synthesized. In particular, larger particles tend to be produced at a lower acidic pH value compared to high pH values



(Sathishkumar *et al.*, 2009; Dubey *et al.*, 2010). The rod-shaped AuNPs nanoparticles synthesized using *Avena sativa* (Oat) biomass were larger (25 to 85 nm) when formed at pH 2 and relatively smaller (5 to 20 nm) at pH 3 (Armendariz *et al.*, 2004). At pH 2 fewer functional groups were available and resulted in particle aggregation to form larger AuNPs. In a similar study, AgNPs were synthesized using *Cinnamon zeylanicum* bark extract and the number of particles synthesized increased with increasing concentrations of bark extract and at higher pH values (pH 5 and above) the shape of the spherical nanoparticles (Sathishkumar *et al.*, 2009).

#### I.1.3.2.2 Reactant Concentration

A study by Huang *et al.* (2007) found that varying the amount of sundried *Cinnamomum camphora* (camphor) leaf extract in the reaction medium could significantly influence the shape of the synthesized AuNPs and AgNPs. Similarly, varying the amount of *Aloe vera* leaf extract in the reaction medium containing chloroaurate ions (Chandran *et al.*, 2006). Furthermore, decahedral, hexagonal, triangular, and spherical Ag nanoparticle shapes were produced by varying the concentration of *Plectranthus amboinicus* leaf extract in the reaction medium (Narayanan and Sakthivel, 2010).

#### I.1.3.2.3 Reaction Time

Ahmad and Sharma. (2012) revealed that the reaction time to synthesize spherical Ag nanoparticles using *Ananas comosus* (Pineapple) extract is an important factor. The reaction continued up to 5 min, but after that, only a slight colour variation could be observed. In a similar study by Dwivedi and Gopal. (2010) *Chenopodium album* leaf extract was used to produce AgNPs and AuNPs. Moreover, a study by Kumar *et al.* (2012) revealed that when *Azadirachta indica* leaf extract and AgNO<sub>3</sub> were combined, increasing the reaction time tended to produce particles with increasing size.

#### I.1.3.2.4 Temperature

Temperature is also an important factor in determining the size, shape, and yield of nanoparticles synthesized via plant extracts (Song *et al.*, 2009; Sathishkumar *et al.*, 2010). The synthesis of AgNPs at a reaction temperature of 25 °C via *Citrus sinensis* (sweet orange) peel extract produced particles with an average size of around 35 nm. However, as the reaction temperature increased to 60 °C the average particle size decreased to 10 nm (Kaviya *et al.*,

2011). *Diospyros kaki* (persimmon) leaf extract was able to synthesize stable AgNPs over a reaction temperature range from 25 to 95 °C. It was also found by Armendariz *et al.* (2004) that thermal variation in the reaction conditions for *Avena sativa* (oat) biomass resulted in changes in the size and shape of Au nanoparticles formed. Gericke and Pinches. (2006) showed that higher temperatures promote the higher formation rate for AuNPs. Nanoparticles reaction rate and particle formation rate appear to become faster when reaction temperature increases, however, the average particle size decreases with increasing temperature.

### I.1.3.2.5 Nature Of Extracts

The nature and source of plant extract influence the morphology of synthesized NPs (Mukunthan and Balaji, 2012).

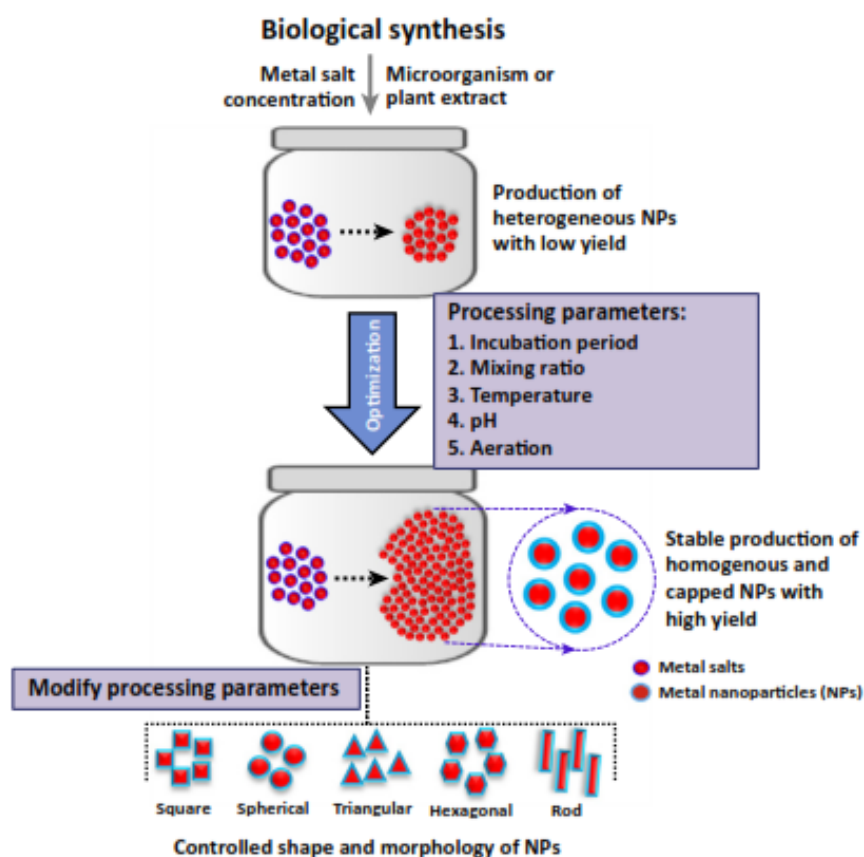


**Figure 12:** Critical biophysical parameters that can influence the production of monodisperse, stable, high-yield nanoparticles (Mukunthan and Balaji, 2012).

## I.2 Broad Applications Of Metallic Nanoparticles & Biologically Inspired Templates

Nowadays, the high impact that nanotechnology has on both science and society offers new research possibilities (Barabadi *et al.*, 2017). The green bionanomaterials involving inorganic metals NPs such as gold, and silver, prepared from different bio-sources (Figure 14), in particular, have received considerable interest in the fields of electronic components, photonics, medicine, and agriculture (Dreaden *et al.*, 2012; Yeh *et al.*, 2012; Elbagory *et al.*, 2016), medical diagnostic imaging (Youns *et al.*, 2011), pharmaceuticals products and phototherapy of cancer cells or tumours (Puvanakrishnan *et al.*, 2012). They also have technological applications including biomedical services, cosmetics as wound dressing, drug-gene delivery, environmental health, and in food (Liz-Marzan and Kaman, 2003; Kannan *et al.*, 2014).

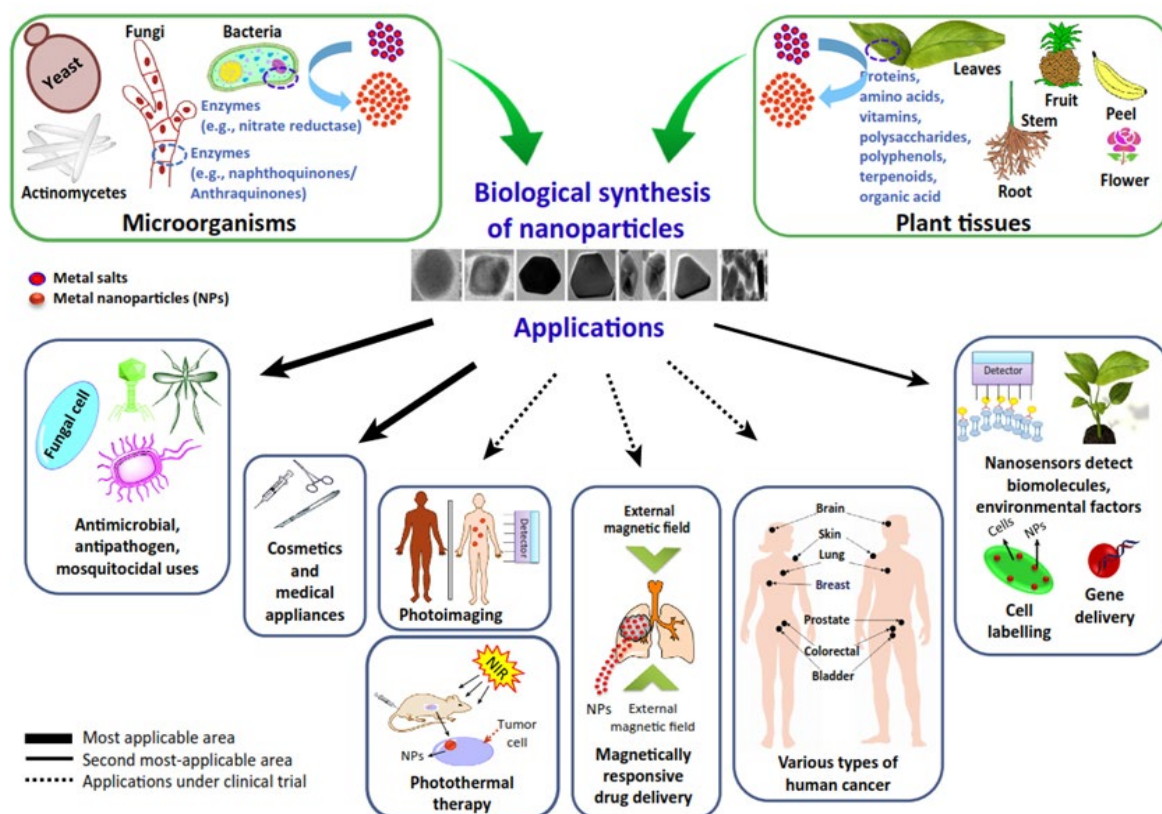
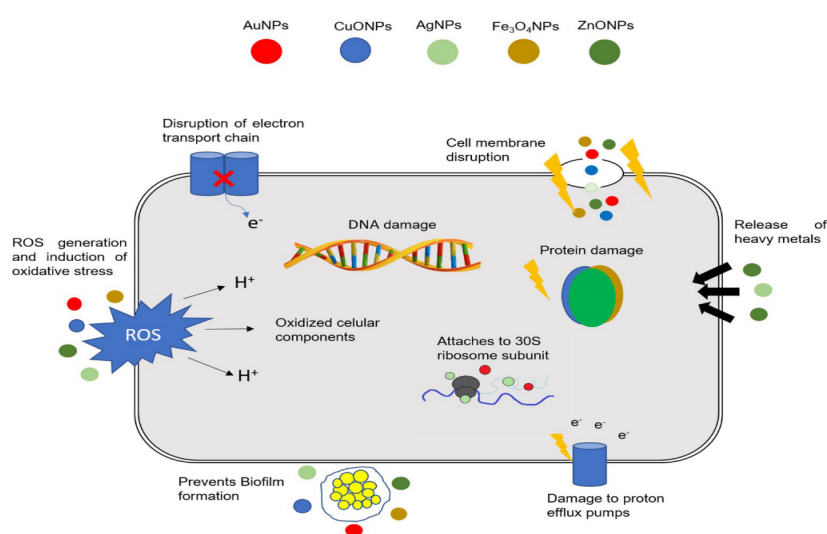


Figure 13: General applications of nanoparticles Adapted with permission from Singh *et al.* (2016).

## I.2.1 Biological And Medical Application Of Silver Nanoparticles

Silver nanoparticles have inherent antimicrobial activity and are already used as an antimicrobial agent in a wide range of commercially available medical and consumer products (Panaček *et al.*, 2006; Pollini *et al.*, 2012) and antimicrobials (Rai *et al.*, 2009). Silver nanoparticles were found to possess both antibacterial and anti-inflammatory properties that can promote faster wound healing. Today, silver nanoparticles, present in metallic nanoparticle groups are frequently used in food shelf life extension, food packaging. The mechanisms of the antibacterial and anticancer activities are shown in Figure 11. Several studies demonstrated the bactericidal properties of the AgNPs. The antimicrobial action of AgNPs is linked with four well-defined mechanisms: (1) adhesion of AgNPs onto the surface of cell wall and membrane, (2) AgNPs penetration inside the cell and damaging of intracellular structures (mitochondria, vacuoles, ribosomes) and biomolecules (protein, lipids, and DNA), (3) AgNPs induced cellular toxicity and oxidative stress caused by the generation of reactive oxygen species (ROS) and free radicals, and (4) Modulation of signal transduction pathways. Besides these four well-recognized mechanisms, AgNPs also modulate the immune system of the human cells by orchestrating inflammatory response (Figure 15) which further aid in the inhibition of microorganisms (Tian *et al.*, 2007). Then, AgNPs cause an increase in ROS inside the microbial cells leading to cell damage, AgNPs modulate the cellular signal system ultimately causing cell death. The antibacterial potential of AgNPs is related to the generation of free radicals and Reactive Oxygen Species (ROS) (Dakal *et al.*, 2016).



**Figure 15:** Diagram represent the different mechanisms of action of NPs including silver nanoparticles in bacterial cells (Baptisa *et al.*, 2018).

## **I.2.2 Biological And Medical Application Of Gold Nanoparticles**

The biological application of AuNPs is rooted in their physicochemical properties. The most important being their smaller size that allows the modification of AuNPs to cross any biological barrier by attaching targeting and therapeutic peptides on their surface (**Cho *et al.*, 2009**). The therapeutic application of gold started centuries ago when gold compounds were used for medical purposes by Chinese and Indian people. For medical purposes, gold was used to treat conditions such as male impotence, epilepsy, syphilis, rheumatic diseases, and tuberculosis. China was the first to discover the longevity effect of red colloidal gold. The application of red colloidal gold continues in India for the same purposes (Ayurvedic medicine for rejuvenation and revitalization) as well as in China by the elderly. Cinnabar-gold (Makaradhwaja) is used for fertility purposes in India, and the USA as a supplement (**Table 2**). Gold was used to treat nervous disorder and epilepsy in Western countries and no toxicity was observed in both *in vitro* and *in vivo* studies (**Bhattacharya *et al.*, 2007**). Since then oral and injectable gold compounds continued to be used especially as treatment of 52 arthritis due to the bacteriostatic effects and proved to be anticancer effects (**Rau and Rheumatol, 2005**). Traditionally, AuNPs were used in several medical applications. Gold nanoparticles were extensively used in biomedical applications (**Bhumkar *et al.*, 2007; Sperling *et al.*, 2008; Doria *et al.*, 2012; Le *et al.*, 2015**), separation sciences (**Sykora *et al.*, 2010**), disease diagnostics (**Torres-Chavolla *et al.*, 2010**), and pharmaceuticals (**Cai *et al.*, 2008**). AuNPs have attracted significant interest over the last decade as a medicinal material in the treatment of tumours. Additionally, studies have also shown that AuNPs are effective antibacterial agents against many bacterial strains (**Pissuwan *et al.*, 2009; Poinern *et al.*, 2013**).

## **I.2.3 Nanomedicine For Cancer Applications**

### **I.2.3.1 Current Challenges In Cancer Therapy**

Cancer is increasingly being recognized as a critical public health problem and the leading cause of death globally with an estimated 18.1 million new cancer cases and 9.6 million cancer deaths worldwide in 2018 (**Bray *et al.*, 2018**). In 2019, 1,762,450 new cancer cases and 606,880 cancer deaths were projected to occur in the United States (**Siegel *et al.*, 2019**). Conventional chemotherapy delivers a cytotoxic agent indiscriminately to neoplastic and normal cells with severe systemic effects. (**Mishra *et al.*, 2013; Akindele *et al.*, 2015**) Among the antineoplastic agents that were investigated as encapsulated drugs for cancer, therapeutics are

doxorubicin (**Table 1**). Those drugs are cytotoxic against different kinds of tumours. They also induce other significant side effects such as cardiotoxicity, and neurotoxicity that can lead to decreased life quality or even death of patients (**Abidemi *et al.* 2015; Wen *et al.*, 2017**). Between 2005 and 2018, over 1,100 anticancer drugs were discovered, most of which are in clinical trials, and a few drugs were waiting for the approval of the Food and Drug Administration. The average amount spent on cancer therapies and supportive care increased to 133 billion dollars in 2017. (**Siegel *et al.*, 2015; Aitken *et al.*, 2018**).

**Table I:** A summary of the various types of chemotherapeutics available for cancer therapy.

Drug Type	Example	Mode of Action
<b>Alkylating agents</b>	<b>Cisplatin</b> <b>Mitomycin C</b>	Cell-cycle independent drugs. Typically, these chemotherapeutics alkylate(bind) DNA base leading to the cross-linking of DNA strands and/or proteins, eventually leading to single and double-stranded DNA breaks, leading to apoptosis ( <b>Puyo et al., 2014</b> ).
<b>Antimetabolites</b>	Methotrexate pemetrexed	Cell cycle-dependent. Small molecules that closely resemble critical metabolites and are capable of interfering with the normal function of metabolic enzymes including those involved in DNA, RNA, and protein synthesis ( <b>Bobrovnikova-Marjon and Hurov, 2014</b> ).
<b>Anti-microtubule agents</b>	Vinca alkaloids (Vincristine, vinblastine, etc); taxanes (Paclitaxel, Docetaxel)	Cell cycle-specific (S-phase) inhibits microtubule function causing mitotic arrest and subsequent apoptosis ( <b>Klute et al., 2014</b> ).
<b>Topoisomerase inhibitors</b>	Irinotecan/topotecan; etoposide Doxorubicin Mitoxantrone, Novobiocin, aciarubicin	Cell cycle-dependent inhibits enzymes (topoisomerase I and II) involved in DNA unwinding, therefore DNA replication and transcription; leading to apoptosis ( <b>Khadka and Cho, 2013</b> ).
<b>Cytotoxic antibiotics</b>	Actinomycin Doxorubicin Epirubicin Mitoxantrone	Cell cycle-dependent. Generally, act to interrupt cell division by intercalating with DNA and preventing the re-sealing of the DNA double helix, triggering the apoptotic pathway ( <b>Tahover et al., 2015</b> ).

Since the approval of Cisplatin (platinum-containing inorganic compound) in 1978 by FDA for cancer treatment, research for medical effects of inorganic metal has been rising. Nano-technology- based therapeutics as an alternative therapy is gaining traction (**Xin et al., 2017**). The nano-drug version of doxorubicin has been approved by the FDA for the treatment of refractory ovarian cancer, breast cancer, and Kaposi's sarcoma in the USA. Biodegradable liposome nanoparticles are used to deliver doxorubicin to the tumour site, and help retain the drug efficacy and circulation longer than the normal drug (**Yezhelyev et al., 2006; and Sasisekharan, 2007**).

### **I.2.3.2 Nanoparticles Based Drugs For Cancer Applications**

The earliest application of nanomedicine was in cancer research where liposomes were used to deliver chemotherapy payloads to the tumour tissues (**Moghimi *et al.*, 2005**). Abraxane (NP albumin-bound paclitaxel) was the first chemotherapeutic NP to be approved by the FDA for the treatment of metastatic breast cancer in the USA (**Yezhelyev *et al.*, 2006**). One important property of gold nanoparticles for cancer applications is their thermal diffusivity. The use of local hyperthermia guided by gold nanoparticle accumulation with the tumour is a recent strategy to provoke cancer cell apoptosis and necrosis (**Kennedy *et al.*, 2011**). The strategy can be applied in various diseases as long as biomarkers exclusively expressed during the development of the disease are known or were identified (**Yezhelyev *et al.*, 2006**). Gold has many applications in medicine and nanotechnology, an anti-angiogenic effect (**Arvizo *et al.*, 2011**). There are currently two AuNP-formulations that have undergone human clinical trials in the treatment of solid tumours. Aurimune (CYT-6091) was the first citrate coated AuNPs to go through clinical trials which started in 2005 for the delivery of anti-cancer therapy. CYT-6091. AuNPs were recently investigated as broadly used nanoparticles for biocompatibility and cytotoxicity in connection with cellular interactions, it is demonstrated that the AuNPs lowered endocytosis and inhibited cancer cell proliferation (**Selim and Hendi 2012; Grijalva *et al.*, 2017**).



**Table II:** Nanoparticles therapeutics undergoing clinical investigations (**Hagaman *et al.*, 2021**).

Name	Formulation	Indications	Company	Current status
<b>Abraxane</b>	<b>Paclitaxel protein bound particles</b> (Breast, and lung cancer)	<b>Microtubules</b> Inhibition and increase the specificity of antineoplastic effect	<b>Celgene</b>	<b>Approval</b>
<b>Caelyx®</b>	Liposomes –doxorubicin (Breast, ovarian cancer)	DNA-intercalating agent and topoisomerase II, much longer circulation time due to the steric barrier provided by the surface-grafted PEG	Janssen Pharmaceutical	<b>Approval</b>
<b>Ferumoxtran-10</b>	Dextran	Inhibit the cancer cells effectively, reduces the size of cancer tissues as therapy	Ferrotran®	Phase 3 clinical trial
<b>GNPS</b>	Gold (Breast, ovarian cancer)	Increase of effects, DNA hybridation detection, protein interaction		Preclinical
<b>S-CKD602</b>	Peglyated liposomal	Topoisomerase inhibitor, greater solubility, eliminated by the reticuloendothelial system (RES), which consists of cells	Alza Corporation	Phase I/II
<b>CRLX101</b>	Polymeric nanoparticle (cyclodextrin) formulation of camptothecin	DNA topoisomerase I, apoptosis, Increase the exposure of tumor cells, while minimizing side effects.	Cerulean Pharma	Phase II
<b>NC-6004</b>	Polymeric nanoparticles (PEG-poly amino acid) Formulation of cisplatin	DNA cross linking agent, DNA synthesis inhibitors	NanoCarrierC0.	Phase I
<b>NK105</b>	Polymeric nanoparticles (PEG-poly aspartate) Formulation of paclitaxel	Antitumor activity and reduction of the associated peripheral nephrotoxicity	Nippon Kayaku C0, Ltd	Phase II
<b>NK911</b>	Polymeric nanoparticle (PEG-poly aspartate formulation of doxorubicin)	Enhanced the delivery of doxorubicin and reduce the associated cardiotoxicity	Nippon Kayaku C0, Ltd	Phase I
<b>Zevalin®</b>	90Y-ibritumomab tiuxetan	combines the benefits of a monoclonal antibody with the efficacy of radiation in the treatment of B-cell non-Hodgkin lymphoma	Bayer Pharma	<b>Approval</b>

### I.2.3.3 Nanoparticles-Induced Cancer Cell Death

Several mechanisms are involved in NP-mediated *in vitro* toxicity in cancerous cells. Cellular responses to NP exposure might include those at the cell, organelle, and gene-level or a combination of them (Patil *et al.*, 2016). The high levels of reactive oxygen species (ROS) production, downregulation of antioxidant enzyme coding genes, lipid peroxidation, and genotoxic effects, among others, may be involved in the integrated cellular response to NPs (Choi *et al.*, 2016; Abdal *et al.*, 2017). The AuNPs and AgNPs were also observed to induce diverse types of cell death, primarily through autophagy, and apoptosis (Sun *et al.*, 2018).

#### I.2.3.3.1 Nanoparticles Induced Apoptosis

Apoptosis is a physiological cell death process (Figure 17). Apoptosis is a sequential signaling pathway that involves protein-cleaving proteases known as cysteinyl-aspartate-specific proteases, caspases (Gullicksen *et al.*, 2003). Morphologically, apoptosis is characterized by loss of cellular contact with the surrounding cells, cytoplasmic contraction, and chromatin condensation. This includes genomic DNA fragmentation, externalization of phosphatidylserine (PS) component of the phospholipid bilayer, and formation of apoptotic bodies that are removed through endocytosis by macrophages before the cells lose their plasma membrane integrity (McConkey 1998; Nelson-Dooley *et al.*, 2005). Although several stimuli appear to trigger the process of apoptosis, there are two major signaling pathways: the death receptor pathway and the mitochondrial pathway (McConkey, 1998; Nelson-Dooley *et al.*, 2005). Extrinsic death signals such as Fas ligand and TNF- $\alpha$  induce cell death from outside of the cell, whereas DNA damage, oxidative stress, toxins, and deficiency of survival factors, are communicated through mitochondria to evoke intrinsic cell death (Asoh and Ohta, 2008).

#### Apoptosis Pathways

Programmed cell death, as the name suggests is a naturally occurring process. Apoptosis continually takes place throughout the growing process, it can be initiated by intrinsic or extrinsic signal pathways and executed by caspases (Mallat and Tedgui, 2000). Both these pathways involve a series of molecular and biochemical steps that lead to the activation of pro-caspases. The activated caspases cleave nuclear and cytoplasmic substrates responsible for the maintenance of nuclear integrity, cell cycle progression, and DNA repair, causing cell death (Nelson-Dooley *et al.*, 2005).

## Intrinsic Pathway

The intrinsic or mitochondrial pathway is initiated by stress molecules (ROS, reactive nitrogen species), (Nelson-Dooley *et al.*, 2005). This pathway is regulated by the Bcl-2 family of proteins, which consist of 3 classes: the pro-apoptotic effectors (Bax and Bak), as the name suggests, the mitochondrial pathway is dependent on the release of cytochrome c from the mitochondria induced by irreparable DNA damage (Figure 16). Depending on the extent of DNA damage, apoptosis can be an immediate or delayed reaction within the cell. The nuclear transcription factor, p53 is often involved in apoptosis. The p53 upregulation activates genes such as Bcl-2 associated protein-X (Bax), resulting in either a decrease in the inner mitochondrial transmembrane potential or opening of the voltage-dependent anion channel (VDAC). Cytochrome c is released from the mitochondria, apoptotic protease activating factor-1 (Apaf-1), procaspase 9, and either ATP or dATP form a complex called apoptosome. Formation of the apoptosome activates caspase 3 leading to cell death (Kiechle and Zhang, 2002). The intrinsic pathway is dependent on the permeability of mitochondrial membranes and the release of cytochrome c as outlined in Figure 1.8. Briefly, the mitochondrial permeability transition pore (PTP) is the key regulator of the intrinsic pathway. The PTP's crucial components inactivation of apoptosis are VDAC-1 in the outer mitochondrial membrane (OMM) and adenine nucleoside translocator (ANT) in the inner mitochondrial membrane (IMM) (Nelson-Dooley *et al.*, 2005; Shore, 2009; Shoshan-Barmatz *et al.*, 2010). Apoptosis can also be induced by an increase in reactive oxygen species (ROS) (Chun *et al.* 2010; Wang *et al.* 2013; Belhadj *et al.* 2014). ROS are by-products generated during oxygen metabolism within mitochondria. Overproduction of ROS can stimulate oxidative stress and damage macromolecules, proteins, lipids, and DNA (Ott *et al.*, 2007). Antioxidant systems help neutralize ROS generation, however a strong imbalance between antioxidants and elevated ROS concentration, upon hyperthermic exposure (Mari *et al.* 2009). Hyperthermia was demonstrated to cause an increase in ROS in the form of hydrogen peroxide, superoxide anion, and hydroxyl radical (Kikusato and Toyomizu 2013). Hyperthermia showed to decrease crucial antioxidant levels such as superoxide dismutase, thus promoting the cell into apoptosis (El-Orabi *et al.* 2011). Most of their functions are executed via ion channels, VDAC in apoptosis. Mitochondria are made up of two distinct and important compartments: the matrix surrounded by the IMM, contains enzymes responsible for  $\beta$ -oxidation and citric acid cycle; the intermembrane space surrounded by the OMM contains several apoptosis-inducing factors (cytochrome

c, procaspases, and AIF). Thus, apoptotic stimuli increase the permeability of the OMM and/or IMM, and induce cytochrome c release (Nelson-Dooley *et al.*, 2005; Shoshan-Barmatz *et al.*, 2010). The release of cytochrome c seals the fate of the cell, which is death. This process can be counteracted by anti-apoptotic proteins (Bcl-2 and Bcl-xL), their increased expression prevents cytochrome C release and promotes cell survival (Kutuk and Basaga, 2006).

#### ✚ Extrinsic Pathway

Extrinsic signals such as cytokines, hormones, and chemotherapeutic, ionizing, or viral agents are also capable of inducing apoptosis. The extrinsic pathway compared to Intrinsic is more acute and massive (Nelson-Dooley *et al.*, 2005). Cell death through this pathway involves recognition of cell membrane death receptors by the ligands from the TNF gene family, the most studied being Fas. The binding of a ligand to the death receptor recruits two signal-transducing molecules: TNF receptor-1 associated death domain protein (TRADD) and Fas-associated protein with death domain (FADD). Either molecule binds procaspase-8 leading to the formation of an intracellular complex known as the death-inducing signal complex (DISC). The formation of DISC results in proteolytic cleavage and activation of procaspase 8 to caspase 8 leading to DNA degradation by cleaving procaspase 3, or truncate Bid to tBid resulting in mitochondrial release of proapoptotic peptides. Binding of tBid to Bak initiates similar steps as in the intrinsic apoptotic pathway, the release of cytochrome c leading to the formation of apoptosome followed by cell death (Kiechle and Zhang, 2002; Nelson-Dooley *et al.*, 2005).

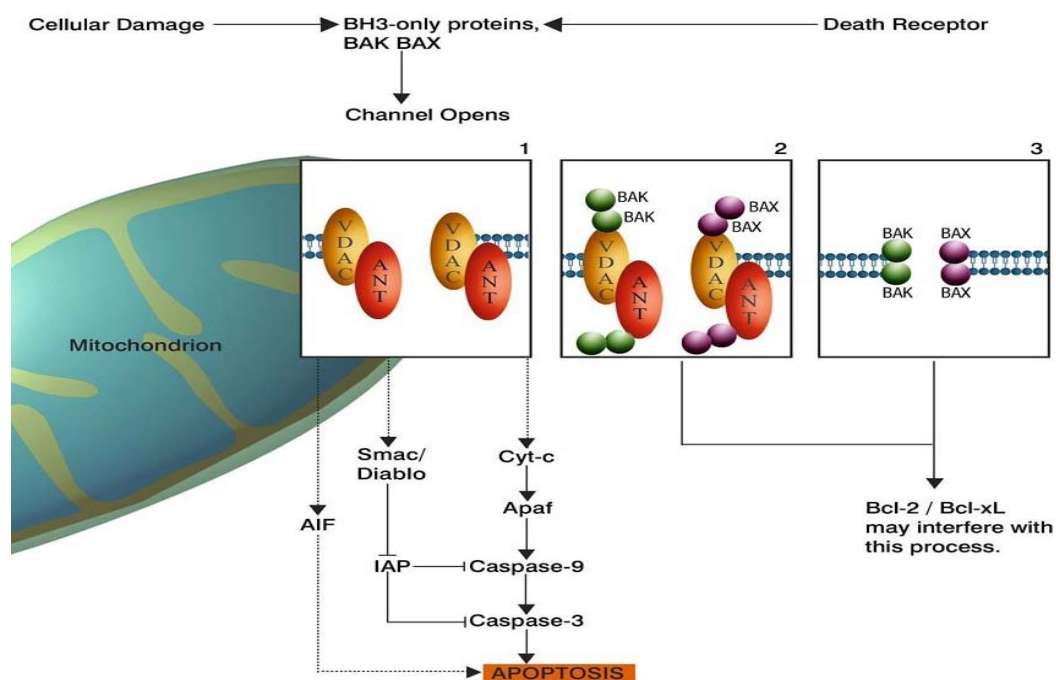


**Figure 14:** Three models for the cytosolic escape of mitochondrial proteins in response to apoptotic stimuli Figure reprinted with permission from Springer (**Kutuk and Basaga, 2006**). Upon an apoptotic stimulus such as cellular stress (oxidative stress, UV irradiation, growth factor withdrawal) or activation of death receptors, a mitochondrial channel could be formed by 1. Voltage-dependent anion channel (VDAC) and adenine nucleotide translocase (ANT), 2. VDAC-ANT-Bcl-2 proteins (Bax, Bak), 3. Only Bcl-2 proteins (Bax, Bak). Anti-apoptotic members of the Bcl-2 protein family (Bcl-2, Bcl-xL) may interfere with the apoptotic process through the inhibition of cytosolic escape of mitochondrial proteins.

### ✚ Apoptosis Assay Analysis By Flow Cytometry Technique

There are many assays available for measuring cell death such as the FITC Annexin V/Dead Cell Apoptosis Kit with FITC annexin V and PI for flow cytometry provides a rapid and convenient assay for apoptosis. Apoptosis assays measure key apoptotic markers, and necrosis typically focuses on the cell permeability that is characteristic of necrotic plasma membrane rupture. Some assays, such as Annexin V, (**Figure 17**) can differentiate between apoptosis and necrosis using a dual-core marker system. Annexin V binding to membrane-bound phosphatidylserine (PS) indicate early apoptosis whereas the propidium iodide (PI) labeling identifies the leaky cell membranes associated with necrosis. Indeed, the morphological and biochemical events in the two pathways can be detected through different assays and techniques: for instance translocation of PS can be detected by flow cytometry using annexin V which binds to externalized PS. DNA fragmentation into 180–200 base-pair units initiated by caspa-

se-3 activation can be determined by agarose gel electrophoresis. (; Sorisky *et al*, 2000; Kiechle and Zhang 2002).

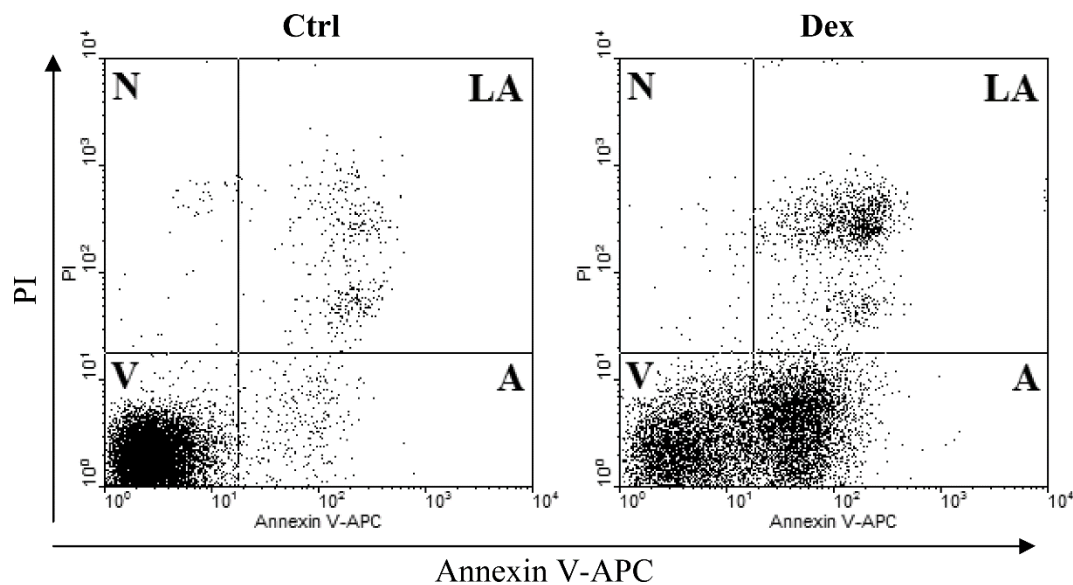


**Figure 15:** Apoptotic changes in the plasma membrane. Detection of apoptosis by concurrent staining with annexin V-APC and PI. Human B-cell lymphoma cells were untreated (left panel) or treated with dexamethasone (right panel), as described. Cells were subsequently stained with annexin V – APC conjugate and PI and their far-red and red fluorescence was measured by flow cytometry. Live cells (V) are both annexin V and PI negative. At the early stage of apoptosis (A), the cells bind annexin V while still excluding PI. At the late stage of apoptosis (N), they bind annexin V-FITC and stain brightly with PI previously (Wlodkovic *et al.*, 2013).

Metallic nanoparticles such as AgNPs and AuNPs induced diverse types of cell death, primarily through intrinsic pathways, including ROS production, mitochondrial function disturbance, and ER stress.

### I.2.3.3.2 Nanoparticles Induced Intracellular ROS And Cell Survival

The reactive oxygen species (ROS) are free radicals of the biological system, including various disease pathogenesis such as cancer (Mitra, 2019). There are three major types of ROS, among others: superoxide anion ( $O_2^-$ ), hydroxyl radical ( $HO\cdot$ ), and hydrogen peroxide ( $H_2O_2$ ), which play a pivotal role in cell metabolism, signaling, and homeostasis. Accumulation of ROS in the cells increases the damage of the proteins, lipids, and nucleic acids (Abdal *et al.*, 2017). Indeed, elevated rates of reactive oxygen species (ROS) have been detected in almost all cancers, where they promote many aspects of tumour development and progression. In cancer cells, high levels of reactive oxygen species can result from increased metabolic activity, mitochondrial dysfunction, peroxisome activity, increased cellular receptor signaling, oncogene activity, increased activity of oxidases, cyclooxygenases, lipoxygenases, and thy-

midine phosphorylase, or through crosstalk with infiltrating immune cells (Pelicano et al., 2004). In this regard, the ability of NPs to generate ROS could potentially be exploited for cancer therapy. In MCF-7 human breast cancer cells, Zn-doped TiO<sub>2</sub> NP exposure leads to drastic decreases in cell viability and increased cell cycle arrest associated with increases in oxidative stress (Ahamed et al., 2016). The NP-mediated ROS generation initiates a sequence of pathological events, including inflammation, fibrosis, genotoxicity, and carcinogenesis, and is modulated by physicochemical features of NPs, such as size, charge, surface area, and chemical structure (Shvedova et al., 2012). NP-related toxicity can trigger increased expression of pro-inflammatory and fibrotic cytokines and activation of inflammatory cells, such as macrophages and neutrophils, which can influence the enhanced generation of ROS (Kennedy et al., 2009; Lee et al., 2009). The mechanism associated with NP-induced ROS generation varies among different NPs (Figure 18), the ability of NPs to depolarize the mitochondrial membrane and to interfere with the electron-transport chain through activation of NADPH-related enzymes was previously described (Xia et al., 2006; Soenen et al., 2011). AgNP-exposed human glioblastoma and human fibroblast cells showed increased accumulation of AgNPs in mitochondria that led to the disruption of the mitochondrial electron-transfer chain and, consequently, high levels of ROS-mediated cytotoxicity (Asharani et al., 2009). The interaction of Ag ions with NADH dehydrogenase, which blocks electron transfer to O<sub>2</sub><sup>2-</sup> and generation of high levels of ROS, was shown in Escherichia coli (Holt and Bard, 2005). (Rissom et al., 2005). NP exposure may cause cancer cell death by oxidative stress through varied mechanisms, including ROS production, inhibition of antioxidant enzymes, mitochondrial damage, and lipid peroxidation (Abdal et al., 2017). For instance, Matulionyte et al. (2017) demonstrated that photoluminescent gold nanoclusters have specific toxicity against MCF-7 breast cancer cells and were less toxic on MDA-MB 231 breast cancer cells, a highly drug-resistant cell line. The mechanism of cell death was apoptosis, necrosis, and generation of ROS, effects that were more evident in MCF-7 cells (Matulionyte et al., 2017). Nanoclusters have specific toxicity against MCF-7 breast cancer cells and were less toxic on MDA-MB 231 breast cancer cells, a highly drug-resistant cell line. The mechanism of cell death was apoptosis, necrosis, and generation of ROS, effects that were more evident in MCF-7 cells.

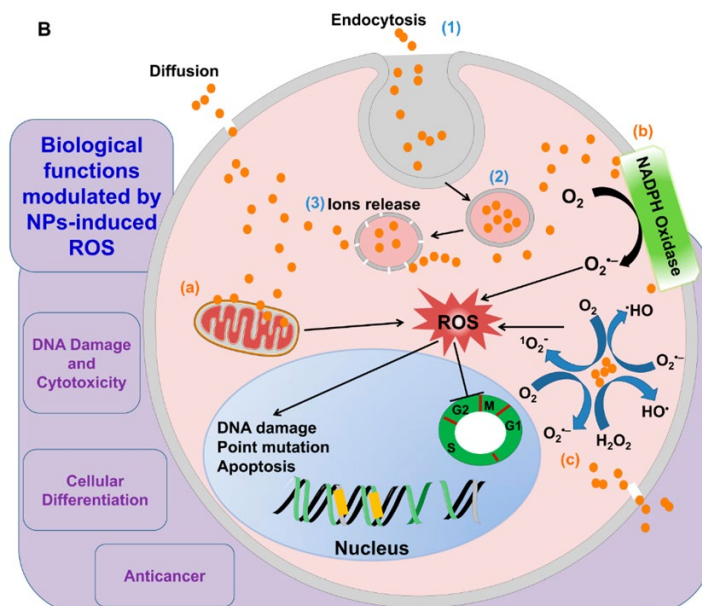


**Figure 16:** Schematic diagram describing the mechanisms implicated in NP-induced ROS production (Abdal *et al.*, 2017). NPs can be internalized into the cell by (1) endocytosis; (2) formation of the endocytotic vesicles; and (3) release of particle ions from vesicles into the cell. The main factors responsible for ROS generation by NPs include: (a) interaction with the mitochondria; (b) interaction with NADPH oxidase; and (c) factors related to the physicochemical properties (size, shape, photoreactive properties, and surface chemistry). These factors lead to ROS generation and its consequences, including DNA damage, cell cycle arrest, alterations in apoptosis, and damage to the cell membrane.

### 1.2.3.3.2 Effects Of Nanoparticles Induce Cellular Responses

Due to the complexity of cell responses to nanoparticles, it is important to evaluate the biological effect of NPs from different perspectives, from toxicology assessment to both *in vitro* and *in vivo* testing, to better understand NP-induced cellular responses and the mechanisms behind them (Figure 19). Nanoparticles have been shown to cause cell cycle arrest, including G<sub>2</sub>/M and G<sub>0</sub>/G<sub>1</sub> arrest (Figure 20). The type and extent of cell cycle arrest vary depending on the composition, size, size distribution, surface modification, and subsequent surface derivatization of nanoparticles (Kim *et al.*, 2013; Wu *et al.*, 2013; Estevez *et al.*, 2014), G<sub>0</sub>/G<sub>1</sub> arrest can be caused by DNA damage and microtubule damage, while nanoparticles in combination with oxidative stress and/or lysosome rupture could lead to the G<sub>0</sub>/G<sub>1</sub> arrest. However, the mechanisms and the factors behind the G<sub>2</sub>/M cell cycle arrest caused by nanoparticles are still unclear. Recently, Mahmoudi *et al.* (2011) speculated that the effects of nanoparticles on the cell cycle may depend on the intracellular location of the nanoparticles. Additionally, it was reported that gold nanoparticles (GNPs) with lysosomal escape ability localized to the tubulin/microtubule system and caused cell cycle arrest at the G<sub>0</sub>/G<sub>1</sub> phase through induction of microtubule damage. However, whether the intracellular localization of nanoparticles is linked with G<sub>2</sub>/M cell cycle arrest is still unknown. Studies on the effects of AuNPs in the cell



cycle are still scarce. However, it has already been reported that AuNPs can interfere in the cell cycle **Mahmoudi et al. (2011)**; and **Roa et al. (2009)** demonstrated that exposure for 24hrs to glucose capped-AuNPs (Glu-AuNPs) accelerated the G0/G1 phase transition in the human prostate cancer cells (DU-145) and resulted in the accumulation of cells in the G2/M phase (29.8 %) comparing with control cells (18.4 %). **Choi et al. (2012)** have also evaluated the effect of serum protein-coated AuNPs in the cell cycle of human lung carcinoma and human epidermoid carcinoma cell lines. The authors observed an increase in the sub-G1 population in the AuNPs-exposed cells compared to control cells, where most cells were in the G1 phase. Also, **Chuang et al. (2013)** performed an extensive evaluation of 10 nm x 45 nm Au nanorods in human lung adenocarcinoma epithelial (A549) and gastric adenocarcinoma (AGS) cells. The effect of AgNPs on the cell cycle has also been studied. In A549 cells, incubation for 24 hrs with a low concentration (2 µg/mL) of AgNPs did not alter the cell cycle progression (**Beer et al., 2012**). However, at a higher concentration (3 µg/mL), a decrease of the cell number in the G1/G0 phase was obtained (**Beer et al., 2012**). In mouse peritoneal macrophage (RAW264.7) cells, exposure to 69 nm AgNPs for 24 hrs resulted in cell arrest at the G1 phase hindering the S phase, followed by cell apoptosis (**Park et al., 2010**). Also, **Asharani et al. (2009)** employed the cell cycle analysis as a complementary study of the oxidative stress caused by starch-coated AgNPs. The fact that cells with DNA damage can accumulate in the G1, S, and G2/M phase, and cells in an irreversible state of damage will accumulate in the sub-G1 phase, the authors reported that these NPs caused cell arrest at the G2/M phase of human lung fibroblast (IMR-90) and human glioblastoma (U251) cells. **Zheng et al. (2013)** used both AuNPs and AgNPs to study their role in the enhancement of radiosensitivity in hepatocellular cells (HepG2). In this study, they have combined AgNPs and AuNPs with irradiation and evaluated whether this combination (AgNPs-irradiation and AuNPs-irradiation) could induce changes in cell cycle compared to control cells (the cells treated with irradiation alone).

## Cell Cycle Analysis By Flow Cytometry Technique

The flow cytometry technique is a valuable tool to analyze the impact of the NPs on the cell cycle. This technique is based on the evaluation of the cell properties in a flow, after staining the cells with propidium iodide (PI), a nucleic acids-binding dye. **Figure 20** is represented a typical histogram of the cell cycle analysis by flow cytometry. The first peak of the histogram is related to the cells in the G<sub>0</sub>/G<sub>1</sub> phase. The cells in the G<sub>2</sub>/M phase are represented in the second peak of the histogram. The space between the peaks corresponds to the cells that are in the S phase. The sub-G<sub>1</sub> area corresponds to cellular debris and late apoptotic and necrotic cells.

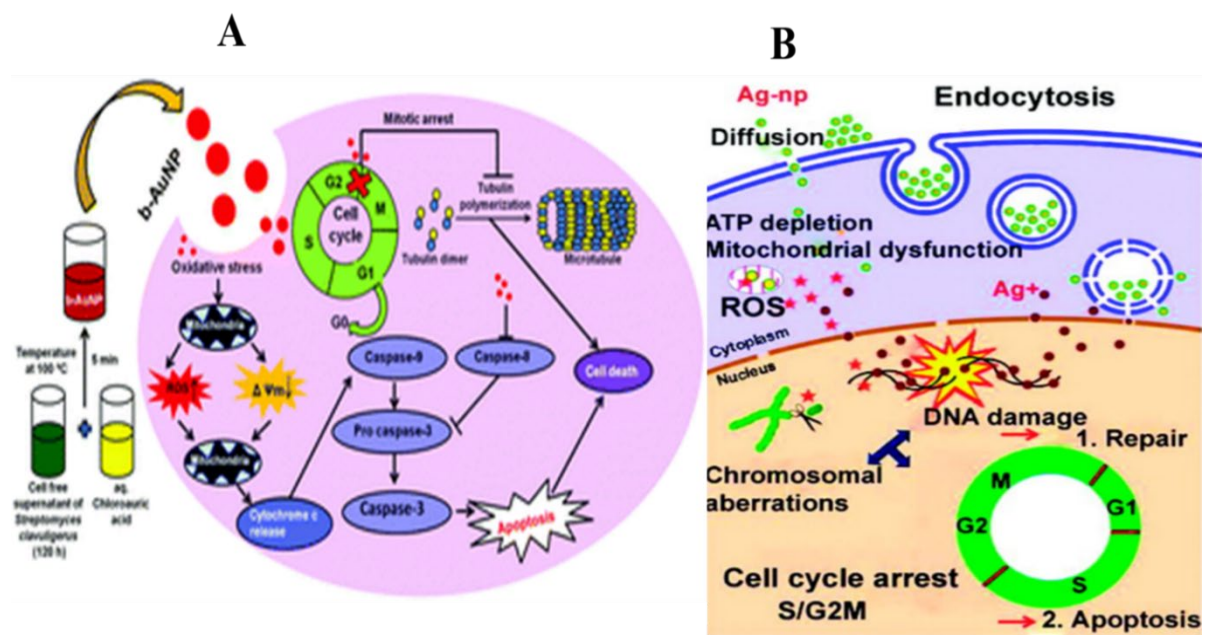


**Figure 17:** Schematic diagram describing the mechanisms implicated in NP on cell cycle arrest (A): Effect of gold nanoparticles (Kumar *et al.*, 2015) and silver nanoparticles (B) on cell cycle arrest (Asharani *et al.*, 2009).

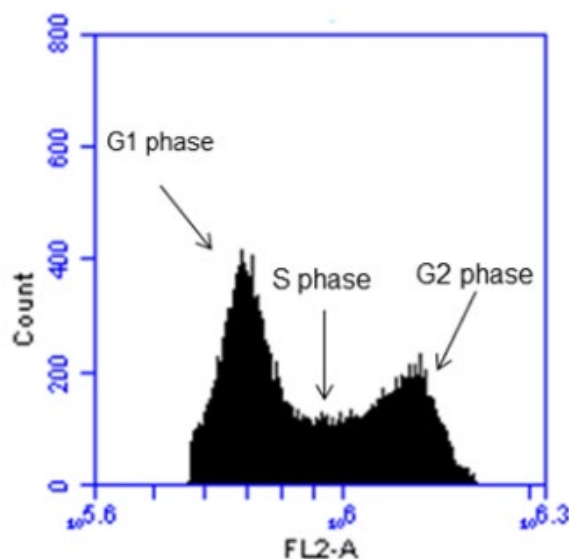


**Figure 18:** Representative cell cycle histogram of Caco-2 cells analyzed by flow cytometry.

Finally, NPs might release ions that enter the nucleus and cause DNA fragmentation/hypermethylation and/or cell cycle arrest in cancer cells. Furthermore, NPs inhibitory effect on cellular viability is due to the downregulation of anti-apoptotic genes, e.g. Bcl2, generation of reactive oxygen species (ROS), mitochondria fission and autophagy, and events that finally induce cell death through apoptosis.

### **I.3 Challenge And Advance In Nanotechnology**

Most of the methods are still in the development stage and the problems experienced are stability and aggregation of nanoparticles, control of crystal growth, morphology, size, and size distribution. The large-scale is interesting because of the lack of surfactants, templates, or other auxiliary substances to stabilize and control nanoparticle shape which could be toxic and persist as residual contaminants in the product (Castro *et al.*, 2014). The use of continuous-flow microreactors should be further examined because they have shown advantages for nanoparticle production. Nowadays, little is known about the mechanistic details of these transformations but this knowledge is necessary for the economic and rational development of new synthetic methods. Genetic engineering techniques can potentially be used to improve the particle properties and to control their composition (Altavilla *et al.*, 2017).

#### **I.3.1 Safety And Environmental Impact Of Nanoparticles**

The application of green nanotechnology has two goals: producing and products without harming the environment or human health and producing nano-products that provide solutions

to environmental problems. Nanomaterials or products directly can clean hazardous waste sites, desalinate water, treat pollutants, or sense and monitor environmental pollutants (Yunus *et al.*, 2012).

### I.3.2 Significance Progress In Green Nanotechnology

Specifically, in the past few years, the production of nanoparticles using plant material have a significant impact on nanotechnology. The emerging biosynthesis using living or dead biomass and derived products is undoubtedly an important field that faces considerable research challenges if the aim is to achieve benefit from nanotechnology minimizing the impact on human health and the environment. Likewise, several studies reported the synthesis of AuNPs using extracts from plants such as Aloe vera (Kumar and Yadav, 2009), *Trianthema decandra* (Geethalakshmi and Sarada, 2012), and *Memecylon umbellatum* (Arunachalam *et al.*, 2013). Chandran and coworkers. (2007) also reported the biogenic gold nano triangles and spherical silver nanoparticles were synthesized by a simple procedure using Aloe vera leaf extract as the reducing agent. Moreover, extracts obtained from plants are found to have several active metabolites like alkaloids, saponins, terpenoids, anthocyanins which are responsible for the possible reduction of complex chemical, silver nitrate, and gold chloride into single-molecule like silver and gold as biometal with bioactivity (Gopinath *et al.*, 2013). Besides, many recent studies used different plant extracts (Table 3) from other *Terminalia* species such as *Terminalia catappa*, *Terminalia bellerica*, *Terminalia bentazoe*, *Terminalia mellueri*, *Terminalia arjuna*, and *Terminalia cheduba* as a mediator for gold and silver nanoparticle formation (Kumar *et al.*, 2012; El-Rafie and Hamed, 2014; Singh *et al.*, 2015). Nevertheless, a survey of literature revealed that very limited species of the genus *Terminalia* are used for the biosynthesis of metal nanoparticles with no report concerning the *Terminalia mantaly* plants (Ankamwar, 2010; Kumar *et al.*, 2012). The present studies attempted to demonstrate the potential of extracts from *Terminalia mantaly* plant to produce crystalline, stable gold and silver nanoparticles and their biological applications.

**Table III:** List of some *Terminalia* species, their parts used, and the biomolecules obtained from the plants responsible for the green synthesis of AgNPs and AuNPs.

Plant species	Part	Actives component	Sizes and Shape	References
<i>Terminalia arjuna</i>	Leaf Bark	Phenol/carboxylic Group Arjunetin, leucoanthocyanidins, and hydrolyzable tannins	Leaf 8–16 nm; spherical and irregular AgNPs 20–60 nm; spherical bimetallic Ag/AuNPs	(Arumugam and Gopinath, 2011). Gopinath <i>et al.</i> , 2013; Ahmed <i>et al.</i> , 2016)
<i>Terminalia catappa</i>	Leaf	Tannins	55–71 nm; cubic, hexagonal, triangular and 10–35 nm, spherical for AgNPs and AuNPs respectively	(Zakir <i>et al.</i> , 2014) and Ankamwar, 2010)
<i>Terminalia chebula</i>	Fruit	Polyphenols	≤100 nm; pentagon, spherical and triangular	(Kumar <i>et al.</i> , 2012)
<i>Terminalia tomentosa</i>	Stem bark	Polyphenols	Spherical AgNPs: 5 to 50 nm	(Shah <i>et al.</i> , 2011)

### I.3.2.1 Description Of Plant Used To This Study

Medicinal plants are a potential source for multiple anticancer, antimicrobial agents, as they produce a wide variety of secondary compounds with several biological activities (Amer *et al.*, 2007). It is well known that more than 400,000 species, as well as *Terminalia* species of tropical flowering plants, have medicinal properties (Odugbemi, 2006). The genus *Terminalia* gets its name from the Latin terminus since the leaves appear at the tips of the shoots (Fahmi *et al.*, 2015).

#### I.3.2.1.1 Terminalia Species

The genus *Terminalia* is the second largest genus of the Combretaceae after Combretum, with about 200 species. *Terminalia* species range from shrubs to large deciduous forest trees. Mostly they are very large trees reaching in height up to 75 m tall. The species, *Terminalia mantaly* are founded in Cameroun and are frequently used in traditional medicine for the treatment of various infectious diseases and chronic diseases as cancer (Ngouana *et al.*, 2015).

### I.3.2.1.2 *Terminalia mantaly* H. Perrier

#### I.3.2.1.2.1 Botanical Description

*Terminalia mantaly* has grown 10-20 m with an erect stem and neat, conspicuously layered branches. Bark pale grey, smooth, and rather mottled (**Figure 22**). The length up to 7 cm, apex broadly rounded, base very tapered, margin wavy (**Figure 22**) (Orwa *et al.*, 2009).



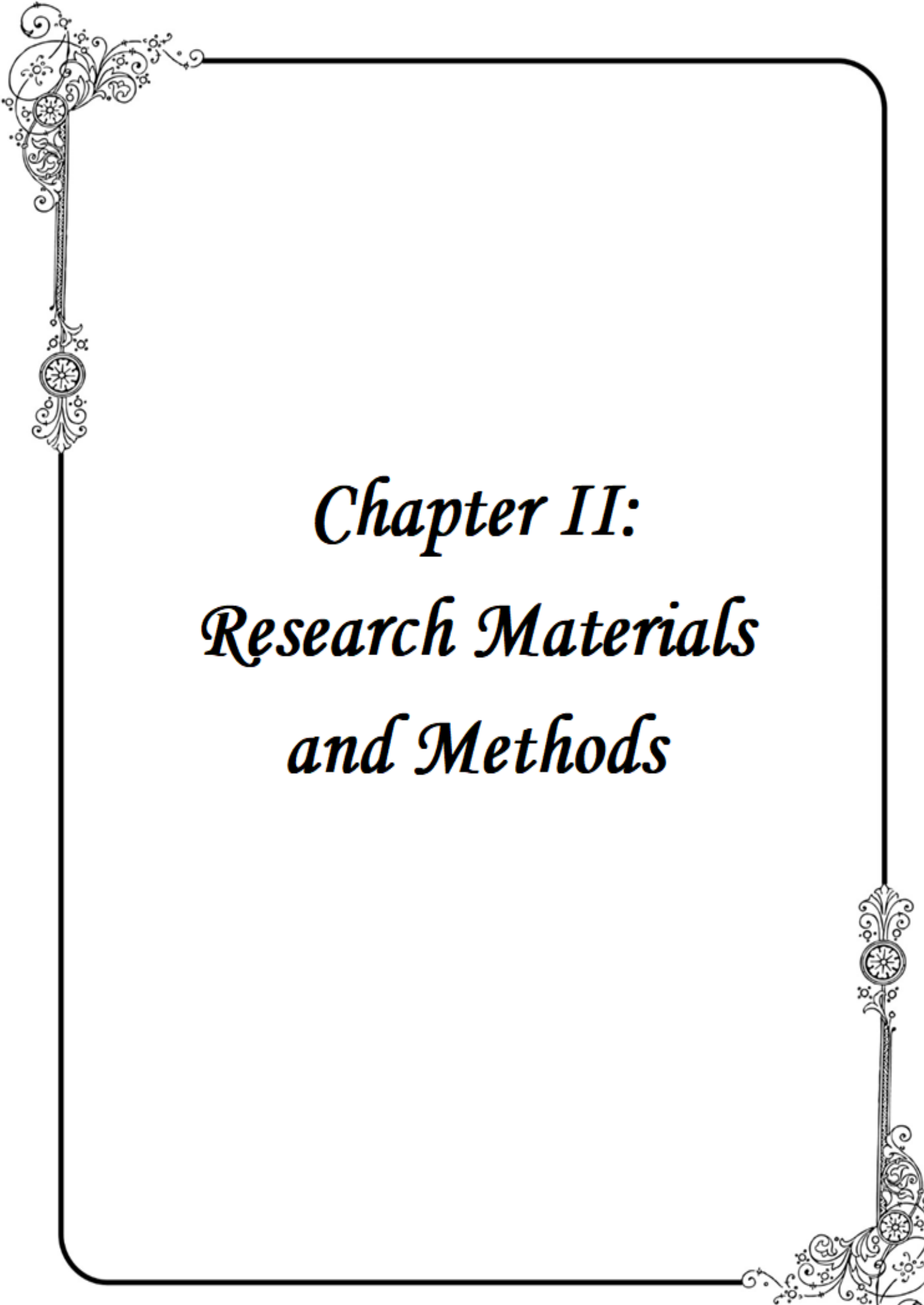
**Figure 19:** *Terminalia mantaly* plant (Combretaceae), (Photographed by Majoumou, 2019).

#### I.3.2.1.2.2 Ethnobotanical And Traditional Used

The wood obtained from the plant is used as ordinary interior joinery in the manufacturer of doors, windows, stairs, partitions, cladding; mounting tools, and firewood (Arbonnier, 2004). Moreover, *Terminalia mantaly* H. Perrier (Combretaceae) is used in the traditional environment to satisfy several troubles such as cancer, diarrhea, dysentery, arterial hypertension, gastroenteritis, mycosis, and bacterial infections (Orwa *et al.*, 2009; Bognan *et al.*, 2013; Fahmy *et al.*, 2015).

#### I.3.2.1.2.3 Previous Work Performed On *Terminalia mantaly* Plant

*Terminalia* species plants especially *Terminalia mantaly* have been used for years in folk medicines and are still used for health benefits. Indeed, several past and recent studies reveal the potential of extracts from these plant species to inhibit the growth of a wide range of pathogenic bacteria (Ngouana *et al.*, 2015; Tchuente *et al.*, 2017). Additionally, Mbouna *et al.* (2018) investigated the antiplasmodial activity of extracts and fractions from *Terminalia mantaly* (Combretaceae) and also their selectivity on non-cancerous kidneys cells line (Hek293T)



*Chapter II:  
Research Materials  
and Methods*

## **CHAPITRE II: MATERIAL AND METHODS**

### **II.1 MATERIALS**

#### **II.1.1 Chemicals Reagents And Their Suppliers**

For this study, silver nitrate and gold salt (sodium tetrachloroaurate (III) dihydrate), and ampicillin were purchased from Sigma-Aldrich (Cape Town, South Africa), Phosphate buffered saline (PBS), and Muller Hinton Broth (MHB) and Muller Hinton Agar (MHA) were purchased from Lonza (Cape Town, South Africa). FBS, Trypsin-EDTA, DMEM, and pen-strep (penicillin-streptomycin) were bought from Thermo Scientific (Ansfrere, South Africa). Polystyrene 96-well microtitre plates were obtained from Greiner bio-one GmbH (Frickenhausen, Germany). Annexin V-Cy3 Apoptosis detection Kit, CM-H2DCFDA probe kit, MTT, propidium iodide, and RNase were purchased from Sigma-Aldrich (Cape Town, South Africa).

#### **II.1.2 Instruments**

UV-Vis spectra were recorded using POLAR star Omega microplate reader (BMG Labtech, Cape Town, South Africa). The size distribution, Pdi, and zeta potential measurements of the synthesized AuNPs and AgNPs in solution were analyzed using Zetasizer (Malvern Instruments Ltd., Malvern, UK). HRTEM analysis was done using FEI Tecnai G2 20 field-emission gun (FEG). The FTIR analysis was done using JASCO 460 plus spectrophotometer with a frequency ranging from 4000-400 cm<sup>-1</sup>. The baseline corrections were performed for all spectra.

#### **II.1.3 Bacteria Strains**

The bacterial strains listed in Table 4 were purchased from Biodefense and Emerging Infections Research Resources Repository (BEI Resources, Rockville, MD 20852) and the American Type Culture Collection (ATCC, Manassas, VA, USA). The microorganisms were maintained on an agar slope at 4 °C and sub-cultured for 24h before use.



**Table IV:** List of bacterial strains used for antibacterial activity.

Bacterial strains	Acronym	Reference No.	Supplier
<i>Streptococcus pneumoniae</i>	<i>S. pneumoniae</i>	ATCC 49619	ATCC
<i>Klebsiella pneumoniae</i>	<i>K. pneumoniae</i>	ATCC 13883	ATCC
<i>Haemophilus influenzae</i>	<i>H. influenzae</i>	ATCC 49247	ATCC
<i>Shigella flexneri</i>	<i>S. flexneri</i>	NR-518	BEI resources
<i>Salmonella enterica</i>	<i>S. enterica</i> <sup>a</sup>	NR-13555	BEI resources
<i>Salmonella enterica</i>	<i>S. enterica</i> <sup>b</sup>	NR-4294	BEI resources
<i>Salmonella enterica enterica</i>	<i>S. enterica enterica</i>	NR-4311	BEI resources
<i>Staphylococcus aureus</i>	<i>S. aureus</i>	NR-45003	BEI resources

**Notes:** *S. enterica* (*Salmonella enterica* subsp. *enterica* A36 (Serovar *Typhimurium*) vs *S. enterica* (*Salmonella enterica* subsp. *enterica* 2004 Pennsylvania Tomato Outbreak, Serovar *Anatum*, Isolate 4)

**Abbreviations:** ATCC, American Type Culture Collection; BEI resources, biodefense, and emerging infections research resources repository.

## II.1.4 Cancer Cells Maintaining

The cell lines provided from ATCC were cultured into DMEM supplemented with 10 % heat-inactivated fetal bovine serum (FBS) and 1 % of penstrep (penicillin-streptomycin) and incubated in a 37 °C humidified incubator with 5 % CO<sub>2</sub> saturation. The cells were obtained from the American Type Culture Collection (ATCC, Manassas, VA, USA).

**Table V:** List of cancer and non-cancerous cells line.

Cells line	Acronym	Resistance status	Gene mutation	Species
Breast cancer	MCF-7	Adenocarcinoma	TP53, CDKN2A, PIK3CA	<i>Homo sapiens</i>
Colorectal cancer	Caco-2	Colorectal adenocarcinoma	PTEN, TP53, APC, MYC	<i>Homo sapiens</i>
Liver cancer	HePG2	Hepatocellular carcinoma	TP53	<i>Homo sapiens</i>
Human fibroblast	KMST-6	nontumorigenic immortalized	N/A	<i>Homo sapiens</i>

**Notes:** MCF-7, Michigan Cancer Foundation-7; Caco-2, Cancer coli-2; CDKN2A, Cyclin-dependent kinase inhibitor 2A; PIK3CA, Phosphatidylinositol-4, 5-bisphosphate 3-kinase, catalytic subunit alpha, PTEN, Phosphatase and tensin homolog; TP53, gene encodes a major tumor suppressor transcription factor; APC, Adenomatous polyposis coli; MYC, proto-oncogene, bHLH transcription factor, N/A, Not applicable.

### **II.1.5 *Terminalia mantaly* Harvest And Identification**

The TM plant materials were collected from Yaoundé (Cameroon, West Africa). Fresh leaves (TML), stem bark (TMSB), and roots (TMR) were harvested from mature TM plant, and identified at the National Herbarium (Yaoundé, Cameroon) by comparison with a voucher specimen bearing the reference number of 64212/HNC.

## **II.2 METHODS**

### **II.2.1 Green synthesis And Characterization Of Gold And Silver Nanoparticles**

#### **II.2.1.1 TM Samples Preparation And Extraction**

The plant material was washed with distilled water, cut into small pieces, and dried at room temperature (25 °C) in the dark. The aqueous and methanolic TM extracts denoted as <sub>a</sub>TM and <sub>m</sub>TM, respectively, were obtained by maceration procedure. Briefly, 100 g fine powder of TML, TMSB, and TMR samples were soaked in 1 L of either methanol (for 48 hrs) or sterile distilled water (for 72 hrs) at room temperature. The extraction procedure was repeated three times and filtered using Whatman No 1 filter paper. The methanolic filtrates were evaporated to dryness using a rotary evaporator (Büchi 011, Flawil, Switzerland). The aqueous filtrates were lyophilized using a Martin Christ Beta 2–8 lyophilizer (Germany). The extracts were stored at 4 °C for further experiments.

#### **II.2.1.2 Phytochemical Screening Of Crude Extracts**

The presence of the following classes of compounds i.e. alkaloids, flavonoids, glycosides, saponins, and tannins, terpenoids, in the TM extracts was performed according to previously described standard procedures of **Harbone. (1976); Odebeyi and Sofowara. (1978)**. Briefly, 50 mg/mL of <sub>a</sub>TM and <sub>m</sub>TM were subjected to different reagents to determine the presence of various phytochemicals using Mayer's reagent (alkaloids), Shinoda test (flavonoids), Fehling solution (glycosides), froth test (saponins), ferric chloride test (tannins and phenolic), Borntrager's reaction test (anthraquinones), and Libermann-Burchard test (sterols and terpenoids).

##### **🚩 Test For Alkaloids**

Fifty milligrams of plant extracts were diluted in 10 mL of 2 % H<sub>2</sub>SO<sub>4</sub>. The mixture was homogenized and warmed for 2 minutes and then filtered. Five drops of Meyer reagent were added to 1 mL of the filtrate. The development of turbidity indicated the presence of alkaloids (**Odebeyi and Sofowara, 1978**).

#### ✚ Test For Phenols

Fifty milligrams of plant extracts were dissolved in 2 mL of methanol and warmed for 5 minutes. Three drops of freshly prepared ferric cyanide solution (1 mL of  $\text{FeCl}_3$  1 % and 1 mL of  $\text{K}_3\text{Fe}(\text{CN})_6$ ) were added. The formation of a green precipitate indicated the presence of phenols (**Harbone, 1976**).

#### ✚ Test For Triterpenes And Sterols

Fifty milligrams of plant extracts were dissolved in 1 mL of chloroform. To this solution, a few drops of acetic anhydride and sulphuric acid were successively added. The formation of violet-red to the green-blue colour indicated the presence of triterpenes and sterols respectively (**Harbone, 1976**).

#### ✚ Test For Saponins

Fifty milligrams of plant extracts were added to 5 mL of dissolved water. After homogenization, the mixture was heated till boiling temperature. The appearance of the foam of more than 1cm in diameter indicated the presence of saponins (**Harbone, 1976**).

#### ✚ Test For Flavonoids

Fifty milligrams mg of plant extracts were dissolved in 5 mL of methanol. Few crystals of magnesium added followed by HCl solution. A brick-red or violet colouration indicated the presence of flavonoids (**Harbone, 1976**).

#### ✚ Test For Tannins

Fifty milligrams of plant extracts were added to 5 mL distilled water. The mixture was warmed and then filtered. A Few drops of 3 % ferric chloride solution were added to the filtrate. Blue-black or dark-green coloration indicated the presence of tannins (**Harbone, 1976**).

#### ✚ Test For Anthraquinones

Fifty milligrams of plant extracts were diluted in 2 mL of chloroform and 2 mL of ether petrol. The mixture obtained was homogenized and filtered. 1 mL of 10 % NaOH was added to 1mL of the filtrate. The red colour formation indicated the presence of anthraquinones (**Odebeyi and Sofowara, 1978**).

### ✚ Test For Glycosides

One gram of plant extracts was dissolved in 5 mL of HCl and then neutralized by 5 mL of 5 % NaOH. Fehling solution was added drop by drop. The formation of a red precipitate indicated the presence of glycosides (Odebeyi and Sofowara, 1978).

### II.2.1.3 Synthesis Of Biogenic Gold And Silver Nanoparticles

The gold and silver nanoparticles were synthesized following a protocol described by Elbagory *et al.* (2016). The stock concentrations (50 mg/mL) of the aqueous and methanolic extracts were prepared in distilled water. The small-scale synthesis was carried out in a 96 well plate to obtain the optimal concentration of TM extracts and temperature. Briefly, 50  $\mu$ L of  $_a$ TM or  $_m$ TM extracts (at concentrations ranging from 0.78 to 50 mg/mL) were placed in a 96 well plate and 250  $\mu$ L of 3 mM AgNO<sub>3</sub> and 1mM of AuCl<sub>4</sub> and 250  $\mu$ L of 1 mM of sodium tetrachloroaurate (III) dehydrate (Sigma-Aldrich, St Louis, USA) respectively to the plant extracts. The samples were prepared in duplicate plates. One plate was incubated at 25 °C and a second plate at 70 °C while shaking at 40 rpm for 24 hrs. The colour change in the solution was used as an indication of AgNPs and AuNPs formation. The optimum concentration of extracts was used to scale up the AgNPs and AuNPs synthesis from 300  $\mu$ L to 2 mL. The nanoparticles were recovered and washed thrice with distilled water, and centrifuged at 14 000 rpm for 10 min to remove the excess of AgNO<sub>3</sub>, AuCl<sub>4</sub>, and the unreacted Au<sup>3+</sup>, Ag<sup>+</sup> ions, and plant extracts. The TM-AgNPs and TM-AuNPs were resuspended in sterile distilled water and stored at 4 °C.

#### II.2.1.3.1 Measurement Of Nanoparticles Concentrations

The nanoparticles were synthesized using a fixed volume of 1 mL in the Eppendorf tube (2 mL) with a precise scale (Appendix 1). After the formation of nanoparticles, the samples were washed thrice with distilled water and centrifuged at 14 000 rpm for 10 mins. The pellet was collected and dried using the Bock Heater (Johannesburg, South Africa) at 25 °C. Finally, the concentration was deducted using the difference in terms of the mass of NPs in 1 mL using this formula.

$$\text{Mass of nanoparticles(Ug)} = \text{Mass of epindoff tube with NPs(ug)} - \text{Mass of the empty epindoff tube(ug)}$$

#### II.2.1.3.2 Characterisation Of Synthesized TM-AgNPs And TM-AuNPs

The formulated nanoparticles gold and silver nanoparticles were characterized by different analyses including UV-Visible Spectroscopy, Dynamic Light Scattering (DLS), High-

Resolution Transmission Electron Microscopy (HRTEM), Energy-Dispersive X-ray Spectroscopy (EDX), and the selected area electron diffraction (SAED) analyses.

#### (i) UV-Visible Spectroscopy Analysis

The formation of TM-AuNPs and TM-AgNPs was preliminarily confirmed by visual observation for a colour change to red wine, yellowish and dark brown, further by UV-visible spectra after 5-24 hrs synthesis. Sharp peaks obtained from the UV-visible spectrum confirmed the presence of AuNPs and AgNPs at the absorption range between 350 and 700 nm using a POLAR star Omega microplate reader (BMG Labtech, Germany). AuNPs synthesis was up-scaled to 2 mL following the optimum conditions.

#### (ii) Dynamic Light Scattering (DLS) Analysis

The TM-AuNPs and TM-AgNPs were washed 3 times with distilled sterile H<sub>2</sub>O and centrifuged at 10000 rpm for 13 min, the nanoparticles were resuspended in double-distilled sterile H<sub>2</sub>O. The AgNPs and AuNPs were analyzed by Dynamic Light Scattering (DLS) to measure their hydrodynamic size, Zeta potential, and Poly dispersity index (Pdi) using a Zetasizer (Malvern Instruments Ltd., Malvern, UK).

#### (iii) Stability Testing Analysis Of Gold And Silver Nanoparticles

The stability of TM-AuNPs and TM-AgNPs in DMEM (Gibco, UK) cell culture media was tested as described by **Elbagory *et al.* (2019)**. The stability of the TM-AuNPs and TM-AgNPs was evaluated by mixing the TM-AuNPs, TM-AgNPs, and the cell culture medium at a 1:1 ratio and incubating the mixture at 37 °C for 24 hrs. The mixtures of the TM-AuNPs, TM-AgNPs, and the cell culture medium were subjected to UV-Vis analysis after the 24 hrs period. The morphology, core size, and crystallinity, of the more stable TM-AgNPs, and TM-AuNPs were performed.

#### (iv) High-Resolution Transmission Electron Microscopy (HRTEM), Energy Dispersive X-Ray Spectroscopy (EDX) And Selected Electron Diffraction (SAED) Pattern Analysis Of More Stable And Bio-active TM-AuNPs And TM-AgNPs

The morphology, core size, and crystallinity of the bio-active TM-AgNPs and TM-AuNPs were characterized by High-Resolution Transmission Election Microscopy (HRTEM) using an FEI Tecnai G2 20 field-emission HRTEM (Oregon, OR, USA). The HRTEM was also used for Energy Dispersive X-ray (EDX) and Selected Area Electron Diffraction (SAED)

analysis. The samples were prepared by drop-coating one drop of each sample onto a carbon-coated copper grid. The samples were dried under a Xenon lamp for 10 min and analyzed by HRTEM. The transmission electron micrographs were captured in bright field mode at an accelerating voltage of 200 KeV. The EDX spectra were collected using an EDX liquid nitrogen cooled Lithium doped Silicon detector. The TEM micrographs were analyzed using Image J Software (50b version 1.8.0\_60, <http://imagej.nih.gov/ij>).

#### (v) Fourier Transform Infrared (FTIR) Analysis Of Active TM-AgNPs And TM-AuNPs

The Fourier Transform Infrared (FTIR) analysis of the active TM-AgNPs and TM-AuNPs and extracts were performed using a JASCO 460 plus spectrophotometer (Perkin Elmer, Massachusetts, MA, USA) with a frequency ranging from 4,000 to 400 cm<sup>-1</sup>. The FTIR analysis is used to identify the type of bonds in the TM phytochemicals that are involved in the synthesis of the AgNPs and AuNPs. The TM-AgNPs and TM-AuNPs were dried in an oven at 70 °C. The TM extracts, AuNPs, and AgNPs powders were mixed with potassium bromide (KBr) powder and pressed into a pellet before FTIR analysis. Background correction was made using a reference blank KBr pellet. The baseline corrections were performed for all spectra.

### **II.2.2 Evaluate *in vitro* Antibacterial Screening And MIC Determination Of The Bio-active Crude Extracts, Gold And Silver Nanoparticles**

The antibacterial activity of the TM extracts AuNPs and AgNPs was assessed on eight bacterial strains according to the guidelines set by the **Clinical Laboratory Standards Institute (M07A9, 2012)** with slight modifications. Some of the bacterial strains that are listed in **Table 6** were a kind gift from Biodefense and Emerging Infections Research Resources Repository (BEI Resources, Rockville, MD 20,852) and some were purchased from the American Type Culture Collection (ATCC, Manassas, VA, USA)

#### **II.2.2.1 Inoculum Preparation**

The Mueller–Hinton broth (Sigma, MO, USA) was inoculated with single bacterial colonies and the cultures were incubated at 37 °C with shaking at 400 rpm for 18–24 hrs. The bacterial suspensions were subsequently standardized to 0.5 Mc Farland ( $\sim 1.5 \times 10^8$  cells/mL) with OD between 0.08 to 0.12 at 600 and 630 nm. The inoculum was diluted to a final concentration of  $5 \times 10^5$  cells/mL.

### II.2.2.2 Screening Of TM Extracts And Derive TM-AgNPs And TM-AuNPs Against A Panel Of Eight Bacteria Strains

The Mueller–Hinton broth (Sigma, MO, USA) was inoculated with single bacterial colonies and the cultures were incubated at 37 °C with shaking at 400 rpm for 18–24 hrs. The bacterial suspensions were subsequently standardized to 0.5 McFarland ( $\sim 1.5 \times 10^8$  cells/mL) at 630 nm. Each inoculum was diluted to a final concentration of  $5 \times 10^5$  cells/mL and further dispensed in a 96 well plate at 100  $\mu$ L per well. The single point inhibitory effect of TM extracts TM-AuNPs and TM-AgNPs was determined against the eight bacterial strains. To this end, 100

Evaluation of spectrum of inhibition (%) =

$$\left( \frac{\text{Number of strains by the test samples}}{\text{Total numbers of tested strains}} \right) \times 100$$

$\mu$ L of TM extracts (500  $\mu$ g/mL), TM-AuNPs or TM-AgNPs (12.5  $\mu$ g/mL) were individually added to wells containing 100  $\mu$ L of bacteria and the plates were incubated for 24 hrs. Ampicillin was used as a positive control at 128  $\mu$ g/mL. The turbidity of the bacterial culture, which was visually examined, was used as an indication of bacterial growth. The growth inhibition was defined as the absence of the turbidity of the bacterial culture. The susceptibility of the bacterial strains to the TM extracts, TM-AuNPs and TM-AgNPs were expressed as the number of the strains that showed growth inhibition spectra action. The percentage of bacteria inhibited or the spectrum of inhibition was calculated according to the following formula:

The active crude extracts and the nanoparticles that inhibited 75 % of tested bacteria were selected for MIC determination using the microdilution assay as described above.

### II.2.2.3 Dose-Response Studies And Evaluation Of The MIC For Active Extracts And TM-AgNPs

The bacteria were treated with increasing concentrations of the crude extracts (0–500  $\mu$ g/mL) and TM-AgNPs (0 –12.5  $\mu$ g/mL). The negative (untreated) and positive (treatment with ampicillin at 0–128  $\mu$ g/mL) controls were also included. After 24 hrs of treatment, the turbidity of the bacterial suspension was visually assessed as an indication of bacterial growth. The lowest concentration that inhibited the visible growth of bacteria was recorded as the MIC. All the experiments were performed in triplicate.

#### **II.2.2.4 Assess The Growth Inhibitory Kinetics Of Promising Silver Nanoparticles On Susceptible Strains**

The bacterial growth kinetics following treatment with  $\alpha$ TMSB and  $\alpha$ TML-AgNPs was studied using a protocol that was previously published by **Cao *et al.* (2012)**. Briefly, the susceptible bacterial strains were treated with the following concentrations:  $1 \times \text{MIC}$ ,  $1/2 \times \text{MIC}$ , and  $1/4 \times \text{MIC}$  of each AgNPs. Ampicillin was used as a positive control at its MIC value. The assays were performed in triplicate in 96 well plates. The OD of bacterial cultures was measured at 630 nm at different time points (2, 3, 4, 6, 7, and 8 hrs) to monitor bacterial growth rate and the growth curves were plotted as absorbance (OD 630 nm) versus time (hrs).

#### **II.2.3 Assesment The Anproliferative Potential Of Extracts, More Stable Gold And Silver Nanoparticles On Four Resistant Models Cells Line**

##### **II.2.3.1 Effect Of The Nanotherapy On Cell Proliferation: MTT Assay Kit**

**The anticancer effect of crude extracts, more stable nanoparticles was carried out on four cell lines according to the methods described by Sibuyi. (2015).**

##### **II.2.3.1.1 Subculture Of Cells**

The cell lines used in this study were obtained from the American Type Culture Collection. The cell lines were regularly cultured in T25 cm (Sigma) at 37 °C in a 5 % CO<sub>2</sub> culture flasks humidified incubator in DMEM cell culture media. The media was supplemented with 10 % heat-inactivated fetal bovine serum (FBS), 1 % penicillin-streptomycin, and 1 % non-essential amino acid solution. The media were changed and replaced with fresh complete media every three days. The procedures were performed in the Biological Safety Cabinet Class II (Laminar flow) using aseptic techniques.

##### **II.2.3.1.2 Cell Splitting And Trypsinization**

The cells were split when they reached 70 % confluency, the media was removed from the flask using a 10 mL serological pipette into a waste beaker. The cells were rinsed with 3 mL of DPBS and discarded into a waste beaker, 3 mL of 2X trypsin was added to the cells and incubated for 1-3 minutes at 37 °C. As soon as the cells start to round up, the detachment was facilitated by gently tapping the flask on the surface to dislodge the cells. The cells that were still attached to the flask were removed by pipetting. The cells were then transferred to the prelabeled 15 mL conical tubes and centrifuged at 3000 rpm for 5 minutes. The cells were resuspended in 1-5 mL complete media, cell count was performed.



### II.2.3.1.3 Cell Count/ Viability: Trypan Blue Exclusion Assay

Cell viability was performed using trypan blue exclusion assay by the Countess® Automated Cell Counter (Life Technologies) following the manufacturer's instructions. Briefly, 10 µL aliquot of trypsinized cell suspension was mixed with 10 µL of 0.4 % trypan blue dye reagent. 10 µL of the cell-dye mixture was loaded into a Countess™ chamber slide (Life Technologies), followed by cell count, the data readout was given in total cells/mL, live cells/mL, dead cells/mL, and percent viability.

### II.2.3.1.4 Antiproliferative MTT Kit Assay

MTT Cell Proliferation Assay Kit provides a simple method for the determination of cell numbers using standard microplate absorbance readers. The determination of cell growth rates is widely used in the testing of drug action and cytotoxic agents and screening other biologically active compounds.

#### (i) Principle of MTT

The MTT assay involves the conversion of the water-soluble MTT (3-(4, 5-dimethylthiazol-2-yl)-2, 5-diphenyltetrazolium bromide) to an insoluble formazan for 2-4 hrs. The formazan is then solubilized, and the concentration is determined by optical density at 570 nm. This reaction is catalyzed by the mitochondrial succinate dehydrogenase enzyme in metabolically living cells, while dead cells showed no activity to generate reducing equivalents such as NADH and NADPH.

#### (ii) Procedure

The viability of the Caco-2, HepG2, and MCF 7 and the non-cancerous human fibroblast cell line (KMST-6), with crude extracts, more stable gold, and silver nanoparticles was evaluated using the MTT assay as described by **Mmola and co-workers. (2016)** with some modifications. The cells were maintained in DMEM containing 10 % FBS and 1 % pen-strep in a 37 °C humidified incubator with 5 % CO<sub>2</sub> saturation. The cells were seeded in 96-well microtitre plates at a density of  $5 \times 10^5$  cells/100 µL/well. The plates were incubated at 37 °C in a humidified CO<sub>2</sub> incubator. After 24 hrs, the culture medium was replaced with a fresh medium containing the nanoparticles at increasing concentrations of high concentration (**Appendix 1**). The stock solutions of nanoparticles were prepared in ddH<sub>2</sub>O and for the extracts (10 mg/mL) were prepared in 10 % dimethyl sulfoxide (DMSO) and two-fold dilutions from 1000 -7.8125 µg/mL and added to the 96-well plate containing the various cell lines. As a positive control,

cells were treated with 10 % DMSO with the final concentration of 1% in each well. Cells were treated without MTT dyes and DMSO concentrated at 100 % was considered as Blank. Untreated cells were used as the negative control. All treatments were done in triplicate. Thereafter, 100  $\mu$ L of MTT reagent (prepared from 5.0 mg/mL stock solution and diluted with

$$\text{Viability (\%)} = \left( \frac{\text{Average absorbance of test ( treated cells)}}{\text{Average absorbance control (untreated cells)}} \right) \times 100$$

DMEM medium using a dilution factor of 1:10) were added to each well. The cells were incubated at 37 °C for 4 hrs and covered in foil and shook for 1 min in an orbital shaker at RT. The MTT reagent was then removed and replaced with 100  $\mu$ L of alkaline DMSO to dissolve the purple formazan crystals as described by **Wang and colleagues. (2012)** and incubated for 30 min. The absorbance of the formazan product formed was measured at 550-570 nm wavelength ( $\lambda$ ), with background subtracted at the  $\lambda$  of 630 nm using a PolarSTAR Omega plate reader. Each sample point was performed in triplicate. The percentage of cell viability was calculated by comparing the absorbance of the test samples with the absorbance of the control (untreated) samples. The average IC<sub>50</sub> for cancer cells and the cytotoxicity concentration (CC<sub>50</sub>) for normal cell values were determined using GraphPad Prism version 8.0.0 for Windows, GraphPad Software, San Diego, California USA, www.graphpad.com. The percentage of cell viability formula was determined using:

### (iii) Selectivity Index (SI) Of Active Extracts And Nanoparticles

The degree of selective toxicity of the active crude extracts and nanoparticles towards cancer cell lines relative to the non-cancerous cell line (KMST-6) was expressed as the selectivity indexes (SI) as outlined by **Badisa et al. (2009)**. The cancer cell line may either be Caco-2, HepG2, and MCF-7. The SI was calculated as:

$$\text{Selective Index (SI)} = \left( \frac{\text{CC}_{50} \text{ in non-cancerous fibroblast cell (KMST-6)}}{\text{IC}_{50} \text{ in cancer cell line}} \right) \times 100$$

## **II.2.3.1.5 Study The Cell Death Mode Of Action Of The Potent Extracts And Nanoparticles**

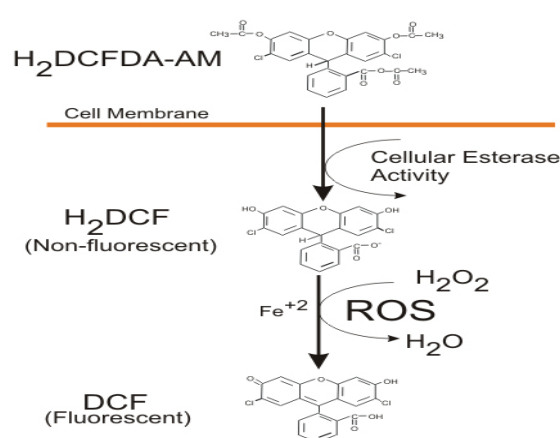
### **II.2.3.1.5.1 Analysis Of Apoptosis Cell Death Induced By Bio-active TM Extracts, TM-AuNPs, And TM-AgNPs**

One of the earliest events to take place during apoptosis is the exposure of phosphatidylserine (PS) residues on the outer leaflet of the cell membrane. Therefore, by exposing cells to fluorescently labeled annexin-V, apoptosis was quantified by the fluorescence intensity measured using flow cytometry (Van, 1998). The percentage of cells undergoing apoptosis was detected and quantified by using the Annexin V-Cy3 Apoptosis Detection Kit (APOAC, Sigma-Aldrich). The cells were seeded in 6 and 12-well culture plates at a density of  $2 \times 10^6$  cells/mL and incubated for 24 hrs at 37 °C. Culture media was then removed and replaced with media containing  $IC_{50}$  AuNPs or AgNPs. The cells were treated with 10  $\mu$ M of cisplatin as a positive control. The cells were then incubated for 24 hrs at 37 °C. Untreated and treated with apoptosis-inducing agents were included as controls. After incubation, all the media from each well containing floating cells were transferred to 15 mL conical tubes using a sterile pipette. The wells were washed with 1 mL DPBS and transferred into the corresponding 15 mL conical tubes containing floating cells. The supernatant was discarded, the pellet was gently re-suspended in APOAC dye (For 10 mL of dye, 100  $\mu$ L of Annexin V Cy3.18 Conjugate (100 mg/mL solution, Catalog Number A 4963, 100  $\mu$ L of 50 mM 6-CFDA in acetone solution, 10 mL Binding Buffer (Catalog Number B9796). The cells were washed three times with 200  $\mu$ L of 1X Binding Buffer each. 100  $\mu$ L of the Double Label Staining Solution (AnnCy3 and 6-CFDA) were added on each 15 mL tube and were covered with aluminum foil. The cells were incubated for further 10 minutes at 37 °C, and 200  $\mu$ L of buffer was added to each tube and centrifuged at 3000 rpm for 5 minutes at RT. The supernatant was discarded and the cell pellets were re-suspended in 200  $\mu$ L of 10 X Binding Buffer on each tube and covered with aluminum foil. The staining was measured by Attune Acoustic flow cytometer (Applied Biosystems, Germany) or Accuri flow cytometer (BD Biosciences). The acquisition was done, in log mode and a maximum of 10000 to 30 000 events per sample was acquired and analyzed using Attune software (Applied Biosystems, German) and Flowjo software.

### II.2.3.1.5.2 Mitochondrial Dysfunction: ROS Activity Of Bio-active TM Extracts, TM-AuNPs And TM-AgNPs

#### (i) Principle Of Chemical Reaction Of H<sub>2</sub>DCFDA

DCFDA-Cellular Reactive Oxygen Species (ROS) assay Kit (ab113851) uses the cell-permeant reagent 2',7'-dichlorofluorescein diacetate (DCFDA, also known as H<sub>2</sub>DCFDA and as DCFH-DA), a fluorogenic dye that measures hydroxyl, peroxy, and other reactive oxygen species (ROS) activity within the cell. DCF is a highly fluorescent compound that is detected by fluorescence spectroscopy with excitation-emission at 495 nm / 529 nm.



#### (ii) Procedure

The intracellular ROS generation in cells exposed to the active crude extracts, AuNPs and AgNPs was investigated using the 5-(and-6)-chloromethyl-2', 7'-dichlorodihydrofluorescein diacetate acetyl ester (CM-H<sub>2</sub>DCFDA) fluorescence probe (Life Technologies). The Caco-2, HepG2 and MCF-7, cells were seeded in a 6 and 12 well plate at  $2 \times 10^5$  cells/mL and cultured at 37 °C overnight. The cells were treated with bio-active crude extracts, AgNPs and AuNPs at IC<sub>50</sub> for 24 hrs. The cells were treated with 0.1 % H<sub>2</sub>O<sub>2</sub> a positive control induction of ROS. Cells were detached using trypsin, washed twice with 2 mL of 1X PBS, and resuspended in 350  $\mu$ L of 7.5  $\mu$ M DCFH-DA prepared in PBS. The pellets were resuspended in 350  $\mu$ L 1X PBS. The mean fluorescence intensity in the cells was determined by Attune or Accuri flow cytometers.

### II.2.3.1.5.3 Cell Cycle Assay of Bio-active TM Extracts, TM-AuNPs, And TM-AgNPs Using Flow Cytometry

The propidium iodide (PI) is a commonly used fluorescent dye for staining DNA in cells. Because it intercalates into the DNA, the fluorescence signal exhibited by PI is directly related to

the amount of DNA within cells. DNA content varies with respect to the cell cycle phase, the percentages of cells in each phase of the cell cycle can be quantified by flow cytometry analysis of PI-stained cells. The Caco-2, HepG2, and MCF-7 cells were seeded in a 12 well plate at  $2 \times 10^6$  cells/mL and cultured at 37 °C overnight. The cells were treated with bio-active TM extracts, TM-AuNPs, TM-AgNPs, at their specific IC<sub>50</sub> for 24 hrs. The cells were treated with 10 µM of cisplatin a positive control. Cells were detached using 400 µL of trypsin-EDTA to each well, washed twice with 2 mL of 1X PBS. Then, the harvested cells were fixed in 70 % ethanol at 20 °C for 2 weeks to permeabilize the cell membrane for efficient dye loading of the relatively impermeable PI dye. After the fixation, the cells were washed with 2X in PBS. Spin at 3000 g in a centrifuge, then, 50 µL of RNA were added (1 mL of RNA (100 µg/mL stock of RNase) prepared in 9 mL of 1X PBS This will ensure only DNA, not RNA, is stained and 200 µL of the fluorescent nucleic acid stain, PI was added (400 uL of PI (50 µg/mL stock solution prepared in 9.6 mL of 1x PBS). The mean fluorescence intensity in the cells was determined by measuring the forward scatter (FS) and side scatters (SS) to identify single cells by Attune or Accuri flow cytometers.

#### **II.2.4 Statistical Analysis**

The values were analyzed using two-way ANOVA using GraphPad Prism version 8.0.0 for Windows, GraphPad Software, San Diego, California USA, [www.graphpad.com](http://www.graphpad.com). Data are expressed as mean  $\pm$  SD of experiments performed in triplicate. Error bars represent the SD and \* $p < 0.0001$ .



*Chapter III:*  
*Results and Discussion*

## CHAPTER III: RESULTS AND DISCUSSION

### III.1 Results Of Green synthesis And Characterization Of Gold And Silver Nanoparticles

The green sources used, the plant extracts are readily available, provide an easy, cost-effective, and simple method that involves just one-step synthesis. Herein we report the enhanced antibacterial potential of twelve AgNPs and twelve AuNPs characterized and synthesized from six aqueous and methanolic extracts prepared of *Terminalia mantaly* plant. The synthesis process was monitored under two different temperature conditions to measure the effect of temperature on the geometric properties of the synthesized AgNPs and AuNPs. The several physical and optical measurement techniques including, Ultraviolet-Visible Spectroscopy (UV-Vis), Dynamic Light Scattering (DLS), High-Resolution Transmission Electron Microscopy (HR-TEM), and Energy-dispersive X-ray spectroscopy (EDX), FTIR were used to characterize the AgNPs and AuNPs and were led to several results.

#### III.1.1 Phytochemicals Composition

The phytochemical composition of TM extracts in **Table 6**, revealed an unequal distribution of different secondary metabolites in both water and methanolic plant extracts. The alkaloids, flavonoids, glucosides, and total phenols were present in all the extracts, and no anthocyanins were found in any of the TM extracts. The <sub>a</sub>TM extracts contained the majority of the phytochemicals, while all the <sub>m</sub>TM extracts lacked steroids. Tannins and triterpenes were not present in TMSB and TMR; TMR and TML lacked anthraquinones. These metabolites contain active functional groups, such as hydroxyl, aldehyde, and carboxyl units, that may play pivotal roles in the chemical reduction processes of gold precursors to produce AgNPs (**Kumar *et al.*, 2012**) and AuNPs (**Ankanwar *et al.*, 2010**). A similar result was reported on other *Terminalia* species by co-workers such as (**Garcez *et al.*, 2003**; **Nagappa *et al.*, 2003**; **Shah *et al.*, 2011**; **Edison and Sethuraman, 2012**; **Gopinath and Arumugam, 2013**).

**Table VI:** Phytochemical composition of TM extracts.

TM Extracts	Alkaloids	Phenolic content	Flavonoids	Tanins	Anthocyanins	Antraquinones	Steroids	Triterpenes	Glucosides	Saponins
<b><sub>a</sub>TMSB</b>	+	+	+	+	-	+	+	+	+	+
<b><sub>m</sub>TMSB</b>	+	+	+	-	-	+	-	-	+	+
<b><sub>a</sub>TMR</b>	+	+	+	+	-	+	-	-	+	+
<b><sub>m</sub>TMR</b>	+	+	+	-	-	-	-	-	+	+
<b><sub>a</sub>TML</b>	+	+	+	+	-	+	+	+	+	+
<b><sub>m</sub>TML</b>	+	+	+	+	-	-	-	+	+	-

**Abbreviations:** TM, *Terminalia mantaly*; TML, TM leaf extract; TMSB, TM stem bark extract; TMR, TM root extract; TML-AgNPs, AgNPs from TM leaf extract; TMSB-AgNPs, AgNPs from TM stem bark extract; TMR-AgNPs, AgNPs from TM root extract, <sub>a</sub> – represents aqueous extracts, <sub>m</sub> – represents methanolic extract.

### III.1.2 Physical Formation Of TM-AgNPs And TM-AuNPs

Small scale AuNPs and AgNPs synthesis were carried out in a 96 well microplate by incubating the fixed concentration of gold (1 mM) and silver (3 mM) salt with increasing concentrations of TM extracts (12.5 to 0.39 mg/mL) within 3 seconds to 5 hrs for AuNPs and 24 hrs for AgNPs. The variation in colours is also dependent on the concentration of the extracts and the temperature applied in the synthesis of the AgNPs and AuNPs.

For biogenic silver nanoparticles **Figure 22, Appendix 2** shows that <sub>a</sub>TMR-AgNPs, <sub>m</sub>TML-AgNPs, <sub>m</sub>TMSB-AgNPs, and <sub>m</sub>TMR-AgNPs produced a yellow colour, while the <sub>m</sub>TML-AgNPs produced a green colour and <sub>a</sub>TMSB-AgNPs produced a brown colour. This is a highly unusual reported AgNPs formation with clear yellowish to brown colours (**Kannan *et al.*, 2014; Govindappa *et al.*, 2016**): The colour of colloidal solutions of AgNPs can vary from yellow-green to blue (**Figure 22**), depending on the size and morphology of synthesized nanoparticles as demonstrated by **Raza *et al.* (2016)**. For AuNPs, the formation of TM-AuNPs was visually observed with the formation of red wine/ruby red colour of the reaction mixture within 3 seconds after addition of TM extracts to the gold salt as shown in **Figure 23, Appendix 3**. The results were obtained by some authors on *Terminalia arjuna* and *Terminalia catappa* (**Ankamwar, 2010**). The appearance of red wine colour in the reaction suggests the formation of AuNPs (**Ankamwar, 2010; Singh *et al.*, 2012; Elia *et al.*, 2014**)



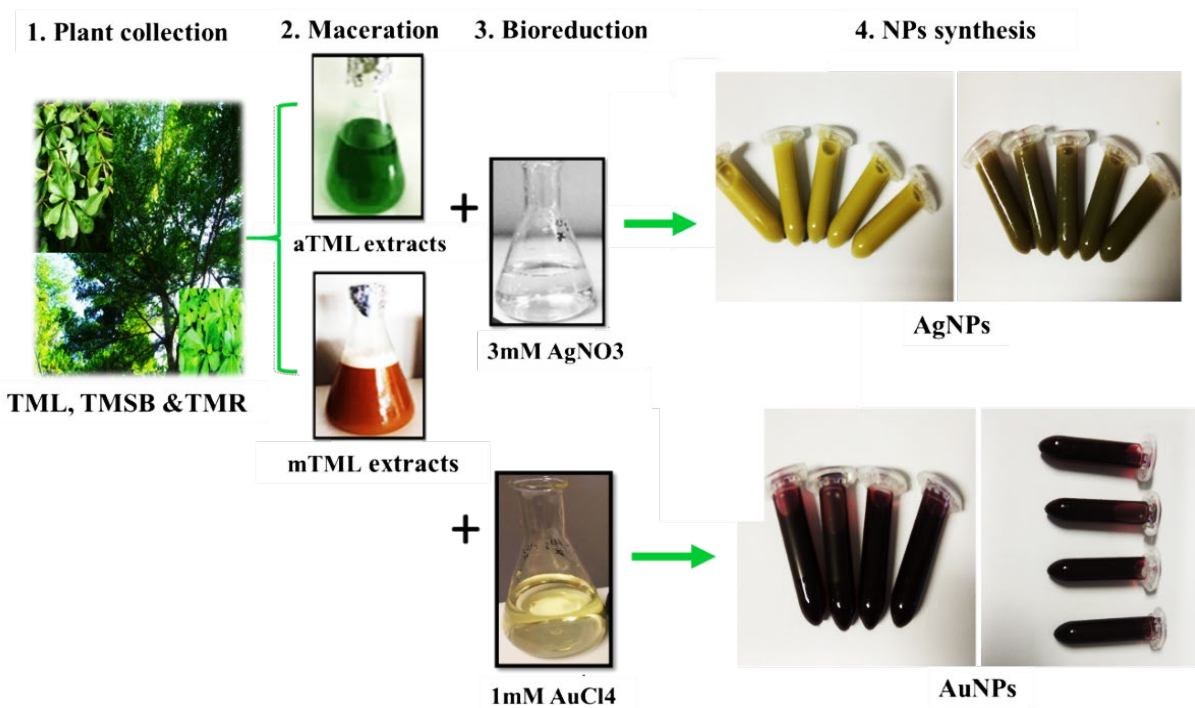


**Figure 20:** One-step synthesis of TM-AgNPs and TM-AuNPs by reduction of gold and silver ions with TM phytochemicals. Colour change denoted the presence of AuNPs and AgNPs.

Note: Aqueous and methanolic TM extracts were used to reduce AgNO<sub>3</sub> into AgNPs, and AuCl<sub>4</sub> into AuNPs, colour change indicates NP formation.

**Abbreviations:** AuNPs, gold nanoparticles; AgNPs, silver nanoparticles; TM, *Terminalia mantaly*; TML, TM leaf extract; TMSB, TM stem bark extract; TMR, TM root extract, a – represents aqueous extracts, m – represents methanolic extracts.

The variation in colours depended on the concentration of the extracts and the temperature applied in the synthesis of the biogenic AgNPs (Moodley *et al.*, 2018) and AuNPs (Ankamwar, 2010). In the one-step reaction, the TM extracts acted as both the reducing, stabilizing and capping agents. The bio-reduction of Ag<sup>+</sup> and Au<sup>3+</sup> ions precursor could be ascribed to various phytochemicals present in the plant extracts such as alkaloids, flavonoids, tannins, steroids, and triterpenes (Table 6) (Huang *et al.*, 2007). The functional groups (hydroxyl, aldehyde, and carboxyl groups) in the extracts play a huge role in the reduction of AuCl<sub>4</sub> into AuNPs and AgNO<sub>3</sub> into AgNPs (Shankar *et al.*, 2004). The phenols due to the scavenging capabilities of their –OH groups have been reported to be involved in the bio-reduction and stabilization of NPs (Ankamwar, 2010). The phenolic compounds along with the water do

mains can synergistically interact with the existing nuclei and lay the foundation to create highly structured sheets of zerovalent gold (Lee *et al.*, 2016).

### III.1.2.1 UV visible Spectrophotometric And Dynamic Light Scattering Analyses Of TM-AuNPs And TM-AgNPs

The green synthesis of AuNPs and AgNPs was directly following by the two characterizations including UV visible spectrophotometric and Dynamic Light Scattering analyses.

#### III.1.2.1.1 UV Visible Spectrophotometric Analyses Of TM-AuNPs

The reaction kinetics of the TM-AuNPs was monitored using a UV-visible spectrophotometer. The optical properties of different TM-AuNPs at 5 hrs are shown in its UV-Vis spectra (**Figure 24**). Their SPR ranged from 535 to 560 nm, which is within the SPR range for AuNPs (Jafarizad *et al.*, 2015). The <sub>a</sub>TMSB-AuNPs-25 °C had the highest intensity at their SPR (560 nm), and a weak plasmon band was observed for <sub>a</sub>TMR-AuNPs-25 °C at 535 nm (**Figure 23, Table 7**). An increase in the absorbance spectra indicates a higher production of AuNPs (Liu *et al.*, 2019). The concentration of extracts plays an important role to control the size and morphology of AuNPs. The variations in the  $\lambda_{max}$  values (SPR) and concentrations of TM-AuNPs vary with the amounts and the quality of phytochemicals present in the TM extracts (**Table 6**). The red wine colour exhibit by AuNPs in water is due to the excitation of Surface Plasmon vibrations (Liu *et al.*, 2019). Furthermore, the SPR of the AuNPs can be affected by factors such as the shape, size, the refractive index of the dispersion medium, and the average distance between neighboring AuNPs (Guo *et al.*, 2015). The UV-Vis spectra of TM-AuNPs (**Figure 21**).

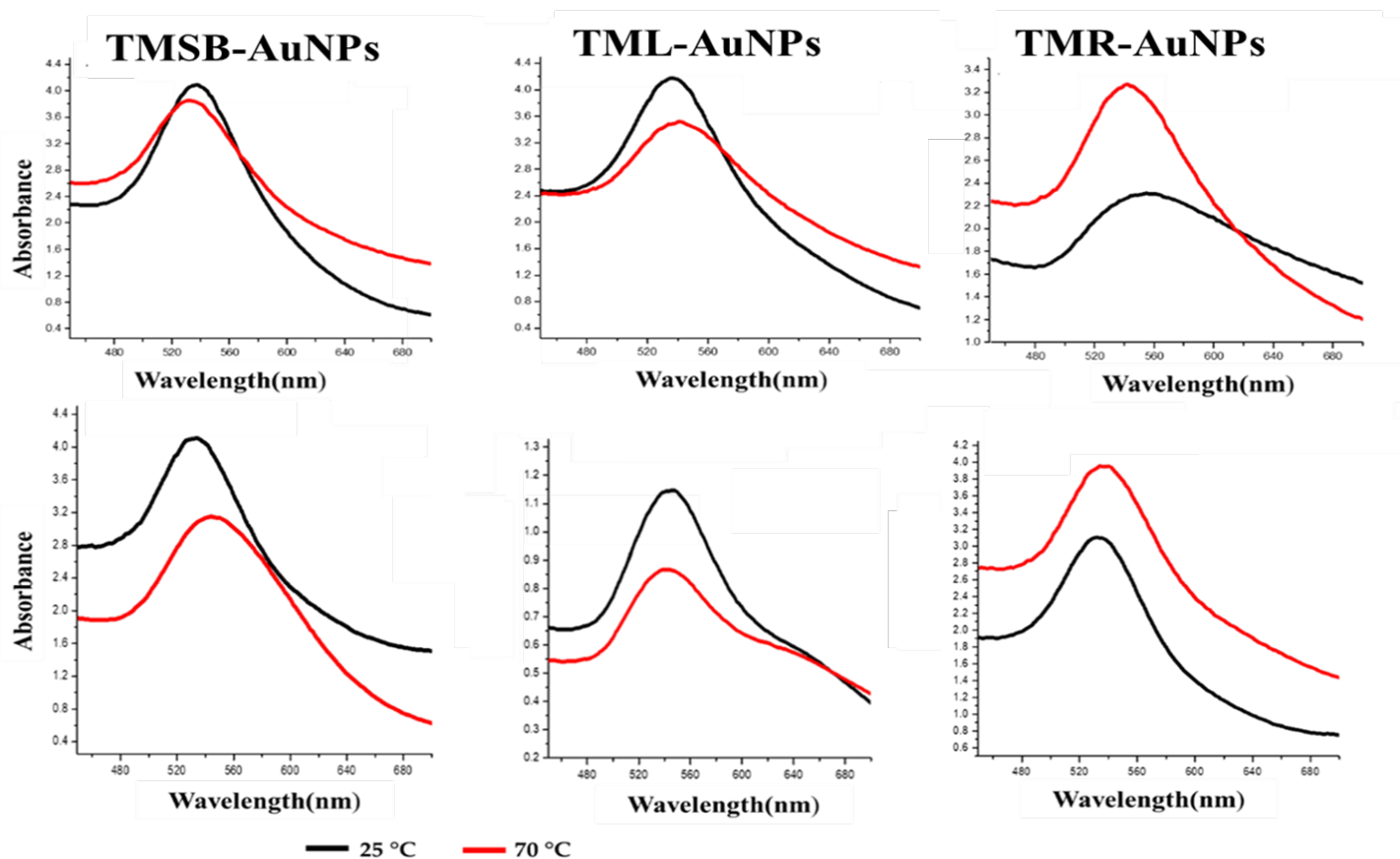


**Figure 21:** UV-vis spectral profiles of TM-AuNPs synthesized at 25 °C and 70 °C.

**Note:** AuNPs were synthesized by reducing AuCl<sub>4</sub> with aqueous and methanolic TM extracts. The optical properties of the NPs were measured by UV-vis spectrophotometry.

**Abbreviations:** AgNPs, silver nanoparticles; TM, *Terminalia mantaly*; TML-AuNPs, AuNPs from TM leaf extract; TMSB-AuNPs, AuNPs from TM stem bark extract; TMR-AuNPs, AuNPs from TM root extract, SPR, Surface plasmon resonance.

The SPR may be related to the amount of the NPs produced, as the OD-value correlates linearly with the concentration of the AuNPs in a solution (**Rastogi and Arunachalam 2012**). There is a significant difference between the bands generated at 25 °C and 70 °C. On the other hand, the sharper bands were also observed at 70 °C with most of the extracts but less asymmetric as compared to 25 °C. It is generally recognized that UV-Vis spectra could be used to examine the size and shape of AuNPs (**Elia et al., 2014; Ngumbi et al., 2018**). The surface plasmon band in the TM-AuNP solution was at  $\geq 535$  nm for all AuNPs, suggesting that these particles are dispersed uniformly in the aqueous solution with no evidence of aggregation (**Abdelhalim et al., 2012**).

### III.1.2.1.2 UV Visible Spectrophotometric Analyses Of TM-AgNPs

Due to surface plasmon resonance (SPR), UV-vis spectrophotometric analysis of AgNPs that are between 10 and 100 nm in size typically produces absorbance peaks ( $\lambda$  max) from 400 to

500 nm. As shown in **Figure 22** and **Table 7**, the absorbance peaks of the TM-AgNPs ranged from 438 to 480 nm. This also confirms the presence of AgNPs following the reactions using TM extracts. The flavonoids and phenolic compounds are the major components in the TM extracts (Ngouana *et al.*, 2015). These phenolic and hydroxylated constituents are most likely responsible for the reduction of AgNO<sub>3</sub> to form the AgNPs (Sharma *et al.*, 2018). The peak intensity of AgNPs synthesized at 70 °C was significantly higher, which suggests that the concentration of the NPs was higher at 70 °C than at 25 °C. Based on UV-vis spectrophotometric analysis, the synthesis of *m*TMSB-AgNPs and *m*TML-AgNPs at 25 °C was not very successful as the peak intensities for these AgNPs were very low. The absorbance peaks for *m*TMR-AgNPs, *a*TMSB-AgNPs and *a*TML-AgNPs produced at 70 °C were much sharper compared to the absorbance peaks for *a*TMR-AgNPs, *m*TMSB-AgNPs and *a*TML-AgNPs (also produced at 70 °C). This suggests that *m*TMR-AgNPs, *a*TMSB-AgNPs and *a*TMR-AgNPs, *a*TML-AgNPs are smaller and more uniform than *m*TMSB-AgNPs and *m*TML-AgNPs.

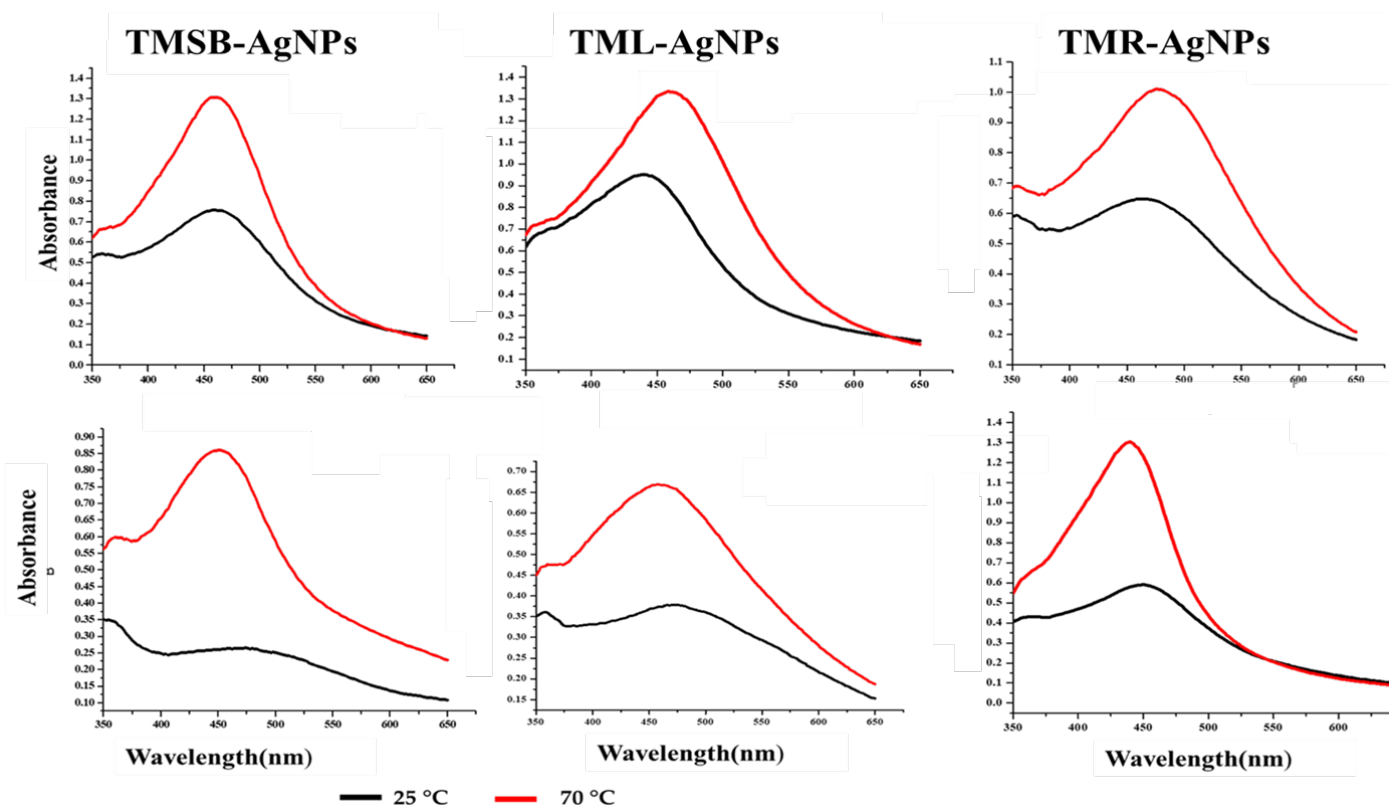


**Figure 22:** UV-vis spectral profiles of TM-AgNPs synthesized at 25 °C and 70 °C.

**Note:** AgNPs were synthesized by reducing AgNO<sub>3</sub> with aqueous and methanolic TM extracts. The optical properties of the NPs were measured by UV-vis spectrophotometry.

**Abbreviations:** AgNPs, silver nanoparticles; TM, *Terminalia mantaly*; TML-AgNPs, AgNPs from TM leaf extract; TMSB-AgNPs, AgNPs from TM stem bark extract; TMR-AgNPs, AgNPs from TM root extract, SPR, Surface plasmon resonance.

The size distribution, charge, and surface chemistry of NPs are particularly important since they strongly influence the mobility and bioavailability of NPs within the physiological conditions; and can be used to predict their state in solution (**Pavlin and Vladimir, 2012**).

### III.1.2.2 Dynamic Light Scattering Analyses (DLS) Of TM-AuNPs And TM-AgNPs

The hydrodynamic diameter, zeta potential, and polydispersity index (Pdi) of the TM-AuNPs and TM-AgNPs were measured by the DLS analysis. The sizes of the TM-AgNPs and TM-AuNPs varied depending on the extract used for the synthesis and temperature (25 °C versus 70 °C). The hydrodynamic diameter ranged from 39 to 79 nm and 11 to 83 nm for TM-AuNPs and TM-AgNPs respectively as shown in **Table 7**. For AuNPs, the extracts (<sub>m</sub>TML, <sub>a</sub>TMR, and <sub>m</sub>TML) produced AuNPs with sizes that differ slightly at the two temperatures. A significant difference was observed for TMSB (aqueous and methanolic) and <sub>a</sub>TMR extracts produced smaller sized (39, 44 and 66 nm) NPs at 25 °C, the sizes increased by  $\geq 8$  nm at 70 °C; while the size difference in others was negligible (1-4 nm). The change in size at high temperatures could be due to various factors, the reducing and capping agents at 25 °C might be different at high temperatures (70 °C). At high temperatures, the active phytochemicals at 25 °C might be preserved and others will then act as reducing agents (**Amendola et al., 2017**). An independent study also reported that at low temperatures the sizes of AuNPs produced from plant extracts were significantly small (**Zhang et al., 2018**). Therefore, this data suggest that temperature could be one of the critical parameters controlling the size of NPs. For AgNPs, the Small sizes of 11 nm were obtained with <sub>a</sub>TML-AgNPs-25 °C and the higher size of 56 and 83 nm with <sub>m</sub>TMR-AgNPs-25 °C, <sub>a</sub>TMSB-AgNPs-70 °C respectively. For AgNPs, the TML extract produced smaller AgNPs compared to the other extracts. Zeta potential provides pivotal information on the dispersion of NPs as the magnitude of the charge and indicates the mutual repulsion (**Clayton et al., 2016**). Additionally, zeta potential is an important parameter used to assess the charge of the NP surface and predicts the long-term stability of the nanoparticles. Nanoparticles with negative zeta potential values suggest there are strong repulsion forces between the NPs, which will prevent the agglomeration of the NPs in solution. Nanoparticles with a zeta potential within +30 mV to -30 mV range are considered to be stable (**Chanda et al., 2011; Cooper, 2015**), while those outside this range will likely aggregate due to inter-particle van der Waal's attractions. The zeta potential of the synthesized TM-AgNPs ranged from -12 to -37 mV. The TMSB-AgNPs were the only NPs with zeta potential

values outside this range (-34 and -37 mV for TM-AgNPs synthesized at 25 °C and 70 °C, respectively) (**Table 7**). This suggests that all the TM-AgNPs except for TMSB-AgNPs are stable. The TM-AuNPs had Zeta potential values that ranged from -10 to -37 mV. This indicates that the NPs repel each other with no tendency to aggregate as they possess the compulsory repulsive forces to remain stable when in solution (**Grabinski, 2015; Clayton et al., 2016**). As well, except for the <sub>m</sub>TML-AuNPs, all the TM-AuNPs are highly stable.

The polydispersity index (Pdi), which is an indication of uniformity, is an important parameter of NPs to consider when assessing the application of NPs, since Pdi can affect the surface conjugation chemistry and nanoparticle aggregation (**Clayton et al., 2016**). According to the International Organization For Standardization (ISO), NPs with a Pdi > 0.5 indicate that the NPs are polydispersed and non-uniform (**Zhang et al., 2018**), while a Pdi < 0.5 indicates that the NPs are mostly uniform or monodispersed (**Elbagory and co-workers, 2016; Mervat et al., 2019**). NPs with low Pdi value is likely to be monodispersed. The polydispersity index (Pdi) of various TM-AuNPs at different temperatures is also shown in Table 3. Based on the Pdi values obtained the TM-AgNPs such as <sub>a</sub>TML-AgNPs, <sub>a</sub>TMSB-AgNPs, <sub>a</sub>TMR-AgNPs and <sub>m</sub>TMR-AgNPs synthesised at 25 °C are monodispersed. Similarly, <sub>a</sub>TML-AgNPs and <sub>a</sub>TMSB-AgNPs synthesised at 70 °C are also monodispersed. The TM-AuNPs had Pdi range between 0.4-0.7 (**Table 6**) and were mainly monodispersed and less aggregated at 25 °C. NPs are known to agglomerate in the presence of salts due to a reduction in the electronic double layer around each particle, allowing for adhesion through van der Waals forces (**Mittal et al., 2014**). The <sub>a</sub>TML-AuNPs had a Pdi of 0.6 at 25 °C, indicating that these NPs might be aggregated, this could happen because some components in the buffer absorb on the surface of the gold salt and form crosslinks in between the AuNPs. However, an increase in size for <sub>m</sub>TMR-AuNPs resulted in polydispersed NPs as reflected by a change Pdi (0.4) at 25 °C to a Pdi = 0.5 at 70 °C. The change may be due to a decrease in NP surface area. The TM-AuNPs with the lower Pdi values indicate that the AuNPs could be monodispersed, uniform in size and shape, no aggregation, and are stable in colloidal form.

**Table VII:** SPR and DLS analysis of TM-AgNPs and TM-AuNPs synthesized at 25 °C and 70 °C.

TM-NPs	NPs parameters									
	25 °C					70 °C				
	[Extract] (mg/mL)	$\lambda_{max}$ (nm)	PD (nm)	Pdi	ZP (mV)	[Extract] (mg/mL)	$\lambda_{max}$ (nm)	PD (nm)	Pdi	ZP (mV)
<sup>a</sup> TML-AgNPs	0.78	438	11	0.50	-24	1.56	460	18	0.40	-26
<sup>a</sup> TML-AuNPs	1.56	540	43	0.60	-37	1.56	545	44	0.70	-35
<sup>m</sup> TML-AgNPs	1.56	474	44	0.60	-22	1.56	458	22	0.80	-29
<sup>m</sup> TML-AuNPs	3.12	544	55	0.4	-29	1.56	544	51	0.50	-10
<sup>a</sup> TMSB-AgNPs	0.78	464	28	0.22	-34	1.56	460	56	0.46	-37
<sup>a</sup> TMSB-AuNPs	1.56	545	39	0.50	-27	1.56	540	57	0.30	-28
<sup>m</sup> TMSB-AgNPs	1.56	480	60	0.62	-12	1.56	458	58	0.53	-12
<sup>m</sup> TMSB-AuNPs	1.56	550	44	0.50	-36	1.56	535	52	0.50	-29
<sup>a</sup> TMR-AgNPs	3.12	472	39	0.40	-23	3.125	478	30	0.88	-24
<sup>a</sup> TMR-AuNPs	6.25	560	66	0.70	-32	6.25	550	79	0.80	-29
<sup>m</sup> TMR-AgNPs	0.78	450	83	0.48	-22	0.78	438	67	0.51	-28
<sup>m</sup> TMR-AuNPs	1.56	540	44	0.40	-30	1.56	550	48	0.50	-32

**Abbreviations:** AuNPs, gold nanoparticles, AgNPs, silver nanoparticles; TM, *Terminalia mantaly*, <sup>a</sup>, represents aqueous extracts ;<sup>m</sup>, represents methanolic extracts; TML-AgNPs, AgNPs from TM leaf extracts; TMSB-AgNPs, AgNPs from of TM stem bark extracts; TMR-AgNPs, AgNPs from TM root extracts; SPR, surface plasmon resonance; UV, ultraviolet; PD, particle diameter; ZP, Zeta potential; Pdi, Polydispersity index; DLS, dynamic light scattering.

### III.1.3 HRTEM, SAED, EDX Analyses And FTIR Analyses Of Bio-Active TM-AgNPs and TM-AuNPs

#### III.1.3.1 HRTEM And SAED Pattern Of Bio-Active TM-AgNPs

The morphology and size of <sup>a</sup>TML-AgNPs and <sup>a</sup>TMSB-AgNPs varied as demonstrated by the HRTEM micrographs in **Figure 25**. The AgNPs displayed heterogeneous and polydispersed characteristics. The TML produced mostly spherical AgNPs at 25 °C whereas the same sample produced various geometric shapes such as triangular, tetrahedral, and hexagonal shapes at 70 °C. Similar shapes as those of TML-AgNPs were observed in AgNPs synthesized by the <sup>a</sup>TMSB extract. These anisotropic shapes were likely due to the reducing and capping phytochemicals which not only provided thermodynamic stability but also defined the NP bio-activities (**Kumar et al., 2012**). The crystalline nature of the biogenic AgNPs was confirmed by their SAED patterns highlighted in **Figure 26**. The Bragg reflection planes on the face-centered cubic (fcc) patterns of TM-AgNPs, i.e. (111), (200), (220), (311), and (331) matched those in the database of the Joint Committee on Powder Diffraction Standards (JCPDS no. 00-

004-0784, USA) (Bagherzade *et al.*, 2017; .Singh *et al.*, 2018) and confirmed that the synthesized AgNPs are composed of pure crystalline silver. These findings are further supported by similar fcc patterns reported for the AgNPs synthesized from *Cannabis sativa*. (Bagherzade *et al.*, 2017; Escárcega-González *et al.*, 2018; Singh *et al.*, 2018).

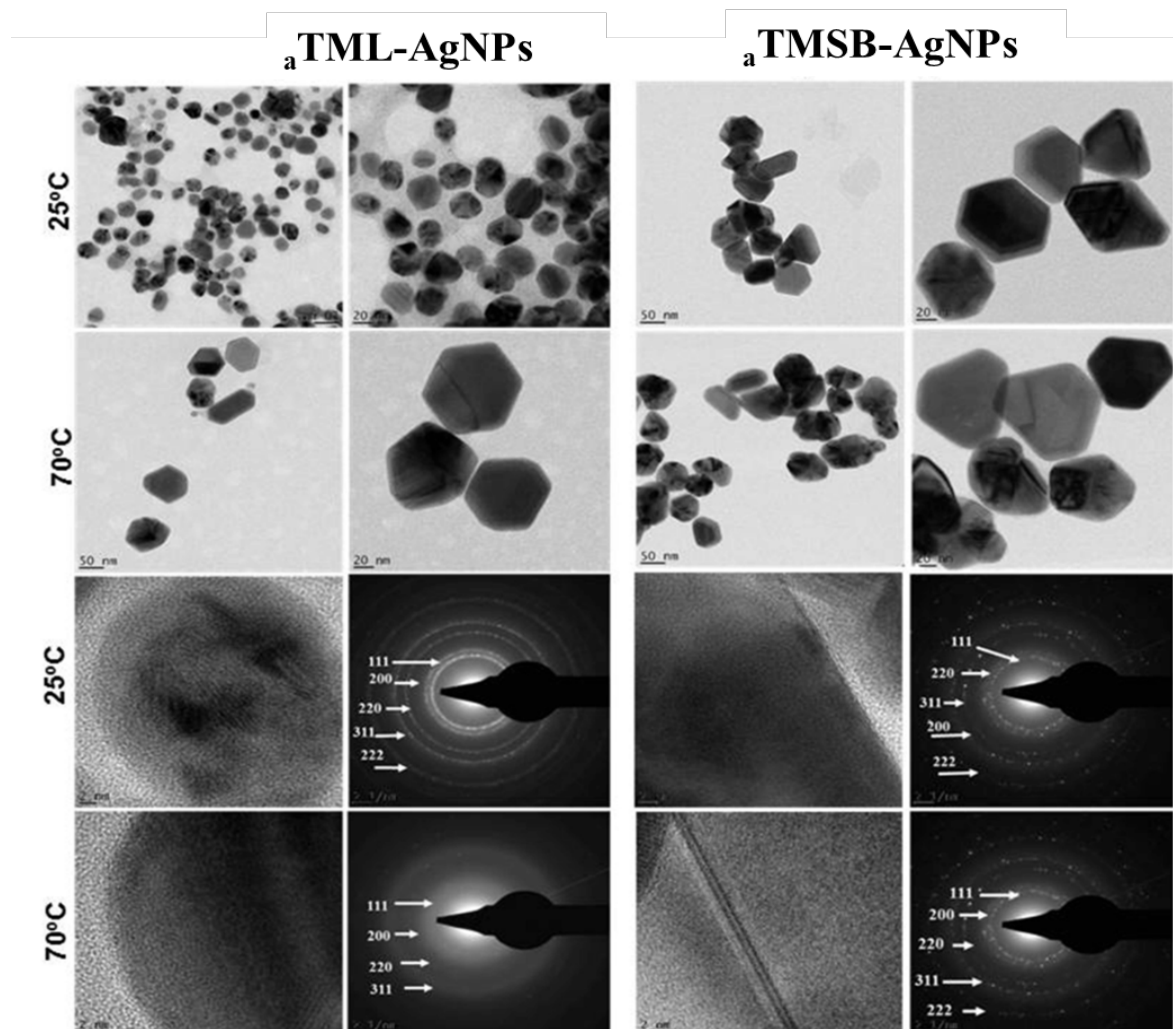


**Figure 23:** HRTEM micrographs and SAED patterns of selected TM-AgNPs.

**Notes:** The size, shape (A) and SAED patterns (B) of  ${}^a\text{TML-AgNPs-25 } ^\circ\text{C}$  and  ${}^a\text{TMSB-AgNPs-70 } ^\circ\text{C}$  AgNPs were analyzed by HRTEM. Scale bar from 20 to 50 nm.

**Abbreviations:** AgNPs, silver nanoparticles; TM, *Terminalia mantaly*;  ${}^a\text{TML}$ , aqueous TM leaf extract;  ${}^a\text{TMSB}$ , aqueous TM stem bark; HRTEM, High resolution transmission electron microscope; SAED, selected area electron diffraction.

The size distribution of TM-AgNPs was calculated from the HRTEM micrograph, the representative histograms (Figure 26) demonstrate that  ${}^a\text{TML-AgNPs-25 } ^\circ\text{C}$  and  ${}^a\text{TMSB-AgNPs-70 } ^\circ\text{C}$  synthesized at 25 °C and 70 °C had a diameter of 9.3 and 6.2 nm, respectively. The



$^a$ TMSB-AgNPs-70 °C produced at 70 °C had a smaller core size (6.2 nm), this might suggest that TMSB might be richer in reducing and capping agents. These results were comparable to those reported by **Zakir *et al.* (2014)** on AgNPs synthesized from leaf extract obtained from *Terminalia catappa*. The NPs were also spherical in morphology, with average sizes ranged from 55-71 nm. Generally, the sizes were smaller and could be directly correlated to the observed activity of TM-AgNPs.

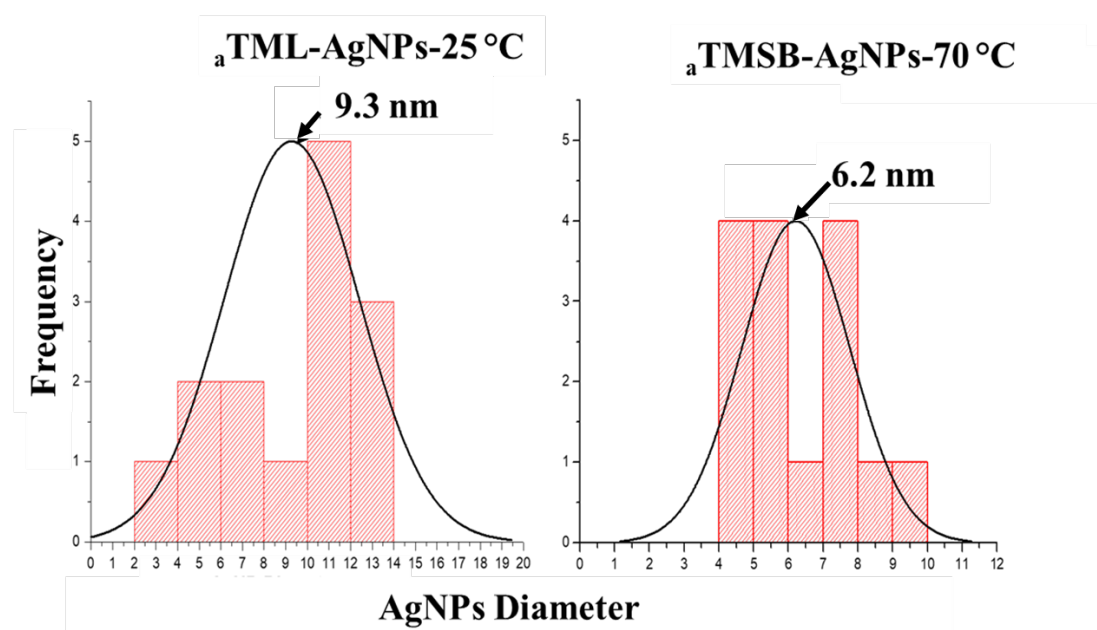


**Figure 24:** Particles size distribution of more stable and bioactive TM-AgNPs.

**Note:** The size, shape were analyzed by HRTEM. Scale bar from 20 to 50 nm using Image G and origin software. The diameter of 9.3 and 6.2 nm was obtained with  $^a$ TML-AgNPs and  $^a$ TMSB-AgNPs.

Abbreviations: AgNPs, silver nanoparticles; TM, Terminalia mantaly;  $^a$ TML, aqueous TM leaf extract;  $^a$ TMSB, aqueous TM stem bark; HRTEM, High Resolution Transmission Electron Microscope.

### III.1.3.1.1 EDX Of Bio-active TM-AgNPs

The Energy Dispersive Absorption photographs of the selected TM-AgNPs in **Figure 27** displays the  $\text{Ag}^+$  peaks at 3 keV. Metallic AgNPs typically show a strong signal peak at this position due to their SPR (**Prakash *et al.*, 2013**). The peaks of other elements such as Cu and C were also detected, where C corresponds to the organic matrix and lacey carbon on the TEM grid, Cu is observed since the grid is made up of Cu, and the S, Si, Cl and N peaks correspond to the molecules capping the TM-AgNPs.

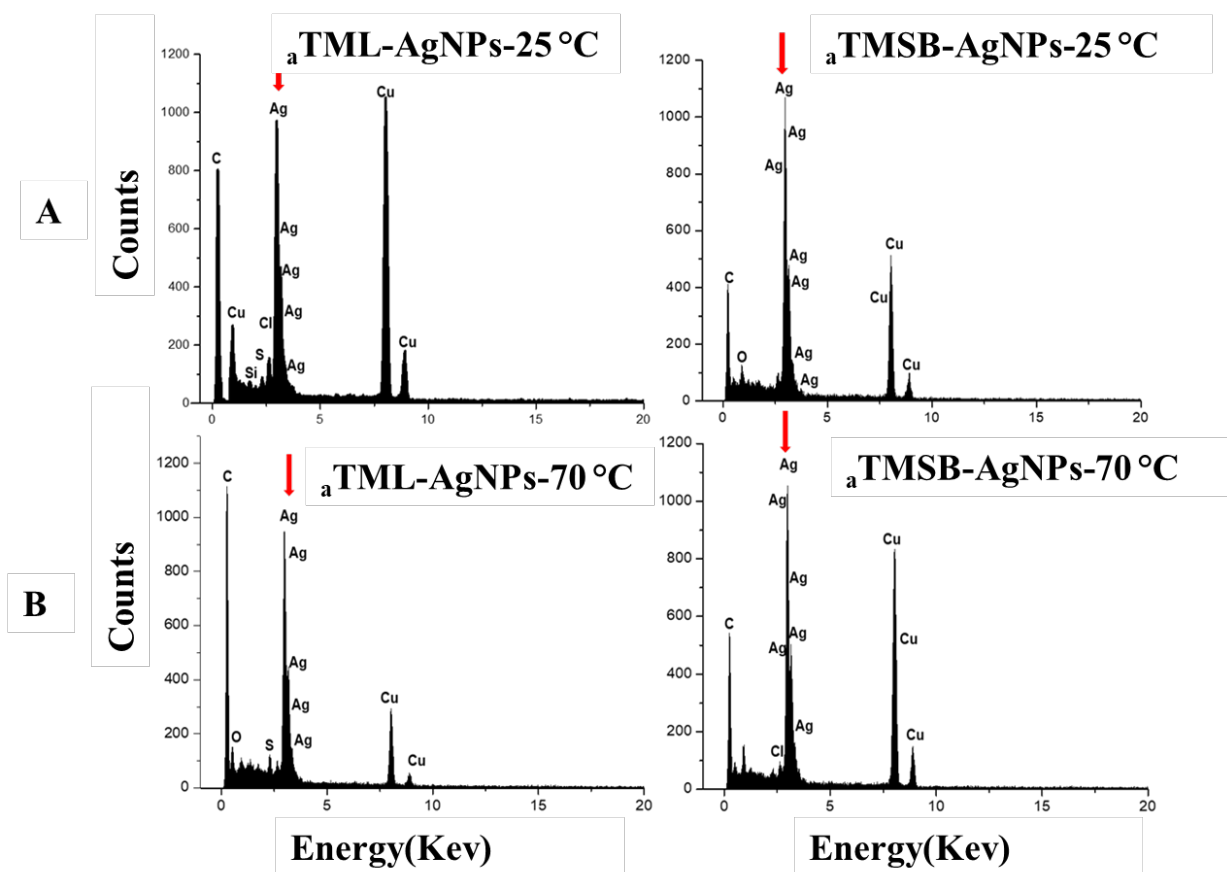


**Figure 25.** EDX spectra of AgNPs synthesized from a TML and aTMSB AgNPs.

Notes: Silver nanocrystallites display an optical absorption band peak at approximately 3 keV (red arrow), which is typical of the absorption of metallic silver nanocrystallites due to SPR.

**Abbreviations:** AgNPs, silver nanoparticles; TM, *Terminalia mantaly*; aTML, aqueous TM leaf extract; aTMSB, aqueous TM stem bark; EDX, Energy Dispersive X-ray.

### III.1.3.1.2 FTIR Analysis Of Bio-active TM-AgNPs

The FTIR analysis of the bio-active TM-AgNPs and their originated plant extracts was performed. The functional group(s) in the aqueous TML and TMSB extracts that are responsible for the reduction of  $\text{Ag}^+$  and stabilization of AgNPs were identified through the FTIR analysis. The phytochemicals play a role in the synthesis of AgNPs (Singh *et al.*, 2016). The comparative FTIR spectroscopy analysis between the TM extracts and the accompanying AgNPs (Appendix 4 and 5). The FTIR data from spectrum of aTML-AgNPs synthesized at 25 °C was compared to the spectrum of the TML extract, while the aTMSB-AgNPs synthesized at 70 °C was compared to the TMSB extract. Several commonalities between the spectra of the extracts and their respective TM-AgNPs could be identified. This suggests that the extracts and their respective TM-AgNPs share similar functional groups, which originate from phytochem-

icals that were involved in the synthesis of the TM-AgNPs. Shifts in the peak in the FTIR spectra of <sup>a</sup>TMSB and <sup>a</sup>TML extracts and their respective AgNPs are summarized in **Table 8**. In particular, the spectra of TML extract and AgNPs produced at 25 °C were characterized by methyl (C-H) rock alkanes vibration band at 1338.32 and 1384.39 cm<sup>-1</sup> and the C-H stretching observed between 2946.61 and 2830.64 cm<sup>-1</sup>. Moreover, there was a C=C double-bond stretching at 1640.29 and 1638.56 cm<sup>-1</sup>. Additionally, strong OH group vibrations assigned to phenol bands at 3647.29 and 3712.96 cm<sup>-1</sup> were detected in both samples (Appendix 1). The FTIR spectra of TMSB and AgNPs produced at 70 °C showed fewer similarities between the two samples. The spectra of <sup>a</sup>TML-AgNPs synthesized at 25 °C, <sup>a</sup>TMSB, and <sup>a</sup>TMSB-AgNPs synthesized at 70 °C. The <sup>a</sup>TML revealed intense bands at 1048.80 cm<sup>-1</sup> attributed to carbon-yls (C=O) vibrations that were absent on TMSB-AgNPs produced. Some similarities in the two samples were observed; the spectra of TMSB extract and AgNPs revealed bands at 1384.03 and 1384.96 corresponding to methyl (C-H) rock alkanes deformation, 1639.21 and 1638.68 cm<sup>-1</sup> bands attributed to stretch alkenes (C=C), 2930.41 and 2789.28 cm<sup>-1</sup> bands corresponding to C-H stretching, 3717.06 and 3731.61 cm<sup>-1</sup> intense bands attributed to O-H from alcohols and phenols vibrations. The shift in the different functional groups might be caused by the polyphenolics, flavonoids, and terpenoids present in the TM extracts. The same phytochemicals might be responsible for reducing, capping, and stabilization of the biogenic AgNPs. Several studies reported that the active components in the plant extracts such as terpenoids and flavonoids act as reducing agent of the silver precursor to form AgNPs (**Ankamar, 2010; Mittal et al., 2013; Fahmy et al., 2015; Elbagory et al., 2017**). Different chemical classes influence the production of AgNPs, as well as their shape, size, and bio-activity. (**Elbagory et al., 2017**). The IR bands and transmittance peak positions in the FTIR spectra of the extracts were compared to their respective AgNPs as shown in **Table 8**. The comparison of differences and similarities in the bonds between the extracts and AgNPs showed that the major peaks in the FTIR spectra of the TMSB and TML extracts and AgNPs with similar functional groups may be key players in the synthesis of the TM AgNPs. The shift in the peak in the FTIR spectra of <sup>a</sup>TMSB and <sup>a</sup>TML extracts and their respective AgNPs are summarized in Table 3. In particular, the spectra of <sup>a</sup>TML extract and AgNPs produced at 25 °C were characterized by methyl (C-H) rock alkanes vibration band at 1338.32 and 1384.39 cm<sup>-1</sup>, and the C-H stretching observed between 2946.61 and 2830.64 cm<sup>-1</sup>. Moreover, there was a C=C double-bond stretching at 1640.29 and 1638.56 cm<sup>-1</sup>. Finally, OH group strong vibrations

assigned to phenol bands at 3647.29 and 3712.96  $\text{cm}^{-1}$  were detected in both samples (Figure 4A and B). The FTIR spectra of <sup>a</sup>TMSB extract and AgNPs produced at 70 °C showed fewer similarities between the two samples (**Appendix 5**). The spectra of <sup>a</sup>TMSB extract revealed intense bands at 1048.80  $\text{cm}^{-1}$  attributed to carbonyls (C=O) vibrations that were absent on <sup>a</sup>TMSB-AgNPs produced. Some similarities in the two samples were observed; the spectra of <sup>a</sup>TMSB extract and AgNPs revealed bands at 1384.03 and 1384.96  $\text{cm}^{-1}$  corresponding to methyl (C-H) rock alkanes deformation, 1639.21 and 1638.68 bands attributed to stretch alkenes (C=C), 2930.41 and 2789.28  $\text{cm}^{-1}$  bands corresponding to C-H stretching, 3717.06 and 3731.61  $\text{cm}^{-1}$  intense bands attributed to O-H from alcohols and phenols vibrations. The shift in the different functional groups might be caused by the polyphenolics, flavonoids, and terpenoids present in the TM extracts (**Table 6**). The same phytochemicals might be responsible for reducing, capping, and stabilization of the biogenic AgNPs (**Ankamwar, 2010; Mittal et al., 2013; Fahmy et al., 2015; Bagherzade et al., 2017**). Several studies reported that the active components in the plant extracts such as terpenoids and flavonoids act as reducing agents of the silver precursor to form AgNPs.

**Table VIII:** Comparison FTIR spectra of TM extracts and their respective most active TM-AgNPs.

<sup>a</sup> TML			<sup>a</sup> TMSB		
Peak position in extracts ( $\text{cm}^{-1}$ )	Peak position in AgNPs at 25 °C ( $\text{cm}^{-1}$ )	Type of Chemical Bond	Peak position in extracts ( $\text{cm}^{-1}$ )	Peak position in AgNPs at 70 °C ( $\text{cm}^{-1}$ )	Type of Chemical bond
1338.32	1384.39	C-H methyl rock alkanes	1048.80	-----	C-O Stretch
1640.29	1638.56	-C=C-stretch alkenes	1131.16	-----	
1876.99	1884.90	C=O Anhydrides	1384.03	1384.96	C-H methyl rock alkanes
2946.61	2830.64	H-C=O:C-H stretch aldehydes	1639.21	1638.68	-C=C- stretch alkenes
3530.47	3417.07		2016.03	2034.58	-C≡C- stretch alkynes
3545.10	3417.99		2930.41	2789.28	H-C=O:C-H stretch aldehydes
3647.29	3712.96	OH Alcohol, phenols	3530.72	3530.35	
			3544.94	3544.99	OH Alcohol, phenols
			3717.06	3731.61	

**Abbreviations:** AgNPs, silver nanoparticles; TM, *Terminalia mantaly*; <sup>a</sup>TML, aqueous TM leaf extracts; <sup>a</sup>TMSB, aqueous TM stem bark, FTIR, Fourier-transform infrared.

### III.1.3.2 Full characterization Of Bio-active TM-AuNPs Using HRTEM, SAED EDX, And FTIR Analyses

#### III.1.3.2.1 Morphology And Particle Size Distribution Of Bio-active AuNPs

A variety of geometrical shapes of nanocrystals were identified in the Bio-active TM-AuNPs by HRTEM as shown in **Figure 28**, most of the NPs (**Appendix 6**) were spherical with some triangular, hexagonal and pentagonal shapes. The NPs had well-defined edges and most of them were well dispersed without any sign of agglomeration. The  $m$ TMSB-AuNPs, and  $m$ TMR-AuNPs generated different types of NPs, some anisotropic particles including the spherical shapes at both temperatures. The non-uniform profiles and mixture of geometrical shapes obtained with the other nanoparticles are very common with plant-based nanoparticle synthesis (**Moraes *et al.*, 2010**). This is mostly due to the presence of numerous phytochemicals in the extracts that might act in synergy to reduce the gold salt and form AuNPs with a mixture of geometrical shapes (**Grabinski, 2015**). TM extracts (**Table 5**) which can actively reduce metal ions to form NPs with different sizes and shapes. The polyphenols were reported to produce NPs with different shapes (**Ankamwar, 2010**) and that the polar and water-soluble compounds are the ones mostly involved in the synthesis of AuNPs (**Lee *et al.*, 2016**). The biomolecules that contain high polar groups (e.g.,  $-OH$ ) on their surface may increase the rate of nucleation and induce AuNPs formation (**Ankamwar, 2010**)

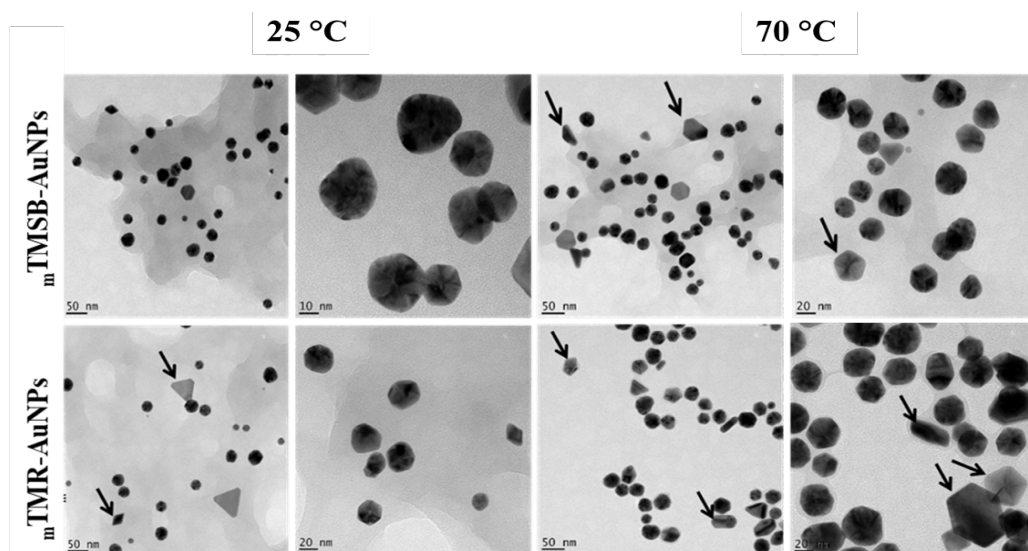


**Figure 26:** HRTEM images of TM-AuNPs synthesized at 25 °C and 70 °C. The arrows point at different NP shapes. The scale bar at 10, 20, and 50 nm.

Notes: The size, shape (A) of  $m$ TMR and  $m$ TMSB. AgNPs were analyzed by HRTEM. Scale bar from 20 to 50 nm.

**Abbreviations:** AuNPs, gold nanoparticles; TM, *Terminalia mantaly*;  $m$ TMSB, methanolic TM Stem Bark extract;  $m$ TMR, methanolic TM root extract; HRTEM, High resolution transmission electron microscope.

The size distribution of TM-AuNPs was calculated from the HRTEM micrograph, the representative histograms (**Figure 29, Appendix 6**) demonstrate that  $m$ TMSB-AuNPs synthesized at 25 °C and 70 °C had a diameter of 25.5 and 28.3 nm, respectively. The  $m$ TMR-AuNPs produced at 25 °C had a smaller core size (21 nm), this might suggest that TMR might be richer in reducing and capping agents. Similar results were reported by **Ankamwar. (2010)** on AuNPs synthesized from leaf extract obtained from *Terminalia Catappa*. The NPs were also spherical in morphology, with an average core size of 21.9 nm. The average sizes of the  $m$ TMSB-AuNPs-70 °C (28.3 nm) bigger compared to the sizes of the  $m$ TMR-AuNPs-25 °C (21 nm). Generally, the core sizes smaller at 25 °C and could be directly correlated to the rapid formation AuNPs from TM plant at this temperature (**Figure 24**).

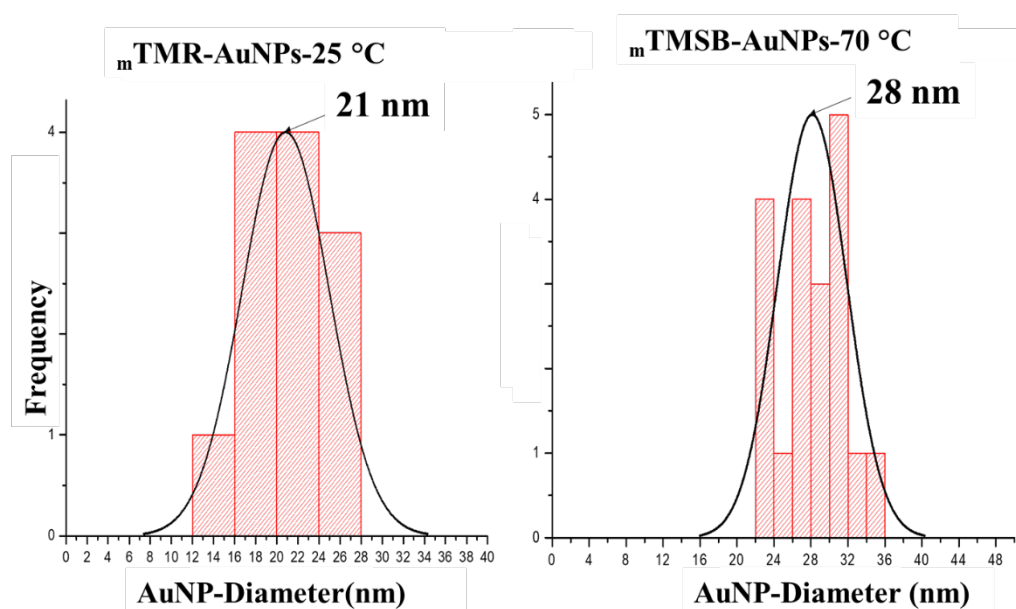


**Figure 27:** The particle size distribution of more stable and bio-active TM-AuNPs.

**Note:** The size, shape were analyzed by HRTEM. Scale bar from 20 to 50 nm using Image G and origin software. The diameter of 21 nm and 28 nm was obtained with  $m$ TMR-AuNPs and  $m$ TMSB-AuNPs.

**Abbreviations:** AuNPs, gold nanoparticles; TM, Terminalia mantaly;  $m$ TMR, methanolic TM Root extract;  $m$ TMSB, methanolic TM stem bark; HRTEM, High Resolution Transmission Election Microscope.

### III.1.3.2.2 Study Of Crystalline Effect Of Bio-active AuNPs Using SAED Analysis

The crystalline effect of NPs, SAED analysis was performed. The fringe lattice values ranged from 0.167 to 0.257 nm and the SAED pattern, which confirmed the crystalline nature of the TM-AuNPs varied between AuNPs synthesized at 25 °C and 70 °C. As an example,  $m$ TMSB-AuNPs synthesized at 70 °C have a typical HRTEM image with clear lattice fringes (**Figure 30**). Furthermore, a d-spacing or inter-planar distance of 0.233 nm was obtained for TM-AuNPs, which was comparable with 0.2355 nm, corresponding to the (111) planes of face-centered cubic (fcc) gold single crystals (**Appendix 7**). The clear lattice fringes in HRTEM images and the typical SAED pattern with bright circular rings corresponding to the (111), (200), (220) and (311) planes were obtained in most TM-AuNPs. This was an indication that the NPs obtained were highly crystalline, confirming the fcc crystalline geometry of AuNPs (JCPDS file no. 4-0783) (**Grabinski, 2015**). This may be indexed based on the fcc structure of gold. However, the lattice plane was predominantly (111)-oriented. The amorphous effect (diffuse rings) was observed with  $a$ TMSB and  $m$ TMR AuNPs at 70 °C, and the Bragg reflections were weak and considerably broadened relative to the intense (111) and (200) reflections.

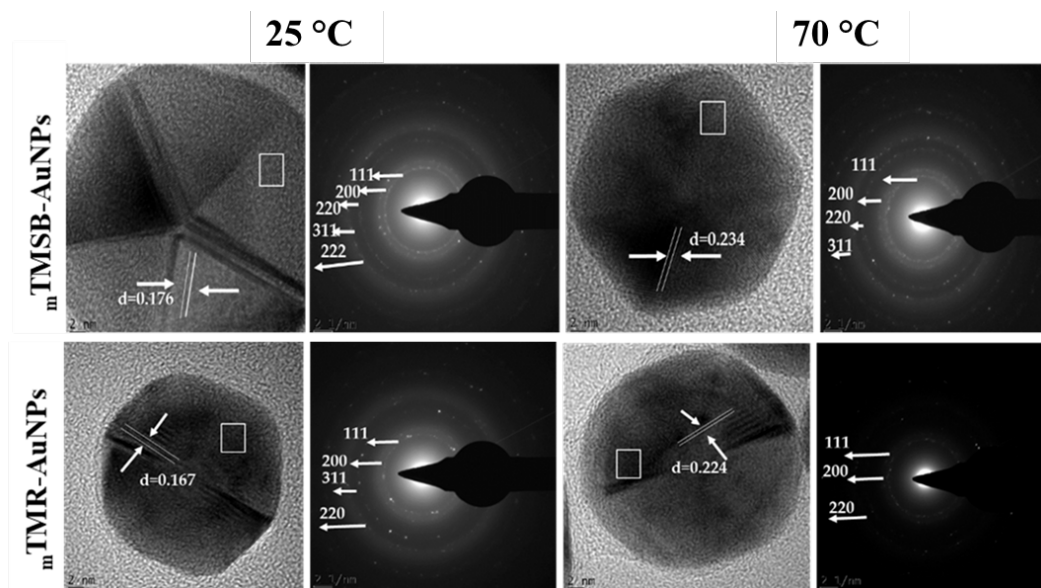


**Figure 28:** SAED patterns of TM-AuNPs showing single facets of NPs in TEM micrographs.

The HRTEM images of gold nanoprism show a fringe spacing of TM-AuNPs synthesized at 25 °C and 70 °C.

Notes: SAED patterns of  $m$ TMSB and  $m$ TMR. AuNPs were analyzed by HRTEM. Scale bar from 20 to 50 nm.

**Abbreviations:** AuNPs, gold nanoparticles; TM, *Terminalia mantaly*;  $m$ TMR, methanolic TM root extract;  $m$ TMSB, methanolic TM stem bark; HRTEM, High resolution transmission electron microscope, SAED. Surface Area Electron Diffraction.

### III.1.3.2.3 EDX Analysis Of Bio-active Active Gold Nanoparticles

The EDX spectra of TM-AuNPs are displayed in **Figure 31**, the spectra confirmed the presence of gold ions in all the AuNPs (**Appendix 8**). The Au peaks were acquired around 2.3 keV, 9.7 keV, and 11.3 keV. In some AuNPs, the EDX spectrum showed the presence of Silicon (Si) which might be due to a high degree of crystallinity. These results further confirmed the SAED patterns in Figure 5. The weak signals for oxygen in the spectra may have originated from the biomolecules bound to the surface of the NPs (**Patel and Agrawal, 2011**), Cu from the support HRTEM grid and film, and Co from the lenses of the microscope (**Elbagory et al., 2017**).

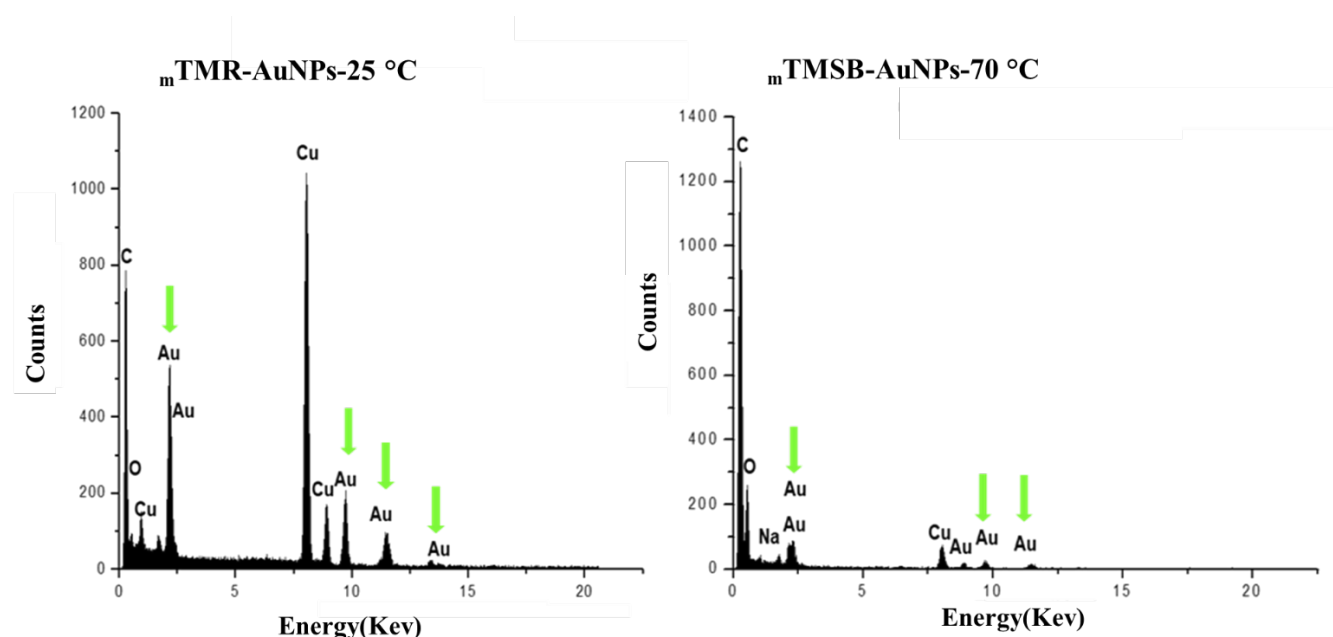


**Figure 29:** EDX spectra of bioactive TM-AuNPs.

**Notes:** Silver nanocrystallites display an optical absorption band peak at approximately 2.3, 9.7, and 11.3 keV (Green arrow), which is typical of the absorption of metallic silver nanocrystallites due to SPR.

**Abbreviations:** AuNPs, gold nanoparticles; TM, *Terminalia mantaly*; <sub>a</sub>TML, aqueous TM leaf extract; <sub>a</sub>TMSB, aqueous TM stem bark, <sub>m</sub>TMSB, methanolic TM stem bark, <sub>m</sub>TMR, methanolic TM root, EDX, Energy Dispersive X-ray.



#### III.1.3.2.4 FTIR Analyses Of Bio-active TM-AuNPs

FTIR analysis was carried out to with bio-active  $mTMR$ ,  $mTMSB$ ,  $mTMR$ - AuNPs -25 °C,  $mTMSB$ -AuNPs-70 °C to identify the possible functional chemical bonds from the phytochemicals in the TM extracts that are responsible for reduction, capping and stabilization of AuNPs (Kumar *et al.*, 2012; Balashanmugam *et al.*, 2016). The FTIR spectra are shown in Table 9, Appendix 9, and 10, highlighting some of the chemical bonds involved in NP synthesis. Generally, the chemical bonds identified in the TM extracts and AuNPs include C-O, C-H,  $-C=C-$ ,  $H-C=O$ ,  $-C\equiv C-$ , and O-H. Some of the peaks were absent in the AuNPs depending on the temperature (25 °C and 70 °C). The FTIR spectra of  $mTMSB$ ,  $mTMSB$ -AuNPs synthesized at 25 °C and at 70 °C (Appendix 9) showed prominent absorption bands at (1044  $cm^{-1}$ , 1330  $cm^{-1}$ , 1692  $cm^{-1}$ , 2958,  $cm^{-1}$ , 3645  $cm^{-1}$ ), (1104  $cm^{-1}$ , 1626  $cm^{-1}$ , 2938  $cm^{-1}$ , 3417  $cm^{-1}$ ) and (1032  $cm^{-1}$ , 1396  $cm^{-1}$ , 1638  $cm^{-1}$ , 2927 and 3474 $cm^{-1}$ ), respectively . The shoulder at 1044  $cm^{-1}$ , 1104  $cm^{-1}$ , 1032  $cm^{-1}$  is characteristic of C=O vibrations, while the stretch at, 1330  $cm^{-1}$ , 1396  $cm^{-1}$  arises from the C-H methyl rock alkanes stretching but was absent on  $mTMSB$ -AuNPs at 25 °C. The recorded peaks at 1692  $cm^{-1}$ , 1626  $cm^{-1}$ , and 1638  $cm^{-1}$  are due to the vibration of  $-C=C-$  stretch alkenes. The broad stretching at 2958  $cm^{-1}$ , 2938  $cm^{-1}$ , and 2927  $cm^{-1}$  arises from the vibrations of  $H-C=O$ : C-H stretch aldehydes. Moreover, the presence of the shifted band at 3645  $cm^{-1}$ , 3417  $cm^{-1}$ , and 3474  $cm^{-1}$ , in the FTIR spectrum of  $mTMSB$ ,  $mTMSB$ -AuNPs at 25 °C and  $mTMSB$ -AuNPs at 70 °C respectively, can be attributed to the OH groups of alcohol or phenols groups. Moreover, the FTIR analysis showed the presence of OH, COOH chemical bonds in the TM extracts and AuNPs which could be the most dominant in the synthesis of AuNPs (Kumar *et al.*, 2012). These groups (-OH, -COOH, and long alkyl chains) are the most commonly used to functionalize metal NPs, especially gold. The recorded FTIR spectra confirm that the chemical functional groups in the TM active metabolites acted as reducing and stabilizing agents in the synthesis of TM-AuNPs (Arumugam & Gopinath, 2013; Lee *et al.*, 2016).

**Table IX:** Comparison FTIR spectra of TM extracts and their respective TM-AuNPs.

Extracts	Peak position in extracts (cm <sup>-1</sup> )	Peak position in AuNPs at 25 °C (cm <sup>-1</sup> )	Peak position in AuNPs at 70 °C (cm <sup>-1</sup> )	Possible chemical groups
<b>mTMSB</b>	1044	1104	1032	C-O carboxylic acids, esters, ethers C-H methyl rock alkanes -C=C- stretch alkenes H-C=O: C-H stretch aldehydes O-H Alcohol, phenol
	1330	-----	1396	
	1692	1626	1638	
	2958	2938	2927	
	3645	3417	3474	
<b>mTMR</b>	1044	1109	1099	C-O carboxylic acids, esters, ethers C-H methyl rock alkanes -C=C- stretch alkenes H-C=O: C-H stretch aldehydes O-H Alcohol, phenol
	1363	1334	1377	
	1597	1626	1637	
	2075	2088	2095	
	3156	3450	3473	

**Abbreviations:** AuNPs, gold nanoparticles; TM, *Terminalia mantaly*; mTMSB, methanolic TM stem bark extracts; mTMR, methanolic TM root; FTIR, Fourier-transform infrared.

## III.2. Antibacterial Activity Of TM extracts, And Derived TM-AuNPs And TM-AgNPs

### III.2.1. Preliminary Antibacterial Screening: Evaluation Of spectra Of Activity

The antibacterial effects of six TM extracts, twelve AuNPs, and twelve AgNPs were evaluated against eight bacterial strains, of which two were Gram-positive (*S. pneumoniae* and *S. aureus*) and the other six were Gram-negative (*S. enterica*<sup>a</sup>, *S. enterica enterica*, *H. influenzae*, *S. flexineri*, *K. pneumoniae*, *S. enterica*<sup>b</sup>). The bacterial cultures were treated with a single dose of 500 µg/mL of TM extracts and 12.5 µg/mL of TM-AgNPs and TM-AuNPs. This was done as a quick and easy test of the antimicrobial activity of the TM extracts and TM-AgNPs. The antibacterial activity in **Figure 32** and **Table 10** showed that four of the treatments (<sub>a</sub>TML-AgNPs-25 °C, <sub>a</sub>TML-AgNPs-70 °C, <sub>a</sub>TMSB-AgNPs-25 °C, and <sub>m</sub>TMSB) inhibited the growth in a significant number of bacterial strains tested in this study. <sub>a</sub>TML-AgNPs-25 °C and <sub>a</sub>TML-AgNPs-70 °C inhibited the growth in all strains, while <sub>a</sub>TMSB-AgNPs-70 °C inhibited the growth of 80 % and 50 % of the strains, respectively and <sub>m</sub>TMSB was the most active extract and inhibited the growth of four strains. Generally, three of the strains (*K.*

*pneumoniae*, *H. influenzae*, and *S. flexneri*) were more susceptible to the effects of the treatments, while *S. enterica enterica* was more resistant (**Table 9**). The lowest concentration required to inhibit the visible growth of the bacteria (i.e. the MIC) treated with the TM extracts and AgNPs was determined. The results showed that the synthesized TM-AuNPs showed no effects against any bacteria at the tested concentrations. The gold nanoparticles are not stable inside the bacteria media and consequently are generally not bactericidal or only weakly at high concentrations (**Zhang et al., 2015**). Many reports also demonstrated that AuNPs exhibited no antibacterial effects against several pathogen bacteria (**Dorosti and Jamshidi, 2016**). **Amin et al. (2009)** investigated the effect of 15 nm citrate capped AuNPs on the growth of *Escherichia coli* and pointed out that no significant inhibitory effect was caused by gold nanoparticles. **Nur. (2013)** found that no significant inhibition effect with both 14.8 nm core size and 5 nm core size citrate capped AuNPs on the growth of *Pseudomonas fluorescens*. **Sri-Ramkumar et al. (2014)** also showed that synthesized AuNPs using *Turbinaria conoides* aqueous extract and AuNPs alone did not show any antibacterial activity. Similarly, AuNPs induced the cell division without any endocytosis and inhibitory effect on *E. coli* (**Cui et al., 2012**).

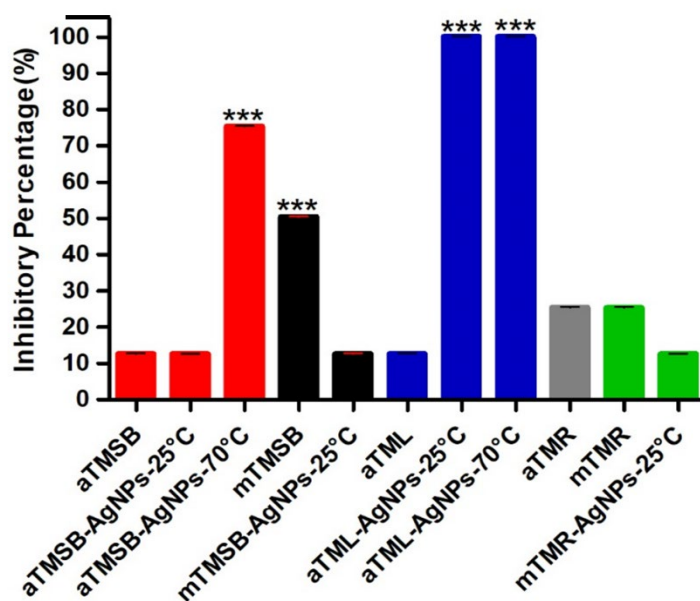


**Figure 30:** Screening of the antibacterial effects of TM extracts and AgNPs against a panel of eight bacterial strains.

**Notes:** Eight bacterial strains were treated with TM extracts and AgNPs for 24 hrs. Inhibitory effects of TM samples are expressed based on the number of strains that showed growth inhibition. \*\*\*P < 0.001.

**Abbreviations:** AgNPs, silver nanoparticles; TM, *Terminalia mantaly*; a, represents aqueous extracts; m, represents methanolic extracts; TML, TM leaf extracts; TMR, TM root extracts; TMSB, TM stem bark extracts..

**Table X:** Comparison of the bacterial susceptibility to TM extracts and TM-AgNPs.

Treatment	Bacterial strains							
	<i>S. enterica</i> <sup>a</sup>	<i>S. pneumoniae</i>	<i>S. aureus</i>	<i>K. pneumoniae</i>	<i>S. enterica enterica</i>	<i>S. enterica</i> <sup>b</sup>	<i>S. flexneri</i>	<i>H. influenzae</i>
Percentage of inhibition (%)								
<sup>a</sup> TMSB	-	-	-	-	-	-	-	✓
<sup>a</sup> TMSB-AgNPs-25 °C	-	-	-	✓	-	-	✓	✓
<sup>a</sup> TMSB-AgNPs-70 °C	-	✓	✓	✓	✓	✓	✓	-
<sup>m</sup> TMSB	-	✓	-	-	✓	-	✓	✓
<sup>m</sup> TMSB-AgNPs-25 °C	-	-	-	-	-	-	-	✓
<sup>a</sup> TML	-	✓	-	-	-	-	-	-
<sup>a</sup> TML-AgNPs-25 °C	✓	✓	✓	✓	✓	✓	✓	✓
<sup>a</sup> TML-AgNP-70 °C	✓	✓	✓	✓	✓	✓	✓	✓
<sup>a</sup> TMR	-	✓	-	-	-	-	-	✓
<sup>m</sup> TMR	-	✓	-	-	-	-	-	✓
<sup>m</sup> TMR-AgNPs-25 °C	-	✓	-	-	-	-	-	-

**NOTE:** Eight bacterial strains were treated with 1M extracts and AgNPs for 24 hrs. Inhibitory effects of 1M samples were visually assessed to identify the strains that were susceptible to TM extracts and AgNPs. The TM-AgNPs were the most active and inhibited growth of all bacterial strains, compared to the crude extracts and other AgNPs. *S. enterica*<sup>a</sup> (*Salmonella enterica* subsp. *enterica* A36 (Serovar *Typhimurium*) vs *S. enterica*<sup>b</sup> (*Salmonella enterica* subsp. *enterica* 2004 Pennsylvania Tomato Outbreak, Serovar *Anatum*, Isolate 4).

**Abbreviations:** AgNPs, Silver nanoparticles; TM, *Terminalia mantaly*; <sup>a</sup>, represents aqueous extracts; <sup>m</sup>, represents methanolic extracts; TML, TM leaf extracts; TMR, TM root extracts; TMSB, TM stem bark extracts; *S. pneumoniae*, *Streptococcus pneumoniae*; *S. enterica enterica*, *Salmonella enterica enterica*; *H. influenzae*, *Haemophilus influenzae*, *S. flexneri*, *Shigella flexneri*; *K. pneumoniae*, *Kbsiella pneumoniae*; *S. aureus*, *Staphylococcus aureus*, *S. enterica*- *Salmonella enterica*; -, no bacterial activity; ✓, bacterial activity.

The crude extracts and TM-AgNPs that inhibit at least 25 % and 75 % of tested bacteria respectively were selected for MIC determination

### III.2.2 Determination Of The Minimal Inhibitory Concentration (MIC) Of The More Active TM Extracts And TM-AgNPs

The MIC values for the treatments are summarized in **Table 11**. The lowest MIC value (3.12 µg/mL) was obtained for <sup>a</sup>TMSB-AgNPs-70 °C and <sup>a</sup>TML-AgNPs-25 °C against *H. influenzae*. The <sup>a</sup>TML-AgNPs-25 °C and <sup>a</sup>TMSB-AgNPs-70 °C appear to have more significant antimicrobial activity than the other TM-AgNPs. MIC values for <sup>a</sup>TML-AgNPs-25 °C varied between 6.24 and 12.50 µg/mL in six out of eight strains, while the MIC values for <sup>a</sup>TMSB-AgNPs-70 °C varied between 3.12 and 6.24 µg/mL in five out of eight strains.

NPs with smaller sizes are usually more efficient as they can easily pass through cellular barriers and disrupt the physiological functions (**Anandalakshmi et al., 2016, Aljabali et al., 2018**). As such, the efficacy of TML-AgNPs could be attributed to their smaller diameter (**Mmola et al., 2016**). Furthermore, the active phytochemicals at specific temperatures might be responsible for the biological activities of the AgNPs (**El-Rafie and Hamed, 2014**). Only *S. enterica enterica*, *S. flexineri*, and *H. influenzae* were susceptible to the <sup>m</sup>TMR, <sup>a</sup>TMSB and <sup>m</sup>TMSB extracts. The MIC for these extracts was 125 µg/mL. Previous studies have demonstrated the antifungal activity of the aqueous and ethanolic TML and TMSB extracts against *Candida* species (*C. albicans*, *C. glabrata*, and *C. parapsilosis*) and *Cryptococcus neoformans* with MIC values ranging from 0.04 to 0.16 mg/mL (**Ngouana et al., 2015**). Although the extracts did not show the same response in bacteria, their respective AgNPs possess enhanced anti-bacterial activities against both Gram-negative and Gram-positive strains.

•

**Table XI** MIC for crude TM extracts and derivate TM-AgNPs on selected bacteria strains.

Treatment	MIC ( $\mu\text{g/mL}$ )							
	<i>S. enterica</i> <sup>a</sup>	<i>S. pneumoniae</i>	<i>S. aureus</i>	<i>K. pneumoniae</i>	<i>S. enterica enterica</i>	<i>S. enterica</i> <sup>b</sup>	<i>S. flexneri</i>	<i>H. influenzae</i>
<sup>a</sup> TMSB	>500	>500	>500	>500	>500	>500	>500	125
<sup>a</sup> TMSB-AgNPs-25 °C	>12.50	>12.50	>12.50	6.24	>12.50	6.24	>12.50	3.12
<sup>a</sup> TMSB-AgNPs-70 °C	>12.50	6.24	12.50	6.24	12.50	12.50	>12.50	>12.50
<sup>m</sup> TMSB	>500	>500	>500	>500	>500	>500	125	>500
<sup>m</sup> TMSB-AgNPs-25 °C	>12.50	>12.50	>12.50	>12.50	>12.50	>12.50	>12.50	6.24
<sup>a</sup> TML	>500	>500	>500	>500	>500	>500	>500	>500
<sup>a</sup> TML-AgNPs-25 °C	6.24	6.24	6.24	6.24	>12.50	6.24	>12.50	3.12
<sup>a</sup> TML-AgNPs-70 °C	>12.50	6.24	12.50	6.24	>12.50	6.24	>12.50	>12.50
<sup>a</sup> TMR	>500	>500	>500	>500	>500	>500	>500	500
<sup>m</sup> TMR	>500	>500	>500	>500	125	>500	>500	>500
<sup>m</sup> TMR-AgNPs25 °C	>12.50	>12.50	>12.50	>12.50	>12.50	>12.50	>12.50	>12.50
<b>Ampicilin</b>	32	4	8	16	32	16	32	16

**Notes:** *S. enterica*<sup>a</sup> (*Salmonella enterica* subsp. *enterica* A36 (Serovar Typhimurium) vs *S. enterica*<sup>b</sup> (*Salmonella enterica* subsp. *enterica* 2004 Pennsylvania Tomato Out-break, Serovar Anatum, Isolate 4).

**Abbreviations:** AgNPs, Silver nanoparticles; TM, *Terminalia mantaly*; <sup>a</sup>, represents aqueous extracts; <sup>m</sup>, represents methanolic extracts; TML, TM leaf extracts; TMR, TM root extracts; TMSB, TM stem bark extracts; *S.pneumoniae*, *Streptococcus pneumoniae*; *S. enterica enterica*, *Salmonella enterica enterica*; *H.influenzae*, *Haemphilus influenzae*, *S.flexineri*, *Shigella flexineri*; *K. pneumoniae*, *Kbsiella pneumoniae*; *S. aureus*, *Staphylococcus aureus*; *S. enterica*, *Salmonella enterica*.

Based on the antibacterial results (Tables 4). The  $^a$ TML-AgNPs synthesized at 25 °C ( $^a$ TML-AgNPs-25 °C) and synthesized at 70 °C ( $^a$ TMSB-AgNPs-70 °C) showed higher antibacterial activities and were selected for the growth inhibitory study.

### III.2.3. Growth Inhibitory Kinetics Of TM-AgNPs

The bacterial growth kinetics of several bacterial strains was evaluated in response to treatment with TM-AgNPs. As shown in **Figure 33**, both TM-AgNPs caused a time- and dose-dependent growth inhibition in the selected strains. Of the two  $^a$ TM-AgNPs,  $^a$ TMLAgNPs-25 °C (**Table 7**) was more effective and with the highest bactericidal effect on the microorganisms. The  $^a$ TML-AgNPs-25 °C suppressed the growth of the six bacterial strains tested. Interestingly, the growth curve for *S. enterica* shows that the inhibitory effects of ampicillin diminish after 4 hrs, while inhibitory effects of  $^a$ TML-AgNPs-25 °C are maintained for the duration of the experiment at all the concentrations tested. The bacteriostatic effects of  $^a$ TMSB-AgNPs-70 °C were observed against all strains except for *H. influenzae* and *S. aureus* (**Figure 34**). The growth curves of *S. enterica enterica* and *S. flexneri* show that  $^a$ TMSB-AgNPs-70 °C can effectively inhibit the growth of these two organisms from 2 to 8 hrs at all the concentrations tested. Only higher concentrations (6.24 µg/mL) of  $^a$ TMSB-AgNPs-70 °C were effective on *S. pneumoniae* and *S. aureus* at all time points. In general, the Gram-negative bacteria were more susceptible to the effects of the TM-AgNPs than Gram-positive bacteria (*S. pneumoniae* and *S. aureus*). This might be due to the structural differences between the two bacterial types, a key component being the cell membrane of the Gram-positive bacteria, where the thick peptidoglycan layer acts as a barrier against penetration of foreign materials (**Holowachuk et al., 2003; Dakal et al., 2016**). The thick and negatively charged peptidoglycan layer in Gram-positive bacteria has been shown to entrap Ag<sup>+</sup> ions onto the cell wall and block their activity. However, the exact mechanism of action of antibacterial of AgNPs is not yet known (**Feng et al., 2000; Kim et al., 2007**). Nonetheless, several studies demonstrated that the bactericidal effects of the AgNPs are strongly influenced by their size, shape, concentration, and colloidal state (**Jiang et al., 2009; Rai et al., 2016**).

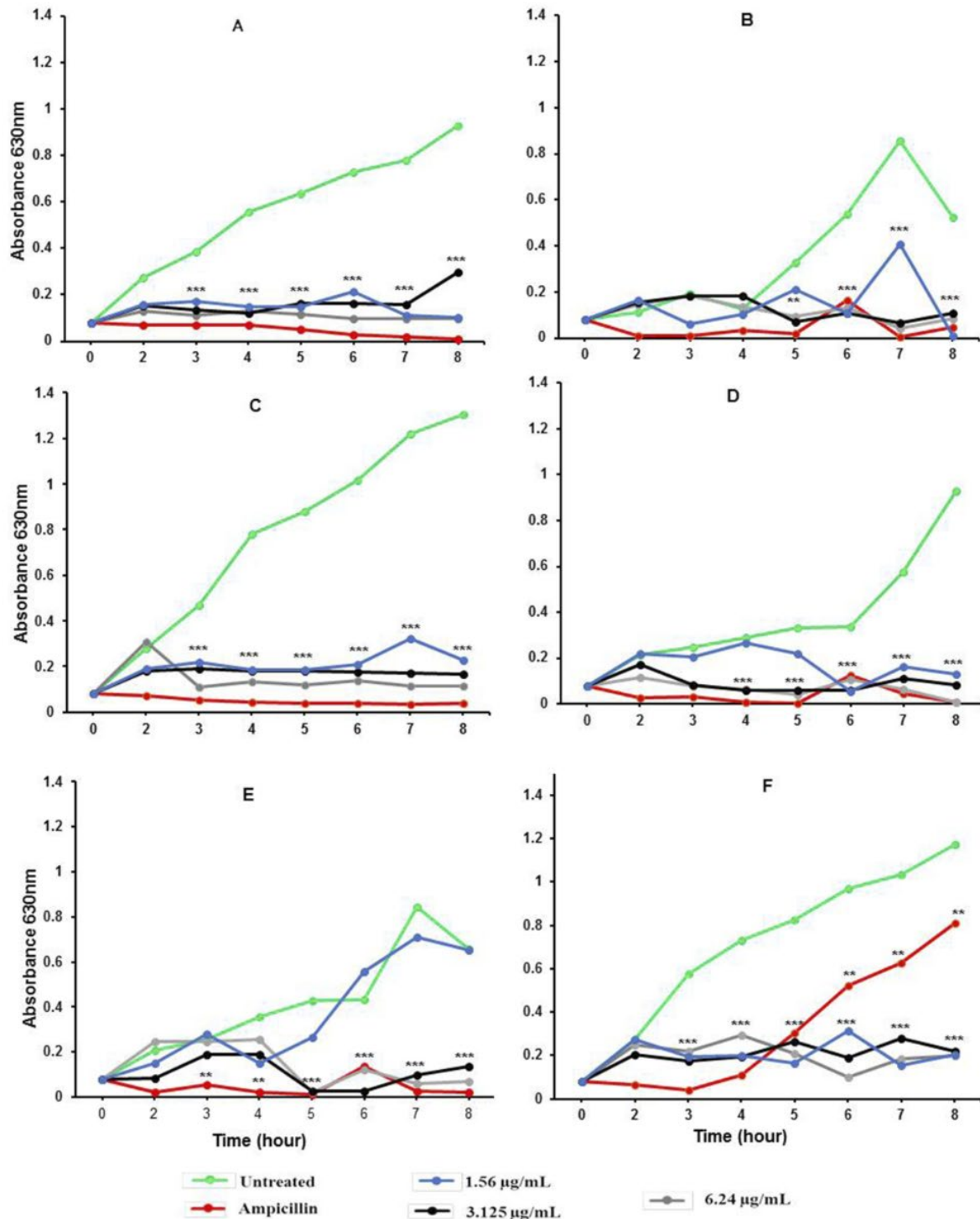


**Figure 33:** Growth inhibitory activities of TML-AgNPs-25 °C against selected bacterial strains.  
**Notes:** Growth curves of (A) *S. pneumoniae*, (B) *S. enterica enterica*, (C) *H. influenzae*, (D) *S. flexneri*, (E) *K. pneumoniae*, and (F) *S. enterica<sup>a</sup>* (*Salmonella enterica* subsp. *enterica* A36 Serovar *Typhimurium*) after 24 hrs treatment. \*\*P < 0.01, \*\*\*P < 0.001.

**Abbreviations:** AgNPs, silver nanoparticles; TM, *Terminalia mantaly*; TML-AgNPs, AgNPs synthesized from aqueous leaf extracts from TM; *S. pneumoniae*, *Streptococcus pneumoniae*; *S. enterica enterica*, *Salmonella enterica enterica*; *H. influenzae*, *Haemophilus influenzae*, *S. flexneri*, *Shigella flexneri*; *K. pneumoniae*, *Klebsiella pneumoniae*; *S. aureus*, *Staphylococcus aureus*; *S. enterica*, *Salmonella enterica*.



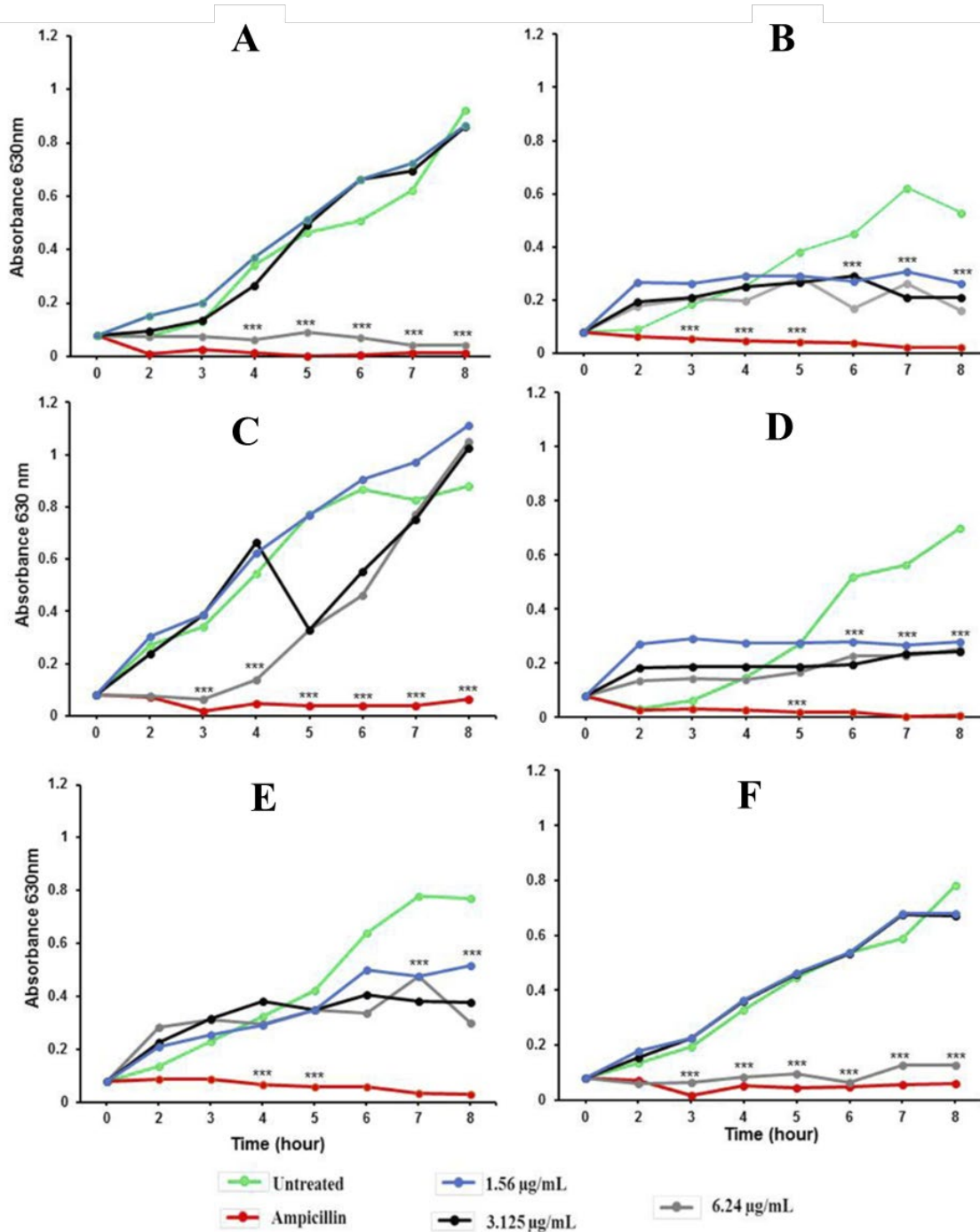


**Figure 31:** Growth inhibitory activities of TMSB-AgNPs-70 °C against selected bacterial strains.

**Notes:** Growth curves of (A) *S. pneumoniae* (B) *S. enterica enterica*, (C) *H. influenzae*, (D) *S. flexneri*, (E) *K. pneumoniae*, and (F) *S. aureus* after 24 hrs treatment. \*\*\*P < 0.001.

**Abbreviations:** AgNPs, Silver nanoparticles; TM, *Terminalia mantaly*; <sub>a</sub>TMSB-AgNPs, AgNPs synthesized from aqueous Stem Bark extracts from TM; *S. pneumoniae*, *Streptococcus pneumoniae*; *S. enterica enterica*, *Salmonella enterica enterica*; *H. influenzae*, *Haemphilus influenzae*, *S. flexneri*, *Shigella flexneri*; *K. pneumoniae*, *Klebsiella pneumoniae*; *S. aureus*, *Staphylococcus aureus*; *S. enterica*, *Salmonella enterica*.

### **III.3 Potential Antiproliferative Effect Of Extracts, And The More Stable Gold And Silver Nanoparticles Against A Panel Of Three Resistant Cancer Cells Line And Study Of Mechanism Of Cell Death**

The application of nanotechnology in medicine is looking very promising, in particular for the development of effective therapies for chronic diseases; bringing about the exciting era of nanomedicine. Nanomaterials have physicochemical properties that make them useful in therapeutics, diagnostics (Lysik and Wu-Pong, 2003; Provenzale and Silva, 2009). However, applications in therapeutics could be limited by their possible toxicity. The green synthesis of nanomaterials has generated great interest as it provides a simple, cost-effective, readily scalable, and eco-friendly products with minimal toxicity towards human beings. Natural products are used extensively as reducing as well as capping agents to prevent agglomeration and increase the stability of the synthesized NPs (Elbagory *et al.*, 2019). The goal of the present section was to develop a nanotherapy for cancer by investigating the therapeutic potential of TM extracts, most stable TM-AuNPs and TM-AgNPs-targeted nanotherapy on the model cell line (Caco-2, HepG2, and MCF-7), the Annexin V-Cy3<sup>TM</sup> Apoptosis detection kit (APOAC), CM-H<sub>2</sub>DCFDA probe to quantify ROS generation and cell cycle analysis using flow cytometry and were also lead to interesting and important data.

#### **-III.3.1 Effect Of TM Crude Extract, Stable TM Gold And Silver Nanoparticles On Cell Proliferation Of Cancer Cells**

The stability of TM-AuNPs and TM-AgNPs in PBS, DMEM (Gibco, UK) cell culture media was tested as described previously by Elbagory *et al.*, (2019) and the most stable gold (TM-AuNPs) and silver (TM-AgNPs) nanoparticles were selected for the anticancer potential. The anti-proliferative activity of six TM extract, the more stable twelve gold, and two silver nanoparticles was evaluated on Caco-2, HepG2, and MCF-7 cells spectrophotometrically by measuring the degree of mitochondrial reduction of the tetrazolium salt, MTT. The potential toxicity of the bioactive crude extract, gold, and silver nanoparticles on non-cancerous human fibroblast skin cells (KMST-6) was investigated using the same methods. The number of viable cells was proportional to the extent of formazan production. The results of MTT assays revealed that most of TM extracts, TM-AuNPs and TM-AgNPs exerted significant cytotoxicity to Caco-2, MCF-7 and HepG2 cells in a dose-dependent manner and were statistically significant at all concentrations tested when compared to the negative controls (untreated cells). The results revealed that most of the TM extracts, TM-AgNPs and TM-AuNPs exerted signif-

icant cytotoxicity on the cells in a dose-dependent manner. The IC<sub>50</sub> values are summarized in **Table 12**, they ranged from 0.18 to 93.73 µg/mL. This study found for the first time that methanol extracts of TM root, stem, and bark are particularly toxic to the human breast cancer (MCF-7) cell line. In general, the IC<sub>50</sub> values of the TM-AuNPs, TM-AgNPs were higher than that of the TM extracts, suggesting that the TM-AuNPs and TM-AgNPs were more cytotoxic than the TM extracts (**Table 12**). The <sub>m</sub>TMR and <sub>m</sub>TMSB extracts were more toxic than the other 4 extracts. However, MCF-7 cells in particular were highly susceptible to the effects of <sub>m</sub>TMR and <sub>m</sub>TMSB extracts, with IC<sub>50</sub> values 2.73 and 19.73 µg/mL, respectively.

*Terminalia* species are known for their anti-tumour activity. *Terminalia ferdinandiana* fruit and leaf extracts exhibited cytotoxicity against human carcinoma cell lines including Caco-2 cells (IC<sub>50</sub> = 102 µg/mL) (**Shalom J and Cock, 2018**). **Nandagopal et al., 2014** demonstrated the cytotoxicity of *Terminalia cheduba* seed extracts against HepG2 cells (IC<sub>50</sub>= 40 µg/mL). Likewise, acetone extracts of *Terminalia belerica* and *Terminalia chebula* exhibited differential cytotoxic activities in several cancer cell lines, with the breast cancer cell line, MCF-7 being highly susceptible to the effects of this extract (**Kaur et al., 2005**). **Saleem et al. (2002)** reported that methanol extracts of the *Terminalia chebula* fruit reduced cell viability and inhibited cell proliferation in several malignant cell lines including MCF-7 cells. Phytochemical analysis of TM has revealed the presence of alkaloids, flavonoids, glucosides, and total phenols (Table 1), these secondary metabolites were reported to have anti-tumour activities. The TM-AgNPs were the most potent with an IC<sub>50</sub> values of (0.006, 0.575, 4.406, µg/mL), and (0.008, 0.488, 2.060 µg/mL) on HepG2, Caco-2 and MCF-7 cells for <sub>a</sub>TML-AgNPs-25 °C and <sub>a</sub>TMSB-AgNPs-70 °C respectively. Compare to the two TM-AgNPs, the <sub>a</sub>TMSB-AgNPs -70 °C was most active on Caco-2 (0.488 µg/mL) and (2.060 µg/mL) MCF-7 cells. Overall, the silver nanoparticles had a higher cytotoxicity potency than gold nanoparticles when the same plant's extracts from *Terminalia mantaly* were used for the synthesis, irrespective of the cancer cell type tested. Cytotoxicity was discussed by **Bupesh et al. (2016)** and showed the anticancer activity of AgNPs nanoparticles from *Terminalia cheduba* against HT-29 colon cancer. AgNPs synthesized from *Annona squamosa* leaf extracts possessed potential cytotoxicity against breast cancer (MCF-7) cells (**Rao et al., 2016**). A study conducted by **Hassanien et al. (2019)** demonstrated that AgNPs showed effectiveness on three types of cancer (MCF-7, HepG2, and Caco-2 cells). **Premasudha et al. (2015)** study the biological synthesis and characterization of silver nanoparticles using *Eclipta Alba* leaf extract and evaluation of its cytotoxic potential. Another example of naturally coated AgNPs includes the effect of the *Erythrina indica* extract causing a dose-dependent reduction of viability in

HepG2 hepatocellular carcinoma (Vimbela *et al.*, 2017). For instance, green biosynthesized AgNPs (*Tanacetum vulgare*) can exert a lethal effect on MCF-7 cells (El-Naggar *et al.*, 2017). The elevated anticancer activity of the TM AgNPs could be attributed to a synergy between AgNPs and the covering polyphenols (Figure 32). Furthermore, most TM-AuNPs showed some activity to the three tested cells. For example, while the IC<sub>50</sub> values for <sub>a</sub>TML-AuNPs-25 °C and <sub>a</sub>TML-AuNPs-70 °C was only 5.71 µg/mL in the Caco-2 cell line, the cytotoxicity of these NPs was very different in the MCF-7 and HepG2 cell lines. The IC<sub>50</sub> value for <sub>a</sub>TML-AuNPs-25°C in the MCF-7 cell line was 6.56 µg/mL, while the IC<sub>50</sub> value for <sub>a</sub>TML-AuNPs-70°C at 32.59 µg/mL was much higher. Similarly, <sub>m</sub>TMR-AuNPs-25°C and <sub>m</sub>TMR-AuNPs-70°C displayed very different cytotoxicity in HepG2 cells. With an IC<sub>50</sub> value of 0.18 µg/mL, <sub>m</sub>TMR-AuNPs-25°C was highly toxic to HepG2 cells, but <sub>m</sub>TMR-AuNPs-70 °C was less toxic to these cells with an IC<sub>50</sub> value of 90.85 µg/mL. It has been demonstrated that AuNPs exert *in vitro* cytotoxicity on several human cancer cells including HepG2 and triple negative breast cancer cells (MDA-MB-231) (Malugin and Ghandehari, 2010; Paino *et al.*, 2010; Moses and Edwards, 2016). KS *et al.*, (2016) synthesized AuNPs from *Cassia tora* leaf extracts demonstrated the cytotoxic efficacy against colon cancer (Col320) cell lines. AuNPs from *Gymnema sylvestre* leaf extracts were also investigated for their anticancer effects against HT-29 cells. The study revealed that these AuNPs exerted significant cytotoxic effects against HT-29 cancer cells at a maximal concentration of 95 µg/mL (Arunachalam *et al.*, 2014).

The activity of TM-AuNPs might be because of the size, shape, or other intrinsic properties of the nanoparticles (Appendix 23, and Appendix 10). It has been reported that spherical and rod-shaped AuNPs are more efficient in reducing cell proliferation of cancer cells than AuNPs with other shapes (Wozniak, *et al.* (2017). TM-AuNPs studied here were mostly spherical which possibly contributes to the high cytotoxicity of these AuNPs. The capping agents (phytochemicals) that play a role in the synthesis of biogenic AuNPs can also affect the cytotoxicity of AuNPs (Ankanwar, 2010; Wu *et al.*, 2011). Phytochemical analysis showed that the chemical composition of the various extracts was very different. This may account for the differences in the physical characteristics of the TM-AgNPs and TM-AuNP as well as the differences in cytotoxicity. This finding supports the traditional use of *Terminalia mantaly* plant and derived TM-AuNPs in the treatment of cancer.

**Table XII:** Cytotoxicity responses of TM extracts and the more stable TM-AuNPs and TM-AgNPs against, Caco-2, HepG2 and MCF-7, cell lines.

Acronym	IC <sub>50</sub> values (µg/mL)		
	HepG2	Caco-2	MCF-7
<sub>m</sub> TML-AuNPs-25 °C	38.750±0.001	41.200±0.030	15.370±0.060
<sub>m</sub> TML-AuNPs-70 °C	85.070±0.005	18.370±0.410	54.560±0.002
<sub>a</sub> TML-AuNPs-25 °C	63.098±0.001	5.714±0.030	6.567±0.010
<sub>a</sub> TML-AuNPs -70 °C	41.740±0.060	5.714±0.310	32.590±0.101
<sub>m</sub> TMSB-AuNPs-25 °C	30.560±0.101	75.837±0.010	54.460±0.010
<sub>m</sub> TMSB-AuNPs-70 °C	36.260±0.070	6.558±0.050	1.240±0.000
<sub>a</sub> TMSB-AuNPs -25 °C	66.290±0.010-	20.340±0.050	65.150±0.018
<sub>a</sub> TMSB-AuNPs-70 °C	63.098±0.210	7.040±0.010	1.776±0.010
<sub>m</sub> TMR-AuNPs -25 °C	0.1971±0.010	23.580±0.020	3.356±0.200
<sub>m</sub> TMR-AuNPs -70 °C	90.845±0.080	31.510±0.030	6.225±0.010
<sub>a</sub> TMR -AuNPs-25 °C	88.591±0.111	4.736±0.010	1.240±0.010
<sub>a</sub> TMR-AuNPs -70 °C	58.028±0.410	40.420±0.040	6.287±0.012
<sub>a</sub> TML-AgNPs -25 °C	0.006±0.011	0.575±0.070	4.406±0.017
<sub>a</sub> TMSB-AgNPs -70 °C	0.008±0.010	0.489±0.101	2.060±0.094
<sub>a</sub> TML	61.188±0.001	90.189±0.121	66.840±0.006
<sub>m</sub> TML	75.069±0.011	87.341±0.001	72.440±0.003
<sub>a</sub> TMSB	93.730±0.001	62.658±0.005	49.230±0.001
<sub>m</sub> TMSB	41.280±0.021	76.372±0.008	19.730±0.023
<sub>a</sub> TMR	90.470±0.011	73.031±0.001	43.300±0.001
<sub>m</sub> TMR	43.240±0.130	89.021±0.000	2.731±0.011

**Note:** Six extracts, twelve gold nanoparticles, and two AgNPs were treated with Caco-2, HepG2, and MCF-7 cells for 24 hrs. The decrease of the viability of cells was in a concentration-dependent manner and the TM-AgNPs were the most active against the, compared to the crude extracts. The <sub>m</sub>TMR-AuNPs-25 °C and <sub>m</sub>TMSB-AuNPs-70 °C were the most active. MCF-7 cells were more sensitive to the treatment.

**Abbreviations:** AuNPs, gold nanoparticles; AgNPs, silver nanoparticles; TM, *Terminalia mantaly*; <sub>a</sub>, represents aqueous extracts; <sub>m</sub>, represents methanolic extracts; TML, TM leaf extracts; TMR, TM root extracts; TMSB, TM stem bark extracts; Caco-2, human colorectal adenocarcinoma; MCF-7, human breast adenocarcinoma; HepG2, human liver carcinoma; IC<sub>50</sub>, 50% Inhibitory Concentration.

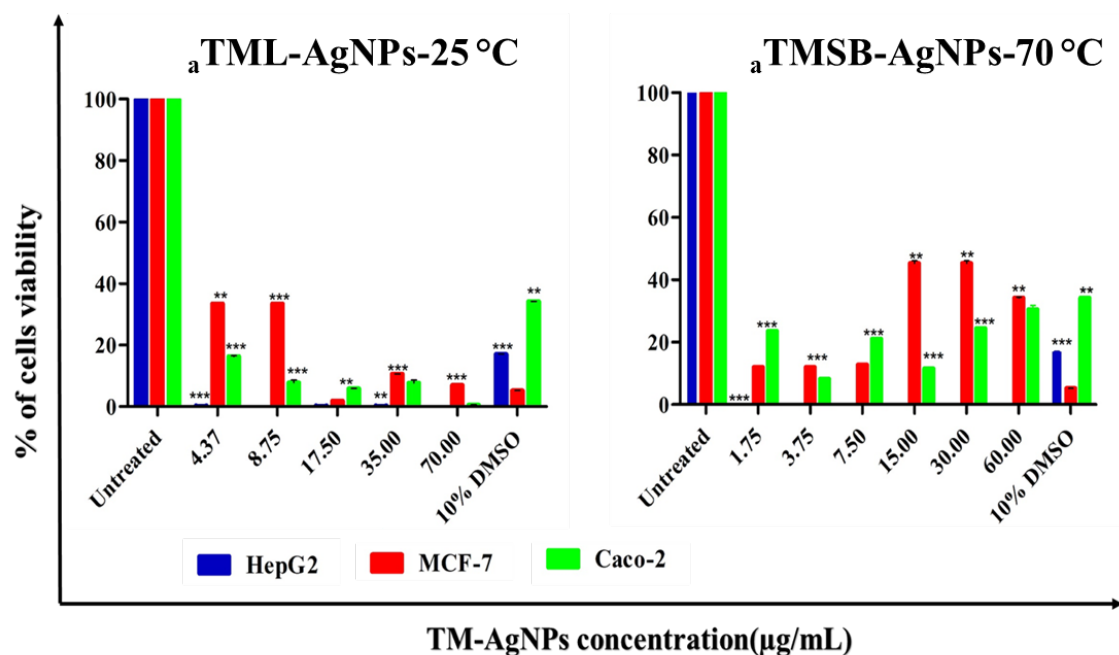


**Figure 32:** Effects of increasing concentrations of silver nanoparticles on the viability of Caco-2, HepG2 and MCF-7 cells.

Note: Cell viability was analyzed using the MTT assay. Cells were treated with increasing concentrations of <sup>a</sup>TML-AgNPs-25 °C and <sup>a</sup>TMSB-AgNPs-70 °C with Caco-2, MCF-7 and HepG2 cells for 24 hrs.

Results represent the average of two independent experiments performed in triplicate. A two-tailed, unpaired t-test was used to analyze significance. \*p<0.05, \*\* p<0.001, \*\*\*p<0.0001, significant difference compared to untreated sample.

**Abbreviation:** AgNPs, silver nanoparticles; TM, *Terminalia mantaly*; a, represents aqueous extracts; m, represents methanolic extracts; TML, TM leaf extracts; TMSB, TM stem bark extracts; Caco-2, human colorectal adenocarcinoma; MCF-7, human breast adenocarcinoma; HepG2, human liver carcinoma.

The anti-carcinogenic effect of phytoconstituents-mediated AuNPs (Patil *et al.*, 2018) and AgNPs (Devaraj *et al.*, 2014) creates a center of attention on the growing interest in AuNPs and AgNPs synthesis, which are being well-thought-out as novel agents. In this report, we elucidated the therapeutic anti-carcinogenic effect of bio-active nanoparticles (<sup>a</sup>TMR-AuNPs-25 °C, <sup>m</sup>TMSB-AuNPs-70 °C, <sup>a</sup>TML-AgNPs-25 °C, <sup>a</sup>TMSB-AgNPs-70 °C) and bio-active extracts (<sup>m</sup>TMSB and <sup>m</sup>TMR) against MCF-7, HepG2 and Caco-2 cancer cells and non-cancerous fibroblast cell line (KMST-6). Most of the tested samples showed the anticancer activity and the cytotoxicity of TM-AuNPs was lower than that of the TM-AgNPs. This difference could be attributed to the surface charges between NPs. MCF-7 cells were more sensitive to the treatment compared to HepG2 and Caco-2 cells. Such variation in cytotoxicity from one cell to another is due to differences in their origin, morphology, and genomes (Diab *et al.*, 2015). The study also highlighted the selective effect of bio-active TM extracts and

TM-AuNPs on non-cancerous fibroblast cells (KMST-6) and could be used as a potent therapeutic agent for further development of anticancer drugs.

According to this criterion of National Cancer Institute (NCI), plant-derived products are generally considered to have *in vitro* cytotoxic activity if the IC<sub>50</sub> value in cancer cells is ≤ 30 µg/mL following incubation between 48-72 hrs (Talib and Mahasheh, 2010), <sup>a</sup>TML-AgNPs-25 °C, <sup>a</sup>TMSB-AgNPs-70 °C, and <sup>m</sup>TML-AuNPs-25 °C were highly cytotoxic. Additionally, base on the availability of kit reagent of Annexin V-Cy3<sup>TM</sup> Apoptosis detection kit, CM-H<sub>2</sub>DCFDA probe to quantify ROS generation and Propidium iodide cell cycle kit analysis, gold nanoparticles (<sup>m</sup>TMSB-AuNPs-70 °C) with IC<sub>50</sub> ≤40 µg/mL and extracts (<sup>m</sup>TMSB and <sup>m</sup>TMR) with IC<sub>50</sub> ≥ 50 µg/mL at least 2 cancer cell lines were also selected for further experiment.

### III.3.2 Effect Of The Selective Crude Extract, More Stable Gold And Silver Nanoparticles On A Normal Fibroblast Cells Line (KMST-6)

The selectivity assay was performed with the two bio-active <sup>m</sup>TMSB, <sup>m</sup>TMR, <sup>m</sup>TMR-AuNPs-25 °C, <sup>m</sup>TMSB-AuNPs-70 °C, <sup>a</sup>TML-AgNPs-25 °C and <sup>a</sup>TMSB-AgNPs-70 °C on non-cancerous fibroblast skin cell line (KMST-6). The values CC<sub>50</sub> are summarized in **Table 13** and ranged from 9.380 to 961.300 µg/mL and the selective indexes were ranged from 0.739 to 1563.330. The <sup>m</sup>TMSB and <sup>m</sup>TMR were non-toxic with high selectivity index especially with Caco-2 cells and <sup>m</sup>TMR (SI=168.144 ug/mL). Similarly, the TM-AuNPs showed no significant toxicity towards KMST-6 cells (**Figure 36**). The values CC<sub>50</sub> of 275.700 µg/mL and the selectivity index of 1399.492 was obtained with <sup>m</sup>TMR-AuNPs-25 °C towards HepG2. The results corroborate with the finding of Elbagory *et al.* (2017) that showed that synthesize biogenic AuNPs from the South African *Galenia africana* and *Hypoxis hemerocal-lidea* plants extracts showed that there was no significant reduction in viability of KMST-6 cell after 24 hrs treatment with different concentrations (up to 32 nM) of the AuNPs. The same finding has been demonstrated by Patra *et al.* (2020), showing that AuNPs were non-toxic towards Hek293T cells signified that the AuNPs can be used for drug delivery as well as bio-imaging applications. Studies have shown that biocompatible AuNPs can be delivered and minimizing treatment duration and side effects (Mitra *et al.*, 2015). These findings suggested that AuNPs-assisted thermotherapy could cause targeted cancer cell ablation while avoiding damage to surrounding noncancerous cells (Grijalva *et al.*, 2018). Regarding silver nanoparticles, the selectivity index of <sup>a</sup>TMSB-AgNPs-70 °C and <sup>a</sup>TML-AgNPs-25 °C was higher on HepG2 with selectivity index of 190.500 and 1563.330 % respectively and which may suggest

that these nanoparticles can be safely used in cancer therapy. Controversy, TM-AgNPs were most toxic compared to TM-AuNPs especially with <sup>a</sup>TMSB-AgNPs-70 °C that revealed the CC<sub>50</sub> value of 1.524 µg/mL on KMST-6 and selectivity index (SI) of 0.739 towards MCF-7 cells. **Ahamed and coworkers. (2019)** demonstrated the adverse effects of AgNPs in mammalian cells. Moreover, according to the previous studies, AgNPs causes cytotoxicity of the fibroblast cells by altering the morphology, reducing the viability along with oxidative stress (**Aziz et al., 2019**). In context to normal cells exposed to AgNPs, an increase in cytotoxicity, genotoxicity, and activation of signaling and inflammatory response, to a large extent, is associated with the generation of ROS, free radicals and consequently buildup of oxidative stress (**Ahamed et al., 2019**). Some authors also evaluated the contribution of Ag<sup>+</sup> ions present in the AgNPs particles itself and not by the ions released in solution (**Beer et al., 2012**). However, contradicting data has been presented in other studies that show that Ag ions are the ones responsible for AgNPs-induced toxicity (**Miura and Shinohara, 2009; Li et al., 2010**).

**Table XIII:** Cytotoxicity evaluation of most promising crude extracts, AuNPs, and AgNPs against non-cancerous fibroblast KMST-6 cells.

Acronym	Non-cancerous	Cancer cells line		
	Fibroblast cell			
	line	KMST-6	MCF-7	HepG2
	CC <sub>50</sub> (µg/mL)	Selectivity index (CC <sub>50</sub> /IC <sub>50</sub> )		
<sup>m</sup> TMR	459.200±0.0120	168.144±0.010	10.619±0.120	5.147±0.010
<sup>m</sup> TMSB	961.300±0.030	23.722±0.050	23.332±0.010	12.597±0.110
<sup>m</sup> TMR-AuNPs-25 °C	275.700±0.010	82.050±0.010	1531.660±0.100	11.690±0.500
<sup>m</sup> TMSB-AuNPs-70 °C	334.500±0.020	269.750±0.100	9.225±0.110	50.990±0.100
<sup>a</sup> TML-AgNPs-25 °C	9.380±0.400	2.128±0.050	1563.330±0.140	16.31±0.000
<sup>a</sup> TMSB-AgNPs-70 °C	1.524±0.330	0.739±0.610	190.500±0.500	3.116±0.610

**Abbreviations:** AuNPs, gold nanoparticles; AgNPs, silver nanoparticles; TM, *Terminalia mantaly*; <sup>a</sup>, represents aqueous extracts; <sup>m</sup>, represents methanolic extracts; TML, TM leaf extracts; TMR, TM root extracts; TMSB, TM stem bark extract; KMST-6, non-cancerous human fibroblast cells; CC<sub>50</sub>, 50% cytotoxicity concentration; SI, selectivity index.



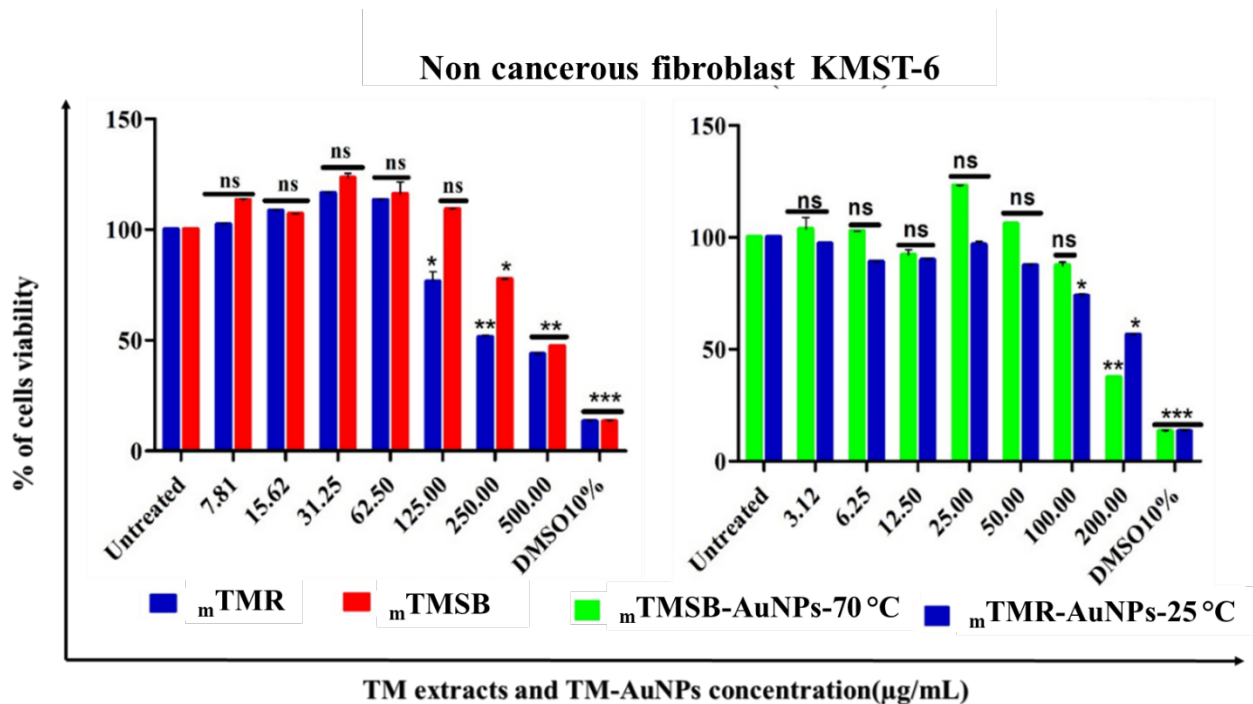


**Figure 33:** Cytotoxicity evaluation of bio-active TM extracts and TM-AuNPs at various concentrations against KMST-6 fibroblast normal cells.

**Note:** Results represent the average of two independent experiments performed in triplicate. A two-tailed, unpaired t-test was used to analyze significance. \* $p < 0.05$ , \*\*  $p < 0.001$ , \*\*\* $p < 0.0001$ , significant difference compared to untreated sample.

**Abbreviation:** AuNPs, gold nanoparticles; TM, *Terminalia mantaly*; a, represents aqueous extracts; m, represents methanolic extracts; TMR, TM root extracts; TMSB, TM stem bark extracts; KMST-6, non-cancerous fibroblast cell line.

To better understand the cancer cells death mode of action induced by most potent extracts, gold and silver nanoparticles, the Annexin V-Cy3<sup>TM</sup> Apoptosis detection kit, CM-H<sub>2</sub>DCFDA probe to quantify the intracellular ROS generation and cell DNA propidium iodide staining cycle analysis using flow cytometry were performed.

### III.3.3 Therapeutic Potential Of Targeted Nanotherapy: Investigation Into The Mode Of Cell Death Induced By Bio-active Crude Extracts, AuNPs, And AgNPs

Biochemical assays such as Annexin V-Cy3<sup>TM</sup> Apoptosis detection kit, CM-H<sub>2</sub>DCFDA probe to quantify the intracellular ROS generation and cell DNA propidium iodide staining cycle analysis using flow cytometry were used to determine the therapeutic potential of selected samples including mTMR, mTMSB, mTMR-AuNPs-25 °C, mTMSB-AuNPs-70 °C, aTML-AgNPs-25 °C, and aTMSB-AgNPs-70 °C on three cancer cells line (Caco-2, HepG2, and MCF-7) and non-cancerous fibroblast cell line (KMST-6).

### III.3.3.1 Annexin V-Cy3 Apoptosis Detection Assay, Induced By Bio-active Extracts, TM-AuNPs And TM-AgNPs On Caco-2, HepG2, and MCF-7 Cells

Apoptosis is a form of programmed cell death and one of the roles of apoptosis is to prevent the development of cancer. The extracts and nanoparticles with pro-apoptotic activities in cancer cells are therefore potentially useful in anti-cancer drug research (Saibu *et al.*, 2015). In this study, the apoptotic effects of the selected samples including  $_m$ TMR,  $_m$ TMSB,  $_m$ TMR-AuNPs-25 °C,  $_m$ TMSB-AuNPs-70 °C,  $_a$ TML-AgNPs-25 °C, and  $_a$ TMSB-AgNPs-70 °C and cisplatin at their IC<sub>50</sub> values exposed by Caco-2, HepG2 and MCF-7 cells were examined using Annexin V-Cy3<sup>TM</sup> Apoptosis detection assay. Concerning MCF-7 cells, apoptotic population ranged from 6.60 to 79.00% (Table XIV). While the percentage varied from 6.60 to 31.60 %, 21.70 to 79.00, and 5.60 to 26.50 % at early apoptotic, late apoptotic, and necrosis phase respectively in a dose-dependent manner (Appendix 11). For HepG2 cells, the percentage of apoptotic varied from 18.22 to 79.85 %, 1.55 to 60.53 %, and 60.53 to 15.16 %, at early apoptotic, late apoptotic and necrosis phase respectively (Table XIV, Appendix 12). The percentage of apoptotic Caco-2 cells varied from 66.24 to 83.86 %, at early apoptotic, late apoptotic, and necrosis phase respectively (Table XIV, Appendix 13). The bio-active TM extracts, TM-AuNPs and TM-AgNPs mostly induced the MCF-7 cell death at the late apoptotic phase and could be explained by the fact that the bio-active extracts and nanoparticles induced the DNA fragmentation content of MCF-7 cells, also the activation of mitochondrial pathways mediated by the family of proteins known as caspases (Reed *et al.*, 2005). Whereas, the bio-active TM extracts, TM-AuNPs, and TM-AgNPs mostly induced the Caco-2 and HepG2 cells death at the early apoptotic phase. The increase of the population at the early apoptotic can be explained by the presence of alterations in membrane asymmetry (i.e., translocation of phosphatidylserine from the cytoplasmic to the extracellular side of the membrane) and a prelytic DNA fragmentation (Jyotirmoy, 2012). The  $_m$ TMSB induced more apoptotic on Caco-2 cells (78.01%) when compared to  $_m$ TMR (66.24%). This result is consistent with what has been obtained by Shalom J and Cock. (2018) that demonstrated that the fruits extracts from *Terminalia ferdinandiana* possessed apoptotic activities against a panel of human carcinoma cell lines including Caco-2 cells. Cell imaging studies detected morphological features consistent with apoptosis in Caco-2 cells exposed to ethyl acetate, methanolic, and aqueous extracts. Caspase 3 activity was significantly elevated in Caco-2 cells exposed to these extracts, indicating that apoptosis was induced. Pucci *et al.* (2000) showed the extracts of *A. santolina* and *R. sativus* induced apoptosis and necrosis in Caco-2 cells with a higher

apoptotic effect (18.2 %) than treatment of *A. santolina* extract (9.6 %). This could be due to the effect of higher phenolic content on cells at G1 phase which is the state preceding DNA replication in which factors such as cellular conditions (metabolism, signaling, and cell size) influence cell cycle progression. The <sub>m</sub>TMR (44.60 %) induced a less apoptotic effect on MCF-7 cells when compared to <sub>m</sub>TMSB (62.50 %). Nevertheless, the <sub>m</sub>TMR (26.50 %) also induced a more necrotic effect on MCF-7 cells compared to <sub>m</sub>TMSB (16.90 %). The results were inconsistent with the previous finding that showed no toxic effects of TM extracts (<sub>m</sub>TMSB and <sub>m</sub>TMR) against non-cancerous KMST-6 cells. The study conducted by **Salem *et al.* (2002)** showed that some apoptosis was induced on MCF-7 cells by the extract at lower concentrations, but at higher concentrations, necrosis was the major mechanism of cell death. The <sub>m</sub>TMSB induced more apoptotic (70.23 %) and less necrotic effect (1.99 %) on HepG2 cells when compared to <sub>m</sub>TMR with a percentage of 35.96 % and 15.16 % for early apoptotic and necrotic phase respectively (**Table XIV**). The results were concordant with those from the study of **Sivalokanathan *et al.* (2006)** that demonstrated that *Terminalia arjuna* bark extract has shown profound effects on HepG2 cells and exhibits its cytotoxicity to these cells and the cell death is mediated by apoptosis. Nanoparticles induced more apoptotic effects in Caco-2, HepG2, and MCF-7 cells compared to extracts. Indeed, the high early apoptotic cells population was obtained with <sub>a</sub>TMSB-AgNPs-70 °C (79.85 %) compared to <sub>a</sub>TML-AgNPs-70 °C (68.86 %) with HepG2 cells. Besides, TM-AgNPs revealed a high population at the late apoptotic with MCF-7 cells and the percentage was highest with <sub>a</sub>TML-AgNPs-70 °C (67.35 %) compared to <sub>m</sub>TMSB-AgNPs-25 °C (35.69 %). The apoptotic effect found in this study is in agreement with findings from other studies. For instance, **Krishnaraj *et al.* (2014)** reported that AgNPs biosynthesized nanoparticles with *Acalypha indica* extract exerted a cytotoxic effect in MDA-MB-231 human breast cancer cells. Moreover, the green synthesized AgNPs from *Cynara scolymus* leaf extract, showed efficient anti-cancer activities via mitochondrial apoptosis in MCF-7 cells (**Erdogan *et al.*, 2019**). As well, it has been proven that AgNPs exposure resulted in alterations in apoptosis evident in the activation of caspase-3 and led to significant suppression of cell growth of human breast cancer cells (MDA-MB-231) (**Gurunathan *et al.*, 2013**). Regarding gold nanoparticle, the <sub>m</sub>TMSB-AuNPs-70 °C (63.75 %), was able to induce more than 50 % apoptosis effect on MCF-7 cells compared to <sub>m</sub>TMR-AuNPs-25 °C (16.61 %). **Banu and coworkers. (2018)** demonstrated the enhanced ability of gold and silver nanoparticles biomimetically synthesized using Date Palm Pollen extract to induce apoptosis in human breast adenocarcinoma cells (MCF-7). The TM-AuNPs showed a similar early apoptotic effect on Caco-2 and HepG2 cells. For example, the early apoptotic

effect of *m*TMSB-AuNPs-25 °C (73.61%) was higher when compared to *m*TMR- AuNPs-25 °C (65.42 %) with HepG2 cells. Similar results were obtained on the biosynthesis of AuNPs using the seed coat of *Cajanus cajan* which led to HepG2 cell apoptosis with spherical shapes of AuNPs having the size of 9 to 41 nm in diameter (**Ashokkumar *et al.*, 2014**). The bioactive nanoparticles previously showed smaller particle sizes. Smaller nanoparticles show a higher accumulation at tumour sites and prolong *in vivo* half-life due to their avoidable capture by the reticuloendothelial system (**Loutfy *et al.*, 2015**). This phenomenon, called enhanced permeability and retention (EPR) effect, provides higher accumulations of nanoparticles with a smaller particle size than 100 nm into the tumour (**Erdogan *et al.*, 2019**). The apoptosis effects of TM extracts could be due to their flavonoid contents. Medicinal plants are a source of a large number of bioactive that are excellent anticancer agents as they have the efficiency to regulate the molecular mechanisms and various signaling pathways involved in carcinogenesis such as oxidation, apoptosis, cell proliferation, metastasis, and angiogenesis. **Park *et al.* (2008)** claimed that flavonoids would induce apoptosis in cancer cells. The results of this study suggest that the differences in the mechanisms of toxicity induced by extracts and nanoparticles may be large as a consequence of the type of cells used. This differential rather than the universal response of different cell types exposed to extracts and nanoparticles may play an important role in the mechanism of their toxicity (**Sahu *et al.*, 2014**). Therefore, those nanoparticles may act as new cell death regulators. Nanoparticles -induced DNA damage often leads to activation of the cytoplasmic protein p53 and activation of caspase.

**Table XIV:** Apoptotic effects of more potent extracts, TM-AuNPs and TM-AgNPs against Caco-2, HePG2 and MCF-7 cells.

Acronym	Annexin V –Cys <sup>TM</sup> Apoptosis Cells population (%)											
	MCF-7				HePG2				Caco-2			
	Viable cells	Early apoptotic	Late apoptotic	Necrotic	Viable cells	Early apoptotic	Late apoptotic	Necrotic	Viable cells	Early apoptotic	Late apoptotic	Necrotic
<b>Crtl</b>	99.90±1.68	0.00±0.00	0.00±0.00	0.1±1.09	94.18±4.15	0.00±0.00	0.07±0.06	5.81±4.13	94.83±0.78	0.73±0.46	0.53±0.05	3.91±1.29
<b>Cisplatin</b>	8.70±1.98	6.60±1.95	79.00±3.80	5.60±0.16	18.37±0.36	18.22±0.02	60.53±0.47	2.98±0.01	10.25±0.25	83.86±0.02	5.75±0.24	0.16±0.02
<b>mTMR-AuNPs-25 °C</b>	36.80±1.81	31.60±3.79	21.70±5.09	9.90±0.52	35.09±0.08	65.42±3.42	2.08±0.07	1.82±0.02	12.42±0.79	82.61±0.74	4.22±0.33	0.76±0.28
<b>mTMSB-AuNPs-70 °C</b>	11.40±0.04	10.5±6.21	70.00±6.27	8.11±0.02	24.21±3.61	73.61±3.50	24.21±3.61	1.58±0.01	17.83±0.03	82.29±1.14	0.91±0.01	0.12±0.04
<b>mTMSB</b>	9.60±1.51	11.00±1.11	62.5±2.76	16.90±0.11	26.47±0.03	70.23±0.18	1.55±0.01	1.99±0.01	12.42±0.69	78.01±0.43	7.52±0.13	2.06±0.13
<b>mTMR</b>	19.80±2.61	9.10±0.65	44.60±7.22	26.50±3.96	46.20±0.01	35.96±0.04	2.76±0.01	15.16±0.02	25.94±1.00	66.24±4.05	6.06±2.21	1.78±0.82
<b>aTML-AgNPs-25 °C</b>	30.40±13.16	9.00±1.67	52.10±16.97	8.70±3.98	30.25±0.01	68.86±0.01	2.52±0.02	0.39±0.02	14.93±0.01	83.65±0.05	1.42±0.01	0.05±0.00
<b>aTMSB-AgNPs-70 °C</b>	17.30±0.71	7.30±0.46	68.70±1.38	6.70±0.20	16.5±0.40	79.85±0.94	2.91±0.76	2.45±0.04	26.21±0.92	73.33±1.06	0.26±0.01	0.76±0.28

**Note:** Data represents the mean ± standard error of the mean (SD) of three independent experiments (n = 3 per group). Significance was accepted at a P-value = 0.05. No differences were found in active TM extracts, TM-AuNPs, and TM-AgNPs-exposed cells compared with controls (untreated cells).

**Abbreviations:** AuNPs, gold nanoparticles, AgNPs, silver nanoparticles; TM, *Terminalia mantaly*, a, aqueous extracts; m, methanolic extracts; TML-AgNPs, AgNPs from TM leaf extracts; TMSB-AgNPs, AgNPs from of TM stem bark extracts; TMR-AuNPs, AuNPs from TM root extracts; MCF-7, Human breast adenocarcinoma cells, HePG2, Human Hepatocellular Carcinoma, Caco-2, Colorectal adenocarcinoma.

### III.3.3.2 Detection Of Intracellular Oxidative Stress-Induced By Bio-active Extracts, TM-AuNPs And TM-AgNPs On Caco-2, HepG2 and MCF-7 Cells

Apoptosis can be triggered by increased intracellular ROS levels, which are strong evidence involved in the induction of apoptosis (Li *et al.*, 2014). To further explore if the mitochondrial dysfunction was related to the generation of ROS, we determined the ROS level in MCF-7 HepG2 and Caco-2 cells stained with H<sub>2</sub>DCF-DA by using confocal microscopy and the flow cytometry. As shown in **Table XV**. The effect of the bio-active TM extracts, and TM-AuNPs and TM-AgNPs conjugates on mitochondrial function and oxidative stress were assessed to determine the health status of the cells. The amount of ROS within the cells was examined to determine whether the various samples induce cellular oxidative stress. The CM-H<sub>2</sub>DCFDA probe was used to detect and quantify the intracellular ROS produced by the cells. CM-H<sub>2</sub>DCFDA is a nonfluorescent ROS indicator that is oxidized to 2', 7'-dichlorofluorescein (DCF) in the presence of ROS. CM-H<sub>2</sub>DCFDA is a cell-permeable fluorogenic probe that can be used to assess oxidative stress in cultured cells (Wu and Yotnda, 2011). When the CM-H<sub>2</sub>DCFDA probe is taken up by the cells, the cellular esterases deacetylate the probe to a non-fluorescent compound that is later oxidized by ROS into the highly fluorescent compounds, DCF. The intracellular ROS levels were examined in MCF-7, HepG2 and Caco-2 cells treated with selected samples including *m*TMR, *m*TMSB, *m*TMR-AuNPs-25 °C, *m*TMSB-AuNPs-70 °C, *a*TML-AgNPs-25°C, *a*TMSB-AgNPs-70 °C and 0.1 % H<sub>2</sub>O<sub>2</sub> as positive control by flow cytometric analysis (**Appendix 14, 15 and 16**). An increase in cell fluorescence was an indication of ROS production in the cells. Concerning MCF-7 cells, the percentage of positive ROS ranged from 3.40 to 69.37 % (**Table XV**). For HepG2 cells, the percentage of positive ROS varied from 6.95 to 62.83 % (**Table XV**). Regarding Caco-2 cells, the percentage of positive ROS ranged from 4.2 to 65 % (**Table XV**). Gold nanoparticles generated an increased ROS level compared to the extracts and silver nanoparticles in a concentration-dependent manner (**Appendix 14, 15, and 16**). For example, *m*TMSB-AuNPs-70 °C generated a positive cellular ROS population of 62.83 % on HepG2 cells. However, cells treated with *m*TMSB showed higher ROS levels of 38.56 % and 45.87 % on HepG2 and Caco-2 cells respectively. Similarly, cells treated with *a*TML-AgNPs-25 °C showed higher ROS levels compared to *a*TMSB-AgNPs-70 °C especially on Caco-2 cells with a percentage of 63.36%. The results corroborate those of Boca and coworkers (2011) that found an increased level of intracellular ROS in HT-29 cells treated with silver nanoparticles. Besides, Bohmert *et al.* (2012) reported that AgNPs increased ROS production and cytotoxic effects in human colo-

rectal adenocarcinoma (Caco-2) cells. Furthermore, one of the most important mechanisms of the toxicity of AgNPs is that excessive levels of intracellular ion concentration increase the production of ROS, which is produced by cellular oxygen metabolism (Carlson *et al.*, 2008) and uncontrolled ROS production can lead to serious cellular injuries, such as DNA damage and mitochondria-involved apoptotic cell death (Gurunathan *et al.*, 2013). Oxidative stress is a response for an increased generation or elimination of ROS which induce cellular injury at cellular levels. Increased generation of free radicals induces by lipid peroxidation which is the major consequence of oxidative stress and antioxidant depletion in cancer cell lines. Zorov *et al.* (2014) demonstrated that the overproduction of ROS levels by a cellular disruption in many cellular processes that occurs during cell proliferation, inflammation and apoptosis, further increased ROS generation triggers cell death have been reported apoptosis can be triggered by increased intracellular ROS levels, which are also strong evidence involved in the induction of apoptosis (Li *et al.*, 2014). The observed activity with TM extracts might be attributed to their high phenolic contents. The phytochemical studies previously revealed the presence of phenols and flavonoids. Most Terminalia species were reported to possess antioxidant activity. The antioxidant activity of the *Terminalia arjuna* bark and *Terminalia chebula* a fruit extract was studied and showed that they possessed a potent antioxidant activity (Fahmi *et al.*, 2015). In terms of acute toxic effects to cells, noble gold and silver metallic nanoparticles have been shown to induce oxidative damage (Conde *et al.*, 2012). Matulionyte *et al.* (2017) demonstrated that photoluminescent gold nanoclusters have specific toxicity against MCF-7 breast cancer cells by increasing the ROS generation. Mechanistic studies have shown that exposure to AgNPs is associated with the generation of ROS, DNA damage, lipid peroxidation that often leads to cytotoxicity, and ultimately cell death (Lima *et al.*, 2012). AgNPs may trigger oxidative stress by reactive oxygen species (ROS) production (Zhang and Gurunathan, 2016) causing a variety of intracellular responses and alterations in antioxidant systems (Zorov *et al.*, 2014) which finally could lead to apoptosis or necrosis. AgNPs action mechanisms involve the release of silver cations and further interaction with biomolecules such as DNA and proteins, affecting cell membrane integrity, lactate dehydrogenase (LDH) levels, and mitochondrial permeability and leading finally to oxidative stress and apoptosis (Li *et al.*, 2005; Salazar *et al.*, 2018). AgNPs and AuNPs with elevated activity due to their large surface to volume ratio could easily enter the cells, interact with cell constituents, and thus disturb the cellular signaling pathways (Park *et al.*, 2010). Importantly, the ROS leads to the activation of caspase-3 which is responsible for cell apoptosis by arresting the cell cycle at the G2/M phase (Rai *et al.*, 2016). The findings suggest that the Caco-2,

HepG2, and MCF-7 cells cytotoxicity induced by the TM extracts ( $m$ TMSB), TM-AgNPs ( $a$ TML-AgNPs-25 °C) and TM-AuNPs ( $m$ TMR-AuNPs-70 °C) is somehow mediated through the induction of increased levels of oxidative stress.

**Table XV:** Effects of more potent extracts, TM-AuNPs and TM-AgNPs on ROS generated by MCF-7, HePG2 and Caco-2 cells

Acronym	Intracellular positive ROS percentage (%)		
	MCF-7	HepG2	Caco-2
<b>Crtl</b>	3.4±0.10	6.95±0.01	4.12±0.02
<b>H<sub>2</sub>O<sub>2</sub></b>	69.37±0.00	48.00±0.10	65.00±0.01
<b><math>m</math>TMR-AuNPs-25 °C</b>	53.87±0.01	38.88±0.01	53.58±0.00
<b><math>m</math>TMSB-AuNPs-70 °C</b>	53.89±0.02	62.83±0.01	58.28±0.02
<b><math>m</math>TMSB</b>	8.35±0.18	24.81±0.05	37.84±0.03
<b><math>m</math>TMR</b>	11.23±0.02	38.56±0.02	45.85±0.00
<b><math>a</math>TML-AgNPs-25 °C</b>	21.83±0.01	18.83±0.10	63.36±0.05
<b><math>a</math>TMSB-AgNPs-70 °C</b>	19.71±0.05	13.78±0.03	36.96±0.02

**Abbreviations:** AuNPs, gold nanoparticles, AgNPs, silver nanoparticles; TM, *Terminalia mantaly*, a, aqueous extracts; m, methanolic extracts; TML-AgNPs, AgNPs from TM leaf extracts; TMSB-AgNPs, AgNPs from of TM stem bark extracts; TMR-AuNPs, AuNPs from TM root extracts; MCF-7, Human breast adenocarcinoma cells, HePG2, Human Hepatocellular Carcinoma, Caco-2, Colorectal adenocarcinoma.

**Note:** Data represents the mean ± standard error of the mean (SD) of three independent experiments (n = 3 per group). Significance was accepted at a P-value = 0.05. No differences were found in active TM extracts, TM-AuNPs, and TM-AgNPs-exposed cells compared with controls (untreated cells).



### III.3.3.3 DNA Staining Cell Cycle Of Bio-active Extracts, TM-AuNPs And TM-AgNPs On Caco-2, HepG2 And MCF-7 Cells

Flow cytometry cell cycle analysis using propidium iodide (PI) DNA staining was performed with bio-active including  $mTMR$ ,  $mTMSB$ ,  $mTMR$ -AuNPs-25 °C,  $mTMSB$ -AuNPs-70 °C,  $aTML$ -AgNPs-25 °C,  $aTMSB$ -AgNPs-70 °C and cisplatin their  $IC_{50}$  values with Caco-2, MCF-7, and HepG2 cells. The different phase G<sub>0</sub>/G<sub>1</sub>, S Phase, G<sub>2</sub>/M phase was significantly increased in a dose-dependent manner (**Appendix 17, 18, and 19**).

Concerning MCF-7, the cells population ranged from 7.05 to 71.00 % (**Table XVI**). For HepG2, the cells population ranged from 10.15 to 73.71 % (**Table XVI**). Regarding Caco-2, the cells population varied from 7.65 to 84.05 % (**Table XVI**). Generally, the bioactive gold nanoparticles efficiently arrests the cell-cycle progression of MCF-7, HepG2, and Caco-2 cells at the G<sub>2</sub>/M phase (**Table XVI**). For example, the  $mTMR$ -AuNPs-25 °C were more encountered in G<sub>2</sub>/M (51.90 %) especially with MCF-7 and it consequently leads to apoptosis. Biogenic AuNPs mostly induced the G<sub>2</sub>/M arrest that could be through microtubule stabilization (**Cardoso et al., 2009; Kim et al., 2011; Chen et al., 2015**). Also, **Fraga et al. (2013)** reported that 20 nm Cit-AuNPs induced DNA damage (G<sub>2</sub>/M) in HepG2 cells at the 24hrs of exposure. The  $mTMR$ , and  $mTMSB$  (28.70 % and 27.40 %) were slightly found to be in the G<sub>2</sub>/M phase after 24 hrs of treatment with MCF-7 cells. Similar results obtained by **Sundarraaj et al. (2012)** who reported that *Acacia nilotica* extract inhibited the cell proliferation in human breast MCF-7 cancer cells by blocking the G<sub>2</sub>/M phase. **Sundarraaj et al. (2012)** reported that *Acacia nilotica* extract inhibited the cell proliferation in human breast MCF-7 cancer cells by blocking the G<sub>2</sub>/M phase.

Biocompatible TM-AuNPs could inhibit lysosome rupture and switched G<sub>0</sub>/G<sub>1</sub> arrest to G<sub>2</sub>/M arrest. Finally, TM-AuNPs could act by stabilizing microtubules and caused G<sub>2</sub>/M arrest by inducing interactions between lysosomes and microtubules. Therefore, the transport of nanoparticles can affect dynamic changes in microtubules. Microtubule-interfering drugs affect the cell cycle distribution by impairing the mitotic checkpoint and regulating the activity of cyclins and CDKs. The stabilization and destabilization of microtubules could impair the mitotic checkpoint and cause G<sub>2</sub>/M arrest. (**Sudo et al., 2004; Nakayama et al., 2009**). Generally, Caco-2 and HePG2 cells treated with bioactive extracts and silver nanoparticles were found to be in the G<sub>0</sub>/G<sub>1</sub> phase. Notably,  $mTMSB$  (70.10 %) and,  $mTMR$  (73.5 %) treated with HepG2 cells were found to be in the G<sub>0</sub>/G<sub>1</sub> phase, compared with 69.55 % in the control group.

A similar study was conducted using an ethanol extract of mastic have been also studied for their anticancer potential and the extracts caused tumour growth suppression of colon cancer cells and G0/G1 cell cycle arrest (**Fitsiou and Pappa, 2019**). The treated HepG2 cells with 1/10 of IC<sub>50</sub> of *A. santolina* induce sub G0 phase apoptosis (**SánchezCarranza et al., 2017**).

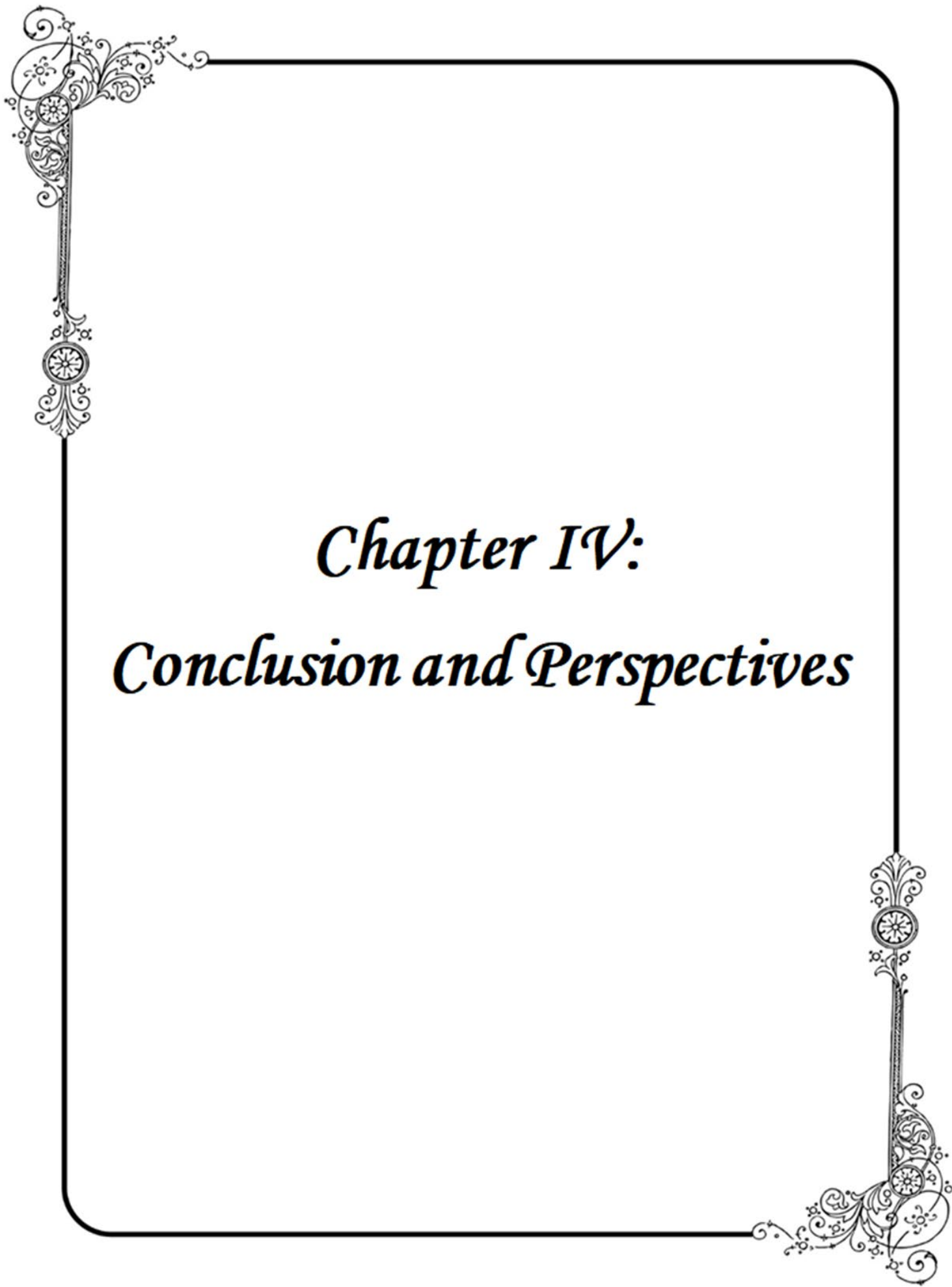
The plant extracts showed a strong effect on G1 checkpoint arrest and induced a high effect on cell apoptosis (**Bortolotto et al., 2016**). This also may due to higher antioxidant activity of flavonoids and phenolic compounds on G1 checkpoints. This result is in agreement with recent *in vitro* studies performed on different cancer cell lines which were treated with extracts of some medicinal plants (*Glycyrrhiza glabra* and *Lepidium sativum*) which contain high levels of polyphenols and flavonoid compounds. Moreover, <sup>a</sup>TML-AgNPs-25 °C, <sup>a</sup>TMSB-AgNPs-70 °C treated with HepG2 (65 and 68.45 %) and Caco-2 (62.75 and 84.05 %) were found to be in the G0/G1 phase, compared with 69.55 in the control group.

However, Caco-2 and HePG2 cells treated with <sup>m</sup>TMR and <sup>a</sup>TMSB-AgNPs-70 °C gave a percentage of 81.45 and 84.05 % were found to be in G0/G1 phase (**Table XVI**). Notably, for the HepG2 cells treated with <sup>m</sup>TMSB (70.10 %), <sup>m</sup>TMR (73.50 %), <sup>a</sup>TML-AgNPs-25 °C (65.00 %), and <sup>a</sup>TMSB-AgNPs-70 °C (68.45 %) were found to be in the G0/G1 phase, compared with 69.55 % in the control group. Our results effects are similar in previous studies of polyphenols on cell cycle G1 arrest and induce an apoptotic effect on colon cancer cells (**Huang et al., 2017; López de las Hazas et al., 2017**). Recently, **De Matteis et al. (2015)** proposed that endocytosed AgNPs are degraded in the lysosomes, and the release of Ag<sup>+</sup> ions in the cytosol induces cell damages. We found that cell cycle arrest was different according to the cancer cells and the type and extent of cell cycle arrest varies depending on the composition, size distribution, surface modification, and subsequent surface derivatization of nanoparticles (**Kim et al., 2013; Wu et al., 2013; Estevez et al., 2014**). The link between the effect of silver and gold nanoparticles on apoptotic, chromosomal aberrations, and oxidative damage of DNA of cancer cells was previously reported (**Xie et al., 2011**). The main factors responsible for ROS generation by NPs include interaction with the mitochondria, interaction with NADPH oxidase, and factors related to the physicochemical properties (size, shape, photoreactive properties, and surface chemistry). These factors lead to ROS generation and its consequences, including DNA damage, cell cycle arrest, alterations in apoptosis, and damage to the cell membrane (**Abdal et al., 2017**). Indeed, the potential of nanoparticles to cause DNA damage can be attributed to the generation of the free radical HO<sub>2</sub>, which interacts with DNA to form 8-hydroxyl-2-deoxyguanosine (8-OHdG) that ultimately leads to DNA damage (**Valavanidis**

*et al., 2009*). In HO mediated DNA damage, 8-OHdG is significantly increased during *in vitro* and *in vivo* exposure to nanoparticles (**Eblin *et al.*, 2006**).

**Table XVI:** Apoptotic effects of more potent extracts, TM-AuNPs and TM-AgNPs against MCF-7, HePG2 and Caco-2 cells.

Acronym	Cells cycle phase population (%)								
	MCF-7			HepG2			Caco-2		
	G0/G1	S phase	G2/M	G0/G1	S phase	G2/M	G0/G1	S phase	G2/M
<b>Crtl-</b>	68.70±0.01	9.50±0.03	22.38±0.03	69.55±0.05	14.20±0.20	14.65±0.05	73.7±1.80	7.65±6.55	23.31±2.59
<b>Cisplatin/H<sub>2</sub>O<sub>2</sub></b>	71.00±0.24	8.56±0.06	20.86±0.05	73.71±0.01	14.65±0.15	10.15±0.05	70.52±0.01	8.61±0.01	19.62±1.19
<b>mTMR-AuNPs-25 °C</b>	34.50±0.3	14.10±0.07	51.90±0.04	48.83±0.18	15.30±0.00	35.34±0.56	62.75±0.05	6.85±0.05	30.76±0.06
<b>mTMSB-AuNPs-70 °C</b>	65.40±0.01	10.20±0.05	24.80±0.10	46.60±0.10	17.55±0.15	35.15±0.55	60.95±0.05	6.25±0.05	33.25±0.05
<b>mTMSB</b>	56.00±0.05	14.45±0.05	28.45±0.04	70.10±0.10	11.70±0.20	16.15±0.02	58.40±0.30	14.48±0.08	27.40±0.01
<b>mTMR</b>	58.70±0.22	14.40±0.03	27.40±0.21	73.5±0.05	11.70±0.20	16.15±0.05	81.45±0.05	2.95±0.05	16.05±0.02
<b>aTML-AgNPs-25 °C</b>	57.40±0.04	17.20±0.05	7.1±0.20	65.00±0.00	16.75±0.05	19.65±0.05	62.75±0.05	13.65±0.02	22.60±0.10
<b>aTMSB-AgNPs-70 °C</b>	54.10±0.01	18.00±0.02	11.4±0.05	68.45±0.05	12.35±0.05	19.15±0.05	84.05±4.05	9.25±0.05	3.35±0.03



*Chapter IV:*  
*Conclusion and Perspectives*

## CHAPTER IV: CONCLUSION AND PERSPECTIVES

### IV-1-CONCLUSION

This study investigated the synthesis and characterization of AuNPs and AgNPs, and to evaluate their effects on cancer cells and bacteria strains, the following conclusions were drawn.

- ✚ The SPR values were ranged from 535 to 560 nm, and 438 to 480 nm and thereby confirming the production of gold and silver nanoparticles with monodisperse and mostly spherical in shapes ( ${}_{aTML-AgNPs-25\text{ }^{\circ}C}$  (9.3 nm),  ${}_{aTMSB-AgNPs-70\text{ }^{\circ}C}$  (6.2 nm),  ${}_{mTMR-AuNPs-25\text{ }^{\circ}C}$  (21 nm), and  ${}_{mTMSB-AuNPs-70\text{ }^{\circ}C}$  (28 nm)).
- ✚ The MIC values were ranged from 3.125 and 500  $\mu\text{g/mL}$ . The  ${}_{aTML-AgNPs-25\text{ }^{\circ}C}$  and  ${}_{mTMSB-AuNPs-70\text{ }^{\circ}C}$  were more potent and the  ${}_{aTML-AgNPs-25\text{ }^{\circ}C}$  was bactericidal on all the six susceptible bacteria.
- ✚ The  $IC_{50}$  values ranged from 0.006 to 93.730  $\mu\text{g/mL}$  and nanoparticles were more active than extracts. The MCF-7 cells, were highly susceptible to the effects of  ${}_{mTMR}$  and  ${}_{mTMSB}$  extracts. The  ${}_{aTML-AgNPs-25\text{ }^{\circ}C}$  and  ${}_{aTMSB-AgNPs-70\text{ }^{\circ}C}$  were more promising on the three tested cells line ( $IC_{50}$  of 0.006 and 0.008  $\mu\text{g/mL}$ ), especially on HepG2 cells. Similarly,  ${}_{mTMR-AuNPs-25^{\circ}C}$  displayed cytotoxicity on HepG2 and MCF-7 cells with  $IC_{50}$  values of 0.18 and 6.56  $\mu\text{g/mL}$ . The bio-active extracts and gold nanoparticles showed no significant effect on KMST-6 cells. The  ${}_{mTMSB}$  exhibited a more apoptotic effect (62.5, 70.23, and 78.01 %) and mostly induced cell arrest in G0/G1. The nanoparticles ( ${}_{mTMSB-AuNPs-70\text{ }^{\circ}C}$  and  ${}_{aTML-AgNPs-25\text{ }^{\circ}C}$ ) elucidated more apoptotic effect (70.00, 73.61 and 82.29 %), and (52.10, 68.86, 83.65 %), also induced the cells arrest in G2/M phase ( ${}_{mTMSB-AuNPs-70\text{ }^{\circ}C}$ ) mediated through the induction of increased levels of oxidative stress especially on Caco-2 (63.36%) and HepG2 (62.83) cells line.

## IV-2 PERSPECTIVES

In view of completing the above data and in the perspective to develop 10 years nanoproducts, moreover carrying out the following investigations in the near future;

- ✚ Initiate the procedure to protect these nanoparticles: obtention of patent and IP;
- ✚ Fabrication of target-specific gold and silver nanostructures using cisplatin, and ampicillin;
- ✚ Test the bioactive extracts, gold and silver nanoparticles against other cancer cell lines and also improve the cell death mechanism of action (caspases 3, 9 and Bcl2 regulation) including the study of several signaling pathways and evaluate their *In vivo* anticancer studies.
- ✚ Demonstrate the safety of synthesized nanoparticles on normal cells and also at chronic stage on humans.
- ✚ Evaluate the pharmacokinetics and dynamics properties of synthesized nanoparticles.
- ✚ Functionalize the most active nanoparticles (AgNPs) with peptide (pegylated poly(lactic-co-glycolic (PEG-PLGA) or aptamers following by the docking analysis;
- ✚ Isolation of protein corona from cells enriched with nanoparticles and analyzed using proteomics following by the gene expression as a new approach for cancer treatment.



# *References*



## REFERENCES

- Abbas AK, Janeway CA.** Immunology: improving on nature in the twenty-first century. *Cell*. 2000;100(1):129-38.
- Abdal Dayem A, Hossain MK, Lee SB, Kim K, Saha SK, Yang GM, Choi HY, Cho SG.** The role of reactive oxygen species (ROS) in the biological activities of metallic nanoparticles. *International Journal of Molecular Sciences*. 2017;18(1):120.
- Adiseshiaiah PP, Crist RM, Hook SS, McNeil SE.** Nanomedicine strategies to overcome the pathophysiological barriers of pancreatic cancer. *Nature Reviews Clinical Oncology*. 2016;13(12):750.
- Ahamed M, AlSalhi MS, Siddiqui M.** Silver nanoparticle applications and human health. *Clinica Chimica Acta*. 2010;411(23-24):1841-8.
- Ahamed M, Khan MM, Akhtar MJ, Alhadlaq HA, Alshamsan A.** Role of Zn doping in oxidative stress mediated cytotoxicity of TiO<sub>2</sub> nanoparticles in human breast cancer MCF-7 cells. *Scientific Reports*. 2016;6:30196.
- Ahmad N, Sharma S.** Green synthesis of silver nanoparticles using extracts of *Ananas comosus*. 2012.
- Ahmed S, Chaudhry SA, Ikram S.** A review on biogenic synthesis of ZnO nanoparticles using plant extracts and microbes: a prospect towards green chemistry. *Journal of Photochemistry and Photobiology Biology*. 2017;166:272-84.
- Akindele AJ, Wani ZA, Sharma S, Mahajan G, Satti NK, Adeyemi OO, Mondhe DM, Saxena AK.** *In vitro* and *in vivo* anticancer activity of root extracts of *Sansevieria liberica* Gerome and Labroy (Agavaceae). *Evidence-Based Complementary and Alternative Medicine*. 2015;2015.
- Aljabali AA, Akkam Y, Al Zoubi MS, Al-Batayneh KM, Al-Trad B, Abo Alrob O, Alkilany AM, Benamara M, Evans DJ.** Synthesis of gold nanoparticles using leaf extract of *Ziziphus zizyphus* and their antimicrobial activity. *Nanomaterials*. 2018;8(3):174.
- Alshaye N, Elobeid M, Alkhalifah D, Mohammed A.** Characterization of biogenic silver nanoparticles by *Salvadora persica* leaves extract and Its application against some MDR pathogens *E. coli* and *S.* *Research Journal of Microbiology*. 2017;12:74-81.
- Al-Sheddi ES, Farshori NN, Al-Oqail MM, Al-Massarani SM, Saquib Q, Wahab R, Musarrat J, Al-Khedhairi AA, Siddiqui MA.** Anticancer potential of green synthesized silver nanoparticles using extract of *Nepeta deflersiana* against human cervical cancer cells (HeLA). *Bioinorganic Chemistry and Applications*. 2018;2018.
- Altavilla C, Ciliberto E, editors.** Inorganic nanoparticles: synthesis, applications, and perspectives. *Chemical rubber company press*. 2017 Dec 19.
- Amendola V, Pilot R, Frascioni M, Maragò OM, Iati MA.** Surface plasmon resonance in gold nanoparticles: a review. *Journal of Physics: Condensed Matter*. 2017;29(20):203002.
- Amer S, Aly M, Sabbagh S.** Biocontrol of dermatophytes using some plant extracts and actinomycetes filtrates. *Egyptian Journal of Biotechnology*. 2006;14:291-315.

- Amin RM, Mohamed MB, Ramadan MA, Verwanger T, Krammer B.** Rapid and sensitive microplate assay for screening the effect of silver and gold nanoparticles on bacteria. *Nanomedicine*. 2009;4(6):637-43.
- Anandalakshmi K, Venugobal J, Ramasamy V.** Characterization of silver nanoparticles by green synthesis method using *Petalium murex* leaf extract and their antibacterial activity. *Applied Nanoscience*. 2016;6(3):399-408.
- Ankamwar B.** Biosynthesis of gold nanoparticles (green-gold) using leaf extract of *Terminalia catappa*. *E-Journal of Chemistry*. 2010;7.
- Arbonnier M.** Trees, shrubs and lianas of West African dry zones: Quae; 2004.
- Armendariz V, Herrera I, Jose-yacaman M, Troiani H, Santiago P, Gardea-Torresdey JL.** Size controlled gold nanoparticle formation by *Avena sativa* biomass: use of plants in nanobiotechnology. *Journal of Nanoparticle Research*. 2004;6(4):377-82.
- Arumugam A, Gopinath K.** *In-vitro* callus development of different explants used for different medium of *Terminalia arjuna*. *Asian Journal Biotechnology*. 2011;3(6):564-72.
- Arunachalam KD, Arun LB, Annamalai SK, Arunachalam AM.** Potential anticancer properties of bioactive compounds of *Gymnema sylvestre* and its biofunctionalized silver nanoparticles. *International Journal of Nanomedicine*. 2015;10:31.
- Arvizo RR, Rana S, Miranda OR, Bhattacharya R, Rotello VM, Mukherjee P.** Mechanism of anti-angiogenic property of gold nanoparticles: role of nanoparticle size and surface charge. *Nanomedicine: Nanotechnology, Biology and Medicine*. 2011;7(5):580-7.
- AshaRani P, Low Kah Mun G, Hande MP, Valiyaveetil S.** Cytotoxicity and genotoxicity of silver nanoparticles in human cells. *ACS nano*. 2009;3(2):279-90.
- Ashokkumar T, Prabhu D, Geetha R, Govindaraju K, Manikandan R, Arulvasu C, Singaravelu G.** Apoptosis in liver cancer (HepG2) cells induced by functionalized gold nanoparticles. *Colloids and Surfaces B: Biointerfaces*. 2014;123:549-56.
- Asoh S, Ohta S.** PTD-mediated delivery of anti-cell death proteins/peptides and therapeutic enzymes. *Advanced Drug Delivery Reviews*. 2008;60(4-5):499-516.
- Assadi Z, Emtiazi G, Zarrabi A.** Novel synergistic activities of tetracycline copper oxide nanoparticles integrated into chitosan micro particles for delivery against multiple drug resistant strains: generation of reactive oxygen species (ROS) and cell death. *Journal of Drug Delivery Science and Technology*. 2018;44:65-70.
- Aziz N, Faraz M, Sherwani MA, Fatma T, Prasad R.** Illuminating the anticancerous efficacy of a new fungal chassis for silver nanoparticle synthesis. *Frontiers in Chemistry*. 2019;7:65.
- Badisa RB, Darling-Reed SF, Joseph P, Cooperwood JS, Latinwo LM, Goodman CB.** Selective cytotoxic activities of two novel synthetic drugs on human breast carcinoma MCF-7 cells. *Anticancer Research*. 2009;29(8):2993-6.
- Bagherzade G, Tavakoli MM, Namaei MH.** Green synthesis of silver nanoparticles using aqueous extract of saffron (*Crocus sativus* L.) wastages and its antibacterial activity against six bacteria. *Asian Pacific Journal of Tropical Biomedicine*. 2017;7(3):227-33.

- Banu H, Renuka N, Faheem SM, Ismail R, Singh V, Saadatmand Z, Khan SS, Narayanan K, Raheem A, Premkumar K, Vasanthakumar G.** Gold and silver nanoparticles biomimetically synthesized using date palm pollen extract-induce apoptosis and regulate p53 and Bcl-2 expression in human breast adenocarcinoma cells. *Biological trace element research*. 2018;186(1):122-34.
- Barabadi H, Ovais M, Shinwari ZK, Saravanan M.** Anti-cancer green bionanomaterials: present status and future prospects. *Green Chemistry Letters and Reviews*. 2017;10(4):285-314.
- Baptista PV, McCusker MP, Carvalho A, Ferreira DA, Mohan NM, Martins M, Fernandes AR.** Nano-strategies to fight multidrug resistant bacteria—"A Battle of the Titans". *Frontiers in microbiology*. 2018 2;9:1441.
- Beer C, Foldbjerg R, Hayashi Y, Sutherland DS, Autrup H.** Toxicity of silver nanoparticles—nanoparticle or silver ion? *Toxicology letters*. 2012;208(3):286-92.
- Belhadj Slimen I, Najjar T, Ghram A, Dabbebi H, Ben Mrad M, Abdrabbah M.** Reactive oxygen species, heat stress and oxidative-induced mitochondrial damage. A review. *International Journal of Hyperthermia*. 2014;30(7):513-23.
- Berne BJ, Pecora R.** Dynamic light scattering: with applications to chemistry, biology, and physics: *Courier Corporation*; 2000.
- Bhattacharya R, Patra CR, Earl A, Wang S, Katarya A, Lu L, Kizhakkedathu JN, Yaszemski MJ, Greipp PR, Mukhopadhyay D, Mukherjee P.** Attaching folic acid on gold nanoparticles using noncovalent interaction via different polyethylene glycol backbones and targeting of cancer cells. *Nanomedicine: Nanotechnology, Biology and Medicine*. 2007;3(3):224-38.
- Bhumkar DR, Joshi HM, Sastry M, Pokharkar VB.** Chitosan reduced gold nanoparticles as novel carriers for transmucosal delivery of insulin. *Pharmaceutical Research*. 2007;24(8):1415-26.
- Bobrovnikova-Marjon E, Hurov JB.** Targeting metabolic changes in cancer: novel therapeutic approaches. *Annual Review of Medicine*. 2014;65.
- Boca SC, Potara M, Gabudean AM, Juhem A, Baldeck PL, Astilean S.** Chitosan-coated triangular silver nanoparticles as a novel class of biocompatible, highly effective photothermal transducers for *in vitro* cancer cell therapy. *Cancer Letters*. 2011;311(2):131-40.
- Bognan AJAA, Guillaume YY, Felix YH, Mathieu KAK, Joseph DA.** Antifungal Activity of *Terminalia mantaly* on the *in vitro* Growth of *Cryptococcus neoformans*. 2013.
- Boldt K, Bruns OT, Gaponik N, Eychmüller A.** Comparative examination of the stability of semiconductor quantum dots in various biochemical buffers. *The Journal of Physical Chemistry B*. 2006;110(5):1959-63.
- Bray F, Ferlay J, Soerjomataram I, Siegel RL, Torre LA, Jemal A.** Global cancer statistics 2018: GLOBOCAN estimates of incidence and mortality worldwide for 36 cancers in 185 countries. *CA: A Cancer Journal for Clinicians*. 2018;68(6):394-424.

- Britto J, Sebastian SR.** Biosynthesis of silver nano particles and its antibacterial activity against human pathogens. *International Journal of Pharmacy and Pharmaceutical Sciences*. 2011;5:257-9.
- Bupesh G, Manikandan E, Thanigaiarul K, Magesh S, Senthilkumar V.** Enhanced antibacterial, anticancer activity from *Terminalia chebula*. Medicinal plant rapid extract by phytosynthesis of silver nanoparticles core-shell structures. *Journal of Nanomedicine & Nanotechnology*. 2016;7:355.
- Buzea C, Pacheco II, Robbie K.** Nanomaterials and nanoparticles: sources and toxicity. *Bio-interphases*. 2007;2 (4):MR17-71.
- Cai W, Gao T, Hong H, Sun J.** Applications of gold nanoparticles in cancer nanotechnology. *Nanotechnology, Science and Applications*. 2008;1:17.
- Cao L, Dai C, Li Z, Fan Z, Song Y, Wu Y, Cao Z, Li W.** Antibacterial activity and mechanism of a scorpion venom peptide derivative *in vitro* and *in vivo*. *PloS one*. 5;7(7):e40135.
- Cardoso CM, Groth-Pedersen L, Høyer-Hansen M, Kirkegaard T, Corcelle E, Andersen JS, Jäättelä M, Nylandsted J.** Depletion of kinesin 5B affects lysosomal distribution and stability and induces peri-nuclear accumulation of autophagosomes in cancer cells. *PloS one*. 2009;4(2):e4424.
- Castro L, Blázquez ML, González FG, Ballester A.** Mechanism and applications of metal nanoparticles prepared by bio-mediated process. *Reviews in Advanced Sciences and Engineering*. 2014;3(3):199-216.
- Cayado P, De Keukeleere K, Garzón A, Perez-Mirabet L, Meledin A, De Roo J, Vallés F, Mundet B, Rijckaert H, Pollefeyt G, Coll M.** Epitaxial YBa<sub>2</sub>Cu<sub>3</sub>O<sub>7-x</sub> nanocomposite thin films from colloidal solutions. *Superconductor Science and Technology*. 2015;28(12):124007.
- Chanda N, Shukla R, Zambre A, Mekapothula S, Kulkarni RR, Katti K, Bhattacharyya K, Fent GM, Casteel SW, Boote EJ, Viator JA.** An effective strategy for the synthesis of biocompatible gold nanoparticles using cinnamon phytochemicals for phantom CT imaging and photoacoustic detection of cancerous cells. *Pharmaceutical Research*. 2011;28(2):279-91.
- Chandran SP, Chaudhary M, Pasricha R, Ahmad A, Sastry M.** Synthesis of gold nanotriangles and silver nanoparticles using *Aloevera* plant extract. *Biotechnology progress*. 2006;22(2):577-83.
- Chen R, Wu J, Li H, Cheng G, Lu Z, Che CM.** Fabrication of gold nanoparticles with different morphologies in HEPES buffer. *Rare Metals*. 2010;29(2):180-6.
- Chen Y, Hancock WO.** Kinesin-5 is a microtubule polymerase. *Nature communications*. 2015;6(1):1-10.
- Cheng Y, Samia AC, Li J, Kenney ME, Resnick A, Burda C.** Delivery and efficacy of a cancer drug as a function of the bond to the gold nanoparticle surface. *Langmuir*. 2010;26(4):2248-55.
- Chitgupi U, Qin Y, Lovell J.** Targeted Nanomaterials for Phototherapy. *Nanotheranostics* 2017; 1 (1): 38-58.

- Cho WS, Cho M, Jeong J, Choi M, Cho HY, Han BS, Kim SH, Kim HO, Lim YT, Chung BH, Jeong J.** Acute toxicity and pharmacokinetics of 13 nm-sized PEG-coated gold nanoparticles. *Toxicology and Applied Pharmacology*. 2009;236(1):16-24.
- Choi SY, Jeong S, Jang SH, Park J, Park JH, Ock KS, Lee SY, Joo SW.** *In vitro* toxicity of serum protein-adsorbed citrate-reduced gold nanoparticles in human lung adenocarcinoma cells. *Toxicology in vitro*. 2012;26(2):229-37.
- Choi YJ, Park JH, Han JW, Kim E, Jae-Wook O, Lee SY, Kim JH, Gurunathan S.** Differential cytotoxic potential of silver nanoparticles in human ovarian cancer cells and ovarian cancer stem cells. *International Journal of Molecular Sciences*. 2016;17(12):2077.
- Chuang SM, Lee YH, Liang RY, Roam GD, Zeng ZM, Tu HF, Wang SK, Chueh PJ.** Extensive evaluations of the cytotoxic effects of gold nanoparticles. *Biochimica et Biophysica Acta (BBA)-General Subjects*. 2013;1830(10):4960-73.
- Chun JN, Choi B, Lee KW, Lee DJ, Kang DH, Lee JY, Song IS, Kim HI, Lee SH, Kim HS, Lee NK.** Cytosolic Hsp60 is involved in the NF- $\kappa$ B-dependent survival of cancer cells via IKK regulation. *PLoS One*. 2010;5(3):e9422.
- Clayton KN, Salameh JW, Wereley ST, Kinzer-Ursem TL.** Physical characterization of nanoparticle size and surface modification using particle scattering diffusometry. *Biomicrofluidics*. 2016;10(5):054107.
- Conde J, Doria G, Baptista P.** Noble metal nanoparticles applications in cancer. *Journal of Drug Delivery*. 2012;2012.
- Cooper R.** Behavior of gold nanoparticles in physiological environment and the role of agglomeration and fractal dimension: *Wright State University*; 2015.
- Cruz DM, Tien-Street W, Zhang B, Huang X, Crua AV, Nieto-Argüello A, Cholula-Díaz JL, Martínez L, Huttel Y, González MU, García-Martín JM.** Citric juice-mediated synthesis of tellurium nanoparticles with antimicrobial and anticancer properties. *Green Chemistry*. 2019;21(8):1982-98.
- Dakal TC, Kumar A, Majumdar RS, Yadav V.** Mechanistic basis of antimicrobial actions of silver nanoparticles. *Frontiers in microbiology*. 2016;7:1831.
- Danhier F, Ansorena E, Silva JM, Coco R, Le Breton A, Prétat V.** PLGA-based nanoparticles: an overview of biomedical applications. *Journal of Controlled Release*. 2012;161(2):505-22.
- Daniel SK, Banu BN, Harshiny M, Nehru K, Ganesh PS, Kumaran S, Sivakumar M.** Ipomea carnea-based silver nanoparticle synthesis for antibacterial activity against selected human pathogens. *Journal of Experimental Nanoscience*. 2014;9(2):197-209.
- Das SK, Khan MMR, Guha AK, Naskar N.** Bio-inspired fabrication of silver nanoparticles on nanostructured silica: characterization and application as a highly efficient hydrogenation catalyst. *Green Chemistry*. 2013;15(9):2548-57.
- Datar R, Cote R.** Nanomedicine: concepts, status and the future. *Medical Innovation & Business*. 2010;2(3):6-17.
- De Matteis V, Malvindi MA, Galeone A, Brunetti V, De Luca E, Kote S, Kshirsagar P, Sabella S, Bardi G, Pompa PP.** Negligible particle-specific toxicity mechanism of

- silver nanoparticles: the role of Ag<sup>+</sup> ion release in the cytosol. *Nanomedicine: Nanotechnology, Biology and Medicine*. 2015;11(3):731-9.
- De Silva DD, Rapior S, Fons F, Bahkali AH, Hyde KD.** Medicinal mushrooms in supportive cancer therapies: an approach to anti-cancer effects and putative mechanisms of action. *Fungal Diversity*. 2012;55(1):1-35.
- Devaraj P, Aarti C, Kumari P.** Synthesis and characterization of silver nanoparticles using *Tabernaemontana divaricata* and its cytotoxic activity against MCF7 cell line. *International Journal of Pharmacy and Pharmaceutical Sciences*. 2014;6(8):86-90.
- Devika R, Elumalai S, Manikandan E, Eswaramoorthy D.** Biosynthesis of silver nanoparticles using the fungus *Pleurotus ostreatus* and their antibacterial activity. *Scientific Reports*. 2012;1:557.
- Diab KA, Guru SK, Bhushan S, Saxena AK.** *In vitro* anticancer activities of *Anogeissus latifolia*, *Terminalia bellerica*, *Acacia catechu* and *Moringa oleifera* Indian plants. *Asian Pacific Journal of Cancer Prevention*. 2015;16(15):6423-8.
- Doria G, Conde J, Veigas B, Giestas L, Almeida C, Assunção M, Rosa J, Baptista PV.** Noble metal nanoparticles for biosensing applications. *Sensors*. 2012;12(2):1657-87.
- Dreaden EC, Austin LA, Mackey MA, El-Sayed MA.** Size matters: gold nanoparticles in targeted cancer drug delivery. *Therapeutic Delivery*. 2012;3(4):457-78.
- Dubey SP, Lahtinen M, Sillanpää M.** Tansy fruit mediated greener synthesis of silver and gold nanoparticles. *Process Biochemistry*. 2010;45(7):1065-71.
- Dwivedi AD, Gopal K.** Biosynthesis of silver and gold nanoparticles using *Chenopodium album* leaf extract. *Colloids and Surfaces A: Physicochemical and Engineering Aspects*. 2010;369(1-3):27-33.
- Eblin KE, Bowen ME, Cromey DW, Bredfeldt TG, Mash EA, Lau SS, Gandolfi AJ.** Arsenite and monomethylarsonous acid generate oxidative stress response in human bladder cell culture. *Toxicology and Applied Pharmacology*. 2006;217(1):7-14.
- Edison TJI, Sethuraman M.** Instant green synthesis of silver nanoparticles using *Terminalia chebula* fruit extract and evaluation of their catalytic activity on reduction of methylene blue. *Process Biochemistry*. 2012;47(9):1351-7.
- Egerton RF.** Physical principles of electron microscopy: Springer; 2005.
- Elbagory AM, Cupido CN, Meyer M, Hussein AA.** Large scale screening of Southern African plant extracts for the green synthesis of gold nanoparticles using microtitre-plate method. *Molecules*. 2016;21(11):1498.
- Elbagory AM, Hussein AA, Meyer M.** The *In vitro* immunomodulatory effects of gold nanoparticles synthesized from *hypoxis hemerocallidea* aqueous extract and hypoxoside on macrophage and natural killer cells. *International Journal of Nanomedicine*. 2019;14:9007.
- Elbagory AM, Meyer M, Cupido CN, Hussein AA.** Inhibition of bacteria associated with wound infection by biocompatible green synthesized gold nanoparticles from South African plant extracts. *Nanomaterials*. 2017;7(12):417.

- Elia P, Zach R, Hazan S, Kolusheva S, Porat Ze, Zeiri Y.** Green synthesis of gold nanoparticles using plant extracts as reducing agents. *International Journal of Nanomedicine*. 2014;9:4007.
- El-Naggar NE-A, Hussein MH, El-Sawah AA.** Bio-fabrication of silver nanoparticles by phycoerythrin, characterization, *in vitro* anticancer activity against breast cancer cell line and *in vivo* cytotoxicity. *Scientific Reports*. 2017;7(1):1-20.
- El-Rafie HM, Hamed MAA.** Antioxidant and anti-inflammatory activities of silver nanoparticles biosynthesized from aqueous leaves extracts of four Terminalia species. *Advances in Natural Sciences: Nanoscience and Nanotechnology*. 2014;5(3):035008.
- El-Serag HB.** Epidemiology of viral hepatitis and hepatocellular carcinoma. *Gastroenterology*. 2012;142(6):1264-73. e1.
- Enayati M, Nemati A, Zarrabi A, Shokrgozar MA.** Reduced graphene oxide: An alternative for Magnetic Resonance Imaging contrast agent. *Materials Letters*. 2018;233:363-6.
- Enow Orock G, Ndom P, Doh A.** Current cancer incidence and trends in Yaounde, Cameroon. *Oncology, Gastroenterology and Hepatology Reports*. 2012;1(1):58-63.
- Escárcega-González CE, Garza-Cervantes JA, Vazquez-Rodríguez A, Montelongo-Peralta LZ, Treviño-Gonzalez MT, Castro ED, Saucedo-Salazar EM, Morales RC, Soto DR, González FT, Rosales JC.** *In vivo* antimicrobial activity of silver nanoparticles produced via a green chemistry synthesis using *Acacia rigidula* as a reducing and capping agent. *International Journal of Nanomedicine*. 2018;13:2349.
- Estevez H, Garcia-Lidon JC, Luque-Garcia JL, Camara C.** Effects of chitosan-stabilized selenium nanoparticles on cell proliferation, apoptosis and cell cycle pattern in HepG2 cells: comparison with other seleno species. *Colloids and Surfaces B: Biointerfaces*. 2014;122:184-93.
- Fahmy N, Al-Sayed E, Singab A.** Genus Terminalia: A phytochemical and biological review. Montin) species. *Medicinal & Aromatic Plants*. 2015;4(5):1-22.
- Feng QL, Wu J, Chen G, Cui F, Kim T, Kim J.** A mechanistic study of the antibacterial effect of silver ions on *Escherichia coli* and *Staphylococcus aureus*. *Journal of Biomedical Materials Research*. 2000;52(4):662-8.
- Ferlay J, Soerjomataram I, Dikshit R, Eser S, Mathers C, Rebelo M, Parkin DM, Forman D, Bray F.** Cancer incidence and mortality worldwide: sources, methods and major patterns in GLOBOCAN 2012. *International Journal of Cancer*. 2015;136(5):E359-86.
- Fitsiou E, Pappa A.** Anticancer Activity of essential oils and other extracts from aromatic plants grown in Greece. *Antioxidants*. 2019;8(8):290.
- Fraga S, Faria H, Soares ME, Duarte JA, Soares L, Pereira E, Costa-Pereira C, Teixeira JP, de Lourdes Bastos M, Carmo H.** Influence of the surface coating on the cytotoxicity, genotoxicity and uptake of gold nanoparticles in human HepG2 cells. *Journal of Applied Toxicology*. 2013;33(10):1111-9.
- Freese C, Uboldi C, Gibson MI, Unger RE, Weksler BB, Romero IA, Couraud PO, Kirkpatrick CJ.** Uptake and cytotoxicity of citrate-coated gold nanospheres:

- comparative studies on human endothelial and epithelial cells. *Particle and Fibre Toxicology*. 2012;9(1):1-1.
- Garcez FR, Garcez WS, Miguel DL, Serea AA, Prado FC.** Chemical constituents from *Terminalia glabrescens*. *Journal of the Brazilian Chemical Society*. 2003;14(3):461-5.
- Gardea-Torresdey J, Tiemann K, Gamez G, Dokken K, Tehuacanero S, Jose-Yacaman M.** Gold nanoparticles obtained by bio-precipitation from gold (III) solutions. *Journal of Nanoparticle Research*. 1999;1(3):397-404.
- Geethalakshmi R, Sarada D.** Gold and silver nanoparticles from *Trianthema decandra*: synthesis, characterization, and antimicrobial properties. *International Journal of Nanomedicine*. 2012;7:5375.
- Gericke M, Pinches A.** Biological synthesis of metal nanoparticles. *Hydrometallurgy*. 2006;83(1-4):132-40.
- Gmeiner WH, Ghosh S.** Nanotechnology for cancer treatment. *Nanotechnology Reviews*. 2014;3(2):111-22.
- Golombek SK, May JN, Theek B, Appold L, Drude N, Kiessling F, Lammers T.** Tumor targeting via EPR: Strategies to enhance patient responses. *Advanced Drug Delivery Reviews*. 2018;130:17-38.
- Gopinath K, Sundaravadivelan C, Arumugam A.** Green synthesis, characterization of silver, gold and bimetallic nanoparticles using bark extract of *Terminalia arjuna* and their larvicidal activity against malaria vector, *Anopheles stephensi*. *International Journal of Recent Scientific Research*. 2013;4(6):904-10.
- Govindappa M, Farheen H, Chandrappa C, Rai RV, Raghavendra VB.** Mycosynthesis of silver nanoparticles using extract of endophytic fungi, *Penicillium* species of *Glycosmis mauritiana*, and its antioxidant, antimicrobial, anti-inflammatory and tyrosinase inhibitory activity. *Advances in Natural Sciences: Nanoscience and Nanotechnology*. 2016;7(3):035014.
- Grabinski CM.** Nanoparticle Deposition and Dosimetry for *in Vitro* Toxicology: Case Western Reserve University; 2015.
- Gräfe C, Weidner A, vd Lühe M, Bergemann C, Schacher FH, Clement JH, Dutz S.** Intentional formation of a protein corona on nanoparticles: serum concentration affects protein corona mass, surface charge, and nanoparticle–cell interaction. *The International Journal of Biochemistry & Cell Biology*. 2016;75:196-202.
- Grijalva M, Vallejo-López MJ, Salazar L, Camacho J, Kumar B.** Cytotoxic and antiproliferative effects of nanomaterials on cancer cell lines: a review. *Unraveling the Safety Profile of Nanoscale Particles and Materials: From Biomedical to Environmental Applications*. 2018:63.
- Gullicksen P, Della-Fera M, Baile C.** Leptin-induced adipose apoptosis: Implications for body weight regulation. *Apoptosis*. 2003;8(4):327-35.
- Guo L, Jackman JA, Yang HH, Chen P, Cho NJ, Kim DH.** Strategies for enhancing the sensitivity of plasmonic nanosensors. *Nano Today*. 2015;10(2):213-39.
- Gurunathan S, Raman J, Abd Malek SN, John PA, Vikineswary S.** Green synthesis of silver nanoparticles using *Ganoderma neo-japonicum* Imazeki: a potential cytotoxic



- agent against breast cancer cells. *International Journal of Nanomedicine*. 2013;8:4399.
- Haider A, Kang IK.** Preparation of silver nanoparticles and their industrial and biomedical applications: a comprehensive review. *Advances in Materials Science and Engineering*. 2015;2015.
- Hagaman DE, Damasco JA, Perez JV, Rojo RD, Melancon MP.** Recent Advances in Nanomedicine for the Diagnosis and Treatment of Prostate Cancer Bone Metastasis. *Molecules*. 2021;26(2):384.
- Hansen SF, Michelson ES, Kamper A, Borling P, Stuer-Lauridsen F, Baun A.** Categorization framework to aid exposure assessment of nanomaterials in consumer products. *Ecotoxicology*. 2008;17(5):438-47.
- Harborne A.** Phytochemical methods a guide to modern techniques of plant analysis: *springer Science & Business Media*; 1998.
- Hassanien R, Abed-Elmageed A, Husein D.** Photocatalytic Study and Anticancer activity of Green-Synthesized Ag Nanoparticles Using Drumstick Leaf Extract. *Journal of Nanoscience and Nanotechnology Applications*. 2019;3(1):1.
- Hirsch LR, Gobin AM, Lowery AR, Tam F, Drezek RA, Halas NJ, West JL.** Metal nanoshells. *Annals of Biomedical Engineering*. 2006;34(1):15-22.
- Hirsch LR, Stafford RJ, Bankson JA, Sershen SR, Rivera B, Price RE, Hazle JD, Halas NJ, West JL.** Nanoshell-mediated near-infrared thermal therapy of tumors under magnetic resonance guidance. *Proceedings of the National Academy of Sciences*. 2003;100(23):13549-54.
- Holowachuk SA, Bal'a MF, Buddington RK.** A kinetic microplate method for quantifying the antibacterial properties of biological fluids. *Journal of microbiological methods*. 2003;55(2):441-6.
- Holt KB, Bard AJ.** Interaction of silver (I) ions with the respiratory chain of *Escherichia coli*: an electrochemical and scanning electrochemical microscopy study of the antimicrobial mechanism of micromolar Ag<sup>+</sup>. *Biochemistry*. 2005;44(39):13214-23.
- Huang J, Li Q, Sun D, Lu Y, Su Y, Yang X, Wang H, Wang Y, Shao W, He N, Hong J.** Biosynthesis of silver and gold nanoparticles by novel sundried *Cinnamomum camphora* leaf. *Nanotechnology*. 2007;18(10):105104.
- Iqbal SS, Mayo MW, Bruno JG, Bronk BV, Batt CA, Chambers JP.** A review of molecular recognition technologies for detection of biological threat agents. *Biosensors and Bioelectronics*. 2000;15(11-12):549-78.
- ISO13321.** Methods for determination of particle size distribution part 8: Photon correlation spectroscopy. *International Organisation for Standardisation (ISO)*. 1996.
- Jafarizad A, Safae K, Gharibian S, Omidi Y, Ekinci D.** Biosynthesis and *in-vitro* study of gold nanoparticles using mentha and pelargonium extracts. *Procedia Materials Science*. 2015;11:224-30.
- Jiang J, Oberdörster G, Biswas P.** Characterization of size, surface charge, and agglomeration state of nanoparticle dispersions for toxicological studies. *Journal of Nanoparticle Research*. 2009;11(1):77-89.

- Jeevanandam J, Barhoum A, Chan YS, Dufresne A, Danquah MK.** Review on nanoparticles and nanostructured materials: history, sources, toxicity and regulations. *Beilstein Journal of Nanotechnology*. 2018;9(1):1050-74.
- Jung JH, Oh HC, Noh HS, Ji JH, Kim SS.** Metal nanoparticle generation using a small ceramic heater with a local heating area. *Journal of Aerosol Science*. 2006;37(12):1662-70.
- Kalishwaralal K, Deepak V, Pandian SRK, Gurunathan S.** Biological synthesis of gold nanocubes from *Bacillus licheniformis*. *Bioresource Technology*. 2009;100(21):5356-8.
- Kannan N, Shekhawat M, Ravindran C, Manokari M.** Preparation of silver nanoparticles using leaf and fruit extracts of *Morinda coreia* Buck. Ham.-A green approach. *International Journal of Scientific Innovations*. 2014;3(3):315-8.
- Kaur S, Michael H, Arora S, Härkönen PL, Kumar S.** The *in vitro* cytotoxic and apoptotic activity of Triphala—an Indian herbal drug. *Journal of Ethnopharmacology*. 2005;97(1):15-20.
- Kaviya S, Santhanalakshmi J, Viswanathan B, Muthumary J, Srinivasan K.** Biosynthesis of silver nanoparticles using *Citrus sinensis* peel extract and its antibacterial activity. *Spectrochimica Acta Part A: Molecular and Biomolecular Spectroscopy*. 2011;79(3):594-8.
- Kelly KL, Coronado E, Zhao LL, Schatz GC.** The optical properties of metal nanoparticles: the influence of size, shape, and dielectric environment. *ACS Publications*. 2003.
- Kennedy IM, Wilson DW, Barakat AI.** Uptake and inflammatory effects of nanoparticles in a human vascular endothelial cell line. *Research Report (Health Effects Institute)*. 2009(136):3-32.
- Kennedy LC, Bickford LR, Lewinski NA, Coughlin AJ, Hu Y, Day ES, West JL, Drezek RA.** A new era for cancer treatment: gold-nanoparticle-mediated thermal therapies. *Small*. 2011;7(2):169-83.
- Khan I, Saeed K, Khan I.** Nanoparticles: Properties, applications and toxicities. *Arabian Journal of Chemistry*. 2019;12(7):908-31.
- Kharissova OV, Dias HR, Kharisov BI, Pérez BO, Pérez VMJ.** The greener synthesis of nanoparticles. *Trends in Biotechnology*. 2013;31(4):240-8.
- Khatami M, Soltani Nejad M, Pourseyedi S.** Biogenic synthesis of silver nanoparticles using mustard and its characterization. *International Journal of Nanoscience and Nanotechnology*. 2015;11(4):281-8.
- Khatoon N, Yasin HM, Younus M, Ahmed W, Rehman NU, Zakaullah M, Iqbal MZ.** Synthesis and spectroscopic characterization of gold nanoparticles via plasma-liquid interaction technique. *AIP Advances*. 2018;8(1):015130.
- Kiechle FL, Zhang X.** Apoptosis: biochemical aspects and clinical implications. *Clinica Chimica Acta*. 2002;326(1-2):27-45.
- Kikusato M, Toyomizu M.** Crucial role of membrane potential in heat stress-induced overproduction of reactive oxygen species in avian skeletal muscle mitochondria. *PLoS one*. 2013;8(5):e64412.

- Kimling J, Maier M, Okenve B, Kotaidis V, Ballot H, Plech A.** Turkevich method for gold nanoparticle synthesis revisited. *The Journal of Physical Chemistry B*. 2006;110(32):15700-7.
- Kim JA, Åberg C, de Cárcer G, Malumbres M, Salvati A, Dawson KA.** Low dose of amino-modified nanoparticles induces cell cycle arrest. *Acs Nano*. 2013;7(9):7483-94.
- Kim JS, Kuk E, Yu KN, Kim JH, Park SJ, Lee HJ, Kim SH, Park YK, Park YH, Hwang CY, Kim YK.** Antimicrobial effects of silver nanoparticles. *Nanomedicine: Nanotechnology, Biology and Medicine*. 2007;3(1):95-101.
- Kim SH, Lee HS, Ryu DS, Choi SJ, Lee DS.** Antibacterial activity of silver-nanoparticles against *Staphylococcus aureus* and *Escherichia coli*. *Korean Journal of Microbiology and Biotechnology*. 2011;39(1):77-85.
- Kloepfer JA, Bradforth SE, Nadeau JL.** Photophysical properties of biologically compatible CdSe quantum dot structures. *The Journal of Physical Chemistry B*. 2005;109(20):9996-10003.
- Klute K, Nackos E, Tasaki S, Nguyen DP, Bander NH, Tagawa ST.** Microtubule inhibitor-based antibody–drug conjugates for cancer therapy. *OncoTargets and Therapy*. 2014;7:2227.
- Kotnala RK, Shah J.** Ferrite materials: nano to spintronics regime. *In Handbook of Magnetic Materials*. 2015, 291-379.
- Krishnaraj C, Muthukumar P, Ramachandran R, Balakumaran M, Kalaichelvan P.** *Acalypha indica* Linn: biogenic synthesis of silver and gold nanoparticles and their cytotoxic effects against MDA-MB-231, human breast cancer cells. *Biotechnology Reports*. 2014;4:42-9.
- Krishnaswamy K.** Green nanotechnology approach for synthesis and encapsulation of gold nanoparticles from agricultural waste: *McGill University*; 2015.
- KS US, Govindaraju K, Prabhu D, Arulvasu C, Karthick V, Changmai N.** Anti-proliferative effect of biogenic gold nanoparticles against breast cancer cell lines (MDA-MB-231 & MCF-7). *Applied Surface Science*. 2016;371:415-24.
- Kumar CG, Poornachandra Y, Chandrasekhar C.** Green synthesis of bacterial mediated anti-proliferative gold nanoparticles: inducing mitotic arrest (G2/M phase) and apoptosis (intrinsic pathway). *Nanoscale*. 2015;7(44):18738-50.
- Kumar KM, Sinha M, Mandal BK, Ghosh AR, Kumar KS, Reddy PS.** Green synthesis of silver nanoparticles using *Terminalia chebula* extract at room temperature and their antimicrobial studies. *Spectrochimica Acta Part A: Molecular and Biomolecular Spectroscopy*. 2012;91:228-33.
- Kumar V, Yadav SK.** Plant-mediated synthesis of silver and gold nanoparticles and their applications. *Journal of Chemical Technology & Biotechnology: International Research in Process, Environmental & Clean Technology*. 2009;84(2):151-7.
- Kumari P, Ghosh B, Biswas S.** Nanocarriers for cancer-targeted drug delivery. *Journal of drug targeting*. 2016;24(3):179-91.
- Kutuk O, Basaga H.** Bcl-2 protein family: implications in vascular apoptosis and atherosclerosis. *Apoptosis*. 2006;11(10):1661-75.

- Le XT, Poinern GEJ, Subramaniam S, Fawcett D.** Applications of nanometre scale particles as pharmaceutical delivery vehicles in medicine. *Open Journal of Biomedical Materials Research*. 2015;2:11-26.
- Lee HM, Shin DM, Song HM, Yuk JM, Lee ZW, Lee SH, Hwang SM, Kim JM, Lee CS, Jo EK.** Nanoparticles up-regulate tumor necrosis factor- $\alpha$  and CXCL8 via reactive oxygen species and mitogen-activated protein kinase activation. *Toxicology and Applied Pharmacology*. 2009;238(2):160-9.
- Lee SY, Krishnamurthy S, Cho CW, Yun YS.** Biosynthesis of gold nanoparticles using *Ocimum sanctum* extracts by solvents with different polarity. *ACS Sustainable Chemistry & Engineering*. 2016;4(5):2651-9.
- Leonard K, Ahmmad B, Okamura H, Kurawaki J.** In situ green synthesis of biocompatible ginseng capped gold nanoparticles with remarkable stability. *Colloids and Surfaces B: Biointerfaces*. 2011;82(2):391-6.
- Li P, Zhao QL, Wu LH, Jawaid P, Jiao YF, Kadowaki M, Kondo T.** Isofraxidin, a potent reactive oxygen species (ROS) scavenger, protects human leukemia cells from radiation-induced apoptosis via ROS/mitochondria pathway in p53-independent manner. *Apoptosis*. 2014;19(6):1043-53.
- Liu Y, Franzen S.** Factors determining the efficacy of nuclear delivery of antisense oligonucleotides by gold nanoparticles. *Bioconjugate Chemistry*. 2008;19(5):1009-16.
- Liu Y, Kim S, Kim YJ, Perumalsamy H, Lee S, Hwang E, Yi TH.** Green synthesis of gold nanoparticles using *Euphrasia officinalis* leaf extract to inhibit lipopolysaccharide-induced inflammation through NF- $\kappa$ B and JAK/STAT pathways in RAW 264.7 macrophages. *International Journal of Nanomedicine*. 2019;14:2945.
- Loos C, Syrovets T, Musyanovych A, Mailänder V, Landfester K, Simmet T.** Amino-functionalized nanoparticles as inhibitors of mTOR and inducers of cell cycle arrest in leukemia cells. *Biomaterials*. 2014;35(6):1944-53.
- Loutfy SA, Al-Ansary NA, Abdel-Ghani NT, Hamed AR, Mohamed MB, Craik JD, Eldin TA, Abdellah AM, Hussein Y, Hasanin MT, Elbehairi SE.** Anti-proliferative activities of metallic nanoparticles in an *in vitro* breast cancer model. *Asian Pacific Journal of Cancer Prevention*. 2015;16(14):6039-46.
- Mahmoudi M, Azadmanesh K, Shokrgozar MA, Journey WS, Laurent S.** Effect of nanoparticles on the cell life cycle. *Chemical reviews*. 2011;111(5):3407-32.
- Makarov VV, Love AJ, Sinitsyna OV, Makarova SS, Yaminsky IV, Taliansky ME, Kalinina NO.** "Green" nanotechnologies: synthesis of metal nanoparticles using plants. *Acta Naturae*. 2014;6(1 (20)).
- Malarkodi C, Rajeshkumar S, Paulkumar K, Vanaja M, Gnanajobitha G, Annadurai G.** Biosynthesis and antimicrobial activity of semiconductor nanoparticles against oral pathogens. *Bioinorganic Chemistry and Applications*. 2014;2014.
- Mallat Z, Tedgui A.** Apoptosis in the vasculature: mechanisms and functional importance. *British journal of pharmacology*. 2000;130(5):947-62.

- Mansoori B, Mohammadi A, Davudian S, Shirjang S, Baradaran B.** The different mechanisms of cancer drug resistance: a brief review. *Advanced Pharmaceutical Bulletin.* 2017;7(3):339.
- Mari M, Morales A, Colell A, García-Ruiz C, Fernández-Checa JC.** Mitochondrial glutathione, a key survival antioxidant. *Antioxidants & Redox Signaling.* 2009;11(11):2685-700.
- Matulionyte M, Dapkute D, Budenaite L, Jarockyte G, Rotomskis R.** Photoluminescent gold Nanoclusters in cancer cells: cellular uptake, toxicity, and generation of reactive oxygen species. *International Journal of Molecular Sciences.* 2017;18(2):378.
- Mbouna CD, Kouipou RM, Keumoe R, Tchokouaha LR, Fokou PV, Tali BM, Sahal D, Boyom FF.** Potent antiplasmodial extracts and fractions from *Terminalia mantaly* and *Terminalia superba*. *Malaria Journal.* 2018;17(1):142.
- McConkey DJ.** Biochemical determinants of apoptosis and necrosis. *Toxicology Letters.* 1998;99(3):157-68.
- Medintz IL, Uyeda HT, Goldman ER, Mattoussi H.** Quantum dot bioconjugates for imaging, labelling and sensing. *Nature Materials.* 2005;4(6):435-46.
- Meyers MA, Mishra A, Benson DJ.** Mechanical properties of nanocrystalline materials. *Progress in Materials Science.* 2006;51(4):427-556.
- Mishra A, Tripathy SK, Yun SI.** Fungus mediated synthesis of gold nanoparticles and their conjugation with genomic DNA isolated from *Escherichia coli* and *Staphylococcus aureus*. *Process Biochemistry.* 2012;47(5):701-11.
- Mishra J, Drummond J, Quazi SH, Karanki SS, Shaw JJ, Chen B, Kumar N.** Prospective of colon cancer treatments and scope for combinatorial approach to enhanced cancer cell apoptosis. *Critical Reviews in Oncology/Hematology.* 2013;86(3):232-50.
- Mitra AK, Agrahari V, Mandal A, Cholkar K, Natarajan C, Shah S, Joseph M, Trinh HM, Vaishya R, Yang X, Hao Y.** Novel delivery approaches for cancer therapeutics. *Journal of Controlled Release.* 2015;219:248-68.
- Mitra S, Nguyen LN, Akter M, Park G, Choi EH, Kaushik NK.** Impact of ROS generated by chemical, physical, and plasma techniques on cancer attenuation. *Cancers.* 2019;11(7):1030.
- Mittal AK, Bhaumik J, Kumar S, Banerjee UC.** Biosynthesis of silver nanoparticles: elucidation of prospective mechanism and therapeutic potential. *Journal of Colloid and Interface Science.* 2014;415:39-47.
- Mittal AK, Chisti Y, Banerjee UC.** Synthesis of metallic nanoparticles using plant extracts. *Biotechnology Advances.* 2013;31(2):346-56.
- Miura N, Shinohara Y.** Cytotoxic effect and apoptosis induction by silver nanoparticles in HeLa cells. *Biochemical and Biophysical Research Communications.* 2009;390(3):733-7.
- Mmola M, Roes-Hill ML, Durrell K, Bolton JJ, Sibuyi N, Meyer ME, Beukes DR, Antunes E.** Enhanced antimicrobial and anticancer activity of silver and gold nanoparticles synthesised using *Sargassum incisifolium* aqueous extracts. *Molecules.* 2016;21(12):1633.

- Moghimi SM, Hunter AC, Murray JC.** Nanomedicine: current status and future prospects. *The FASEB Journal*. 2005;19(3):311-30.
- Moses S, Edwards V, Brantley E.** Cytotoxicity in MCF-7 and MDA-MB-231 breast cancer cells, without harming MCF-10A healthy cells. *Journal of Nanomedicine & Nanotechnology*. 2016;7(369):2.
- Mughini-Gras L, Schaapveld M, Kramers J, Mooij S, Neefjes-Borst EA, Pelt WV, Neefjes J.** Increased colon cancer risk after severe Salmonella infection. *PloS one*. 2018;13(1):e0189721.
- Mukunthan K, Balaji S.** Cashew apple juice (*Anacardium occidentale* L.) speeds up the synthesis of silver nanoparticles. *International Journal of Green Nanotechnology*. 2012;4(2):71-9.
- Mulvaney P.** Surface plasmon spectroscopy of nanosized metal particles. *Langmuir*. 1996;12(3):788-800.
- Murawala P, Phadnis S, Bhonde R, Prasad B.** *In situ* synthesis of water dispersible bovine serum albumin capped gold and silver nanoparticles and their cytocompatibility studies. *Colloids and Surfaces B: Biointerfaces*. 2009;73(2):224-8.
- Nagappa A, Thakurdesai P, Rao NV, Singh J.** Antidiabetic activity of *Terminalia catappa* Linn fruits. *Journal of Ethnopharmacology*. 2003;88(1):45-50.
- Nakayama S, Torikoshi Y, Takahashi T, Yoshida T, Sudo T, Matsushima T, Kawasaki Y, Katayama A, Gohda K, Hortobagyi GN, Noguchi S.** Prediction of paclitaxel sensitivity by CDK1 and CDK2 activity in human breast cancer cells. *Breast Cancer Research*. 2009;11(1):R12.
- Nandagopal S, Kumar AG, Dhanalaksmi D, Prakash P.** Bio-prospecting the antibacterial and anticancer activities of silver nanoparticles synthesized using *Terminalia chebula* seed extract. *International Journal of Pharmacy and Pharmaceutical Sciences*. 2014;6(2):368-73.
- Narayanan KB, Sakthivel N.** Phytosynthesis of gold nanoparticles using leaf extract of *Coleus amboinicus* Lour. *Materials Characterization*. 2010;61(11):1232-8.
- Nath D, Banerjee P.** Green nanotechnology—a new hope for medical biology. *Environmental Toxicology and Pharmacology*. 2013;36(3):997-1014.
- Nayak D, Ashe S, Rauta PR, Kumari M, Nayak B.** Bark extract mediated green synthesis of silver nanoparticles: evaluation of antimicrobial activity and antiproliferative response against osteosarcoma. *Materials Science and Engineering: C*. 2016;58:44-52.
- Nelson-Dooley C, Della-Fera M, Hamrick M, Baile C.** Novel treatments for obesity and osteoporosis: targeting apoptotic pathways in adipocytes. *Current Medicinal Chemistry*. 2005;12(19):2215-25.
- Ngouana TK, Mbouna CD, Kuipou RM, Tchuenmogne MA, Zeuko'o EM, Ngouana V, Mallié M, Bertout S, Boyom FF.** Potent and synergistic extract combinations from *Terminalia catappa*, *Terminalia mantaly* and *Monodora tenuifolia* against pathogenic yeasts. *Medicines*. 2015;2(3):220-35.
- Ngumbi PK, Mugo SW, Ngaruiya JM.** Determination of gold nanoparticles sizes via surface plasmon resonance. *IOSR Journal of Applied Chemistry*. 2018;11:25-9.

- Nichols JW, Bae YH.** EPR: Evidence and fallacy. *Journal of Controlled Release.* 2014;190:451-64.
- Odebeyi OO and Sofowara FH.** *Planta Médecine.* 1978; 36: 204-207
- Odugbemi T.** Medicinal plants as antimicrobials In: Outline and pictures of Medicinal plants from Nigeria. *University of Lagos press ISBN.* 2006:53-64.
- Orwa C, Mutua A, Kindt R, Jamnadass R, Anthony S.** Agroforestree Database: a tree reference and selection guide version 4.0. *World Agroforestry Centre, Kenya.* 2009;15.
- Ott M, Gogvadze V, Orrenius S, Zhivotovsky B.** Mitochondria, oxidative stress and cell death. *Apoptosis.* 2007;12(5):913-22.
- Panáček A, Kvitek L, Pucek R, Kolář M, Večeřová R, Pizúrová N, Sharma VK, Nevěčná TJ, Zbořil R.** Silver colloid nanoparticles: synthesis, characterization, and their antibacterial activity. *The Journal of Physical Chemistry B.* 2006;110(33):16248-53.
- Park EJ, Yi J, Kim Y, Choi K, Park K.** Silver nanoparticles induce cytotoxicity by a Trojan-horse type mechanism. *Toxicology in vitro.* 2010;24(3):872-8.
- Park H, Kim MJ, Ha E, Chung JH.** Apoptotic effect of hesperidin through caspase3 activation in human colon cancer cells, SNU-C4. *Phytomedicine.* 2008;15(1-2):147-51.
- Parkin DM, Sitas F, Chirenje M, Stein L, Abratt R, Wabinga H.** Part I: Cancer in Indigenous Africans—burden, distribution, and trends. *The lancet Oncology.* 2008;9(7):683-92.
- Patel AP.** Cancer hyperthermia using gold and magnetic nanoparticles: *University of Glasgow;* 2017.
- Patel VR, Agrawal Y.** Nanosuspension: An approach to enhance solubility of drugs. *Journal of Advanced Pharmaceutical Technology & Research.* 2011;2(2):81.
- Patil MP, Jin X, Simeon NC, Palma J, Kim D, Ngabire D, Kim NH, Tarte NH, Kim GD.** Anticancer activity of *Sasa borealis* leaf extract-mediated gold nanoparticles. *Artificial Cells, Nanomedicine, and Biotechnology.* 2018;46(1):82-8.
- Patil MP, Kim GD.** Eco-friendly approach for nanoparticles synthesis and mechanism behind antibacterial activity of silver and anticancer activity of gold nanoparticles. *Applied Microbiology and Biotechnology.* 2017;101(1):79-92.
- Patil NA, Gade W, Deobagkar DD.** Epigenetic modulation upon exposure of lung fibroblasts to TiO<sub>2</sub> and ZnO nanoparticles: alterations in DNA methylation. *International Journal of Nanomedicine.* 2016;11:4509.
- Patra B, Gautam R, Priyadarsini E, Rajamani P, Pradhan SN, Saravanan M, Meena R.** Piper betle: Augmented Synthesis of Gold Nanoparticles and Its *In-vitro* Cytotoxicity Assessment on HeLa and HEK293 Cells. *Journal of Cluster Science.* 2020;31(1):133-45.

- Patra JK, Baek KH.** Novel green synthesis of gold nanoparticles using *Citrullus lanatus* rind and investigation of proteasome inhibitory activity, antibacterial, and antioxidant potential. *International Journal of Nanomedicine*. 2015;10:7253.
- Pavlin M, Bregar VB.** Stability of nanoparticle suspensions in different biologically relevant media. *Digest Journal of Nanomaterials & Biostructures*. 2012;7(4).
- Pelicano H, Carney D, Huang P.** ROS stress in cancer cells and therapeutic implications. *Drug Resistance Updates*. 2004;7(2):97-110.
- Pérez Mirabet L.** Synthesis, characterization and functionalization of metal and metal oxide nanoparticles TEM microscopy study: *Universitat Autònoma de Barcelona*; 2014.
- Pissuwan D, Cortie CH, Valenzuela SM, Cortie MB.** Functionalised gold nanoparticles for controlling pathogenic bacteria. *Trends in Biotechnology*. 2010;28(4):207-13.
- Poinern GEJ, Chapman P, Shah M, Fawcett D.** Green biosynthesis of silver nanocubes using the leaf extracts from *Eucalyptus macrocarpa*. *Nano Bulletin*. 2013;2(1):130101.
- Poinern GEJ.** A laboratory course in nanoscience and nanotechnology: *Chemical Rubber Compagny Press*. 2014.
- Pollini M, Paladini F, Catalano M, Taurino A, Licciulli A, Maffezzoli A, Sannino A.** Antibacterial coatings on haemodialysis catheters by photochemical deposition of silver nanoparticles. *Journal of Materials Science: Materials in Medicine*. 2011;22(9):2005-12.
- Polte J, Erler R, Thunemann AF, Sokolov S, Ahner TT, Rademann K, Emmerling F, Kraehnert R.** Nucleation and growth of gold nanoparticles studied via *in situ* small angle X-ray scattering at millisecond time resolution. *ACS nano*. 2010;4(2):1076-82.
- Prakash P, Gnanaprakasam P, Emmanuel R, Arokiyaraj S, Saravanan M.** Green synthesis of silver nanoparticles from leaf extract of *Mimusops elengi*, Linn. for enhanced antibacterial activity against multi drug resistant clinical isolates. *Colloids and Surfaces B: Biointerfaces*. 2013;108:255-9.
- Premasudha P, Venkataramana M, Abirami M, Vanathi P, Krishna K, Rajendran R.** Biological synthesis and characterization of silver nanoparticles using *Eclipta alba* leaf extract and evaluation of its cytotoxic and antimicrobial potential. *Bulletin of Materials Science*. 2015;38(4):965-73.
- Pucci B, Kasten M, Giordano A.** Cell cycle and apoptosis. *Neoplasia*. 2000;2(4):291-9.
- Puvanakrishnan P, Park J, Chatterjee D, Krishnan S, Tunnell JW.** *In vivo* tumour targeting of gold nanoparticles: effect of particle type and dosing strategy. *International Journal of Nanomedicine*. 2012;7:1251.
- Rai M, Kon K, Ingle A, Duran N, Galdiero S, Galdiero M.** Broad-spectrum bioactivities of silver nanoparticles: the emerging trends and future prospects. *Applied Microbiology and Biotechnology*. 2014;98(5):1951-61.
- Rai M, Yadav A, Gade A.** Silver nanoparticles as a new generation of antimicrobials. *Biotechnology Advances*. 2009;27(1):76-83.



- Rajan R, Chandran K, Harper SL, Yun SI, Kalaichelvan PT.** Plant extract synthesized silver nanoparticles: an ongoing source of novel biocompatible materials. *Industrial Crops and Products*. 2015;70:356-73.
- Rajkumar V, Guha G, Kumar RA.** Antioxidant and anti-neoplastic activities of *Picrorhiza kurroa* extracts. *Food and Chemical Toxicology*. 2011;49(2):363-9.
- Rajoriya P.** Green synthesis of silver nanoparticles, their characterization and antimicrobial potential (Doctoral dissertation, Department of Molecular & Cellular Engineering, Jacob Institute of Biotechnology & Bioengineering, Sam Higginbottom University of Agriculture, Technology & Sciences Allahabad-211007, UP (India) 2017).
- Rao PV, Nallappan D, Madhavi K, Rahman S, Jun Wei L, Gan SH.** Phytochemicals and biogenic metallic nanoparticles as anticancer agents. *Oxidative Medicine and Cellular Longevity*. 2016;2016.
- Rau R.** Have traditional DMARDs had their day? *Clinical Rheumatology*. 2005;24(3):189-202.
- Raza MA, Kanwal Z, Rauf A, Sabri AN, Riaz S, Naseem S.** Size-and shape-dependent antibacterial studies of silver nanoparticles synthesized by wet chemical routes. *Nanomaterials*. 2016;6(4):74.
- Reimer L.** Transmission electron microscopy: physics of image formation and microanalysis: Springer; 2013.
- Richman EK, Hutchison JE.** The nanomaterial characterization bottleneck. *ACS Publications*; 2009.
- Risom L, Møller P, Loft S.** Oxidative stress-induced DNA damage by particulate air pollution. *Mutation Research/Fundamental and Molecular Mechanisms of Mutagenesis*. 2005;592(1-2):119-37.
- Roa W, Zhang X, Guo L, Shaw A, Hu X, Xiong Y, Gulavita S, Patel S, Sun X, Chen J, Moore R.** Gold nanoparticle sensitize radiotherapy of prostate cancer cells by regulation of the cell cycle. *Nanotechnology*. 2009;20(37):375101.
- Rosadi F, Fiorentini C, Fabbri A.** Bacterial protein toxins in human cancers. *Pathogens and Disease*. 2016;74(1).
- Sahu SC.** Altered global gene expression profiles in human gastrointestinal epithelial Caco2 cells exposed to nanosilver. *Toxicology Reports*. 2016;3:262-8.
- Saibu G, Katerere D, Rees D, Meyer M.** *In vitro* cytotoxic and pro-apoptotic effects of water extracts of *Tulbaghia violacea* leaves and bulbs. *Journal of Ethnopharmacology*. 2015;164:203-9.
- Salata OV.** Applications of nanoparticles in biology and medicine. *Journal of Nanobiotechnology*. 2004;2(1):3.
- Salazar L, Vallejo López MJ, Grijalva M, Castillo L, Maldonado A.** Biological effect of organically coated *Grias neuberthii* and *Persea americana* silver nanoparticles on HeLa and MCF-7 cancer cell lines. *Journal of Nanotechnology*. 2018;2018.

- Saleem A, Husheem M, Härkönen P, Pihlaja K.** Inhibition of cancer cell growth by crude extract and the phenolics of *Terminalia chebula* retz. fruit. *Journal of Ethnopharmacology*. 2002;81(3):327-36.
- Sathishkumar M, Sneha K, Won S, Cho CW, Kim S, Yun YS.** Cinnamon zeylanicum bark extract and powder mediated green synthesis of nano-crystalline silver particles and its bactericidal activity. *Colloids and Surfaces B: Biointerfaces*. 2009;73(2):332-8.
- Scanu T, Spaapen RM, Bakker JM, Pratap CB, Wu LE, Hofland I, Broeks A, Shukla VK, Kumar M, Janssen H, Song JY.** Salmonella manipulation of host signaling pathways provokes cellular transformation associated with gallbladder carcinoma. *Cell host & Microbe*. 2015;17(6):763-74.
- Sekhar EC, Rao K, Rao KMS, Alisha SB.** A simple biosynthesis of silver nanoparticles from *Syzygium cumini* stem bark aqueous extract and their spectrochemical and antimicrobial studies. *Journal of Applied Pharmaceutical Science*. 2018;8(1):73-9.
- Selim ME, Hendi AA.** Gold nanoparticles induce apoptosis in MCF-7 human breast cancer cells. *Asia Pacific Organization for Cancer Prevention*. 2012;13(4):1617-20.
- Selim ME, Hendi AA.** Gold nanoparticles induce apoptosis in MCF-7 human breast cancer cells. *Asia Pacific Organization for Cancer Prevention*. 2012;13(4):1617-20.
- Senapati S, Mahanta AK, Kumar S, Maiti P.** Controlled drug delivery vehicles for cancer treatment and their performance. *Signal Transduction and Targeted Therapy*. 2018;3(1):1-19.
- Sengupta S, Sasisekharan R.** Exploiting nanotechnology to target cancer. *British Journal of Cancer*. 2007;96(9):1315-9.
- Shah W, Patil U, Sharma A.** Green synthesis of silver nanoparticles from stem bark extract of *Terminalia tomentosa* Roxb.(Wight & Arn.). *Der Pharma chemica*. 2011;6:6.
- Shalom J, Cock IE.** *Terminalia ferdinandiana* Exell. fruit and leaf extracts inhibit proliferation and induce apoptosis in selected human cancer cell lines. *Nutrition and Cancer*. 2018;70(4):579-93.
- Shankar SS, Ahmad A, Pasricha R, Sastry M.** Bioreduction of chloraurate ions by geranium leaves and its endophytic fungus yields gold nanoparticles of different shapes. *Journal of Materials Chemistry*. 2003;13(7):1822-6.
- Shankar SS, Rai A, Ahmad A, Sastry M.** Rapid synthesis of Au, Ag, and bimetallic Au core–Ag shell nanoparticles using Neem (*Azadirachta indica*) leaf broth. *Journal of Colloid and Interface Science*. 2004;275(2):496-502.
- Sharma NC, Sahi SV, Nath S, Parsons JG, Gardea-Torresde JL, Pal T.** Synthesis of plant-mediated gold nanoparticles and catalytic role of biomatrix-embedded nano-materials. *Environmental Science & Technology*. 2007;41(14):5137-42.
- Sharma R, Dhillon A, Kumar D.** Mentha-Stabilized Silver Nanoparticles for high-performance colourimetric detection of Al (III) in aqueous systems. *Scientific Reports*. 2018;8(1):1-13.
- Sharma S, Jaiswal S, Duffy B, Jaiswal AK.** Nanostructured materials for food applications: spectroscopy, microscopy and physical properties. *Bioengineering*. 2019;6(1):26.

- Shore GC.** Apoptosis: it's BAK to VDAC. *EMBO reports*. 2009;10(12):1311-3.
- Shoshan-Barmatz V, Keinan N, Abu-Hamad S, Tyomkin D, Aram L.** Apoptosis is regulated by the VDAC1 N-terminal region and by VDAC oligomerization: release of cytochrome c, AIF and Smac/Diablo. *Biochimica et Biophysica Acta (BBA)-Bioenergetics*. 2010;1797(6-7):1281-91.
- Shvedova AA, Pietroiusti A, Fadeel B, Kagan VE.** Mechanisms of carbon nanotube-induced toxicity: focus on oxidative stress. *Toxicology and Applied Pharmacology*. 2012;261(2):121-33.
- Sibuyi NRS.** Development of a receptor targeted nanotherapy using a proapoptotic peptide. *University of Western Cape*, 2015.
- Siddiqui MH, Al-Whaibi MH, Mohammad F.** Nanotechnology and plant sciences. *Springer International Publishing, Cham*, 303p . 2015;10:978-3.
- Siegel RL, Miller KD, Jemal A.** Cancer statistics, 2019. *CA: A Cancer Journal for Clinicians*. 2019;69(1):7-34.
- Singh C, Baboota RK, Naik PK, Singh H.** Biocompatible synthesis of silver and gold nanoparticles using leaf extract of *Dalbergia sissoo*. 2012.
- Singh P, Kim YJ, Zhang D, Yang DC.** Biological synthesis of nanoparticles from plants and microorganisms. *Trends in Biotechnology*. 2016;34(7):588-99.
- Singh P, Pandit S, Garnæs J, Tunjic S, Mokkalapati VR, Sultan A, Thygesen A, Mackevica A, Mateiu RV, Daugaard AE, Baun A.** Green synthesis of gold and silver nanoparticles from *Cannabis sativa* (industrial hemp) and their capacity for biofilm inhibition. *International Journal of Nanomedicine*. 2018;13:3571.
- Singh V, Shrivastava A, Wahi N.** Biosynthesis of silver nanoparticles by plants crude extracts and their characterization using UV, XRD, TEM and EDX. *African Journal of Biotechnology*. 2015;14(33):2554-67.
- Sivalokanathan S, Vijayababu MR, Balasubramanian MP.** Effects of *Terminalia arjuna* bark extract on apoptosis of human hepatoma cell line HepG2. *World Journal of Gastroenterology*. 2006;12(7):1018.
- Smith KR, Klei LR, Barchowsky A.** Arsenite stimulates plasma membrane NADPH oxidase in vascular endothelial cells. *American Journal of Physiology-Lung Cellular and Molecular Physiology*. 2001;280(3):L442-L9.
- Soenen SJ, Rivera-Gil P, Montenegro JM, Parak WJ, De Smedt SC, Braeckmans K.** Cellular toxicity of inorganic nanoparticles: common aspects and guidelines for improved nanotoxicity evaluation. *Nano today*. 2011;6(5):446-65.
- Sofowora A.** Medicinal plants and traditional medicine in Africa. Ibadan. *Nigeria: Spectrum Books Ltd*. 1993:191-289.
- Song JY, Jang HK, Kim BS.** Biological synthesis of gold nanoparticles using *Magnolia kobus* and *Diopyros kaki* leaf extracts. *Process Biochemistry*. 2009;44(10):1133-8.
- Sorisky A, Magun R, Gagnon A.** Adipose cell apoptosis: death in the energy depot. *International Journal of Obesity*. 2000;24(4):S3-S7.

- Sperling RA, Gil PR, Zhang F, Zanella M, Parak WJ.** Biological applications of gold nanoparticles. *Chemical Society Reviews*. 2008;37(9):1896-908.
- Virant-Klun I, Stimpfel M.** Novel population of small tumour-initiating stem cells in the ovaries of women with borderline ovarian cancer. *Scientific Reports*. 2016;6:34730.
- Sudo T, Nitta M, Saya H, Ueno NT.** Dependence of paclitaxel sensitivity on a functional spindle assembly checkpoint. *Cancer Research*. 2004;64(7):2502-8.
- Sun H, Jia J, Jiang C, Zhai S.** Gold nanoparticle-induced cell death and potential applications in nanomedicine. *International Journal of Molecular Sciences*. 2018;19(3):754.
- Sundarraaj S, Thangam R, Sreevani V, Kaveri K, Gunasekaran P, Achiraman S, Kannan S.**  $\gamma$ -Sitosterol from *Acacia nilotica* L. induces G2/M cell cycle arrest and apoptosis through c-Myc suppression in MCF-7 and A549 cells. *Journal of Ethnopharmacology*. 2012;141(3):803-9.
- Suvarna S, Das U, Kc S, Mishra S, Sudarshan M, Saha KD, Dey S, Chakraborty A, Narayana Y.** Synthesis of a novel glucose capped gold nanoparticle as a better theranostic candidate. *PloS one*. 2017;12(6):e0178202.
- Sýkora D, Kašička V, Mikšík I, Řezanka P, Záruba K, Matějka P, Král V.** Application of gold nanoparticles in separation sciences. *Journal of Separation Science*. 2010;33(3):372-87.
- Tahover E, Patil YP, Gabizon AA.** Emerging delivery systems to reduce doxorubicin cardiotoxicity and improve therapeutic index: focus on liposomes. *Anti-cancer Drugs*. 2015;26(3):241-58.
- Tchuente Tchuemogne MA, Kammalac TN, Gohlke S, Kouipou RM, Aslan A, Kuzu M, Comakli V, Demirdag R, Ngouela SA, Tsamo E, Sewald N.** Compounds from *Terminalia mantaly* L.(Combretaceae) stem bark exhibit potent inhibition against some pathogenic yeasts and enzymes of metabolic significance. *Medicines*. 2017 Mar;4(1):6.
- Therese K, Bagyalakshmi R, Madhavan H, Deepa P.** *In-vitro* susceptibility testing by agar dilution method to determine the minimum inhibitory concentrations of amphotericin B, fluconazole and ketoconazole against ocular fungal isolates. *Indian Journal of Medical Microbiology*. 2006;24(4):273.
- Tian J, Wong KK, Ho CM, Lok CN, Yu WY, Che CM, Chiu JF, Tam PK.** Topical delivery of silver nanoparticles promotes wound healing. *ChemMedChem*. 2007;2(1):129-36.
- Torres-Chavolla E, Ranasinghe RJ, Alcilja EC.** Characterization and functionalization of biogenic gold nanoparticles for biosensing enhancement. *IEEE transactions on Nanotechnology*. 2010;9(5):533-8.
- Tripathi A, Kumari S, Kumar A.** Toxicity evaluation of pH dependent stable *Achyranthes aspera* herbal gold nanoparticles. *Applied Nanoscience*. 2016;6(1):61-9.
- ud Din F, Aman W, Ullah I, Qureshi OS, Mustapha O, Shafique S, Zeb A.** Effective use of nanocarriers as drug delivery systems for the treatment of selected tumors. *International journal of nanomedicine*. 2017;12:7291.

- Valavanidis A, Vlachogianni T, Fiotakis C.** 8-hydroxy-2'-deoxyguanosine (8-OHdG): a critical biomarker of oxidative stress and carcinogenesis. *Journal of environmental science and health Part C.* 2009;27(2):120-39.
- Van Elsland D, Neefjes J.** Bacterial infections and cancer. *EMBO reports.* 2018;19(11):e46632.
- Van Engeland M, Nieland LJ, Ramaekers FC, Schutte B, Reutelingsperger CP.** Annexin V-affinity assay: a review on an apoptosis detection system based on phosphatidylserine exposure. *The Journal of the International Society for Analytical Cytology.* 1998;31(1):1-9.
- Vijayakumar S, Ganesan S.** *In vitro* cytotoxicity assay on gold nanoparticles with different stabilizing agents. *Journal of Nanomaterials.* 2012;2012.
- Vimbela GV, Ngo SM, Frazee C, Yang L, Stout DA.** Antibacterial properties and toxicity from metallic nanomaterials. *International Journal of Nanomedicine.* 2017;12:3941.
- Wan J, Wang JH, Liu T, Xie Z, Yu XF, Li W.** Surface chemistry but not aspect ratio mediates the biological toxicity of gold nanorods *in vitro* and *in vivo*. *Scientific Reports.* 2015;5:11398.
- Wang H, Wang F, Tao X, Cheng H.** Ammonia-containing dimethyl sulfoxide: an improved solvent for the dissolution of formazan crystals in the 3-(4, 5-dimethylthiazol-2-yl)-2, 5-diphenyl tetrazolium bromide (MTT) assay. *Analytical Biochemistry.* 2012;421(1):324-6.
- Wang Y, He X, Wang K, Zhang X, Tan W.** Barbated Skullcup herb extract-mediated biosynthesis of gold nanoparticles and its primary application in electrochemistry. *Colloids and Surfaces B: Biointerfaces.* 2009;73(1):75-9.
- Wlodkowic D, Skommer J, Darzynkiewicz Z.** Flow cytometry-based apoptosis detection. *Apoptosis: Springer;* 2009. p. 19-32.
- Woźniak A, Malankowska A, Nowaczyk G, Grześkowiak BF, Tuśnio K, Słomski R, Zaleska-Medynska A, Jurga S.** Size and shape-dependent cytotoxicity profile of gold nanoparticles for biomedical applications. *Journal of Materials Science: Materials in Medicine.* 2017;28(6):92.
- Wu D, Yotnda P.** Production and detection of reactive oxygen species (ROS) in cancers. *Journal of Visualized Experiments.* 2011(57):e3357.
- Wu H, Zhu H, Li X, Liu Z, Zheng W, Chen T, Yu B, Wong KH.** Induction of apoptosis and cell cycle arrest in A549 human lung adenocarcinoma cells by surface-capping selenium nanoparticles: an effect enhanced by polysaccharide-protein complexes from *Polyporus rhinocerus*. *Journal of Agricultural and Food Chemistry.* 2013;61(41):9859-66.
- Wu L, Zhang J, Watanabe W.** Physical and chemical stability of drug nanoparticles. *Advanced Drug Delivery Reviews.* 2011;63(6):456-69.
- Xia T, Kovoichich M, Brant J, Hotze M, Sempf J, Oberley T, Sioutas C, Yeh JI, Wiesner MR, Nel AE.** Comparison of the abilities of ambient and manufactured nanoparticles to induce cellular toxicity according to an oxidative stress paradigm. *Nano letters.* 2006;6(8):1794-807.

- Xie H, Mason MM, Wise JP.** Genotoxicity of metal nanoparticles. *Reviews on Environmental Health.* 2011;26(4):251-68.
- Xin Y, Yin M, Zhao L, Meng F, Luo L.** Recent progress on nanoparticle-based drug delivery systems for cancer therapy. *Cancer Biology & Medicine.* 2017;14(3):228.
- Yeh YC, Creran B, Rotello VM.** Gold nanoparticles: preparation, properties, and applications in bionanotechnology. *Nanoscale.* 2012;4(6):1871-80.
- Yezhelyev MV, Gao X, Xing Y, Al-Hajj A, Nie S, O'Regan RM.** Emerging use of nanoparticles in diagnosis and treatment of breast cancer. *The lancet Oncology.* 2006;7(8):657-67.
- Youns M, D Hoheisel J, Efferth T.** Therapeutic and diagnostic applications of nanoparticles. *Current Drug Targets.* 2011;12(3):357-65.
- Yunus IS, Harwin, Kurniawan A, Adityawarman D, Indarto A.** Nanotechnologies in water and air pollution treatment. *Environmental Technology Reviews.* 2012;1(1):136-48.
- Zakir M, Maming EYL, Lembang MS.** Synthesis of silver and gold nanoparticles through reduction method using bioreductor of leaf extract of ketapang (*Terminalia catappa*), 2018.
- Zeng H, Chen W, Zheng R, Zhang S, Ji JS, Zou X, Xia C, Sun K, Yang Z, Li H, Wang N.** Changing cancer survival in China during 2003–15: a pooled analysis of 17 population-based cancer registries. *The Lancet Global Health.* 2018;6(5):e555-67.
- Zhang P, Wang P, Yan L, Liu L.** Synthesis of gold nanoparticles with *Solanum xanthocarpum* extract and their *in vitro* anticancer potential on nasopharyngeal carcinoma cells. *International Journal of Nanomedicine.* 2018;13:7047.
- Zhang X-F, Gurunathan S.** Combination of salinomycin and silver nanoparticles enhances apoptosis and autophagy in human ovarian cancer cells: an effective anticancer therapy. *International Journal of Nanomedicine.* 2016;11:3655.
- Zhang Y, Shareena Dasari TP, Deng H, Yu H.** Antimicrobial activity of gold nanoparticles and ionic gold. *Journal of Environmental Science and Health, Part C.* 2015;33(3):286-327.
- Zhang YB, Pan XF, Chen J, Cao A, Zhang YG, Xia L, Wang J, Li H, Liu G, Pan A.** Combined lifestyle factors, incident cancer, and cancer mortality: a systematic review and meta-analysis of prospective cohort studies. *British Journal of Cancer.* 2020;122(7):1085-93.
- Zhang Z, Berg A, Levanon H, Fessenden RW, Meisel D.** On the interactions of free radicals with gold nanoparticles. *Journal of the American Chemical Society.* 2003;125(26):7959-63.
- Zheng Q, Yang H, Wei J, Tong JI, Shu Yq.** The role and mechanisms of nanoparticles to enhance radiosensitivity in hepatocellular cell. *Biomedicine & Pharmacotherapy.* 2013;67(7):569-75.
- Zheng Y, Sanche L.** Gold nanoparticles enhance DNA damage induced by anti-cancer drugs and radiation. *Radiation Research.* 2009;172(1):114-9.

**Zhou Y, Liang X, Dai Z.** Porphyrin-loaded nanoparticles for cancer theranostics. *Nanoscale*. 2016;8(25):12394-405.



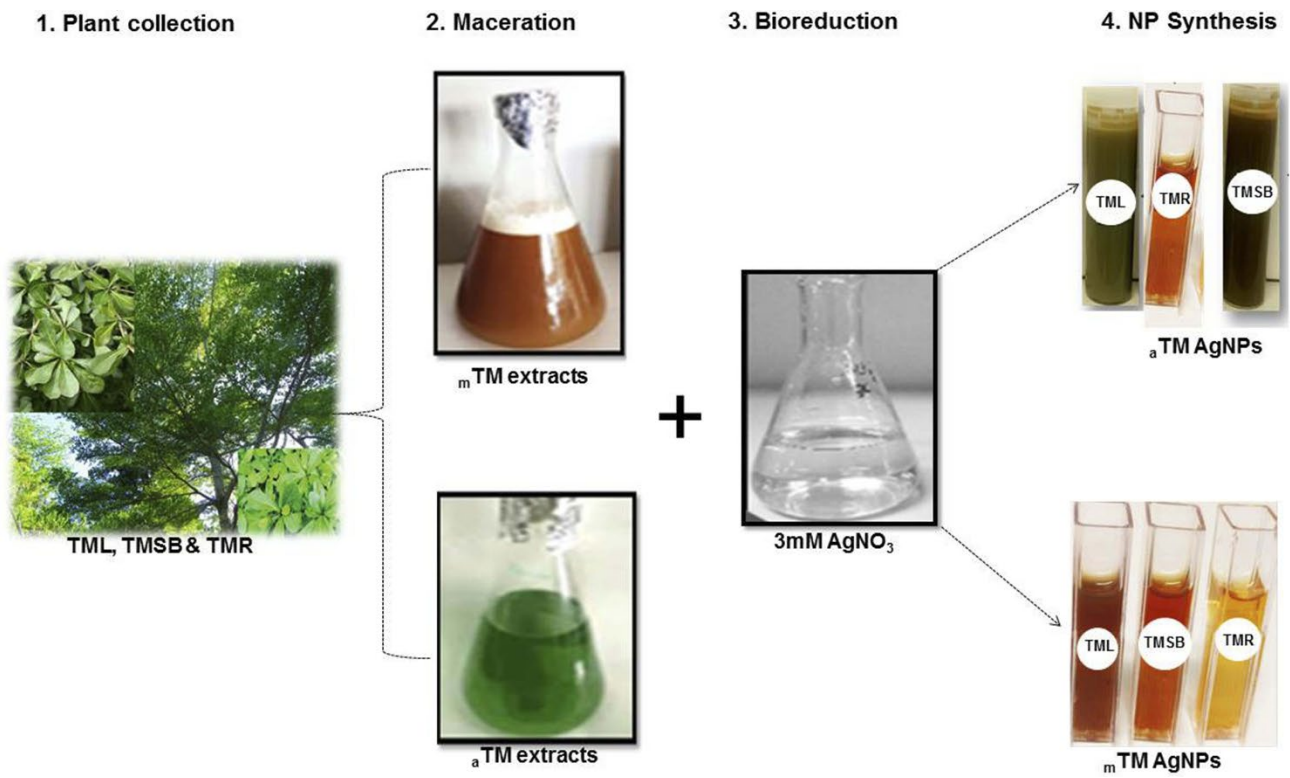
*Appendices*



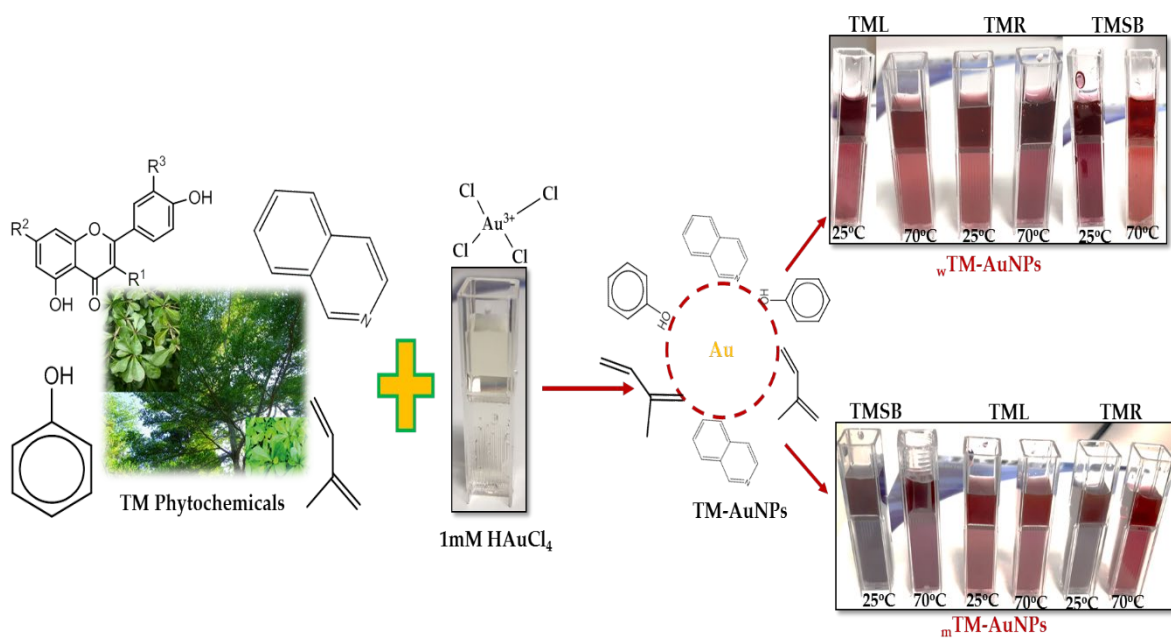
**Appendix 1:** Measurement of nanoparticles concentrations higher concentration of nanoparticles.

Acronym	Concentration (µg/mL)	Acronym	Concentration (µg/mL)
mTML-AuNPs-25 °C	1040	mTML-AgNPs-25 °C	500
mTML- AuNPs-70 °C	1360	mTML-AgNPs-70 °C	500
aTML- AuNPs-25 °C	500	aTML-AgNPs-25 °C	560
aTML- AuNPs-70 °C	880	aTML-AgNPs-70 °C	880
mTMSB-AuNPs-25 °C	720	mTMSB-AgNPs-25 °C	720
mTMSB- AuNPs-70 °C	400	mTMSB-AgNPs-70 °C	400
aTMSB- AuNPs-25 °C	960	aTMSB-AgNPs-25 °C	960
aTMSB- AuNPs-70 °C	240	aTMSB-AgNPs -70 °C	480
mTMR- AuNPs-25 °C	400	mTMR-AgNPs—25 °C	240
mTMR- AuNPs-70 °C	800	mTMR-AgNPs-70 °C	400
aTMR- AuNPs-25 °C	160	aTMR-AgNPs-25 °C	160
aTMR- AuNPs-70 °C	480	aTMR-AgNPs -70 °C	160

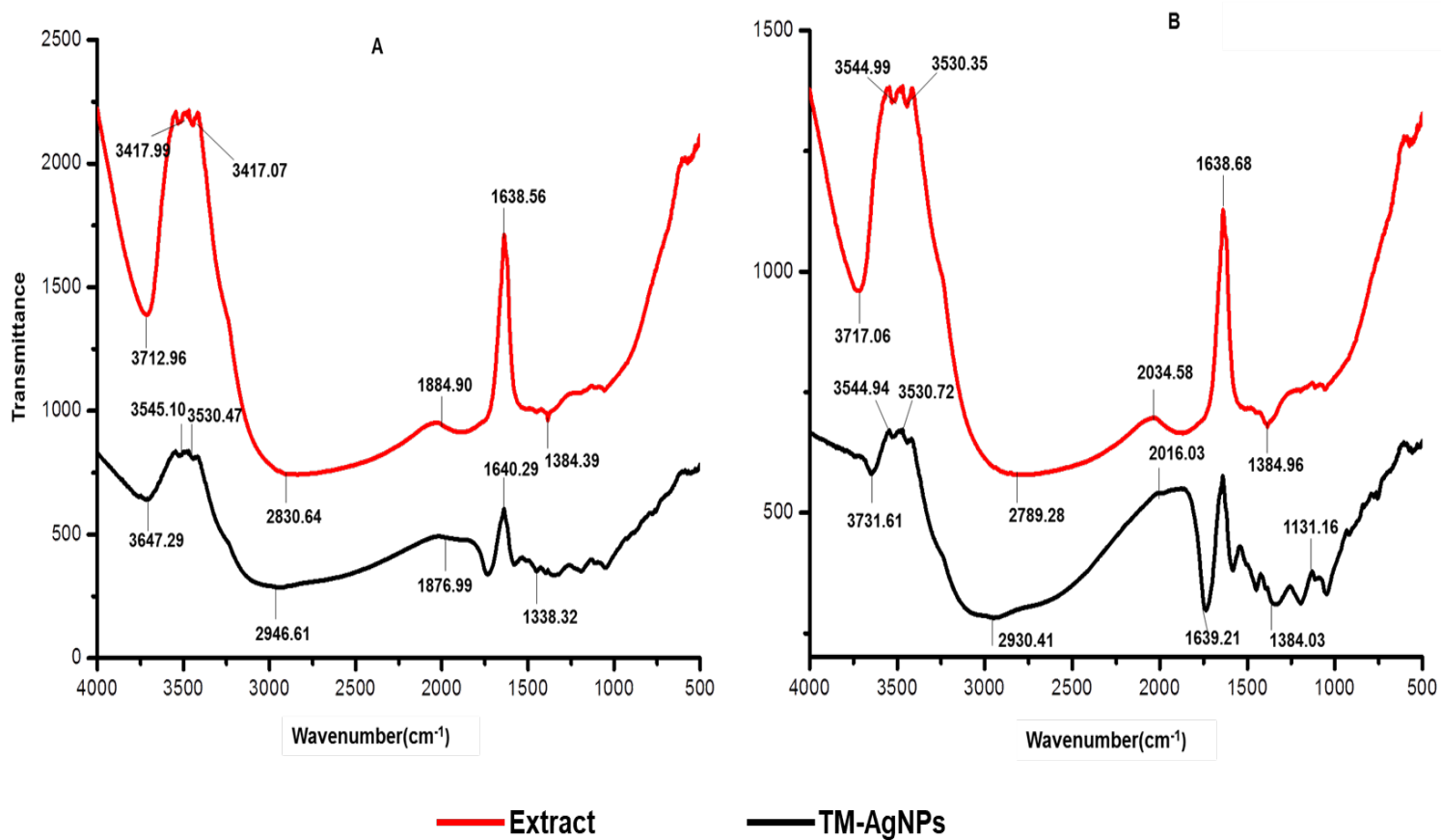
## Appendix 2: Schematic representation of the AgNP synthesis from TM plant extracts



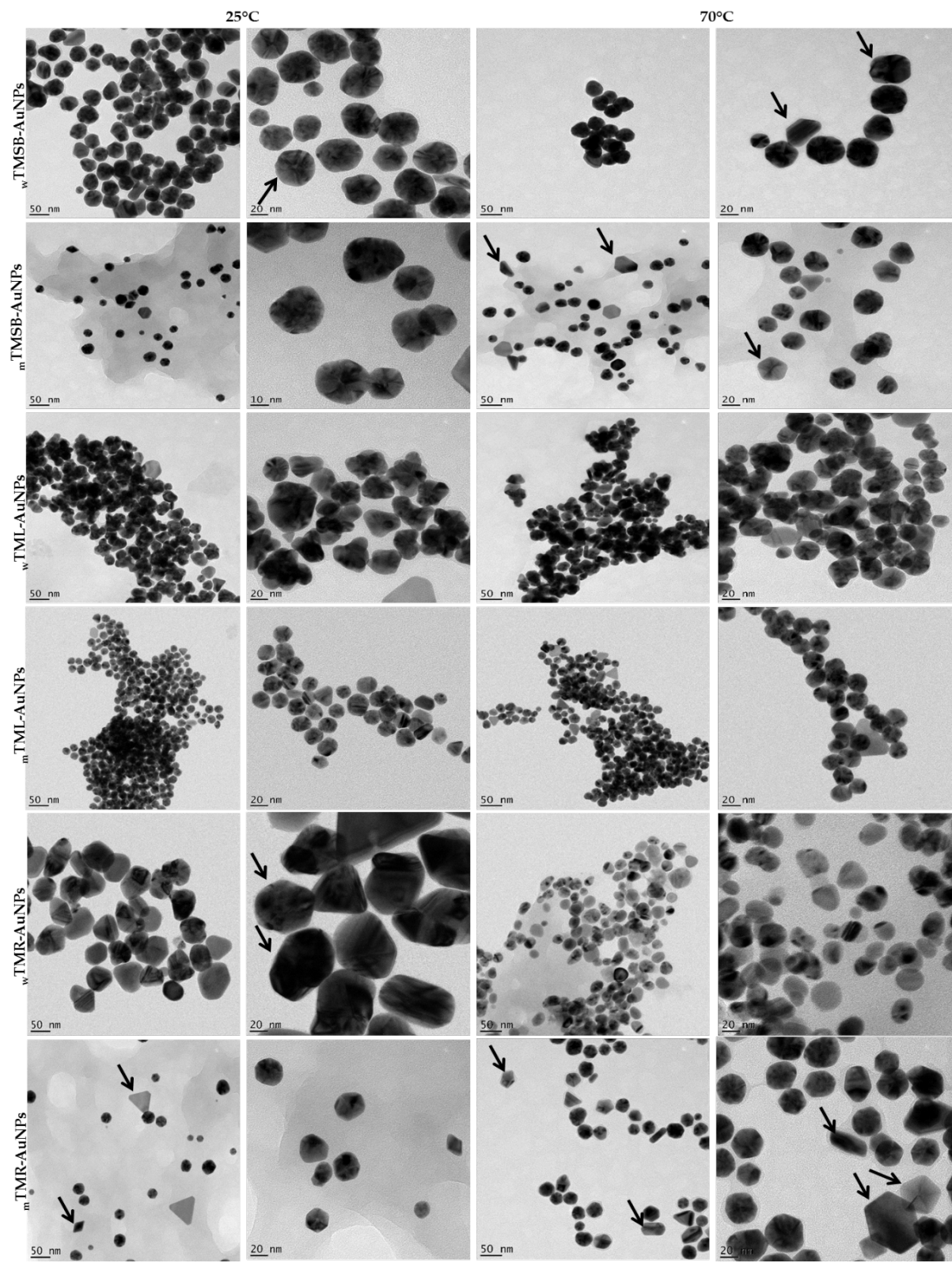
**Appendix 3:** One-step synthesis of TM-AuNPs by reduction of gold ions with TM phytochemicals. Colour change denoted to the presence of AuNPs.



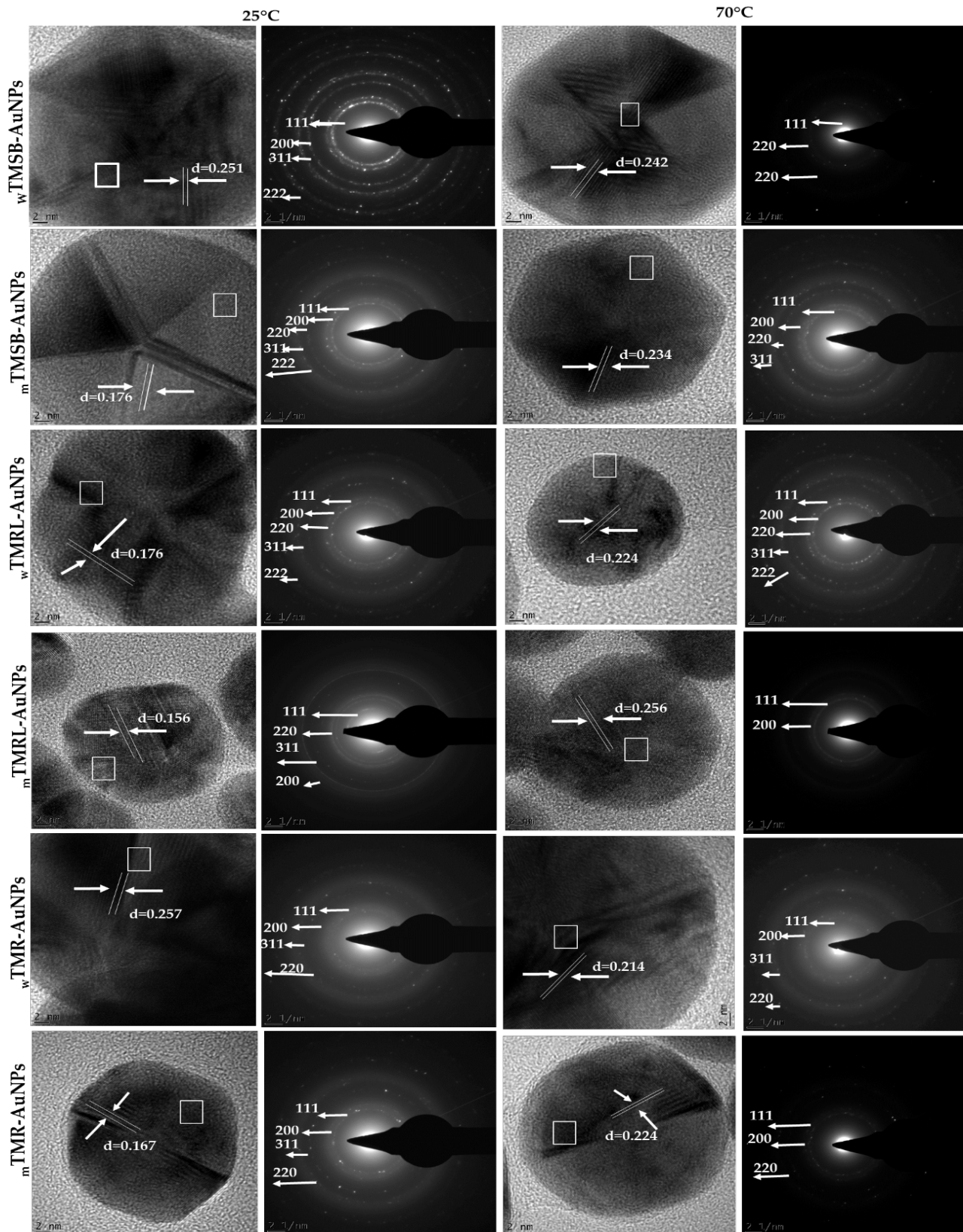
**Appendix 4:** Fourier-transform infrared spectra of (A) extract from (aTMSB) of *Terminalia mantaly* (B) AuNPs- aTMSB prepared at 25 °C and (C) AuNPs-aTMSB synthesized at 70 °C.



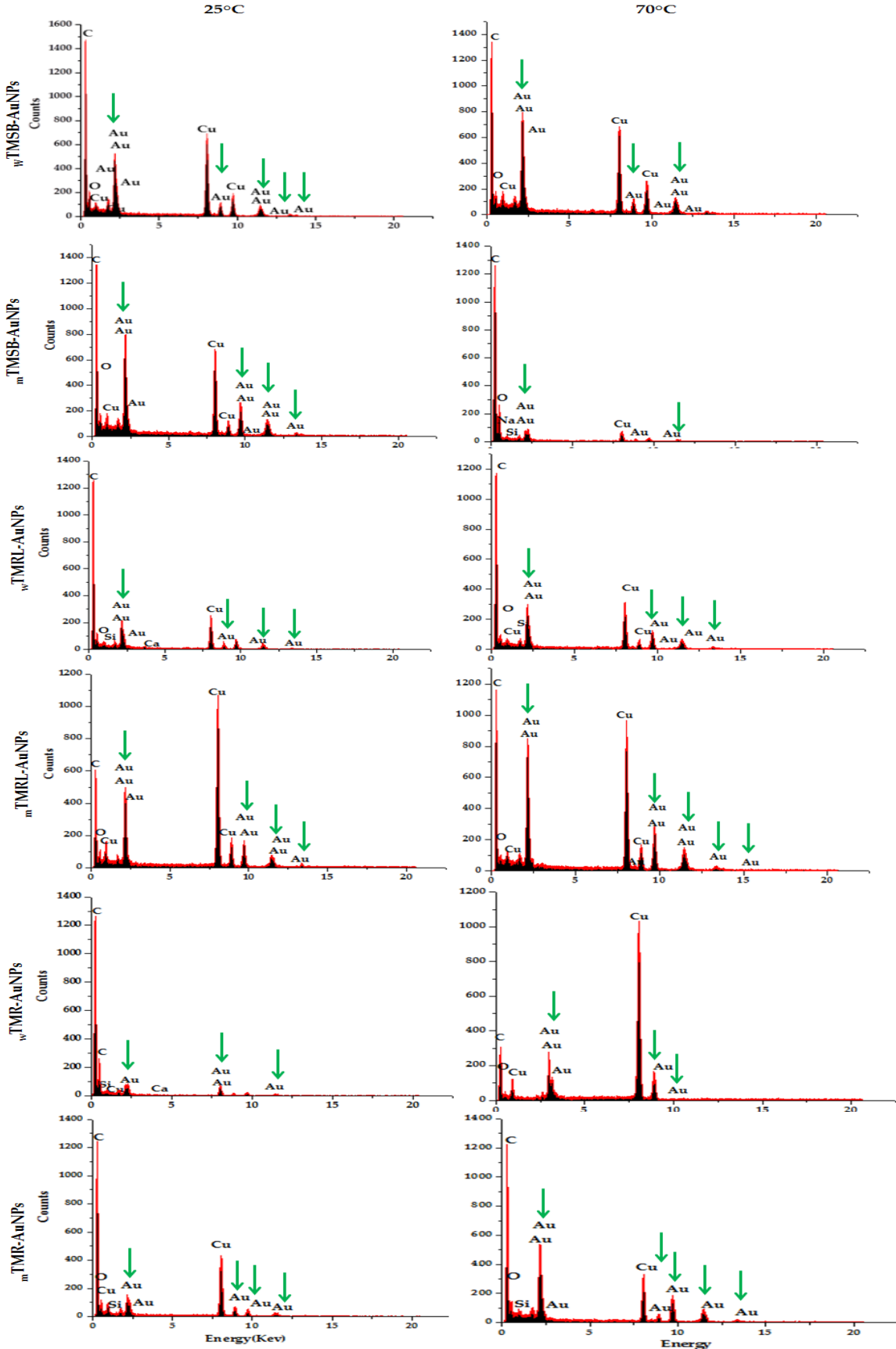
**Appendix 5:** HRTEM images of AuNPs synthesized at 25 °C and 70 °C. The arrows point at different NP shapes. The scale bar at 10, 20 and 50 nm.



**Appendix 6: SAED patterns of TM-AuNPs showing single facets of NPs in TEM micrographs**



**Appendix 7: EDX spectra of TM-AuNPs synthesized at 25 °C and 70 °C.**



## Appendix 8: Core sizes of TM-AuNPs were analyzed by HRTEM

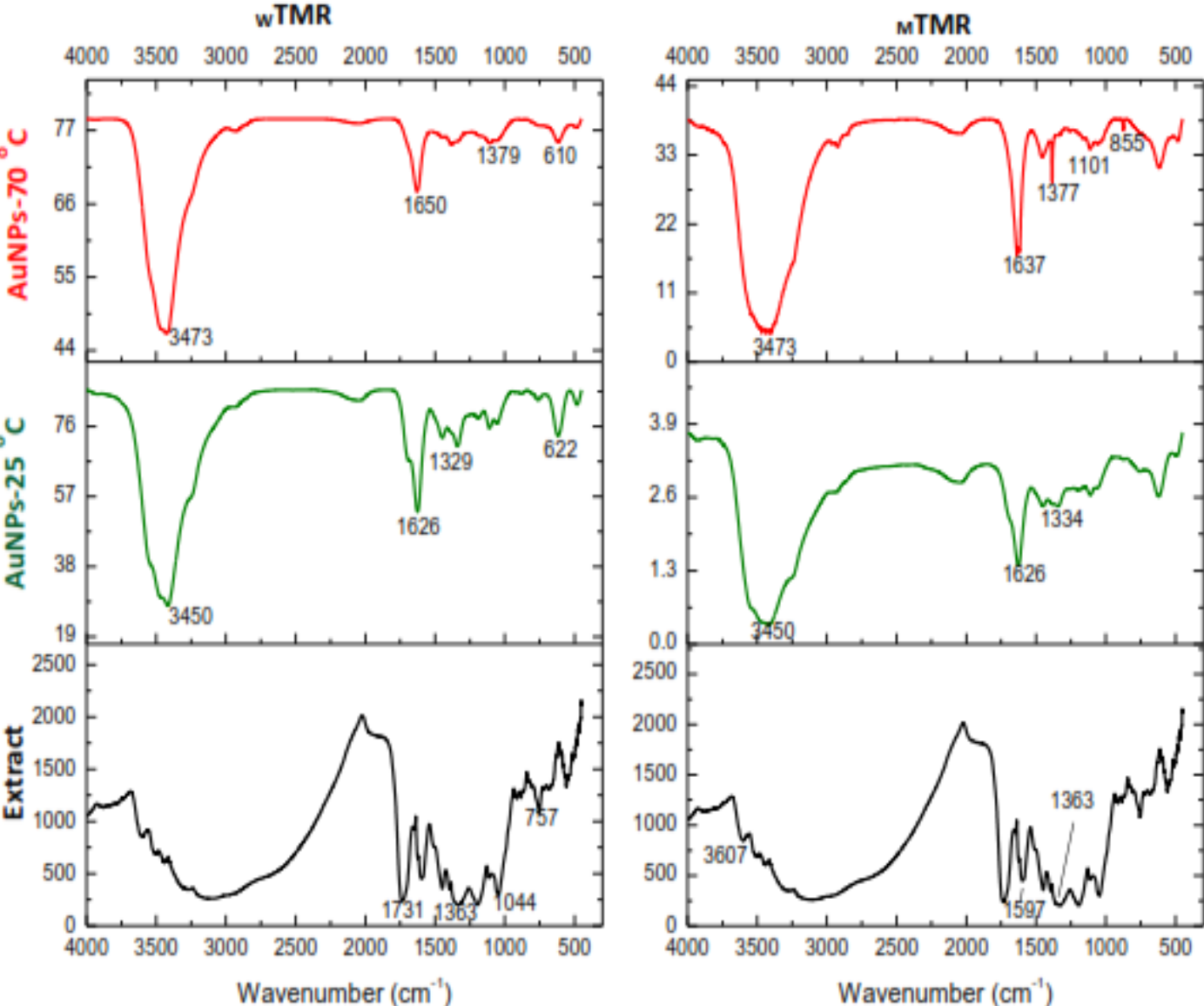
TM Extracts	TM-AuNP core size (nm)	
	25 °C	70 °C
<sup>a</sup> TMSB-AuNPs	35.5	43.0
<sup>m</sup> TMSB-AuNPs	25.5	28.3
<sup>a</sup> TML-AuNPs	26.5	21.5
<sup>m</sup> TML-AuNPs	23.5	25.0
<sup>a</sup> TMR-AuNPs	32.0	33.5
<sup>m</sup> TMR-AuNPs	21.0	29.5

## Appendix 9: FTIR analysis of TM-AuNPs.

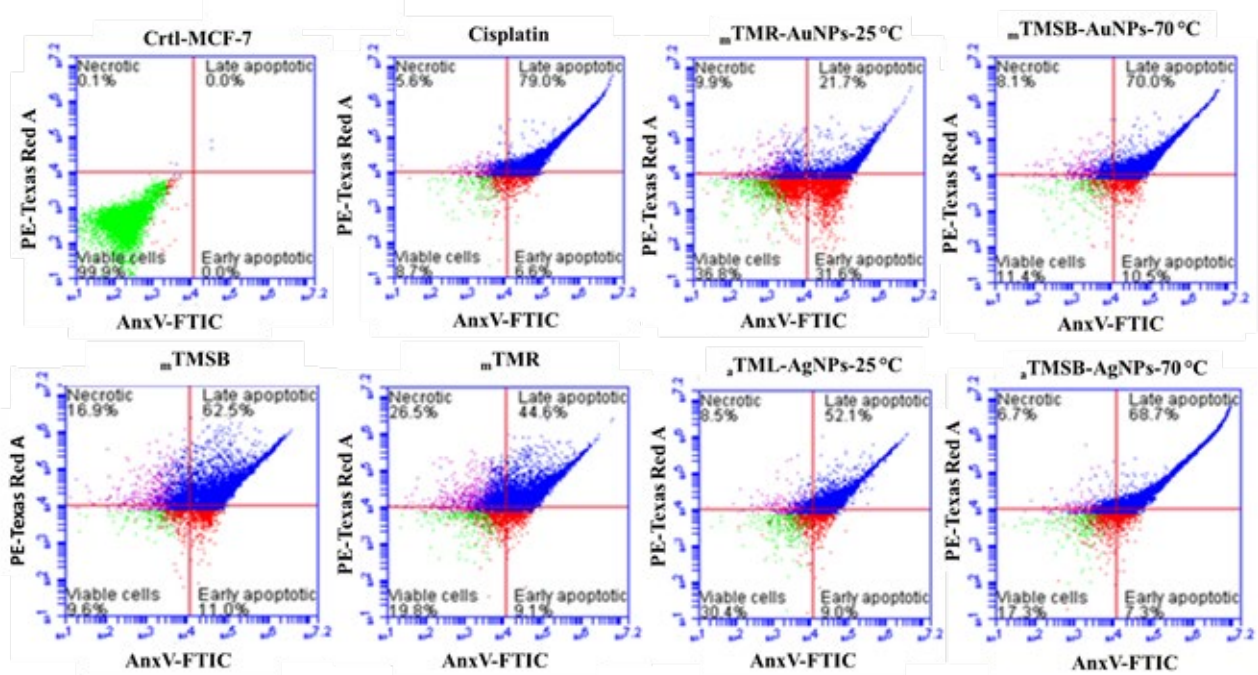
Extracts	Peak position in extracts (cm <sup>-1</sup> )	Peak position in AuNPs at 25 °C (cm <sup>-1</sup> )	Peak position in AuNPs at 70 °C (cm <sup>-1</sup> )	Possible chemicals groups
<sup>a</sup> TMSB	1048	1108	1123	C-O carboxylic acids, esters, ethers C-H methyl rock alkanes -C=C- stretch alkenes H-C=O: C-H stretch aldehydes -C≡C- stretch alkynes O-H, Alcohol, phenol
	1384	1347	-----	
	1639	1627	1636	
	2920	2939	2939	
	2016	2106	2106	
	3717	3409	3452	
<sup>m</sup> TMSB	1044	1104	1032	C-O carboxylic acids, esters, ethers C-H methyl rock alkanes -C=C- stretch alkenes H-C=O: C-H stretch aldehydes O-H Alcohol, phenol
	1330	-----	1396	
	1692	1626	1638	
	2958	2938	2927	
	3645	3417	3474	
<sup>a</sup> TMR	1044	1106	1101	C-O carboxylic acids, esters, ethers C-H methyl rock alkanes -C=C- stretch alkenes O-H Alcohol, phenol
	1318	1338	1379	
	1597	1626	1635	
	3114	3450	3473	
<sup>m</sup> TMR	1044	1109	1099	C-O carboxylic acids, esters, ethers C-H methyl rock alkanes -C=C- stretch alkenes H-C=O: C-H stretch aldehydes O-H Alcohol, phenol
	1363	1334	1377	
	1597	1626	1637	
	2075	2088	2095	
	3156	3450	3473	
<sup>a</sup> TML	1129	1184	1132	C-O Aromatic esters, ethers -C=C- stretch alkenes H-C=O: C-H stretch aldehydes OH, Alcohol, phenol
	1640	1626	1650	
	2946	2828	-----	
	3647	3450	3466	
<sup>m</sup> TML	1066	1163	1066	-O Aromatic esters, ethers C-H methyl rock alkanes -C=C- stretch alkenes H-C=O: C-H stretch aldehydes OH, Alcohol, phenol
	1394	-----	1394	
	1635	1641	1635	
	2991	2991	2989	
	3306	3250	3304	



**Appendix 10:** FTIR spectra of selected TM-AgNPs compared to their respective TM extracts.

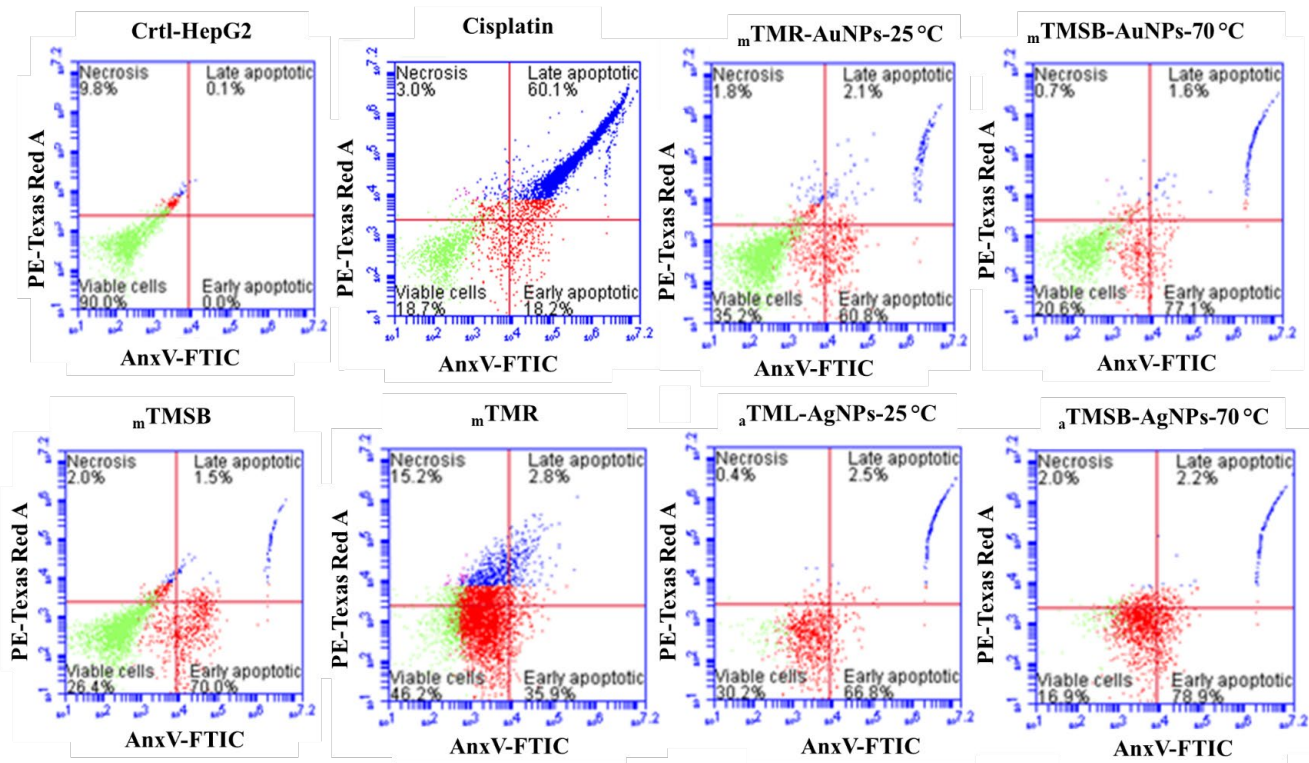


**Appendix 11:** Apoptotic effect of more active crude extracts, gold, and the silver nanoparticle from *Terminalia mantaly* on MCF-7 cells. **Note:** MCF-7 cells were treated with mTMSB, mTMR, mTMR-AuNPs-25 °C, mTMSB-AuNPs-70 °C, aTML-AgNPs-25 °C, aTMSB-AgNPs-70 °C at their specific IC<sub>50</sub> values, cisplatin 10 μM was used at positive control were stained with 20 μL of Annexin V Cy3.18 Conjugate (100 mg/mL solution, Catalog Number A4963), 20 μL of 50 mM 6-CFDA in acetone solution, 200 μL of 10X Binding Buffer (Catalog Number B9796). The experiment was performed thrice, and the representative images of each group are presented.



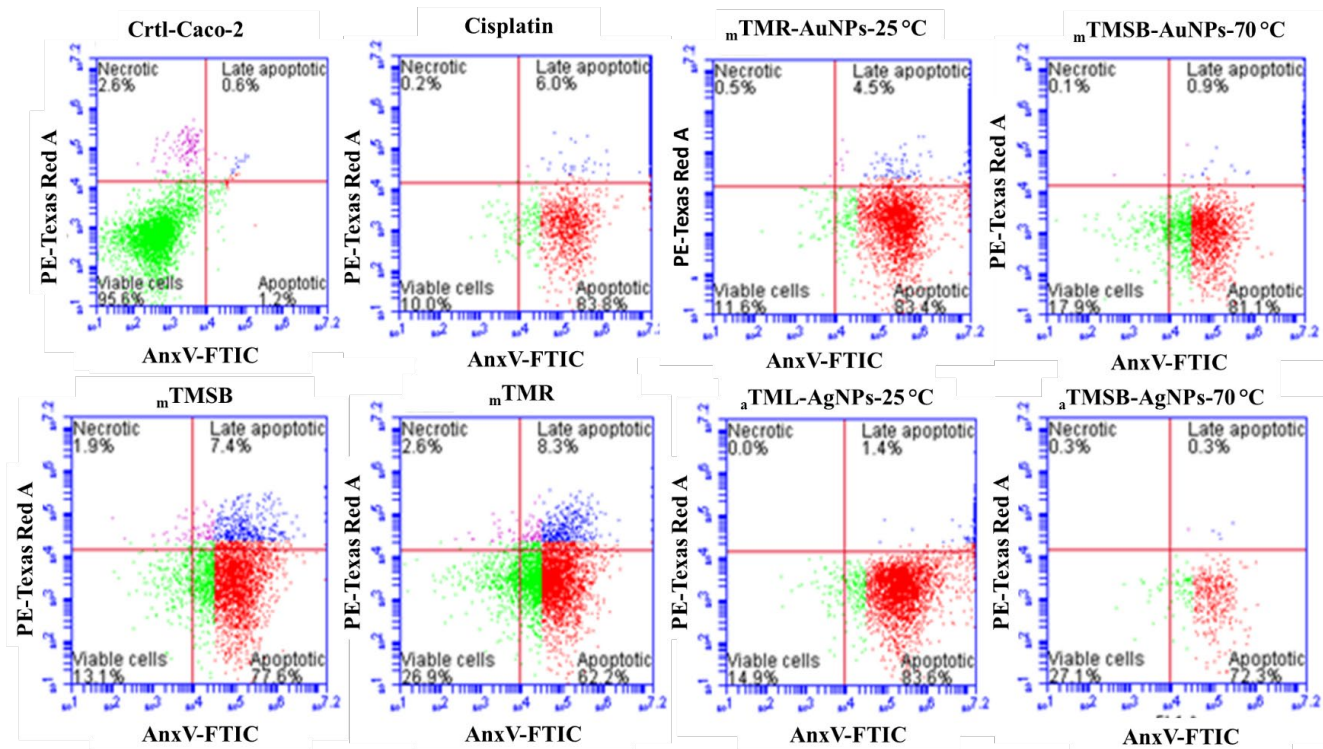
**Appendix12:** Apoptotic effect of more active crude extracts, two active gold and silver nanoparticles from *Terminalia mantaly* on HepG2 cells for 24 hrs.

**Note:** HepG2 cells were treated with  $mTMSB$ ,  $mTMR$ ,  $mTMR-AuNPs-25^\circ C$ ,  $mTMSB-AuNPs-70^\circ C$ ,  $aTML-AgNPs-25^\circ C$ ,  $aTMSB-AgNPs-70^\circ C$  at their specific  $IC_{50}$  values, cisplatin  $10\ \mu M$  was used at positive control were stained with  $20\ \mu L$  of Annexin V Cy3.18 Conjugate (100 mg/mL solution, Catalog Number A4963),  $20\ \mu L$  of 50 mM 6-CFDA in acetone solution,  $200\ \mu L$  of 10X Binding Buffer (Catalog Number B9796). The experiment was performed thrice, and the representative images of each group are presented



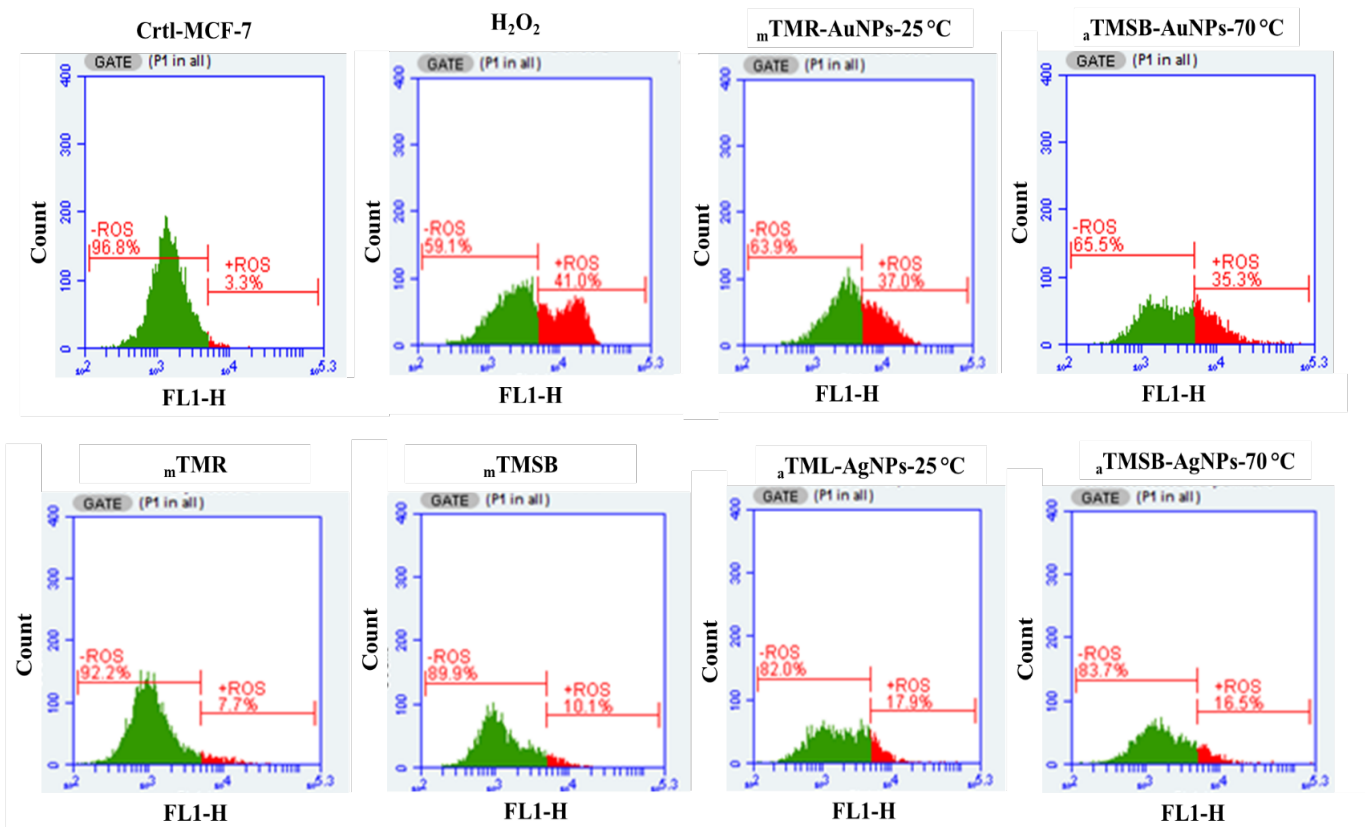
**Appendix13:** Apoptotic effect of more active crude extracts, two active gold and silver nanoparticles from *Terminalia mantaly* on Caco-2 cells for 24 hrs.

**Note:** Caco-2 cells were treated with  $mTMSB$ ,  $mTMR$ ,  $mTMR-AuNPs-25\text{ }^{\circ}C$ ,  $mTMSB-AuNPs-70\text{ }^{\circ}C$ ,  $aTML-AgNPs-25\text{ }^{\circ}C$ ,  $aTMSB-AgNPs-70\text{ }^{\circ}C$  at their specific  $IC_{50}$  values, cisplatin  $10\text{ }\mu M$  was used at positive control were stained with  $20\text{ }\mu L$  of Annexin V Cy3.18 Conjugate ( $100\text{ mg/mL}$  solution, Catalog Number A4963),  $20\text{ }\mu L$  of  $50\text{ mM}$  6-CFDA in acetone solution,  $200\text{ }\mu L$  of  $10X$  Binding Buffer (Catalog Number B9796). The experiment was performed thrice, and the representative images of each group are presented.



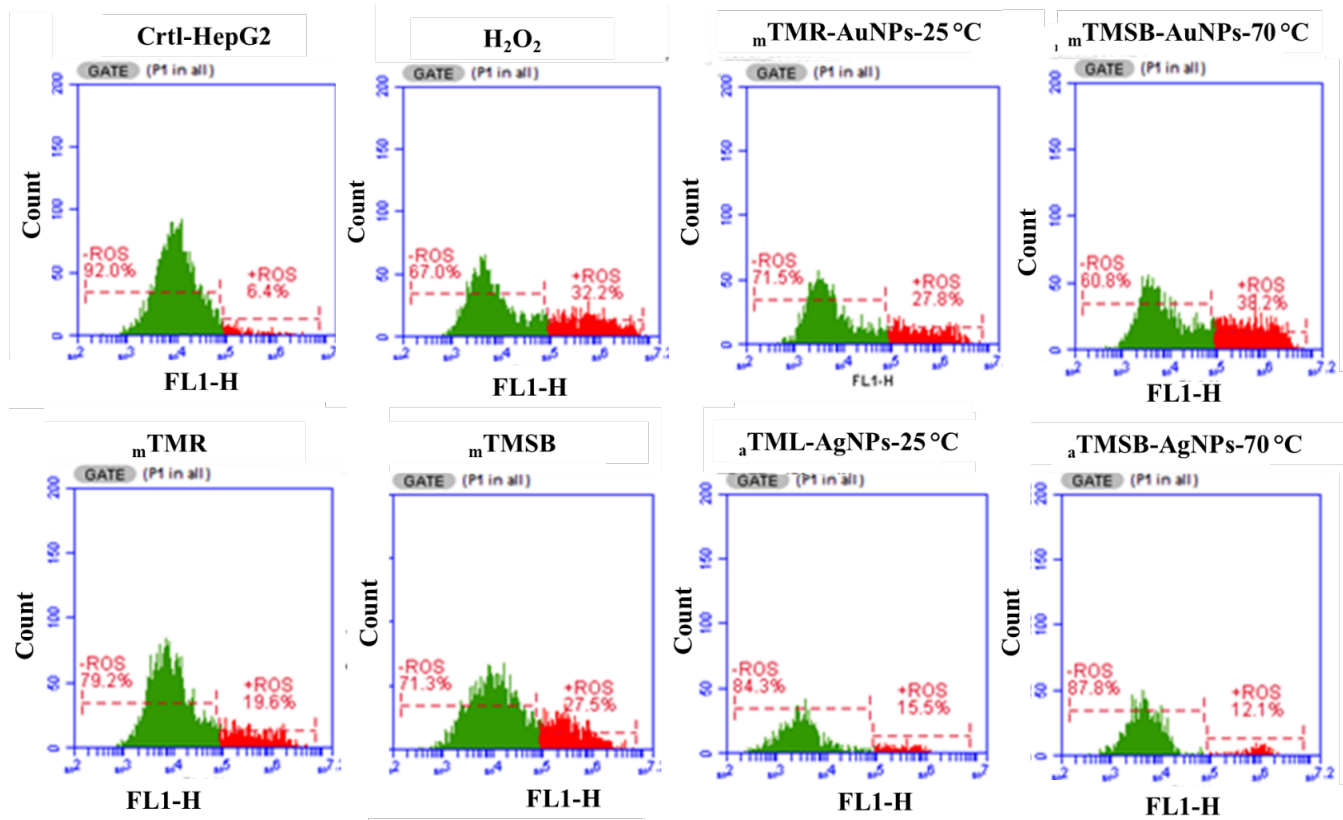
**Appendix14:** ROS activity in response to various treatments. MCF-7 cells were treated with mTMSB, mTMR, mTMR-AuNPs-25 °C, mTMSB-AuNPs-70 °C, aTML-AgNPs-25 °C, and aTMSB-AgNPs-70 °C at their specific IC50 values, 0.1% H2O2 was used as positive control values for 24 hrs.

**Note:** ROS levels were assessed by incubating the cells with 10 μM CM-H2DCFDA at 37 °C for 30 min. The fluorescence staining was analyzed with the Attune flow cytometer. For each sample, 10 000 events were recorded.



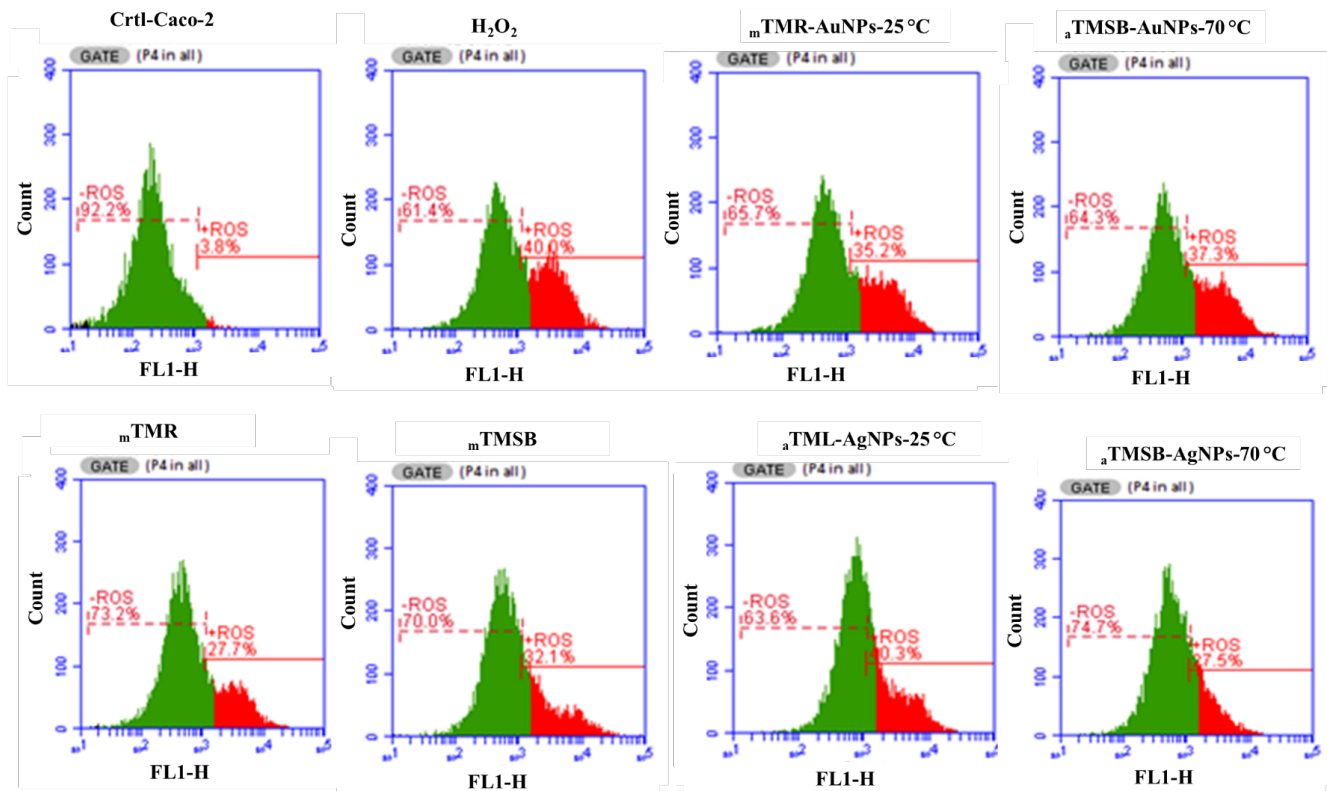
**Appendix15:** ROS activity in response to various treatment. HepG2 cells were treated with with mTMSB, mTMR, mTMR-AuNPs-25 °C, mTMSB-AuNPs-70 °C, aTML-AgNPs-25 °C, and aTMSB-AgNPs-70 °C at their specific IC50 values, 0.1% H2O2 was used as positive control for 24 hrs.

**Note:** ROS levels were assessed by incubating the cells with 10 μM CM-H2DCFDA at 37 °C for 30 min. The fluorescence staining was analyzed with the Attune flow cytometer. For each sample, 10 000 events were recorded.

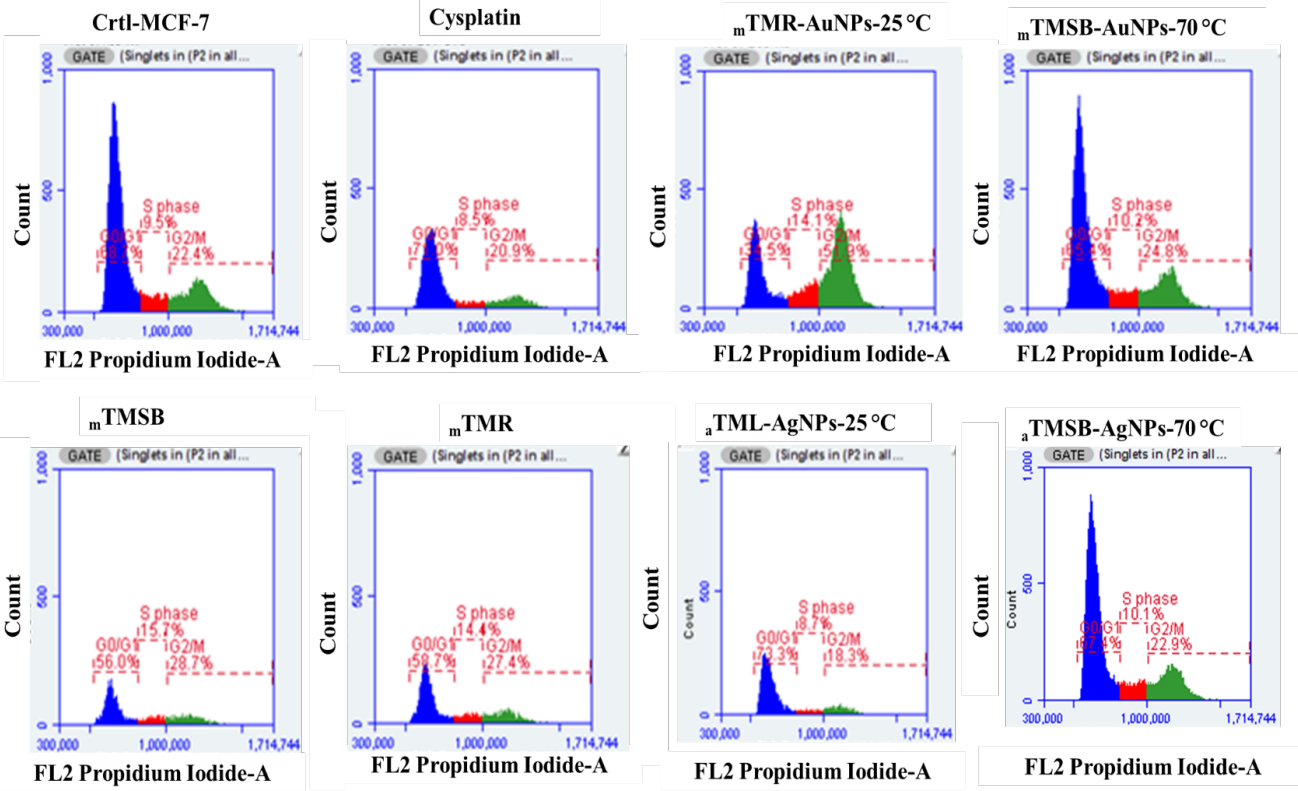


**Appendix16:** ROS activity in response to various treatments. Caco-2 cells were treated with mTMSB, mTMR, mTMR-AuNPs-25 °C, mTMSB-AuNPs-70 °C, aTML-AgNPs-25 °C, and aTMSB-AgNPs-70 °C at their specific IC50 values, 0.1% H2O2 was used as positive control for 24 hrs.

**Note:** ROS levels were assessed by incubating the cells with 10 μM of CM-H2DCFDA at 37 °C for 30 min. The fluorescence staining was analyzed with the Attune flow cytometer. For each sample, 10 000 events were recorded.

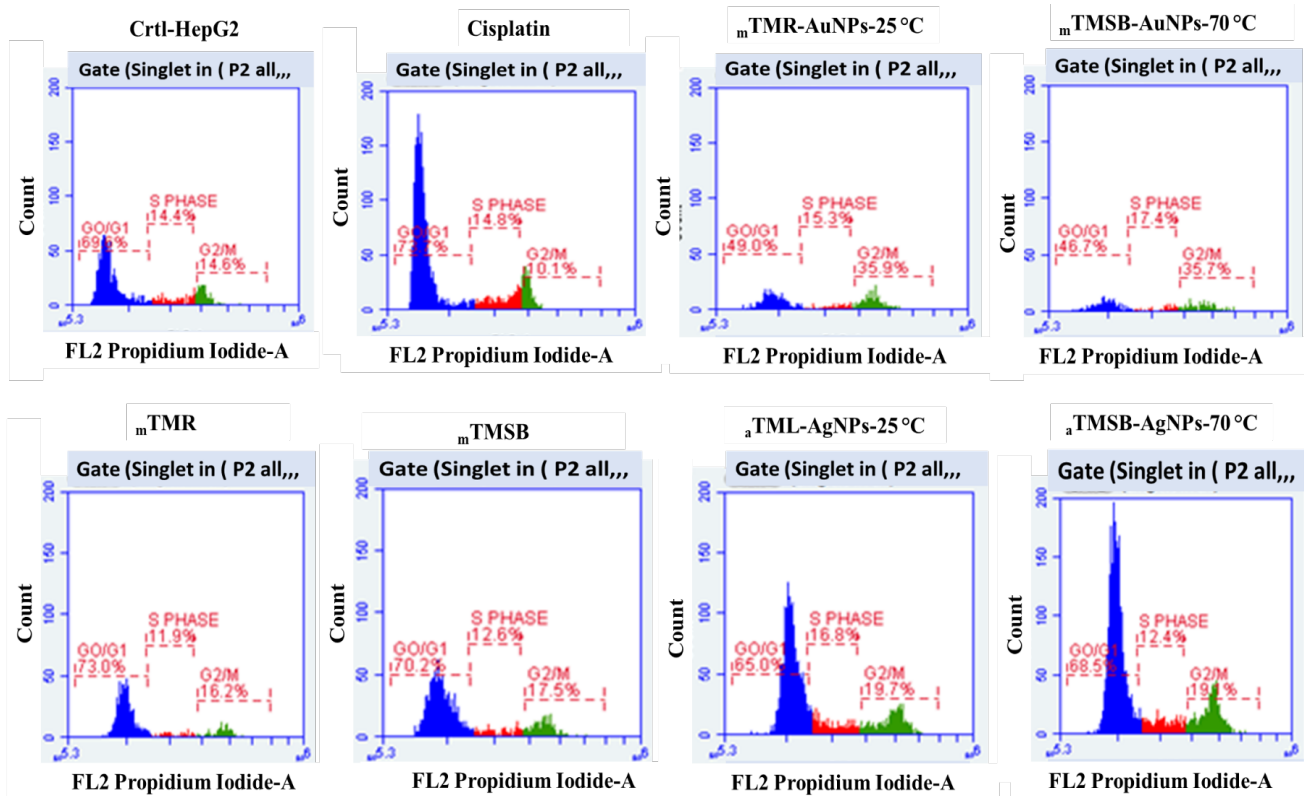


**Appendix17:** Cell cycle analysis after treatment with active mTMR-AuNPs-25 °C, mTMSB-AuNPs-70 °C, aTML-AgNPs-25 °C, aTMSB-AgNPs-70 °C, mTMSB and mTMR in MCF-7 cells at their specific IC50 values, cisplatin 10 μM was used at positive control after 24 hrs.

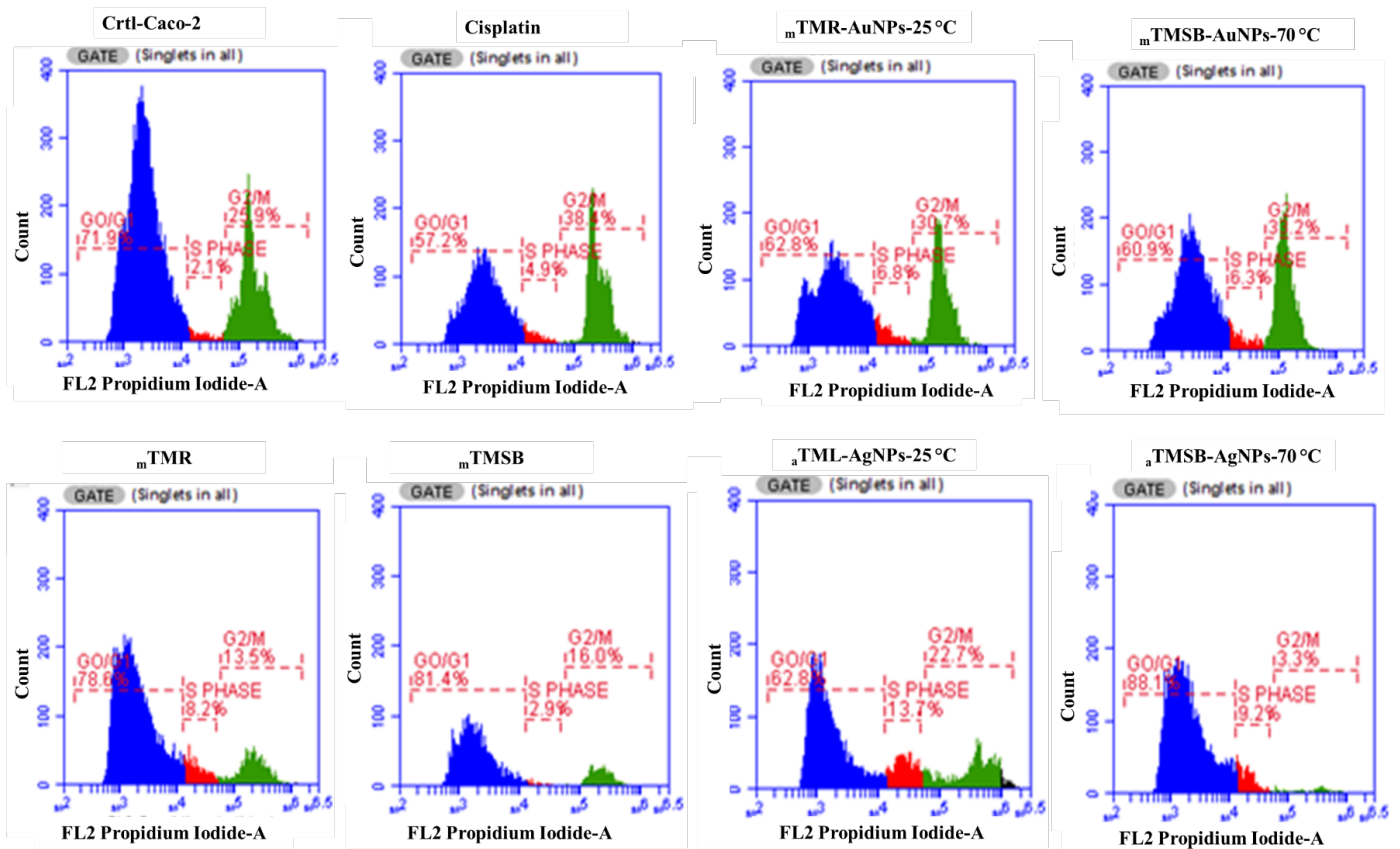




**Appendix18:** Cell cycle analysis after treatment with active mTMR-AuNPs-25 °C, mTMSB-AuNPs-70 °C, aTML-AgNPs-25 °C, aTMSB-AgNPs-70 °C, mTMSB and mTMR in HepG2 cells at their specific IC50 values, cisplatin 10 μM was used as positive control after 24 hrs.



**Appendix19:** Cell cycle analysis after treatment with active mTMR-AuNPs-25 °C, mTMSB-AuNPs-70 °C, aTML-AgNPs-25 °C, aTMSB-AgNPs-70 °C, mTMSB and mTMR in Caco-2 cells after 24 hrs.



## **Appendix 20:** Preparation of solutions and reagents.

### **+ Ampicillin antibiotic**

1 mg/mL Ampicillin was prepared in dH<sub>2</sub>O, filter sterilized. Aliquots of 2mL were stored at -20 °C.

### **+ Preparation of MHA**

38 g of the powder medium was suspended in one liter of dH<sub>2</sub>O. The medium was heated with frequent agitation and boil for one minute to completely dissolve the medium and was autoclave at 121°C for 15 minutes.

### **+ Preparation of MHB**

21 g of the powder medium was suspended in one liter of dH<sub>2</sub>O. The medium was well and was dissolved by heating with frequent agitation. Finally the medium was boiled for one minute until complete dissolution and was dispense into appropriate containers and sterilize in an autoclave at 121°C for 15 minutes.

### **+ Preparation of complete DMEM**

For 500 mL of incomplete DMEM, 100 mL serum (FBS in -80 freezer) and 1mL of penicillin/Streptomycin 1% were added. Then the medium was gently mixed to avoid the formation of the bubble with the serological pipette of 10 mL.

### **+ Preparation of MTT solution.**

12 mM MTT of stock solution was prepared by adding 1 mL of sterile PBS to one 5 mg vial of MTT (Component A). Mix by vortexing or sonication until dissolved and was stored for four weeks at 4°C protected from light. After that, 10 mL of 0.01 M HCl was added to one tube containing 1g of SDS. The solution was gently mixed by inversion or sonication until the SDS dissolves. For the cell viability assay, 1mL of MTT dye solution was diluted with 10 mL of complete DMEM. After the incubation time, 100 µL of DMSO100% was added to each well and mix thoroughly with the pipette, incubate at 37°C for 10 minutes.

### **+ 10 X Phosphate Buffered Saline (PBS):**

80 g NaCl

2.0 g KCl (Merck)

14.4 g Na<sub>2</sub>HPO<sub>4</sub> (Merck)

2.4 g KH<sub>2</sub>PO<sub>4</sub> (Merck)

The ingredients were dissolved in ~800mL distilled H<sub>2</sub>O, adjusted pH to 7.4. Then the final volume was adjusted to 1L with dH<sub>2</sub>O. The buffer was sterilized by autoclaving and stored at RT.

**1X PBS** (makes 1 liter): 100 mL 10X PBS used to make up 1L with dH<sub>2</sub>O, pH 7.2.

#### **✚ Preparation of Annexin V-Cy3 Apoptosis Detection Kit**

**1× Binding Buffer** (10mM HEPES, pH 7.5, containing 140 mM NaCl and 2.5 mM CaCl<sub>2</sub>) - Dilute 10× Binding Buffer (Catalog Number B9796) 10-fold with deionized water.

#### **50 mM 6-CFDA in acetone solution –**

Dissolve 2.32 mg of 6-Carboxyfluorescein diacetate (6-CFDA, Catalog Number C5041) in 0.1 mL acetone. Store the solution in an amber vial and protect it from light. After opening, store the remaining 6-CFDA at –20 °C.

#### **✚ Double Label Staining Solution**

(1 µg/mL AnnCy3 and 500 µM 6-CFDA in 1× Binding Buffer) –

**To prepare 2 mL of Double Label Staining Solution mix the following:**

20 µl Annexin V Cy3.18 Conjugate (100 µg/mL solution, Catalog Number A4963)

20 µl 50 mM 6-CFDA in acetone solution

200 µl 10× Binding Buffer (Catalog Number B9796) 1.76 mL Deionized water

Store the Double Label Staining Solution in an amber vial and protect it from light.

#### **✚ Preparation of the cellular ROS measurement kit**

50 µg dye were centrifuged quickly and were diluted with 500µl of DMSO. Then 434 µl were diluted up to 10 mL of DPBS (1X)

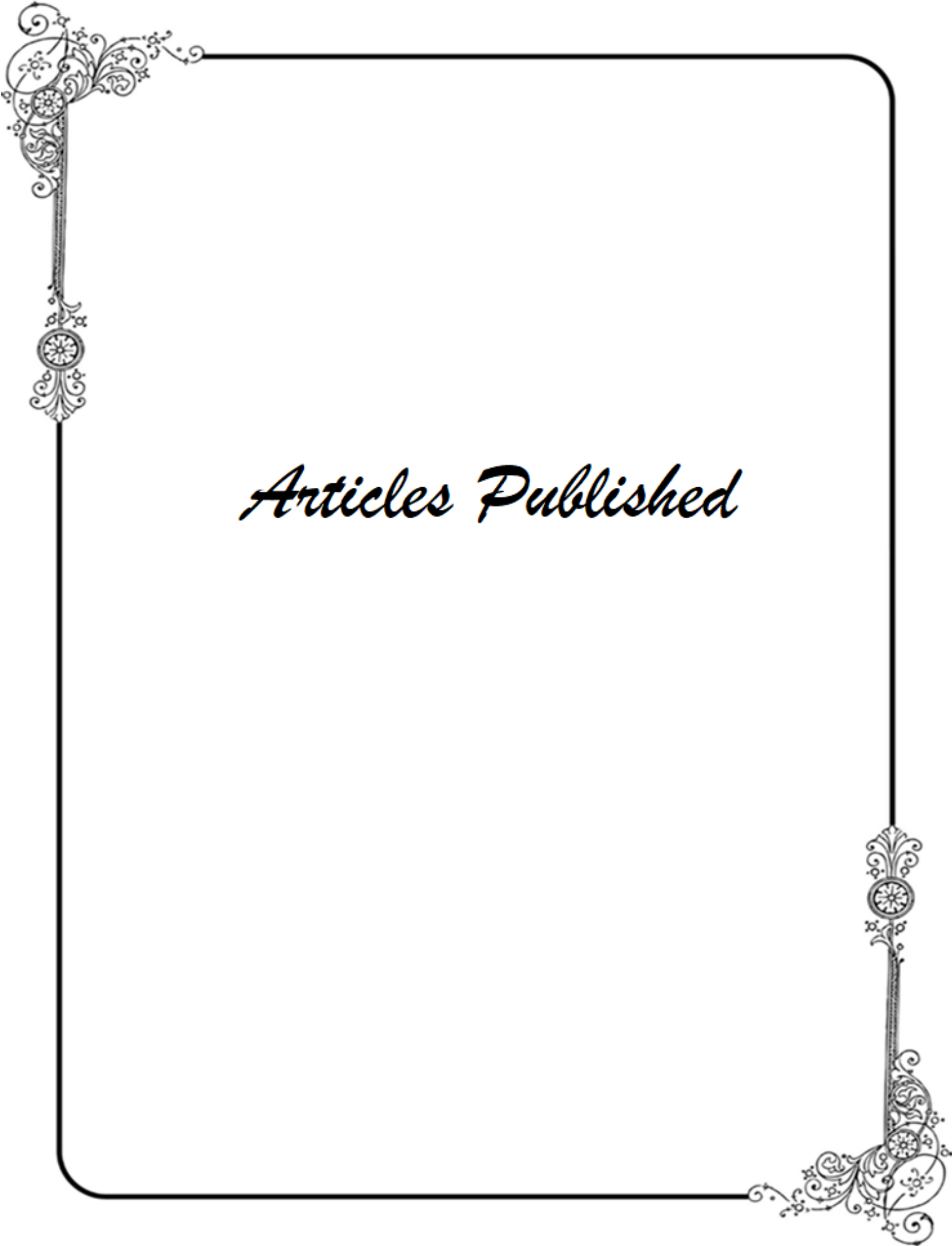
#### **✚ Cell cycle kit preparation**

##### **Preparation of Propidium iodide**

400 ul of PI (50 µg/mL stock solution prepared in 9.6 mL of 1x PBS)

##### **Preparation of RNA**

1mL of RNA (100 µg/mL stock of RNase) prepared in 9 mL of 1XPBS



*Articles Published*



## ARTICLE PUBLISHED

M S Majoumouo, NRS Sibuyi, M B Tincho, M Mbekou, F F Boyom, M Meyer. Enhanced Anti-Bacterial activity of biogenic silver nanoparticles synthesized from *Terminalia mantaly* extracts. *International Journal of nanomedicine*. 2019, 14: 9031-9046.

Majoumouo MS, Sharma JR, Sibuyi NRS, Tincho MB, Boyom FF, Meyer M. Synthesis of biogenic gold nanoparticles from *Terminalia mantaly* extracts and the evaluation of their in vitro cytotoxic effects in cancer cells. *Molecules*. 19p.

# Enhanced Anti-Bacterial Activity Of Biogenic Silver Nanoparticles Synthesized From *Terminalia mantaly* Extracts

This article was published in the following Dove Press journal:  
*International Journal of Nanomedicine*

Michele Stella Majoumouo <sup>1,2</sup>  
Nicole Remaliah Samantha  
Sibuyi <sup>2</sup>  
Marius Belmondo Tincho <sup>2</sup>  
Michele Mbekou<sup>1</sup>  
Fabrice Fekam Boyom <sup>1</sup>  
Mervin Meyer <sup>2</sup>

<sup>1</sup>Antimicrobial & Biocontrol Agents Unit, Laboratory for Phytobiochemistry and Medicinal Plants Studies, Department of Biochemistry, University of Yaoundé I, Yaoundé, Cameroon; <sup>2</sup>Department of Science and Technology (DST)/Mintek Nanotechnology Innovation Centre, Biolabels Node, Department of Biotechnology, University of the Western Cape, Bellville, South Africa

**Background:** The global increase in outbreaks and mortality rates associated with multi-drug-resistant (MDR) bacteria is a major health concern and calls for alternative treatments. Natural-derived products have shown potential in combating the most dreadful diseases, and therefore serve as an effective source of bioactive compounds that can be used as anti-bacterial agents. These compounds are able to reduce metal ions and cap nanoparticles to form biogenic nanoparticles (NPs) with remarkable anti-bacterial activities. This study explores the use of *Terminalia mantaly* (TM) extracts for the synthesis of biogenic silver NPs (TM-AgNPs) and the evaluation of their antibacterial activity.

**Methods:** TM-AgNPs were synthesized by the reduction of AgNO<sub>3</sub> with aqueous and methanolic TM extracts. UV-visible (UV-vis) spectrophotometry, Dynamic Light Scattering (DLS), Transmission Electron Microscopy, and Fourier Transform Infrared (FTIR) analyses were used to characterise the TM-AgNPs. Anti-bacterial activity of the TM extracts and TM-AgNPs was evaluated against eight bacterial strains using the broth microdilution assay. The growth inhibitory kinetics of the bio-active TM-AgNPs was assessed on susceptible strains for a period of 8 hrs.

**Results:** Polycrystalline biogenic AgNPs with anisotropic shapes and diameter range of 11 to 83 nm were synthesized from the TM extracts. The biogenic TM-AgNPs showed significant antibacterial activity compared to their respective extracts. The MIC values for TM-AgNPs and extracts were 3 and 125 µg/mL, respectively. Biogenic AgNPs synthesised from the aqueous TM leaf extract at 25°C (aTML-AgNPs-25°C) showed significant antibacterial activity against all the bacterial strains tested in this study. Their bactericidal effect was particularly higher against the *Streptococcus pneumoniae* and *Haemophilus influenzae*.

**Conclusion:** This study demonstrated the ability of TM extracts to synthesize biogenic AgNPs. The NPs synthesized from the aqueous TM extracts demonstrated higher antibacterial activity against the tested microorganisms compared to the methanolic extracts. Studies are underway to identify the phytochemicals involved in NP synthesis and their mechanism of action.

**Keywords:** antimicrobial resistance, green synthesis, nanotechnology, *Terminalia mantaly*, antibacterial activity

Correspondence: Mervin Meyer  
University of the Western Cape,  
Department of Biotechnology, New Life  
Science Building, Robert Sobukwe Road,  
Bellville 7535, South Africa  
Tel +27 21 9592032  
Fax +27 21 9593505  
Email memeyer@uwc.ac.za

## Introduction

Antimicrobial resistance (AMR) is increasingly recognized as a growing global health problem and accounts for over 700,000 deaths annually.<sup>2</sup> AMR following bacterial infections in particular, is a major concern due to their high prevalence and mortality rates in both developed and developing countries.<sup>1</sup> Europe and the United States of America (USA) have been reported to have high rates of AM-resistant bacterial infections and associated mortality rates. More than 20,000 people in

Europe and the USA succumb to antibiotic-resistant bacterial infections per annum.<sup>2</sup> Thus, the problems associated with the rise of multi-drug-resistant (MDR) bacterial infections have prompted a need for novel and cost-effective antimicrobial agents.<sup>3–5</sup> Recent advancements in nanotechnology-based medicines have opened new horizons for developing strategies that can combat AMR. Silver nanoparticles (AgNPs) have shown excellent bactericidal properties against a range of microorganisms, including the most problematic antibiotic-resistant strains such as *Bacillus subtilis*, *Escherichia coli*, *Neisseria gonorrhoeae*, *Pseudomonas aeruginosa*, *Staphylococcus aureus* and *Streptococcus faecalis*.<sup>6,7</sup>

NPs compared to their bulk counterparts have unique properties attributed to their small size, which can increase the efficacy and bioavailability of antimicrobial agents.<sup>8,9</sup> A variety of protocols for the synthesis of different geometric shapes and sizes of AgNPs have been reported.<sup>10,11</sup> However, most of the protocols involve the use of toxic chemicals as reducing and capping agents which are likely to produce toxic by-products. The by-products might have adverse effects on human health and the environment.<sup>10,11</sup> Conversely, green biosynthetic methods that use natural products as both reducing and capping agents have emerged as alternative synthesis routes. The green synthesis of nanomaterials has generated a great interest as it provides a simple, cost-effective, readily scalable, and eco-friendly products with minimal toxicity towards human beings.<sup>12–15</sup> Natural products are used extensively as reducing as well as capping agents to prevent the agglomeration and increase the stability of the synthesized NPs.<sup>16–18</sup> The synthesis of AgNPs of different shapes and sizes using various plants extracts has been reported.<sup>19–21</sup> Such biogenic AgNPs demonstrated enhanced antibacterial activity on a wide spectrum of multi drug-resistant gram-positive and -negative bacterial pathogens.<sup>22–25</sup> The precise mechanism of antibacterial activity of AgNPs is not fully understood.<sup>20</sup> It is speculated that their small size could increase oxidative stress in the cells by generating reactive oxygen species or attacking the fatty acids in the cell membranes resulting in increased lipid peroxidation.<sup>26</sup> AgNPs once inside the bacterial cells, destabilizes the intracellular structures and biomolecules, consequently inducing death.<sup>27,28</sup>

The current study reports on the synthesis of AgNPs using aqueous and methanolic extracts of the *Terminalia mantaly* (TM) plant. The study also investigates the antibacterial activity of TM extracts and AgNPs. Extracts from *Terminalia* species (Combretaceae) such as *Terminalia catappa*, *Terminalia bellerica*, *Terminalia*

*benzozoe*, *Terminalia mellueri*, *Terminalia arjuna* and *Terminalia cheduba* have been widely used by traditional healers to treat diseases such as cancer, dysentery, diabetes, mycosis and bacterial infections.<sup>19,29</sup> *Terminalia* extracts are commonly rich in phenolics, flavonoids, alkaloids, triterpenoids, and tannins.<sup>30,31</sup> These phytochemicals can potentially be used as reducing agents in the synthesis of colloidal gold and silver metallic NPs. Previous studies have shown that TM extracts can inhibit the growth of a wide range of pathogenic bacteria.<sup>32,33</sup> Moreover, silver and gold NPs synthesized from *Terminalia* species namely *Terminalia cheduba*,<sup>34</sup> *Terminalia catappa*, *Terminalia mellueri*, *Terminalia benzozoe* and *Terminalia bellerica*<sup>19</sup> have demonstrated a wide range of biological activities such as antibacterial, antioxidant and anti-inflammatory properties.<sup>19,34</sup> To the best of our knowledge, this will be the first study to demonstrate the biosynthesis and antibacterial activity of AgNPs produced from TM extracts.

## Materials And Methods

### TM Sample Collection And Identification

The TM plant materials were collected from Yaoundé (Cameroon, West Africa). Fresh leaves (TML), stem bark (TMSB) and roots (TMR) were harvested from mature TM plants. The identity of the plant was confirmed at the National Herbarium (Yaoundé, Cameroon), the reference number of the herbarium sample is 64,212/HNC.

### TM Samples Preparation And Extraction

The plant material was washed with distilled water, cut into small pieces and dried at room temperature (25°C) in the dark. The dried samples were ground into powder using industrial food grinders. The samples were stored in a desiccator at room temperature until further processing.

The aqueous and methanolic TM extracts denoted by <sub>a</sub>TM and <sub>m</sub>TM, respectively, were obtained by maceration procedure. Briefly, 100 g fine powder of TML, TMSB and TMR samples were soaked in 1 L of either methanol (for 48 hrs) or sterile distilled water (for 72 hrs) at room temperature. The extraction procedure was repeated three times and filtered using Whatman No 1 filter paper. The methanolic filtrates were evaporated to dryness using a rotary evaporator (Büchi 011, Flawil, Switzerland). The aqueous filtrates were lyophilized using a Martin Christ Beta 2–8 lyophilizer (Germany). The extracts were stored at 4°C.



## Green Synthesis Of AgNPs Using TM Extracts

The optimal conditions for the synthesis of the AgNPs were obtained using a previously reported method.<sup>35</sup> Stock concentrations (50 mg/mL) of the aqueous and methanolic extracts were prepared in distilled water. Small-scale synthesis was carried out in a 96 well plate to obtain the optimal concentration of TM extracts and temperature. Briefly, 50  $\mu$ L of <sub>a</sub>TM or <sub>m</sub>TM extracts (at concentrations ranging from 0.78 to 50 mg/mL) were placed in a 96 well plate and 250  $\mu$ L of 3 mM AgNO<sub>3</sub> was added to the plant extracts. The samples were prepared in duplicate plates. One plate was incubated at 25°C and a second plate at 70°C, while shaking at 40 rpm for 24 hrs. The optimum concentration of extracts was used to scale up the AgNP synthesis from 300  $\mu$ L to 2 mL. The AgNPs were recovered by centrifuged at 14,000 rpm for 10 min. The AgNPs were washed with sterile distilled water to remove excess AgNO<sub>3</sub> and plant extract. The TM-AgNPs were re-suspended in sterile distilled water and stored at 4°C.

## Characterization Of TM-AgNPs

### UV-Vis Spectrophotometry And DLS Analysis

UV-vis analysis (350–700 nm) of the TM-AgNPs was performed using a POLAR star Omega microplate reader (BMG Labtech, Germany). The hydrodynamic diameter, polydispersity index (Pdi) and zeta potential of the synthesized TM-AgNPs were analysed by DLS using a Malvern Nano ZS90 Zetasizer (Malvern, UK).

### HRTEM Characterization Of TM-AgNPs

The morphology, core size, and the crystallinity of the TM-AgNPs were characterized by High-Resolution Transmission Electron Microscopy (HRTEM) using a FEI Tecnai G2 20 field-emission HRTEM (Oregon, OR, USA). HRTEM was

also used for Energy Dispersive X-ray (EDX) and Selected Area Electron Diffraction (SAED) analysis. The samples were prepared by drop-coating one drop of each sample onto a carbon-coated copper grid. The samples were dried under a Xenon lamp for 10 min and analysed by HRTEM. Transmission electron micrographs were captured in bright field mode at an accelerating voltage of 200 KeV. EDX spectra were collected using an EDX liquid nitrogen cooled Lithium doped Silicon detector. The TEM micrographs were analysed using Image J Software (50b version 1.8.0\_60, <http://imagej.nih.gov/ij>).

### FTIR Analysis Of TM-AgNPs

FTIR analysis of the TM-AgNPs and extracts was performed using a JASCO 460 plus spectrophotometer (Perkin Elmer, Massachusetts, MA, USA) with a frequency ranging from 4,000 to 400  $\text{cm}^{-1}$ . The TM-AgNPs were dried in an oven at 70°C. The TM extracts and AgNPs powders were mixed with potassium bromide (KBr) powder and pressed into a pellet prior to FTIR analysis. Background correction was made using a reference blank KBr pellet. The baseline corrections were performed for all spectra.

## Screening Of Antibacterial Activity Of TM Extracts And AgNPs

The antibacterial activity of the TM extracts and AgNPs was assessed on eight bacterial strains according to the guidelines set by Clinical Laboratory Standards Institute (M07A9, 2012)<sup>36</sup> with slight modifications. Some of the bacterial strains that are listed in Table 1 were a kind gift from Biodefense and Emerging Infections Research Resources Repository (BEI resources, Rockville, MD 20,852) and some were purchased from the American Type Culture Collection (ATCC, Manassas, VA, USA).

**Table 1** List Of Bacterial Strains Used For Anti-Bacterial Activity

Bacterial Strains	Acronym	Reference No.	Supplier
<i>Streptococcus pneumoniae</i>	<i>S. pneumoniae</i>	ATCC 49619	ATCC
<i>Klebsiella pneumoniae</i>	<i>K. pneumoniae</i>	ATCC 13883	ATCC
<i>Haemophilus influenzae</i>	<i>H. influenzae</i>	ATCC 49247	ATCC
<i>Shigella flexneri</i>	<i>S. flexneri</i>	NR-518	BEI resources
<i>Salmonella enterica</i>	<i>S. enterica</i> <sup>a</sup>	NR-13555	BEI resources
<i>Salmonella enterica</i>	<i>S. enterica</i> <sup>b</sup>	NR-4294	BEI resources
<i>Salmonella enterica enterica</i>	<i>S. enterica enterica</i>	NR-4311	BEI resources
<i>Staphylococcus aureus</i>	<i>S. aureus</i>	NR-45003	BEI resources

**Notes:** *S. enterica*<sup>a</sup> (*Salmonella enterica* subsp. *enterica* A36 (Serovar Typhimurium) vs *S. enterica*<sup>b</sup> (*Salmonella enterica* subsp. *enterica* 2004 Pennsylvania Tomato Outbreak, Serovar Anatum, Isolate 4).

**Abbreviations:** ATCC, American Type Culture Collection; BEI resources, biodefense and emerging infections research resources repository.

Mueller–Hinton broth (Sigma, MO, USA) was inoculated with single bacterial colonies and the cultures were incubated at 37°C with shaking at 400 rpm for 18–24 hrs. The bacterial suspensions were subsequently standardized to 0.5 McFarland ( $\sim 1.5 \times 10^8$  cells/mL) at 450 nm. Each inoculum was diluted to a final concentration of  $5 \times 10^5$  cells/mL and further dispensed in a 96 well plate at 100  $\mu$ L per well. Single point inhibitory effect of TM extracts and TM-AgNPs was determined against the eight bacterial strains. To this end, 100  $\mu$ L of  $_a$ TM (500  $\mu$ g/mL),  $_m$ TM extracts (500  $\mu$ g/mL) or TM-AgNPs (12.5  $\mu$ g/mL) were individually added to wells containing 100  $\mu$ L bacteria and the plates were incubated for 24 hrs. Ampicillin was used as the positive control at 128  $\mu$ g/mL. The turbidity of the bacterial culture, which was visually examined, was used as an indication of bacterial growth. Growth inhibition was defined by reduction in the turbidity of the bacterial culture. The susceptibility of the bacterial strains to the TM extracts and TM-AgNPs was expressed as the number of the strains that showed growth inhibition. The percentage of bacterial growth inhibition was calculated according to the following formula:

$$\% \text{ Growth inhibition} = \left( \frac{\text{Number of strains inhibited by the test sample}}{\text{Total number of tested strains}} \right) \times 100$$

### Dose–Response Studies And Evaluation Of The MIC For Active Extracts And TM-AgNPs

MICs were determined for TM-AgNPs that inhibited bacterial growth by more than 75% (i.e. the  $_a$ TMSB-70°C and  $_a$ TML AgNPs-25°C) using the microdilution assay as described above. The bacteria (*S. pneumoniae*, *K. pneumoniae*, *H. influenzae*, *S. flexneri*, *S. enterica*<sup>a</sup>, *S. enterica enterica* and *S. aureus*) were treated with increasing concentrations of the crude extracts (0–500  $\mu$ g/mL) and TM-AgNPs (0–12.5  $\mu$ g/mL). The negative (untreated) and positive (treatment with ampicillin at 0–128  $\mu$ g/mL) controls were also included. After 24 hrs of treatment, the turbidity of the bacterial suspension was visually assessed as an indication of bacterial growth. The lowest concentration that inhibited the visible growth of bacteria was recorded as the MIC. All the experiments were performed in triplicate.

### Bacterial Growth Inhibition Kinetics Of Active TM-AgNPs

The bacterial growth kinetics following treatment with  $_a$ TMSB and  $_a$ TML AgNPs was studied using a protocol that was previously published.<sup>37,38</sup> Briefly, the susceptible bacterial strains were treated with the following

concentrations:  $1 \times \text{MIC}$ ,  $1/2 \times \text{MIC}$  and  $1/4 \times \text{MIC}$  of each AgNPs. Ampicillin was used as a positive control at its MIC value. The assays were performed in triplicate in a 96 well plates. The OD of bacterial cultures was measured at 630 nm at different time points (2, 3, 4, 6, 7 and 8 hr) to monitor bacterial growth rate, and the growth curves were plotted as absorbance (OD 630 nm) versus time (hrs).

### Statistical Analysis

The results were analysed using Graph pad prism 6.0. The data are presented as means  $\pm$  SD according to one-way ANOVA test followed by a post hoc multiple comparisons (Tukey's test). A p value of  $<0.05$  was considered statistical significance and represented by an asterisk (\*). \* $p < 0.05$ , \*\* $p < 0.01$ , \*\*\* $p < 0.001$ .

## Results And Discussion

### Physical And UV Vis Analysis Of TM-AgNPs

The colour of colloidal solutions of AgNPs can vary from yellow-green to blue, depending on the size and morphology of synthesized NPs as demonstrated by Raza et al<sup>39</sup>. For biogenic AgNPs, the variation in colours is also dependent on the concentration of the extracts and the temperature applied in the synthesis of the AgNPs.<sup>38</sup> These colour changes have been reported in several studies.<sup>40,41</sup> Figure 1 shows that the colour of AgNO<sub>3</sub>/TM extract mixtures changed to yellow, brown or green. These colour changes observed during the synthesis of AgNPs is one of the first indications that AgNP synthesis was successful. Figure 1 shows that  $_a$ TMR-AgNP,  $_m$ TML-AgNP,  $_m$ TMSB-AgNP, and  $_m$ TMR-AgNP produced a yellow colour, while  $_a$ TML-AgNP produced a green colour and  $_a$ TMSB-AgNP produced a brown colour.

Due to surface plasmon resonance (SPR), UV-vis spectrophotometric analysis of AgNP that are between 10 and 100 nm in size typically produces absorbance peaks ( $\lambda$  max) from 400 to 500 nm. As shown in Figure 2 and Table 2, the absorbance peaks of the TM-AgNPs ranged from 438 to 480 nm. This also confirms the presence of AgNPs following the reactions using TM extracts. Flavonoids and phenolic compounds are the major components in the TM extracts.<sup>32</sup> These phenolic and hydroxylated constituents are most likely responsible for the reduction of AgNO<sub>3</sub> to form the AgNP.<sup>42</sup> The peak intensity of AgNP synthesised at 70°C was significantly higher, which suggests that the concentration of the NPs was higher at 70°C than at 25°C.

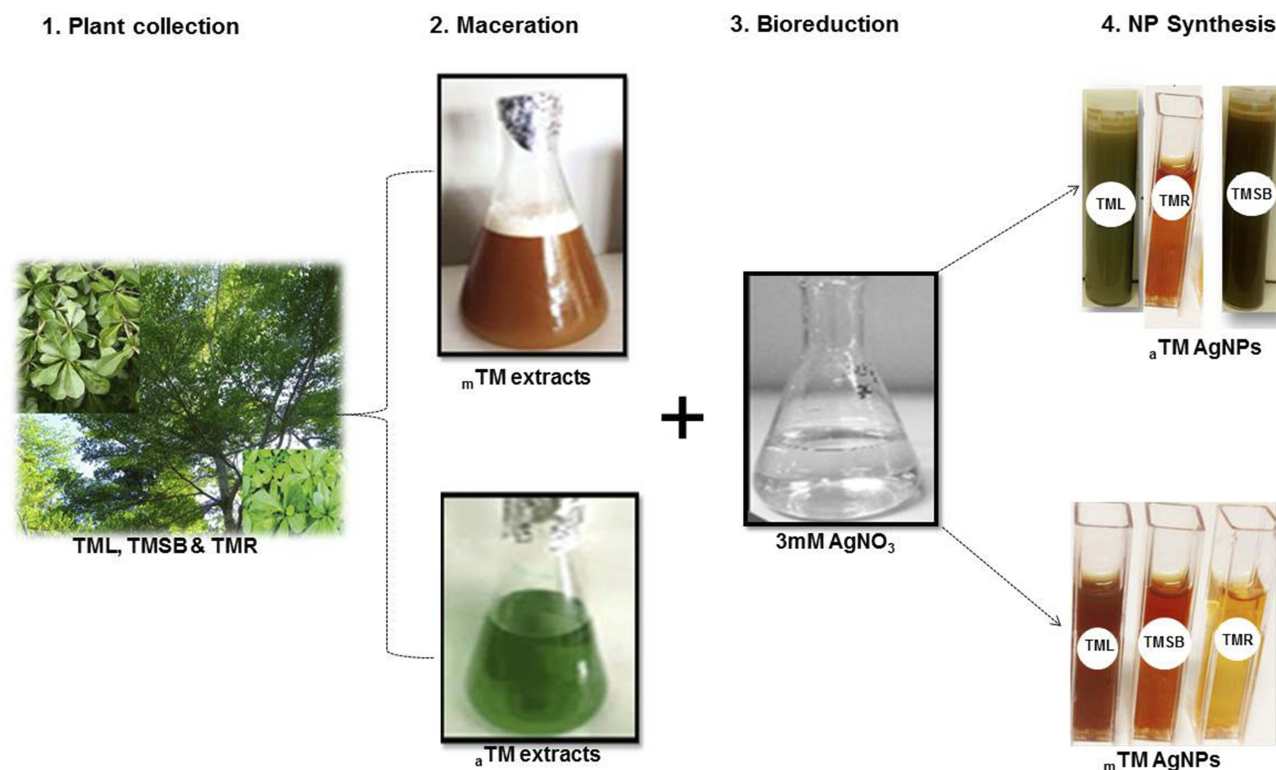


**Figure 1** Schematic representation of the AgNP synthesis from TM plant extracts.

**Notes:** Aqueous and methanolic TM extracts were used to reduce  $\text{AgNO}_3$  into AgNPs, color change indicates NP formation.

**Abbreviations:** AgNPs, silver nanoparticles; TM, *Terminalia mantaly*; TML, TM leaf extract; TMSB, TM stem bark extract; TMR, TM root extract; TML-AgNPs, AgNPs from TM leaf extract; TMSB-AgNPs, AgNPs from TM stem bark extract; TMR-AgNPs, AgNPs from TM root extract; a, aqueous; m, methanolic.

In fact, based on UV-vis spectrophotometric analysis, synthesis of  ${}_m\text{TMSB-AgNP}$  and  ${}_m\text{TML-AgNP}$  at  $25^\circ\text{C}$  was not very successful as the peak intensities for these AgNPs were very low. The absorbance peaks for  ${}_m\text{TMR-AgNP}$ ,  ${}_a\text{TMSB-AgNP}$  and  ${}_a\text{TML-AgNP}$  (produced at  $70^\circ\text{C}$ ) were much sharper compared to the absorbance peaks for  ${}_a\text{TMR-AgNP}$ ,  ${}_m\text{TMSB-AgNP}$  and  ${}_m\text{TML-AgNP}$  (also produced at  $70^\circ\text{C}$ ). This suggests that  ${}_m\text{TMR-AgNP}$ ,  ${}_a\text{TMSB-AgNP}$  and  ${}_a\text{TML-AgNP}$  are smaller and more uniform than  ${}_a\text{TMR-AgNP}$ ,  ${}_m\text{TMSB-AgNP}$  and  ${}_m\text{TML-AgNP}$ .

## DLS And FTIR Analyses Of TM-AgNPs

The hydrodynamic diameter, zeta potential and polydispersity index (Pdi) of the TM-AgNPs were measured by the DLS. As shown in Table 2, the sizes of the TM-AgNPs varied depending on the extract used for the synthesis and temperature ( $25^\circ\text{C}$  versus  $70^\circ\text{C}$ ) at which synthesis was done. The hydrodynamic diameter of the TM-AgNPs ranged from 11 to 83 nm. The  ${}_a\text{TML}$  extract produced smaller AgNPs compared to the other extracts. The zeta potential of the synthesized TM-AgNPs ranged from  $-12$  to  $-37$  mV. Zeta potential is an important parameter used to assess the charge of the NP surface and

predicts the long-term stability of the NPs. NPs with negative zeta potential values suggest there are strong repulsion forces between the NPs, which will prevent the agglomeration of the NPs in solution.<sup>11,43</sup> NPs with a zeta potential within the  $+30$  mV to  $-30$  mV range are considered to be stable, while those outside this range will likely aggregate due to inter-particle van der Waal's attractions. The  ${}_a\text{TMSB-AgNPs}$  were the only NPs with zeta potential values outside this range ( $-34$  and  $-37$  mV for TM-AgNPs synthesized at  $25^\circ\text{C}$  and  $70^\circ\text{C}$ , respectively) (Table 2). This suggests that all the TM-AgNPs except for  ${}_a\text{TMSB-AgNPs}$  are stable. The Pdi, which is an indication of uniformity, is an important parameter of NPs to consider when assessing the application of NPs, since Pdi can affect the surface conjugation chemistry and NP aggregation.<sup>44</sup> According to the International Organization for Standardization (ISO),<sup>45</sup> Pdi values  $>0.7$  indicate that the samples have a very broad size distribution, while Pdi values  $\leq 0.5$  are more monodispersed.<sup>49</sup> Based on the Pdi values obtained for  ${}_a\text{TML-AgNPs}$ ,  ${}_a\text{TMSB-AgNPs}$ ,  ${}_a\text{TMR-AgNPs}$  and  ${}_m\text{TMR-AgNPs}$  synthesised at  $25^\circ\text{C}$ , these TM-AgNPs are monodispersed. Similarly,  ${}_a\text{TML-AgNPs}$  and  ${}_a\text{TMSB-AgNPs}$  synthesised at  $70^\circ\text{C}$  are also monodispersed.

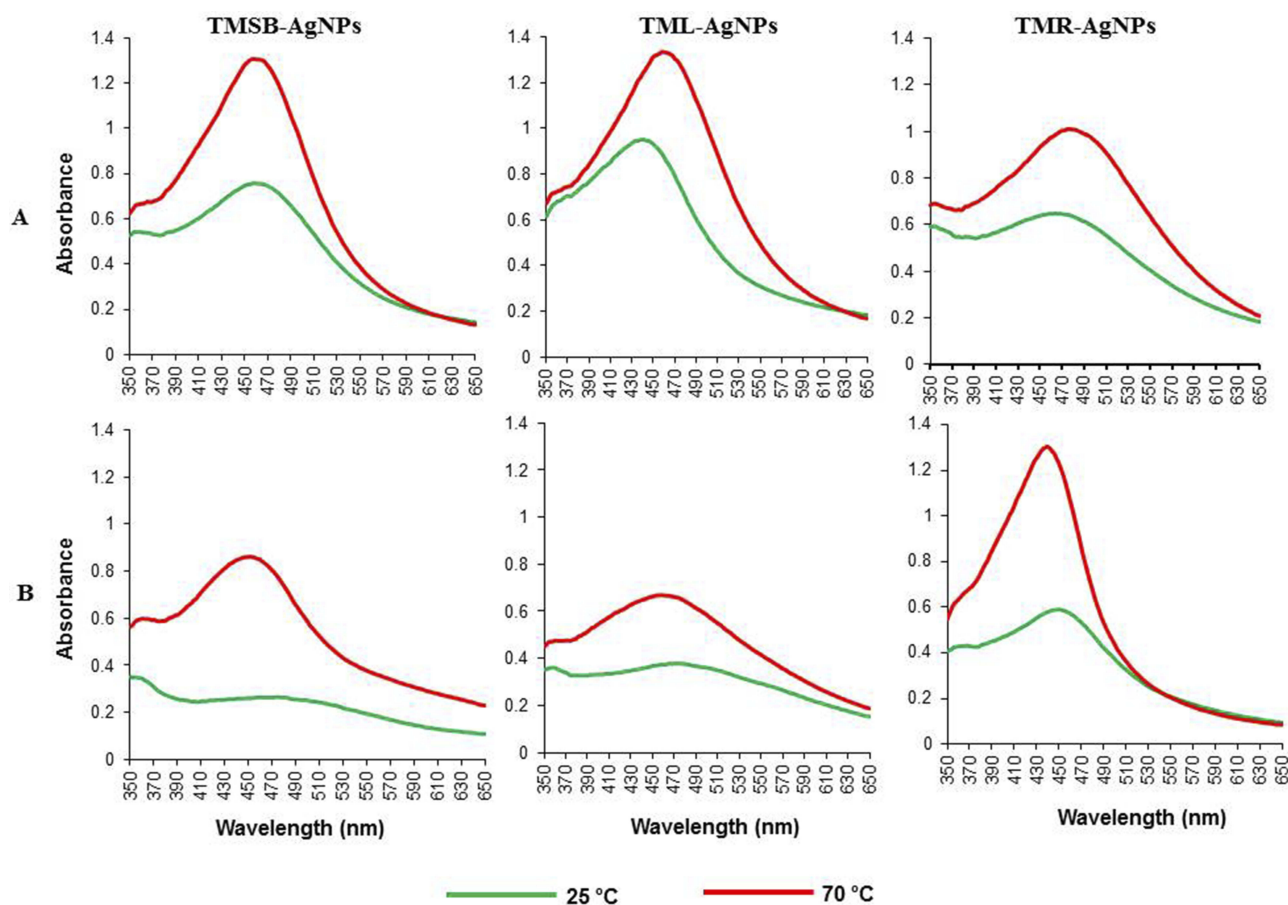


**Figure 2** UV-vis spectral profiles of TM-AgNPs synthesised at 25°C and 70°C.

**Notes:** AgNPs were synthesized by reducing  $\text{AgNO}_3$  with aqueous (A) and methanolic (B) TM extracts. The optical properties of the NPs were measured by UV-vis spectrophotometry.

**Abbreviations:** AgNPs, silver nanoparticles; TM, *Terminalia mantaly*; TML-AgNPs, AgNPs from TM leaf extract; TMSB-AgNPs, AgNPs from TM stem bark extract; TMR-AgNPs, AgNPs from TM root extract.

Various phytochemicals that are present in the plant extracts are expected to play a role in the synthesis of AgNPs.<sup>46</sup> These phytochemicals are involved in the reduction of  $\text{AgNO}_3$  and stabilization of the AgNPs. Different chemical classes influence the production of AgNPs, as well as their shape, size and bio-activity.<sup>47</sup> As

**Table 2** SPR And DLS Analysis Of TM-AgNPs Synthesized At 25°C And 70°C

TM-AgNPs	NP Parameters									
	25°C					70°C				
	[Extract] (mg/mL)	$\lambda_{\text{max}}$ (nm)	PD (nm)	Pdi	ZP (mV)	[Extract] (mg/mL)	$\lambda_{\text{max}}$ (nm)	PD (nm)	Pdi	ZP (mV)
<sub>a</sub> TML-AgNPs	0.78	438	11	0.50	-24	1.56	460	18	0.40	-26
<sub>m</sub> TML-AgNPs	1.56	474	44	0.60	-22	1.56	458	22	0.80	-29
<sub>a</sub> TMSB-AgNPs	0.78	464	28	0.22	-34	1.56	460	56	0.46	-37
<sub>m</sub> TMSB-AgNPs	1.56	480	60	0.62	-12	1.56	458	58	0.53	-12
<sub>a</sub> TMR-AgNPs	3.12	472	39	0.40	-23	3.125	478	30	0.88	-24
<sub>m</sub> TMR-AgNPs	0.78	450	83	0.48	-22	0.78	438	67	0.51	-28

**Abbreviations:** AgNPs, silver nanoparticles; TM, *Terminalia mantaly*; <sub>a</sub>, aqueous extracts; <sub>m</sub>, methanolic extracts; TML-AgNPs, AgNPs from TM leaf extracts; TMSB-AgNPs, AgNPs from TM stem bark extracts; TMR-AgNPs, AgNPs from TM root extracts; SPR, surface plasmon resonance; UV, ultraviolet; PD, particle diameter; ZP, Zeta potential; Pdi, Polydispersity index; DLS, dynamic light scattering.

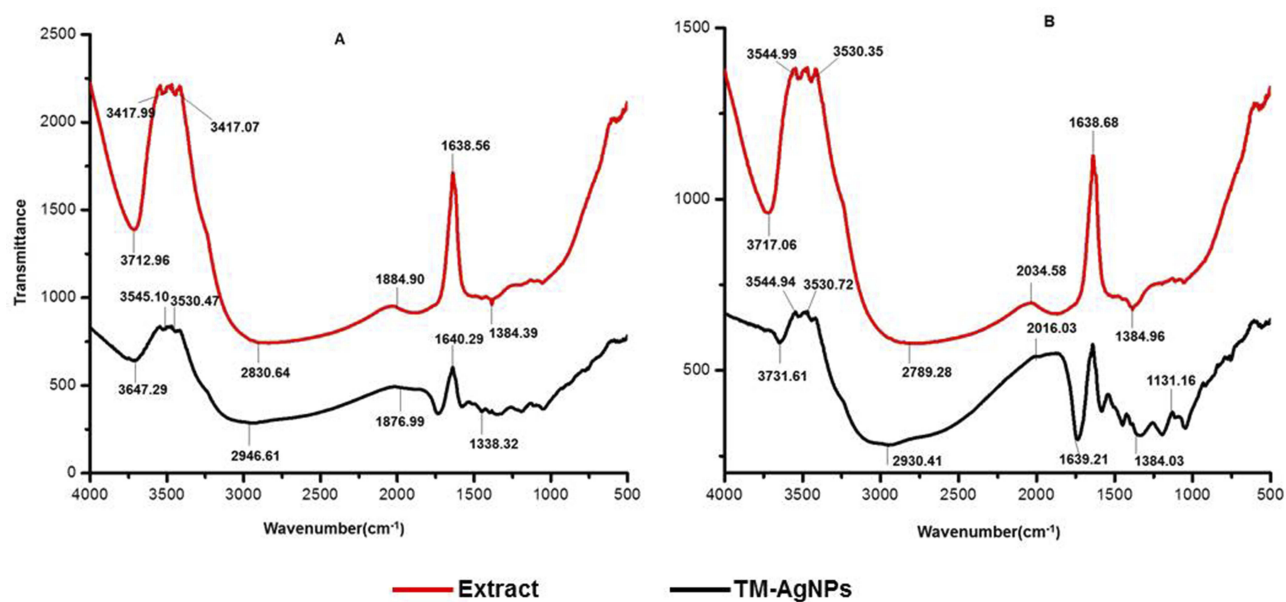


**Figure 3** FTIR spectra of selected TM-AgNPs compared to their respective TM extracts.

**Notes:** FTIR spectra of (A)  $a$ TML extract, (B)  $a$ TML-AgNPs synthesized at 25°C, (C)  $a$ TMSB extract and (D)  $a$ TMSB-AgNPs synthesized at 70°C.

**Abbreviations:** AgNPs, silver nanoparticles; TM, *Terminalia mantaly*;  $a$ TML, aqueous TM leaf extract;  $a$ TMSB, aqueous TM stem bark; FTIR, Fourier-transform infrared.

such, it is expected that some of the phytochemicals that are present in the extract will be present on the TM-AgNPs. Comparative FTIR spectroscopy analysis between the TM extracts and the accompanying AgNPs was used to demonstrate this (Figure 3). In Figure 3, the FTIR spectrum of  $a$ TML-AgNPs synthesized at 25°C is compared to the spectrum of the TML extract, while the  $a$ TMSB-AgNPs synthesised at 70°C is compared to the  $a$ TMSB extract. Several commonalities between the spectra of the extracts and their respective TM-AgNPs could be identified. This suggests that the extracts and their respective TM-AgNPs share similar functional groups, which originate from phytochemicals that were involved in the synthesis of the TM-AgNPs. Shifts in the peak in the FTIR spectra of  $a$ TMSB and  $a$ TML extracts and their respective AgNPs are summarized in Table 3. In particular, the spectra of  $a$ TML extract and AgNPs produced at 25°C were characterized by methyl (C-H) rock alkanes vibration band at 1338.32 and 1384.39  $\text{cm}^{-1}$ , and the C-H stretching observed between 2946.61 and 2830.64  $\text{cm}^{-1}$ . Moreover, there was a C=C double-bond stretching at 1640.29 and 1638.56  $\text{cm}^{-1}$ . Additionally, strong OH group vibrations assigned to phenol bands at 3647.29 and 3712.96  $\text{cm}^{-1}$  were detected in both samples (Figure 4A and B).

The FTIR spectra of  $a$ TMSB extract and AgNPs produced at 70°C showed fewer similarities between the two samples (Figure 3C and D). The spectra of  $a$ TMSB extract

revealed intense bands at 1048.80  $\text{cm}^{-1}$  attributed to carbonyls (C=O) vibrations that were absent on  $a$ TMSB-AgNPs produced. Some similarities in the two samples were observed; the spectra of  $a$ TMSB extract and AgNPs revealed bands at 1384.03 and 1384.96 corresponding to methyl (C-H) rock alkanes deformation, 1639.21 and 1638.68 bands attributed to stretch alkenes (C=C), 2930.41 and 2789.28 bands corresponding to C-H stretching, 3717.06 and 3731.61 intense bands attributed to O-H from alcohols and phenols vibrations. The shift in the different functional groups might be caused by the polyphenolics, flavonoids, and terpenoids present in the TM extracts. The same phytochemicals might be responsible for reducing, capping and stabilization of the biogenic AgNPs.<sup>13,31,48–50</sup> Several studies reported that the active components in the plant extracts such as terpenoids and flavonoids act as reducing agent of the silver precursor to form AgNPs.<sup>51</sup>

## HRTEM And EDX Analyses Of Bio-Active TM-AgNPs

The morphology and size of  $a$ TML-AgNPs and  $a$ TMSB-AgNPs varied as demonstrated by the HRTEM micrographs in Figure 4A. The AgNPs displayed heterogeneous and polydispersed characteristics. The  $a$ TML produced mostly spherical AgNPs at 25°C whereas the same sample produced various geometric shapes such as triangular,

**Table 3** Comparison FTIR Spectra Of TM Extracts And Their Respective AgNPs

$_a$ TML				$_a$ TMSB			
Peak Position In Extracts ( $\text{cm}^{-1}$ )	Peak Position In AgNPs At 25 °C ( $\text{cm}^{-1}$ )	Shift In Position ( $\text{cm}^{-1}$ )	Type Of Chemical Bond	Peak Position In Extracts ( $\text{cm}^{-1}$ )	Peak Position In AgNPs at 70°C ( $\text{cm}^{-1}$ )	Shift In Position ( $\text{cm}^{-1}$ )	Type Of Chemical Bond
1338.32	1384.39	+46.07	C–H methyl rock alkanes	1048.80	-----	-----	C–O Stretch
1640.29	1638.56	–1.73	–C=C–stretch alkenes	1131.16	-----	-----	
1876.99	1884.90	+7.91	C=O Anhydrides	1384.03	1384.96	+0.93	C–H methyl rock alkanes
2946.61	2830.64	–115.97	H–C=O:C–H stretch aldehydes	1639.21	1638.68	–0.53	–C=C–stretch alkenes
3530.47	3417.07	–112.48	OH Alcohol, phenols	2016.03	2034.58	+18.55	–C≡C–stretch alkynes
3545.10	3417.99	–127.11		2930.41	2789.28	–141.13	H–C=O:C–H stretch aldehydes
3647.29	3712.96	+65.67		3530.72 3544.94 3717.06	3530.35 3544.99 3731.61	+0.37 +0.05 +14.55	OH Alcohol, phenols

**Note:** Shift values were calculated by subtracting the peak position in TM-AgNPs from the peak position in TM-extracts.

**Abbreviations:** FTIR, Fourier-transform infrared; AgNPs, silver nanoparticles; TM, *Terminalia mantaly*;  $_a$ TML, aqueous TM leaf extracts;  $_a$ TMSB, aqueous TM stem bark.

tetrahedral and hexagonal shapes at 70°C. Similar shapes as those of  $_a$ TML-AgNPs were observed in AgNPs synthesized by the  $_a$ TMSB extract. These anisotropic shapes were likely due to the reducing and capping phytochemicals which not only provided thermodynamic stability but also defined the NP bio-activities.<sup>34</sup> The crystalline nature of the biogenic AgNPs was confirmed by their SAED patterns highlighted in Figure 4B. The Bragg reflection planes on the face-centered cubic (fcc) patterns of TM-AgNPs, i.e. (111), (200), (220), (311), and (331) matched those in the database of the Joint Committee on Powder Diffraction Standards (JCPDS no. 00-004-0784, USA)<sup>51,52</sup> and confirmed that the synthesized AgNPs are composed of pure crystalline silver. These findings are further supported by similar fcc patterns reported for the AgNPs synthesized from *Cannabis sativa*.<sup>51,53</sup>

Further characterization of the elemental composition of the TM-AgNPs by EDX confirmed the presence of a signal characteristic of elemental silver. The Energy

Dispersive Absorption photographs of the selected TM-AgNPs in Figure 5 displays the  $\text{Ag}^+$  peaks at 3 keV. Metallic AgNPs typically show a strong signal peak at this position due to their SPR.<sup>54</sup> Peaks of other elements such as Cu and C were also detected, where C corresponds to the organic matrix and lacey carbon on the TEM grid, Cu is observed since the grid is made up of Cu, and the S, Si, Cl and N peaks correspond to the molecules capping the TM-AgNPs.

## Antibacterial Activity Of TM Extracts And AgNPs

The antibacterial effects of TM extracts and AgNPs were evaluated against eight bacterial strains, of which two were Gram positive (*S. pneumoniae* and *S. aureus*) and the other six were Gram negative. The bacterial cultures were treated with a single dose of 500  $\mu\text{g/mL}$  of TM extracts and 12.5  $\mu\text{g/mL}$  of TM-AgNPs. This was done as a quick and easy test of the antimicrobial

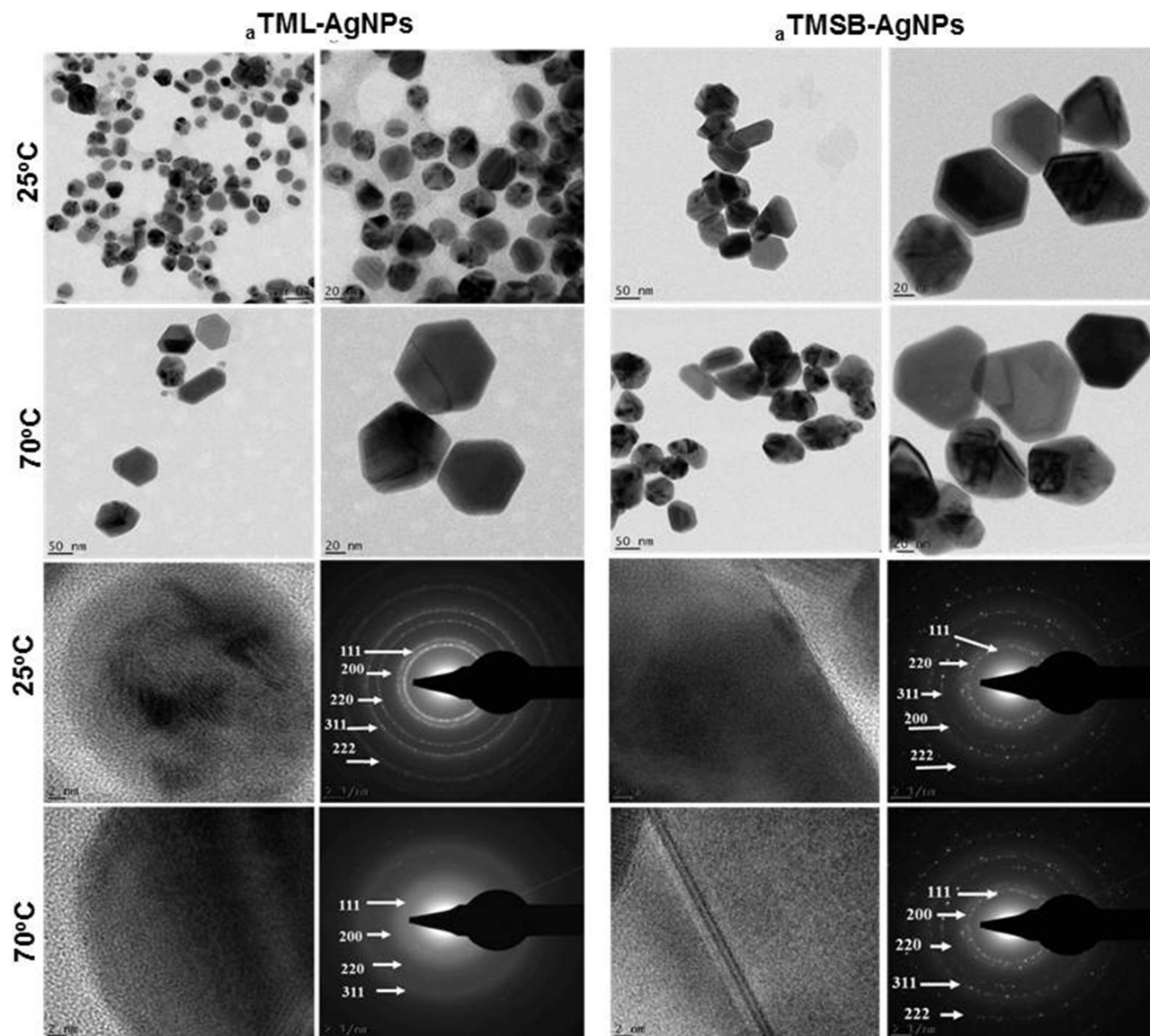


**Figure 4** HRTEM micrographs and SAED patterns of selected TM-AgNPs.

**Notes:** The size, shape and SAED patterns of  ${}_{a}$ TML-25°C and  ${}_{m}$ TML-70°C AgNPs were analyzed by HRTEM. Scale bar from 20 to 50 nm.

**Abbreviations:** AgNPs, silver nanoparticles; TM, *Terminalia mantaly*;  ${}_{a}$ TML, aqueous TM leaf extract;  ${}_{a}$ TMSB, aqueous TM stem bark; HRTEM, high resolution transmission electron microscope; SAED, selected area electron diffraction.

activity of the TM extracts and TM-AgNPs. Figure 6 and Table 4 show that four of the treatments ( ${}_{a}$ TML-AgNPs-25°C ( ${}_{a}$ TML-AgNPs synthesised at 25°C),  ${}_{a}$ TML-AgNPs-70°C ( ${}_{a}$ TML-AgNPs synthesised at 70°C),  ${}_{a}$ TMSB-AgNPs-25°C ( ${}_{a}$ TMSB-AgNPs synthesised at 25°C) and  ${}_{m}$ TMSB) inhibited the growth in a significant number of the eight bacterial strains tested in this study.  ${}_{a}$ TML-AgNPs-25°C and  ${}_{a}$ TML-AgNPs-70°C inhibited the growth in all eight strains, while  ${}_{a}$ TMSB-AgNPs-25°C and  ${}_{m}$ TMSB inhibited the growth in 80% and 50% of the strains, respectively.  ${}_{m}$ TMSB was the

most active extract and inhibited growth in a significant number (four) of the strains. Generally, three of the strains (*K. pneumoniae*, *H. influenzae* and *S. flexneri*) were more susceptible to the effects of the treatments, while *S. enterica enterica* was more resistant (Table 4).

The lowest concentration of the treatments required to inhibit visible growth of the bacteria (i.e. the MIC) was determined after 24 hr treatment with the TM extracts and AgNPs. The MIC values for the treatments are summarized in Table 5. The lowest MIC value (3.12 µg/mL) was obtained for  ${}_{a}$ TMSB-AgNPs-25°C and  ${}_{a}$ TML-AgNPs-25°C against *H. influenzae*.

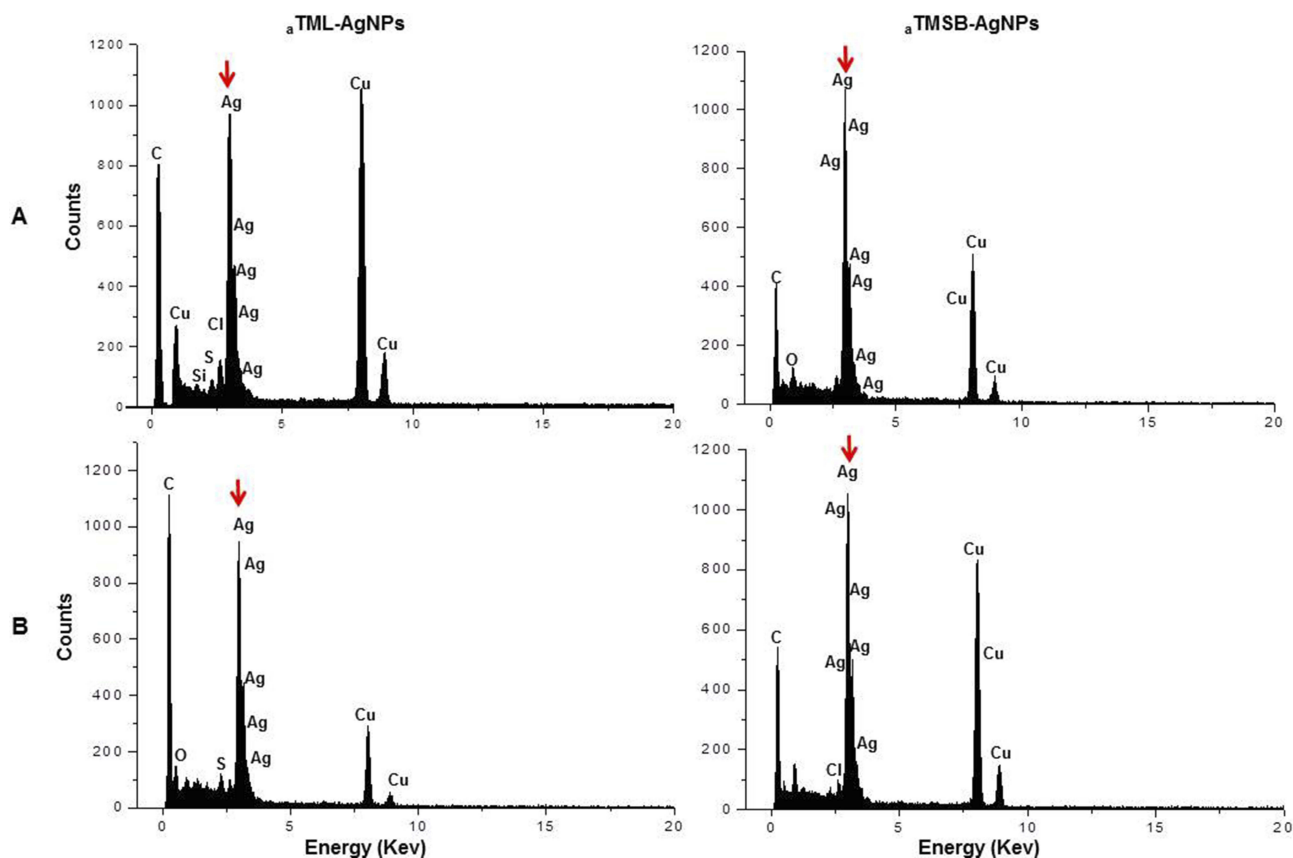


**Figure 5 (A,B)** EDX spectra of AgNPs synthesized from  $a$ TML and  $m$ TMSB AgNPs.

**Notes:** Silver nanocrystallites display an optical absorption band peak at approximately 3 keV (red arrow), which is typical of the absorption of metallic silver nanocrystallites due to their SPR.

**Abbreviations:** AgNPs, silver nanoparticles; TM, *Terminalia mantaly*;  $a$ TML, aqueous TM leaf extract;  $a$ TMSB, aqueous TM stem bark; EDX, Energy Dispersive X-ray.

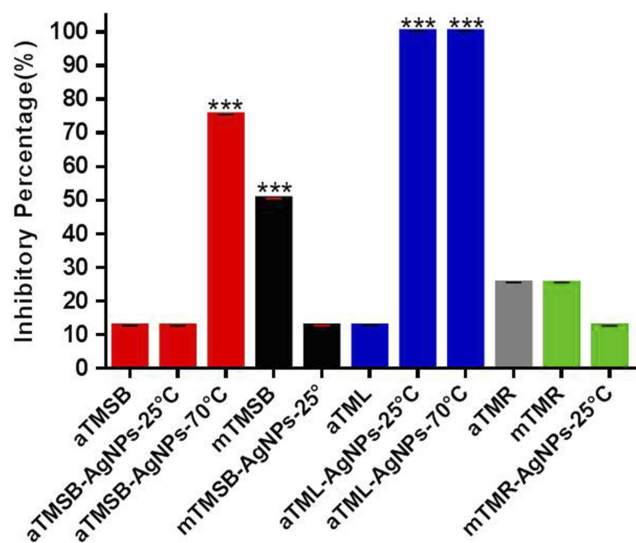


**Figure 6** Screening of the antibacterial effects of TM extracts and AgNPs against a panel of bacterial strains.

**Notes:** Eight bacterial strains were treated with TM extracts and AgNPs for 24 hrs. Inhibitory effects of TM samples are expressed based on the number of strains that showed growth inhibition. \*\*\* $P < 0.001$ .

**Abbreviations:** AgNPs, silver nanoparticles; TM, *Terminalia mantaly*;  $a$ , represents aqueous extracts;  $m$ , represents methanolic extracts; TML, TM leaf extracts; TMR, TM root extracts; TMSB, TM stem bark extracts.

$a$ TML-AgNPs-25°C and  $a$ TMSB-AgNPs-70°C appears to have more significant antimicrobial activity than the other TM-AgNPs. This is based on the findings that these two TM-AgNPs have the lowest MIC values against the largest number of bacterial strains. MIC values for  $a$ TML-AgNPs-25°C varied between 6.24 and 12.50  $\mu$ g/mL in six of the eight strains, while the MIC values for  $a$ TMSB-AgNPs-70°C varied between 3.12 and 6.24  $\mu$ g/mL in five of the eight strains.

The absence of antibacterial activity observed in some of the AgNPs may be due to various factors, either the phytochemicals responsible for capping the NPs had adsorbed to the NPs through its active site,<sup>55</sup> or the phytochemicals simply have no antibacterial activity as demonstrated by the crude extracts. Size of the NPs also plays a role in NP activity. NPs with smaller sizes are usually more efficient as they can easily pass through cellular barriers and disrupt the physiological functions of the bacteria once internalized.<sup>11</sup> As such, the efficacy of  $a$ TML-AgNPs could be attributed to their smaller diameter. Their small size could allow for efficient binding and uptake by bacteria



**Table 4** Comparison Of The Bacterial Susceptibility To TM Extracts And AgNPs

Treatment	Bacterial Strains							
	<i>S. enterica</i> <sup>a</sup>	<i>S. pneumoniae</i>	<i>S. aureus</i>	<i>K. pneumoniae</i>	<i>S. enterica enterica</i>	<i>S. enterica</i> <sup>b</sup>	<i>S. flexneri</i>	<i>H. influenzae</i>
<sup>a</sup> TMSB	-	-	-	-	-	-	-	✓
<sup>a</sup> TMSB-AgNPs-25°C	-	-	-	✓	-	-	✓	✓
<sup>a</sup> TMSB-AgNPs-70°C	-	✓	✓	✓	✓	✓	✓	-
<sup>m</sup> TMSB	-	✓	-	-	✓	-	✓	✓
<sup>m</sup> TMSB-AgNPs-25°C	-	-	-	-	-	-	-	✓
<sup>a</sup> TML	-	✓	-	-	-	-	-	-
<sup>a</sup> TML-AgNPs-25°C	✓	✓	✓	✓	✓	✓	✓	✓
<sup>a</sup> TML-AgNP-70°C	✓	✓	✓	✓	✓	✓	✓	✓
<sup>a</sup> TMR	-	✓	-	-	-	-	-	✓
<sup>m</sup> TMR	-	✓	-	-	-	-	-	✓
<sup>m</sup> TMR-AgNPs-25°C	-	✓	-	-	-	-	-	-

**Notes:** Eight bacterial strains were treated with TM extracts and AgNPs for 24 hrs. Inhibitory effects of TM samples were visually assessed to identify the strains that were susceptible to TM extracts and AgNPs. The <sup>a</sup>TM-AgNPs were the most active and inhibited growth of all bacterial strains, compared to the crude extracts and other AgNPs. *S. enterica*<sup>a</sup> (*Salmonella enterica* subsp. *enterica* A36 (Serovar Typhimurium) vs *S. enterica*<sup>b</sup> (*Salmonella enterica* subsp. *enterica* 2004 Pennsylvania Tomato Outbreak, Serovar Anatum, Isolate 4).

**Abbreviations:** AgNPs, Silver nanoparticles; TM, *Terminalia mantaly*; <sup>a</sup>, represents aqueous extracts; <sup>m</sup>, represents methanolic extracts; TML, TM leaf extracts; TMR, TM root extracts; TMSB, TM stem bark extracts; *S. pneumoniae*, *Streptococcus pneumoniae*; *S. enterica enterica*, *Salmonella enterica enterica*; *H. influenzae*, *Haemphilus influenzae*, *S. flexneri*, *Shigella flexneri*; *K. pneumoniae*, *Kbsiella pneumoniae*; *S. aureus*, *Staphylococcus aureus*, *S. enterica*- *Salmonella enterica*; -, no bacterial activity; ✓, bacterial activity.

**Table 5** MIC For Crude TM Extracts And Its Derivate AgNPs On Selected Bacterial Strains

Treatment	MIC (µg/mL)							
	<i>S. enterica</i> <sup>a</sup>	<i>S. pneumoniae</i>	<i>S. aureus</i>	<i>K. pneumoniae</i>	<i>S. enterica enterica</i>	<i>S. enterica</i> <sup>b</sup>	<i>S. flexneri</i>	<i>H. influenzae</i>
<sup>a</sup> TMSB	>500	>500	>500	>500	>500	>500	>500	125
<sup>a</sup> TMSB-AgNPs-25 °C	>12.50	>12.50	>12.50	6.24	>12.50	6.24	>12.50	3.12
<sup>a</sup> TMSB-AgNPs-70 °C	>12.50	6.24	12.50	6.24	12.50	12.50	>12.50	>12.50
<sup>m</sup> TMSB	>500	>500	>500	>500	>500	>500	125	>500
<sup>m</sup> TMSB-AgNPs-25 °C	>12.50	>12.50	>12.50	>12.50	>12.50	>12.50	>12.50	6.24
<sup>a</sup> TML	>500	>500	>500	>500	>500	>500	>500	>500
<sup>a</sup> TML-AgNPs-25 °C	6.24	6.24	6.24	6.24	>12.50	6.24	>12.50	3.12
<sup>a</sup> TML-AgNP-70 °C	>12.50	6.24	12.50	6.24	>12.50	6.24	>12.50	>12.50
<sup>a</sup> TMR	>500	>500	>500	>500	>500	>500	>500	500
<sup>m</sup> TMR	>500	>500	>500	>500	125	>500	>500	>500
<sup>m</sup> TMR-AgNPs25 °C	>12.50	>12.50	>12.50	>12.50	>12.50	>12.50	>12.50	>12.50
Ampicillin	32	4	8	16	32	16	32	16

**Notes:** *S. enterica*<sup>a</sup> (*Salmonella enterica* subsp. *enterica* A36 (Serovar Typhimurium) vs *S. enterica*<sup>b</sup> (*Salmonella enterica* subsp. *enterica* 2004 Pennsylvania Tomato Outbreak, Serovar Anatum, Isolate 4).

**Abbreviations:** AgNPs, Silver nanoparticles; TM, *Terminalia mantaly*; <sup>a</sup>, represents aqueous extracts; <sup>m</sup>, represents methanolic extracts; TML, TM leaf extracts; TMR, TM root extracts; TMSB, TM stem bark extracts; *S.pneumoniae*, *Streptococcus pneumoniae*; *S. enterica enterica*, *Salmonella enterica enterica*; *H.influenzae*, *Haemphilus influenzae*, *S. flexneri*, *Shigella flexneri*; *K. pneumoniae*, *Kbsiella pneumoniae*; *S. aureus*, *Staphylococcus aureus*; *S. enterica*, *Salmonella enterica*.

resulting in their death.<sup>56</sup> Furthermore, the active phytochemicals at specific temperatures might be responsible for the biological activities of the AgNPs.<sup>19</sup> Only *S. enterica enterica*, *S. flexneri* and *H. influenzae* were susceptible to the <sup>m</sup>TMR, <sup>a</sup>TMSB and <sup>m</sup>TMSB extracts. The MIC for these extracts was 125 µg/mL. The other strains were not susceptible to the effect of the TM extracts at concentrations

up to 500 µg/mL, the MIC values for these extracts could not be established in this study. Previous studies have demonstrated the antifungal activity of the aqueous and ethanolic TML and TMSB extracts against *Candida* species (*C. albicans*, *C. albicans*, *C. glabrata* C, *parapsilosis*) and *Cryptococcus neoformans* with MIC values ranging from 0.04 to 0.16 mg/mL.<sup>32</sup> Although the extracts did not show

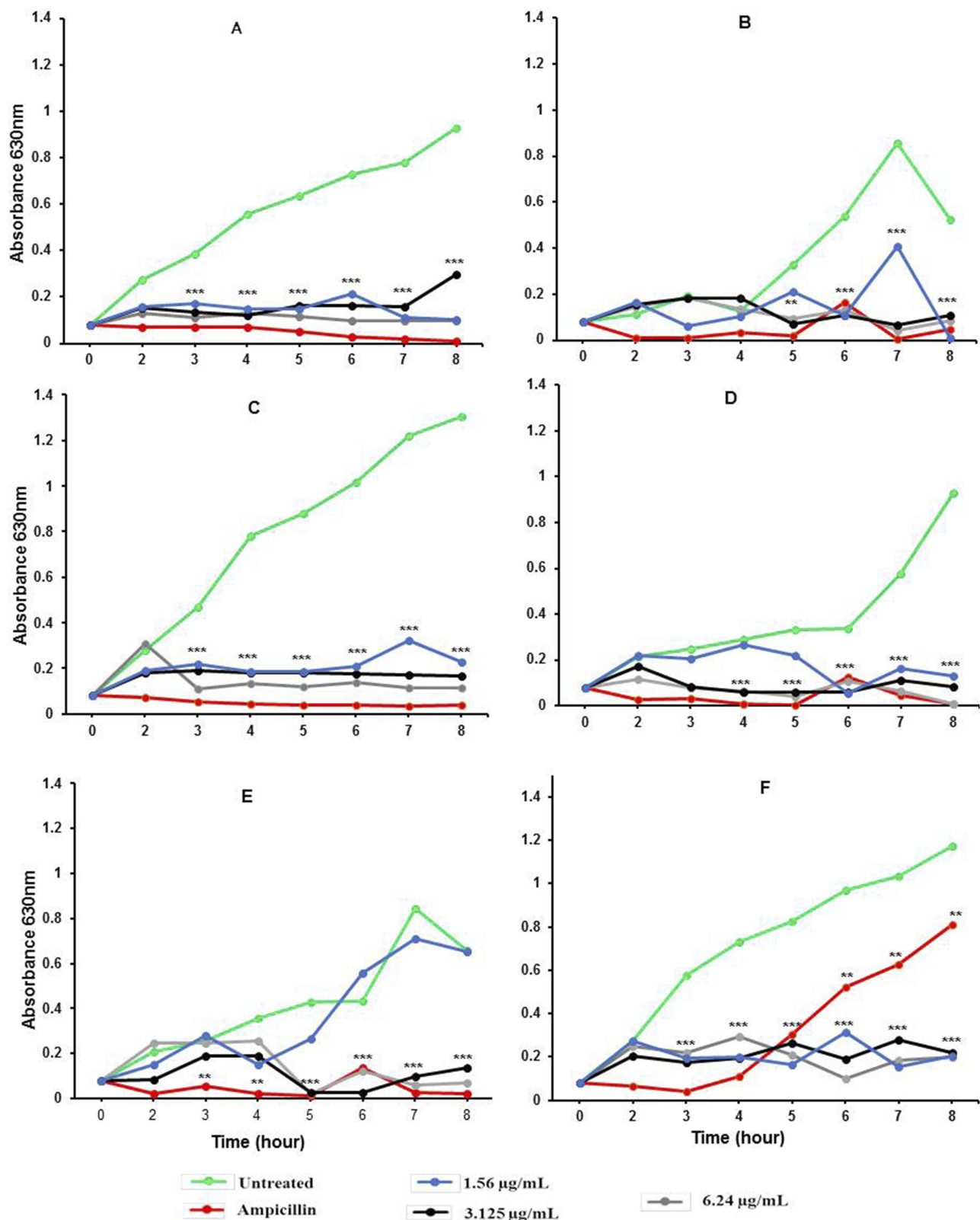


**Figure 7** Growth inhibitory activities of <sup>a</sup>TML-AgNPs-25°C against selected bacterial strains.

**Notes:** Growth curves of (A) *S. pneumoniae*, (B) *S. enterica enterica*, (C) *H. influenzae*, (D) *S. flexneri*, (E) *K. pneumoniae*, and (F) *S. enterica<sup>a</sup>* (*Salmonella enterica* subsp. *enterica* A36 Serovar Typhimurium) after 24 hr treatment. \*\*P < 0.01, \*\*\*P < 0.001.

**Abbreviations:** AgNPs, Silver nanoparticles; TM, *Terminalia mantaly*; <sup>a</sup>TML-AgNPs, AgNPs synthesized from aqueous leaf extracts from TM; *S. pneumoniae*, *Streptococcus pneumoniae*; *S. enterica enterica*, *Salmonella enterica enterica*; *H. influenzae*, *Haemphilus influenzae*, *S. flexneri*, *Shigella flexneri*; *K. Pneumoniae*, *Klebsiella pneumoniae*; *S. aureus*, *Staphylococcus aureus*; *S. enterica*, *Salmonella enterica*.

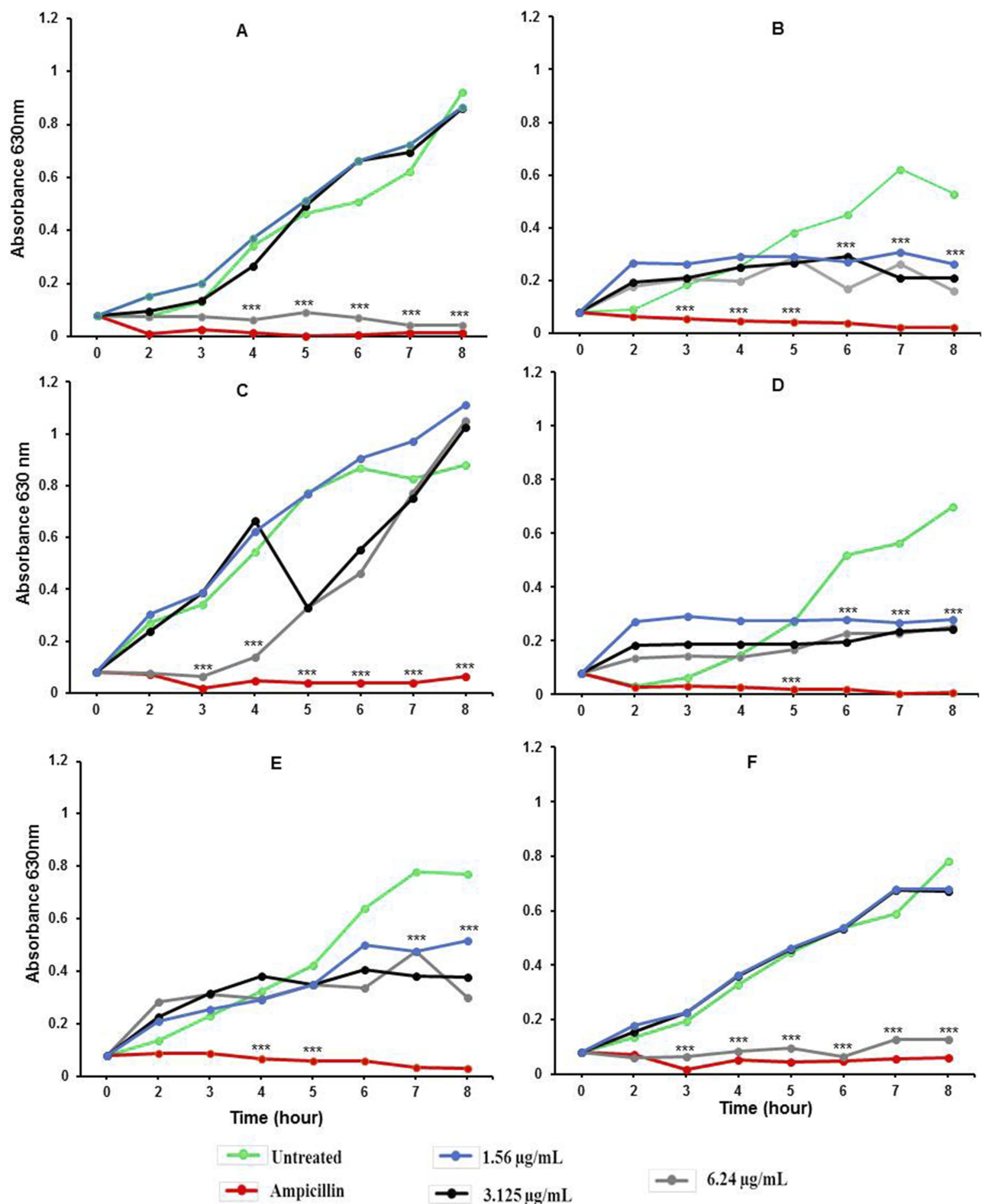


**Figure 8** Growth inhibitory activities of  $a$ TMSB-AgNPs-70°C against selected bacterial strains.

**Notes:** Growth curves of (A) *S. pneumoniae*, (B) *S. enterica*, (C) *H. influenzae*, (D) *S. flexneri*, (E) *K. pneumoniae*, and (F) *S. aureus* after 24 hr treatment. \*\*\*P < 0.001.

**Abbreviations:** AgNPs, Silver nanoparticles; TM, *Terminalia mantaly*;  $a$ TMSB-AgNPs, AgNPs synthesized from aqueous Stem Bark extracts from TM; *S. pneumoniae*, *Streptococcus pneumoniae*; *S. enterica*, *Salmonella enterica*; *H. influenzae*, *Haemophilus influenzae*, *S. flexneri*, *Shigella flexneri*; *K. pneumoniae*, *Klebsiella pneumoniae*; *S. aureus*, *Staphylococcus aureus*; *S. enterica*, *Salmonella enterica*.

the same response in bacteria, their respective AgNPs possess enhanced anti-bacterial activities against both Gram-negative and Gram-positive strains.

## Growth Inhibitory Kinetics Of TM-AgNPs

Based on the results for the antibacterial screening (Figure 6),  ${}^a$ TML-AgNPs synthesised at 25°C ( ${}^a$ TML-AgNPs-25°C) and  ${}^a$ TMSB-AgNPs synthesised at 70°C ( ${}^a$ TMSB-AgNPs-70°C) showed the highest antibacterial activities. The bacterial growth kinetics of several bacterial strains was evaluated in response to treatment with these two TM-AgNPs. Figures 7 and 8 show the effects of  ${}^a$ TML-AgNPs-25°C and  ${}^a$ TMSB-AgNPs-70°C, respectively.

Changes in optical density (OD) were used to assess bacterial growth. This provides an easy and efficient way to quantify bacterial growth over time. A decrease in the absorbance indicates the inhibition of bacterial growth, an effect that can be attributed to the death of cells that is blocked in the stationary phase.<sup>57</sup> As shown in Figures 7 and 8, both TM-AgNPs caused a time- and dose-dependent growth inhibition in the selected strains. Of the two TM-AgNPs,  ${}^a$ TML-AgNPs-25°C (Figure 7) was more effective and had the highest bactericidal effect against the microorganisms.  ${}^a$ TML-AgNPs-25°C suppressed the growth of all six bacterial strains tested. Interestingly, the growth curve for *S. enterica* shows that the inhibitory effects of ampicillin diminish after 4 hrs, while inhibitory effects of  ${}^a$ TML-AgNPs-25°C are maintained for the duration of the experiment at all the concentrations tested. The bacteriostatic effects of  ${}^a$ TMSB-AgNPs-70°C were observed against all strains except for *H. influenzae* and *S. aureus* (Figure 8). The growth curves of *S. enterica enterica* and *S. flexneri* show that  ${}^a$ TMSB-AgNPs-70°C is able to effectively inhibit the growth of these two organisms from 2 to 8 hrs at all the concentrations tested. Only higher concentrations (6.24 µg/mL) of  ${}^a$ TMSB-AgNPs-70°C were effective on *S. pneumoniae* and *S. aureus* at all time points. In general, the Gram-negative bacteria were more susceptible to the effects of the TM-AgNPs than Gram-positive bacteria (*S. pneumoniae* and *S. aureus*). This might be due to the structural differences between the two bacterial types, a key component being the cell membrane of the Gram-positive bacteria, where the thick peptidoglycan layer acts as a barrier against penetration of foreign materials.<sup>20,58</sup> The thick and negatively charged peptidoglycan layer in Gram-positive bacteria has been shown to entrap Ag<sup>+</sup> ions onto the cell wall and block their activity.<sup>59</sup> The exact mechanism of antibacterial action of AgNPs is not yet known.<sup>60,61</sup> Nonetheless, several studies have demonstrated

that bactericidal effects of the AgNPs are strongly influenced by their size, shape, concentration, and colloidal state.<sup>62,63</sup>

## Conclusion

This study reports on a plant-mediated approach to synthesize AgNPs using TM leaf, stem bark and root extracts as both reducing and capping agents. The biogenic TML and TMSB AgNPs remained stable for more than 2 weeks, while those within a diameter ranging from 11 to 60 nm exhibited remarkable antibacterial activity against the tested pathogenic microorganisms. The  ${}^a$ TM AgNPs demonstrated the highest bactericidal effect, and compared to the crude extracts, their activity was ≥20-fold higher. The rise in the number of antimicrobial-resistant bacterial strains underpins the need for alternative antimicrobial agents. The biogenic AgNPs described in this study can potentially be used as an alternative to conventional antimicrobial agents. Further studies are underway to study the anti-microbial mechanism of TM-AgNPs and identify the phytochemicals involved in the synthesis of the NPs.

## Acknowledgment

We thank the Organization for Women in Science for the Developing World (OWSD) for sponsoring Ms Michele Majoumou's PhD studies (2017-2019). We also thank the DST/Mintek NIC and Chemical Industries Education & Training Authority (CHIETA) for financial assistance. This work also received materials and equipment support from Yaoundé-Bielefeld Bilateral Graduate School for Natural Products with Anti-parasite and Antibacterial Activity (YaBiNaPA) and the Seeding Labs' Instrumental Access.

## Disclosure

The authors report no conflicts of interest in this work.

## References

- Laxminarayan R, Matsoso P, Pant S, et al. Access to effective antimicrobials: a worldwide challenge. *Lancet*. 2016;387:168–175. doi:10.1016/S0140-6736(15)00474-2
- CDC: Centers for Disease Control and Prevention. Antibiotic resistance threats in the United States. *Annu Rep*. 2013;508.
- De la Fuente-Núñez C, Reuville F, Fernández L, Hancock RE. Bacterial biofilm development as a multicellular adaptation: antibiotic resistance and new therapeutic strategies. *Curr Opin Microbiol*. 2013;16:580–589. doi:10.1016/j.mib.2013.06.013
- Smith WD, Bardin E, Cameron L, Edmondson CL, Farrant KV, Martin I. Current and future therapies for *Pseudomonas aeruginosa* infection in patients with cystic fibrosis. *FEMS Microbiol Lett*. 2017;364.
- Mohammed EA, Al-Qahtani A, Al-Mutairi A, Al-Shamri B, Aabed K. Antibacterial and cytotoxic potential of biosynthesized silver nanoparticles by some plant extracts. *Nanomaterials*. 2018;8(6):E382.

6. El-Chaghaby GA, Ahmad AF. Biosynthesis of silver nanoparticles using *Pistacial entiscus* leaves extract and investigation of their antimicrobial effect. *Orient J Chem.* 2011;27:929–936.
7. Veerasamy R, Xin TZ, Gunasagaran S, et al. Biosynthesis of silver nanoparticles using Mangosteen leaf extract and evaluation of their antimicrobial activities. *J Saudi Chem Soc.* 2011;15:113–120. doi:10.1016/j.jscs.2010.06.004
8. Ahmed S, Ikram S. Silver nanoparticles: one pot green synthesis using *Terminalia arjuna* extract for Biological application. *Nanomed Nanotechnol.* 2015;6:7.
9. Wang D, Josua M, Yeon-Ju K, et al. Coalescence of functional gold and monodisperse silver nanoparticles mediated by black *Panax ginseng* Meyer root extract. *Int J Nanomedicine.* 2016;14.
10. Yuan CG, Huo C, Gui B, Cao WP. Green synthesis of gold nanoparticles using *Citrus maxima* peel extract and their catalytic/antibacterial activities. *IET Nanobiotechnol.* 2017;11:523–530. doi:10.1049/iet-nbt.2016.0183
11. Aljabali AAA, Yazan Akkam IDY, Al Zoubi IDMS, et al. Synthesis of gold nanoparticles using leaf extract of *Ziziphus zizyphus* and their antimicrobial activity. *Nanomaterials.* 2018;8:174. doi:10.3390/nano8030174
12. Dhillon GS, Brar SK, Kaur S, Verma M. Green approach for nanoparticle biosynthesis by fungi: current trends and applications. *Crit Rev Biotechnol.* 2012;32:49–73. doi:10.3109/07388551.2010.550568
13. Mittal AK, Chisti Y, Banerjee UC. Synthesis of metallic nanoparticles using plant extracts. *Biotechnol Adv.* 2013;31:46–456. doi:10.1016/j.biotechadv.2013.01.003
14. Khatami M, Nejad MS, Pourseyedi SH. Biogenic synthesis of silver nanoparticles using mustard and its characterization. *Int J Nanosci Nanotechnol.* 2015;11(4):281–288.
15. Singh V, Shrivastava A, Wahi N. Biosynthesis of silver nanoparticles by plants crude extracts and their characterization using UV, XRD, TEM and EDX. *Afr J Biotechnol.* 2015;14(33):2554–2567. doi:10.5897/AJB2015.14692
16. Kharisova OV, Dias HV, Kharisov BI, Perez BO, Perez VMJ. The greener synthesis of nanoparticles. *Trends Biotechnol.* 2013;31:240. doi:10.1016/j.tibtech.2013.01.003
17. Malarkodi C, Rajeshkumar S, Paulkumar K, Vanaja M, Gnanajobitha G, Annadurai G. Biosynthesis and antimicrobial activity of semiconductor nanoparticles against oral pathogens. *Bioin Chem Appl.* 2014;2014:1–10. doi:10.1155/2014/347167
18. Sekhar EC, Rao KSKV, Rao MS, Alisha SB. A simple biosynthesis of silver nanoparticles from *Syzygium cumini* stem bark aqueous extract and their spectrochemical and antimicrobial studies. *J Appl Pharm Sci.* 2018;8(1):73–79.
19. El-Rafie MH, Hamed MAA. Antioxidant and anti-inflammatory activities of silver nanoparticles biosynthesized from aqueous leaves extracts of four *Terminalia* species. *Adv Nat Sci Nanosci Nanotechnol.* 2014;5:11.
20. Dakal TC, Kumar A, Majumdar RS, Yadav V. Mechanistic basics of antimicrobials action of silver nanoparticles. *Front Microbiol.* 2016;7:1831. doi:10.3389/fmicb.2016.01831
21. Wang D, Markus J, Wang C, et al. Green synthesis of gold and silver nanoparticles using aqueous extract of *Cibotium barometz* root. *Artif Cells Nanomed Biotechnol.* 2017;45:1548–1555.
22. Sondi I, Salopek-Sondi B. Silver nanoparticles as antimicrobial agent: a case study on *Escherichia coli* as a model for Gram-negative bacteria. *J Colloid Interf Sci.* 2004;275:177–182. doi:10.1016/j.jcis.2004.02.012
23. Jain J, Arora S, Rajwade JM, Omray P, Khandelwal S, Paknikar KM. Silver nanoparticles in therapeutics: development of an antimicrobial gel formulation for topical use. *Mol Pharm.* 2009;6:1388–1401. doi:10.1021/mp900056g
24. Tippayawat P, Phromviyo N, Parichart B, Chompoosor A. Green synthesis of silver nanoparticle using *Aloe vera* plant extract prepared by a hydrothermal method and their synergistic antibacterial activity. *Peer J.* 2016;4:1–16.
25. Alshaye NA, Elobeid MM, Alkhalifah DHM, Mohammed AE. Characterization of biogenic silver nanoparticles by *Salvadora persica* leaves extract and Its application against some MDR pathogens *E. coli* and *S. Aureus.* *Res J Microbiol.* 2017;12:74–81.
26. Hwang ET, Lee JH, Chae YJ, et al. Analysis of the toxic mode of action of silver nanoparticles using stress-specific bioluminescent bacteria. *Small.* 2008;4(6):746–750. doi:10.1002/sml.200700954
27. Panacek A, Kvittek L, Prucek R, et al. Silver colloid nanoparticles synthesis characterization and their antibacterial activity. *J Phys Chem B.* 2006;110(33):16248–16253. doi:10.1021/jp063826h
28. Chwalibog A, Sawosz E, Hotowy A, et al. Visualization of interaction between inorganic nanoparticles and bacteria or fungi. *Int J Nanomed.* 2010;5:1085–1094. doi:10.2147/IJN.S13532
29. Therese KL, Bagyalakshmi R, Madhavan HN, Deepa P. *In vitro* susceptibility testing by agar dilution method to determine the minimum inhibitory concentrations of amphotericin B, fluconazole and ketoconazole against ocular fungal isolates. *Ind J Med Microbiol.* 2006;24:273–279. doi:10.4103/0255-0857.29386
30. Kumar KM, Mandal BK, Kumar KS, Reddy PS. Biobased green method to synthesise palladium and iron nanoparticles using *Terminalia chebula* aqueous extract. *Spectrochim Acta A Mol Biomol Spectrosc.* 2013;102:128–133.
31. Ankamwar B. Biosynthesis of gold nanoparticles (green-gold) using leaf extract of *Terminalia catappa.* *J Chem.* 2010;7:1334–1339.
32. Nguouana KT, Mbouna JCD, Kuipou TRM, et al. Potent and synergistic extract combinations from *Terminalia catappa*, *Terminalia mantaly* and *Monodora tenuifolia* against pathogenic yeasts. *Medicines.* 2015;2:220–235. doi:10.3390/medicines2030220
33. Tchuenmogne TMA, Kammalac NT, Gohlke S, et al. Compounds from *Terminalia mantaly* L. stem bark exhibit potent inhibition against some pathogenic yeasts and enzymes of metabolic significance. *Medicines.* 2017;4:6. doi:10.3390/medicines4010006
34. Kumar KM, Sinha M, Mandal BK, Ghosh AR, Kumar KS, Reddy PS. Green synthesis of silver nanoparticles using *Terminalia chebula* extract at room temperature and their antimicrobial studies. *Spectrochim Acta A.* 2012;91:228–233. doi:10.1016/j.saa.2012.02.001
35. Elbagory AM, Cupido CN, Meyer M, Hussein AA. Large scale screening of southern african plant extracts for the green synthesis of gold nanoparticles using microtitre-plate method. *Molecules.* 2016;20.
36. CLSI. *Methods for Dilution Antimicrobial Susceptibility Tests for Bacteria that Grow Aerobically; Approved Standard-Ninth Edition Document M07A9.* Clinical Laboratory Standard Institute; 2012.
37. Cao L, Dai C, Li Z, et al. Antibacterial activity and mechanism of a scorpion venom peptide derivative in Vitro and in Vivo. *PLoS One.* 2012;7(7):11.
38. Moodley JS, Krishna SBN, Sershen KP, Govender P. Green synthesis of silver nanoparticles from *Moringa oleifera* leaf extracts and its antimicrobial potential. *Adv Nat Sci Nanosci Nanotechnol.* 2018;9.
39. Raza MA, Kanwal Z, Rauf A, Sabri AN, Riaz S, Naseem S. Size and shape-dependent antibacterial studies of silver nanoparticles synthesized by wet chemical routes. *Nanomaterials.* 2016;6:74. doi:10.3390/nano6040074
40. Govindappa M, Farheen H, Chandrappa CP, Channabasava R, Rai RV, Raghavendra VB. Mycosynthesis of silver nanoparticles using extract of endophytic fungi, *Penicillium* species of *Glycosmis mauritiana* and its antioxidant, antimicrobial, anti-inflammatory and tyrosinase inhibitory activity. *Adv Nat Sci Nanosci Nanotechnol.* 2016;7:03501. doi:10.1088/2043-6262/7/3/035014
41. Kannan N, Shekhawat MS, Ravindran CP, Manokari M. Preparation of silver nanoparticles using leaf and fruit extracts of *Morinda coreia* Buck. Ham. -A green approach. *J Sci Innov Res.* 2014;3(3):315–318.
42. Sharma R, Dhillon A, Kumar D. Mentha-Stabilized silver nanoparticles for high performance colorimetric detection of Al (III) in aqueous systems. *Sci Rep.* 2018;8:5189. doi:10.1038/s41598-018-23469-1

43. Hiemenz PC, Rajagopalan R. *Principles Of Colloid And Surface Chemistry*. 3rd ed. New York, NY, USA: Marcel Dekker;1997:650–664.
44. Clayton KN, Salameh JW, Wereley ST, Kinzer-Ursem T. Physical characterization of nanoparticle size and surface modification using particle scattering diffusometry. *Biomicrofluidics*. 2016;10:14. doi:10.1063/1.4962992
45. International Standard ISO13321. *Methods for Determination of Particle Size Distribution Part 8: Photon Correlation Spectroscopy*. ISO;1996.
46. Wu L, Zhang J, Watanabe W. Physical and chemical stability of drug nanoparticles. *Adv Drug Deliv Rev*. 2011;63:456–469. doi:10.1016/j.addr.2011.02.001
47. Singh P, Kim YJ, Zhang D, Yang DC. Biological synthesis of nanoparticles microorganisms. *Trends Biotechnol*. 2016;34:88–599. doi:10.1016/j.tibtech.2016.02.006
48. Elbagory AM, Meyer M, Cupido CN, Hussein AA. Inhibition of bacteria associated with wound infection by biocompatible green synthesized gold nanoparticles from South African plant extracts. *Nanomaterials*. 2017;7:417. doi:10.3390/nano7120458
49. Fahmy NM, Al-Sayed E, Singab AN. Genus *Terminalia*: A phytochemical and biological review. *Med Aromat Plants*. 2015;4:5.
50. Patra JK, Baek KH. Novel green synthesis of gold nanoparticles using *Citrullus lanatus* rind and investigation of proteasome inhibitory activity, antibacterial, and antioxidant potential. *Int J Nanomedicine*. 2015;10:7253–7264. doi:10.2147/IJN.S95483
51. Bagherzade G, Mohmmad MT, Namaei H. Green synthesis of silver nanoparticles using aqueous extract of saffron (*Crocus sativus* L.) wastages and its antibacterial activity against six bacteria. *Asian Pac J Trop Biomed*. 2017;7:227–233. doi:10.1016/j.apjtb.2016.12.014
52. Singh P, Pandit S, Garnæs J, et al. Green synthesis of gold and silver nanoparticles from *Cannabis sativa* (industrial hemp) and their capacity for biofilm inhibition. *Int J Nanomedicine*. 2018;13:3571–3591. doi:10.2147/IJN.S157958
53. Escárcega-González EC, Garza-Cervantes JA, Vázquez-Rodríguez A, et al. In vivo antimicrobial activity of silver nanoparticles produced via a green chemistry synthesis using *Acacia rigidula* as a reducing and capping agent their anticancer activities. *Int J Nanomedicine*. 2018;13:2349–2363. doi:10.2147/IJN.S160605
54. Prakash P, Gnanaprakasam P, Emmanuel R, Arokiyaraj S, Saravanan M. Green synthesis of silver nanoparticles from leaf extract of *Mimusops elengi*, Linn for enhanced antibacterial activity against multi drug resistant clinical isolates. *Colloid Surf B*. 2013;108:255–259. doi:10.1016/j.colsurfb.2013.03.017
55. Anandalakshmi K, Venugobal J, Ramasamy V. Characterization of silver nanoparticles by green synthesis method using *Petalium murex* leaf extract and their antibacterial activity. *Appl Nanosci*. 2016;6:399–408. doi:10.1007/s13204-015-0449-z
56. Mmola M, Le Roes-Hill M, Durrell K, et al. Enhanced antimicrobial and anticancer activity of silver and gold nanoparticles synthesized using *Sargassum incisifolium* aqueous extracts. *Mol*. 2016;21:1633. doi:10.3390/molecules21121633
57. Chudasama B, Vala AK, Andhariya N, Mehta RV, Upadhyay RV. Highly bacterial resistant silver nanoparticles: synthesis and antibacterial activities. *J Nanopart Res*. 2010;12(5):1677–1685. doi:10.1007/s11051-009-9845-1
58. Holowachuk SA, Farid MB, Buddington RK. A kinetic microplate method for quantifying the antibacterial properties of biological fluids. *J Microbiol Methods*. 2003;55:441–446.
59. Hajipour MJ, Fromm KM, Ashkarran AA, et al. Antibacterial properties of nanoparticles. *Trends Biotechnol*. 2012;30:499–511. doi:10.1016/j.tibtech.2012.06.004
60. Feng QL, Wu J, Chen GQ, Gui FZ, Kim TN, Kim JO. Mechanistic study of the antibacterial effect of silver nanoparticles on *Escherichia Coli* and *Staphylococcus aureus*. *J Biomed Mater Res*. 2000;52(4):662–668. doi:10.1002/1097-4636(20001215)52:4<662::aid-jbm10>3.0.co;2-3
61. Kim J, Kuk E, Yu KN, et al. Antimicrobial effects of silver nanoparticles. *Nanomedicine*. 2007;3:95–101. doi:10.1016/j.nano.2006.12.001
62. Jiang J, Oberdörster G, Biswas P. Characterization of size, surface charge, and agglomeration state of nanoparticle dispersions for toxicological studies. *J Nanopart Res*. 2009;11:77–89. doi:10.1007/s11051-008-9446-4
63. Rai M, Kon K, Ingle A, Duran N, Galdiero S, Galdiero M. Broad spectrum bioactivities of silver nanoparticles: the emerging trends and future prospects. *Appl Microbiol Biotechnol*. 2014;98:1951–1961. doi:10.1007/s00253-013-5473-x

## International Journal of Nanomedicine

Dovepress

### Publish your work in this journal






The International Journal of Nanomedicine is an international, peer-reviewed journal focusing on the application of nanotechnology in diagnostics, therapeutics, and drug delivery systems throughout the biomedical field. This journal is indexed on PubMed Central, MedLine, CAS, SciSearch®, Current Contents®/Clinical Medicine,

Journal Citation Reports/Science Edition, EMBase, Scopus and the Elsevier Bibliographic databases. The manuscript management system is completely online and includes a very quick and fair peer-review system, which is all easy to use. Visit <http://www.dovepress.com/testimonials.php> to read real quotes from published authors.

Submit your manuscript here: <https://www.dovepress.com/international-journal-of-nanomedicine-journal>

Article

# Synthesis of Biogenic Gold Nanoparticles from *Terminalia mantaly* Extracts and the Evaluation of Their In Vitro Cytotoxic Effects in Cancer Cells

Michele S. Majoumouo <sup>1,2</sup> , Jyoti R. Sharma <sup>2</sup> , Nicole R. S. Sibuyi <sup>2</sup> , Marius B. Tincho <sup>2</sup> ,  
Fabrice F. Boyom <sup>1</sup>  and Mervin Meyer <sup>2,\*</sup> 

<sup>1</sup> Antimicrobial & Biocontrol Agents Unit, Laboratory for Phytobiochemistry and Medicinal Plants Studies, Department of Biochemistry, University of Yaoundé 1, Yaoundé PO. Box 812, Cameroon; 3770612@myuwc.ac.za (M.S.M.); ffeff@yahoo.com (F.F.B.)

<sup>2</sup> Department of Science and Innovation (DSI)/Mintek Nanotechnology Innovation Centre, Biolabels Node, Department of Biotechnology, University of the Western Cape, Private Bag X17, Bellville 7535, South Africa; Jyt228@gmail.com (J.R.S.); nsibuyi@uwc.ac.za (N.R.S.S.); 3173772@myuwc.ac.za (M.B.T.)

\* Correspondence: memeyer@uwc.ac.za; Tel.: +27-21-9592032

Received: 23 July 2020; Accepted: 12 September 2020; Published: 29 September 2020



**Abstract:** Scientists have demonstrated the potential of plant materials as ‘green’ reducing and stabilizing agents for the synthesis of gold nanoparticles (AuNPs) and opened new ecofriendly horizons to develop effective and less harmful treatment strategies. The current study demonstrated the use of *Terminalia mantaly* (TM) extracts to synthesize AuNPs with enhanced cytotoxic effects. The TM-AuNPs were synthesized at 25 and 70 °C using water (<sub>W</sub>TM) and methanolic (<sub>M</sub>TM) extracts of the leaf, root and stem/bark parts of the plant. The TM-AuNPs were characterized using UV–visible spectrophotometry, dynamic light scattering (DLS), transmission electron microscopy, energy dispersive X-ray (EDX), selection area electron diffraction (SAED) and Fourier transform infrared (FTIR) spectroscopy. Majority of the TM-AuNPs were spherical with a mean diameter between 22.5 and 43 nm and were also crystalline in nature. The cytotoxic effects of TM-AuNPs were investigated in cancer (Caco-2, MCF-7 and HepG2) and non-cancer (KMST-6) cell lines using the MTT assay. While the plant extracts showed some cytotoxicity towards the cancer cells, some of the TM-AuNPs were even more toxic to the cells. The IC<sub>50</sub> values (concentrations of the AuNPs that inhibited 50% cell growth) as low as 0.18 µg/mL were found for TM-AuNPs synthesized using the root extract of the plant. Moreover, some of the TM-AuNPs demonstrated selective toxicity towards specific cancer cell types. The study demonstrates the potential of TM extracts to produce AuNPs and describe the optimal conditions for AuNPs using TM extracts. The toxicity of some the TM-AuNPs can possibly be explored in the future as an antitumor treatment.

**Keywords:** antitumor; gold nanoparticles; green synthesis; nanotechnology; *Terminalia mantaly*

## 1. Introduction

Traditional medicine has always used and relied on the medicinal properties of plants for the treatment of numerous diseases such as bacterial infections, headaches, hypertension, jaundice, leprosy and cancer, among others [1]. Among various plant species used in Cameroonian traditional medicine, *Terminalia mantaly* (TM) has gained scientific recognition due to its reported antitumor, antidiabetic and antihypertensive medicinal properties. TM is a deciduous tree belonging to the flowering plant family, Combretaceae. The genus *Terminalia* comprises of more than 100 species. Numerous scientific studies have explored the antimicrobial, antiprotozoal, antidiarrheal, anti-inflammatory, antitumor and wound healing activities; which can be attributed to phytochemicals present in the plant [1]. A survey

of the literature has revealed that the *Terminalia* genus, TM included; possesses a variety of bioactive phytochemical constituents, such as tannins, pentacyclic triterpenes, glycoside derivatives, flavonoids and phenolic compounds [2].

Green nanotechnology has been applied to synthesize metallic nanoparticles (NPs) from medicinal plants extracts. It has been shown that the phytochemical constituents present in plants can act as reducing and capping agents during the synthesis biogenic metallic NPs, including gold nanoparticles (AuNPs) [3,4]. Several studies have demonstrated the synthesis of biogenic AuNPs using various species of the genus *Terminalia*, which include *T. catappa*, *T. chebula*, *T. arjuna* and *T. bellirica* [5–8]. While TM has been used to produce biogenic silver nanoparticles [3], this species has not been used to produce AuNPs. The conventional physical and chemical methods used for AuNP synthesis involve the use of toxic chemicals, high energy processes and are expensive [9–11]. Studies have highlighted concerns regarding chemically synthesized NPs for biomedical applications due to the use of toxic reducing agents such as sodium citrate, sodium borohydride and byproducts formed during the synthesis process [11,12]. These chemicals are not only corrosive but also generate flammable by products during chemical synthesis. Considering the threats these nanomaterials and the processes used to synthesize these materials pose to the environment and humans, there is a need for the development of more biofriendly nanomaterials using processes that are also more environmentally safe [11].

Scientists have turned to green nanotechnology to produce metallic NPs using biological systems (e.g., microbes and plant extracts) [11–13]. Since biologicals are used in the synthesis process, the expectation is that the nanomaterials will be more biofriendly and the synthesis processes would be more environmentally friendly. This eliminates the use of toxic reducing, stabilizing and capping agents and produces nanoparticles that will have shape and size-dependent biological activities [11,14,15]. Moreover, utilizing plant extracts as reducing agents for the synthesis of AuNPs is advantageous owing to the availability of the plants and simplicity of the approach. Plant-mediated synthesis of AuNPs will not only allow large-scale production but will also reduce cost and time involved in the synthesis [16].

The use of nanotechnology to produce metallic nanostructures has gained interest, especially in medicine [17–19]. The fascinating and insightful use of optical, chemical and catalytic properties of noble metal NPs depends on the metal source, nanoparticle sizes and shapes and surface chemistry. Furthermore, these properties allow NPs to gain impetus in the present century and make them an excellent resource for diverse applications [20–23]. Metallic NPs especially AuNPs have attracted a great deal of attention, owing to their tunable optical and electronic properties [24]. AuNPs have been reported as safe for use in drug delivery system in in vitro and in vivo studies [25]. While the antibacterial activities of some of the biogenic AuNPs produced from *Terminalia* species have been studied, not much is known about the in vitro and in vivo cytotoxicity of these AuNPs. The toxicity of AuNPs synthesized using a water extract of fruit pericarp of *T. bellirica* was tested using the brine shrimp assay and did not show any toxicity [26].

Nanotechnology can play an important role in medicine, specifically in the early disease detection, improved diagnosis, and development of personalized treatments for chronic and infectious diseases [27]. Biocompatible AuNPs have been widely studied and applied in the diagnosis and treatment of cancer [28]. In addition, several studies indicated the intrinsic antitumor property of AuNPs that were able to selectively kill cancer cells [29]. Previous reports described AuNPs that have strong antitumor effects through the induction of apoptosis in colorectal, breast and liver cancer cells [30]. Owing to their small size, AuNPs are well suited for delivering antitumor drugs due to their preferential accumulation at tumor sites through the enhanced permeability retention effect [31].

Herein we describe for the first time the synthesis of biogenic AuNPs from the leaf, root and stem/bark parts of the TM. We evaluated cytotoxic effects of biogenic AuNPs synthesized from six different TM extracts in three human cancer (Caco-2, HepG2 and MCF-7) and one non-cancer (KMST-6) cell lines and found that the AuNPs display selective toxicity towards certain cancer cell lines.



## 2. Results and Discussion

AuNPs have been applied in the development of biosensors, pharmaceuticals, nanoscience and nanotechnology, hence, the term nanomedicine was coined. In nanomedicine, AuNPs can be used as contrast and drug delivery agents for diagnostics and therapeutics, respectively. Traditionally, AuNP are synthesized through physical and chemical methods, these methods are usually limited by their use of toxic chemicals as reducing agents. To overcome the drawbacks of these methods, many studies have opted to use a green approach to synthesize AuNPs [5,32,33]. Among the green sources used, plant extracts are readily available, providing an easy and simple method that involves just one step synthesis. Moreover, utilizing plant extracts as reducing agents in synthesizing AuNPs reduces production time and cost, and offers an opportunity for large-scale production [34]. Biogenic AuNPs have been reported to elicit potent toxic effects and antiproliferative activity against various tumors [35]. The inhibitory mechanism of nanoparticles against cancer cell lines is not well known. However, it was suggested that nanoparticles can block the activity of abnormal signaling proteins or interact with functional groups of intracellular proteins and enzymes, as well as with the nitrogen bases in the DNA molecules, which results in cell death [36]. The current study explored and demonstrated the synthesis of biogenic AuNPs using  $W^{TM}$  and  $M^{TM}$  extracts as both reducing and stabilizing agents, and tested their in vitro cytotoxicity.

### 2.1. Qualitative Analysis of TM Phytochemicals

The phytochemical composition of TM extracts in Table 1, revealed an unequal distribution of different secondary metabolites in  $W^{TM}$  and  $M^{TM}$  extracts. The alkaloids, flavonoids, glucosides and total phenols were present in all the extracts, and no anthocyanins were found in any of the TM extracts. The  $W^{TM}$  extracts contained majority of the phytochemicals. All the  $M^{TM}$  extracts lacked steroids. Tannins and triterpenes were not present in TMSB and TMR, and TMR and TML lacked anthraquinones. Metabolites that contain active functional groups, such as hydroxyl, aldehyde and carboxyl units, may play pivotal roles in chemical reduction processes of the gold precursor to produce AuNPs [5].

**Table 1.** Analysis of phytochemical composition in *Terminalia mantaly* (TM) extracts.

TM Extracts	Alkaloids	Phenolic content	Flavonoids	Tannins	Anthocyanins	Anthraquinones	Steroids	Triterpenes	Glucosides	Saponins
$W^{TMSB}$	+	+	+	+	-	+	+	+	+	+
$M^{TMSB}$	+	+	+	-	-	+	-	-	+	+
$W^{TMR}$	+	+	+	+	-	+	-	-	+	+
$M^{TMR}$	+	+	+	-	-	-	-	-	+	+
$W^{TML}$	+	+	+	+	-	+	+	+	+	+
$M^{TML}$	+	+	+	+	-	-	-	+	+	-

(+) Presence; (-) Absence.

### 2.2. Green Synthesis of AuNPs

Small scale AuNP synthesis was carried out in a 96 well microplate by incubating a fixed concentration (1 mM) of  $NaAuCl_4 \cdot 2H_2O$  with increasing concentrations (0.39–12.5 mg/mL) of the 6 TM extracts ( $W^{TMSB}$ ,  $W^{TMR}$ ,  $W^{TML}$ ,  $M^{TMSB}$ ,  $M^{TMR}$  and  $M^{TML}$ ). The formation of TM-AuNPs was indicated by a color change in the reaction mixture as is shown in Figure 1. The appearance of a red wine/ruby red color after the addition of TM extracts to the  $NaAuCl_4 \cdot 2H_2O$  solution is an indication of AuNP synthesis. Synthesis was performed for 5 h at 25 °C and 70 °C. These temperatures are often

used for the synthesis of AuNPs [18]. The red wine color, which AuNP solutions typically exhibit, is due to the excitation of surface plasmon vibrations in the AuNP solution, and indicates the formation of AuNPs [5,35,37]. TM-AuNPs were successfully synthesized with all six extracts at both 25 °C and 70 °C. In the one step reaction, the phytochemicals in the TM extracts acted as the reducing, stabilizing and capping agents. The bioreduction of the gold precursor could be ascribed to phytochemicals such as alkaloids, flavonoids, tannins, steroids and triterpenes that have been shown to be present in the plant extracts (Table 1) as was suggested in previous studies [32,33]. In particular, it is phytochemicals that contain hydroxyl, aldehyde and carboxyl functional groups that can partake in the bioreduction process [38]. Due to the scavenging capabilities of their –OH groups in phenols, these phytochemicals have been reported to be involved in the bioreduction and stabilization of NPs [33]. The phenolic compounds along with the water domains can synergistically interact with the existing nuclei and lay the foundation to create highly structured sheets of zerovalent gold [23].



**Figure 1.** One step synthesis of TM-gold nanoparticles (AuNPs) by the reduction of chloroaurate ions by TM extracts. The  $w$ TM and  $M$ TM extracts of leaf, root and stem/bark parts of the plant were prepared and mixed with  $\text{NaAuCl}_4 \cdot 2\text{H}_2\text{O}$ . The appearance of a red wine/ruby red color indicated the formation of the AuNPs.

### 2.2.1. Optimization of TM-AuNP Synthesis and UV–Vis Spectroscopy

The synthesis of TM-AuNPs was further confirmed by UV–visible spectrophotometry analysis and this data was used to determine the optimum plant concentration to produce the TM-AuNPs from each of the six TM extracts. The Surface Plasmon Resonance (SPR) of AuNPs results in an absorption maxima (or  $\lambda_{\text{max}}$ ) in the region of 500–600 nm [10,39] as is illustrated in Figure 2, which shows the UV–visible spectra for TM-AuNPs produced with the six different TM extracts at 25 °C and 70 °C. These spectra also represent the AuNPs synthesized with the optimal plant extract concentrations. Table 2 indicates the optimal concentration (OC) of the plant extract and the corresponding  $\lambda_{\text{max}}$  for the respective TM-AuNPs ( $w$ TMSB-AuNPs,  $w$ TMR-AuNPs,  $w$ TML-AuNPs,  $M$ TMSB-AuNPs,  $M$ TMR-AuNPs and  $M$ TML-AuNPs) at both 25 °C and 70 °C. Based on the UV-visible spectrophotometry analysis, the TMR produced AuNPs with a lower peak height or optical density, which is an indication that either the nanoparticle concentration is lower or larger in size [40,41]. Figure 2 also shows that the temperature at which the synthesis was carried out significantly influenced the UV–visible spectra and characteristics of the AuNPs. The same TM extract produced a very different spectrum at the two different temperatures. For example, the optical density of TM-AuNP produced with the  $w$ TML extract produced at 25 °C was significantly higher than the optical density produced for the same extract at 70 °C. The shape of the spectra, which is an indication of the size, shape and uniformity of

the TM-AuNPs were also different. While the  $\lambda_{\max}$  for  $W$ TML-AuNP produced at 25 and 70 °C was the same (544 nm), the  $\lambda_{\max}$  values from the other five extracts were very different at the two temperatures. This all suggests that the concentration of the extract, the phytochemicals and the temperature at which the synthesis was performed all play a role in the synthesis of the AuNPs.

**Table 2.** The OC of TM extracts for AuNP synthesis and the SPR of TM-AuNPs.

AuNPs	AuNPs at 25 °C		AuNPs at 70 °C	
	OC (mg/mL)	$\lambda_{\max}$ (nm)	OC (mg/mL)	$\lambda_{\max}$ (nm)
$W$ TMSB-AuNPs	1.56	545	1.56	540
$M$ TMSB-AuNPs	1.56	550	1.56	535
$W$ TMR-AuNPs	6.25	560	6.25	550
$M$ TMR-AuNPs	1.56	540	1.56	550
$W$ TML-AuNPs	1.56	540	1.56	545
$M$ TML-AuNPs	3.12	544	1.56	544

### 2.2.2. DLS Analysis of TM-AuNPs

The size distribution, charge and surface chemistry of the AuNPs are particularly important since these physicochemical properties strongly influence the mobility and bioavailability of nanoparticles when applied in biological conditions [10,11]. These characteristics can be used to predict the behavior of AuNPs in various biological environments, which is important when designing nanomaterials for biomedical applications. The TM-AuNPs synthesized at 25 and 70 °C had a hydrodynamic diameter ranging from 39 to 79 nm as shown in Table 3. Except for the  $M$ TML, the other five extracts produced larger AuNPs at 70 °C than at 25 °C. The size of the TM-AuNPs increased on average by 9 nm when the synthesis was done at 70 °C. It is possible that the reducing and capping agents are modified at higher temperatures and that the phytochemicals that are involved in the synthesis process at 70 °C differ from the phytochemicals present at 25 °C [42]. An independent study also reported that the sizes of AuNPs produced from plant extracts were significantly smaller at low temperatures [43].

**Table 3.** Dynamic light scattering (DLS) analysis of TM-AuNPs synthesized at 25 and 70 °C.

TM-AuNPs	AuNPs at 25 °C			AuNPs at 70 °C		
	PD (nm)	Pdi	ZP (mv)	PD (nm)	Pdi	ZP (mv)
$W$ TMSB-AuNPs	39	0.5	−27	57	0.3	−28
$M$ TMSB-AuNPs	44	0.5	−36	52	0.5	−29
$W$ TMR-AuNPs	66	0.7	−32	79	0.8	−29
$M$ TMR-AuNPs	44	0.4	−30	48	0.5	−32
$W$ TML-AuNPs	43	0.6	−37	44	0.7	−35
$M$ TML-AuNPs	55	0.4	−29	51	0.5	−10

Note: PD—particle diameter, Pdi—polydispersity index and ZP—zeta potential.

The polydispersity index (Pdi) gives an indication of the degree of uniformity of the size distribution of a nanoparticle in solution. Pdi values above 0.7 indicate that the sample has a very broad particle size distribution [44], and that the nanoparticles may possibly also be aggregated. Except for  $W$ TMR-AuNPs produced at 70 °C, which had a Pdi of 0.8, the Pdi values for all the other TM-AuNPs were less or equal to 0.7 (Table 3), suggesting that these samples have an acceptable level of uniformity. TM-AuNPs with Pdi values less or equal to 0.7 were likely to be monodispersed, uniform in size and shape and stable in colloidal form.

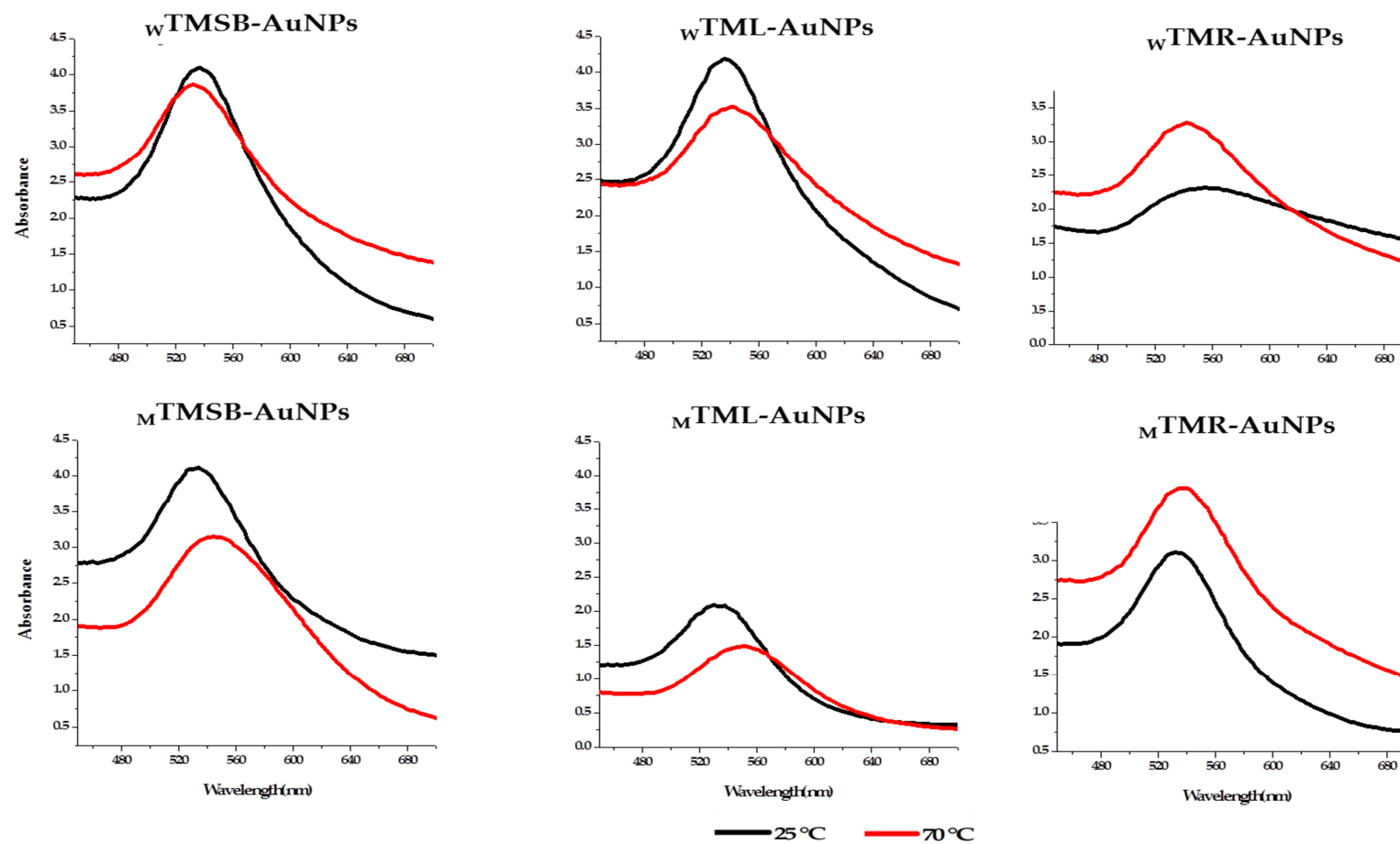


**Figure 2.** The UV-visible spectra of TM-AuNPs. The AuNPs were synthesized at the optimal concentration (OC) of TM-extracts at 25 and 70 °C using  $w$ TM and  $M$ TM extracts.

Nanoparticles are known to agglomerate in the presence of salts due to a reduction in the electronic double layer around each particle, allowing for adhesion through van der Waals forces [45,46]. Aggregation can happen because phytochemicals present in the reaction solution are absorbed on the surface of the AuNPs, resulting in the formation of crosslinks in between the AuNPs.

Zeta potential provides pivotal information on the dispersion of nanoparticles as the magnitude of the charge and indicates the mutual repulsion between particles [47]. Nanoparticles with a zeta potential between 30 and  $-30$  mV are more stable in solution [48] and will repel each other and they tend not to form aggregates in solution [47,49,50]. The zeta potential values for 7 of the 12 TM-AuNPs samples were within this range (Table 3). This included  ${}_W$ TMSB-AuNPs synthesized at both  $25$  °C and  $70$  °C,  ${}_M$ TMSB-AuNPs synthesized at  $70$  °C,  ${}_W$ TMR-AuNPs synthesized at  $70$  °C,  ${}_M$ TMR-AuNPs synthesized at  $25$  °C, and  ${}_M$ TML-AuNPs synthesized at both  $25$  °C and  $70$  °C. Based on the results, these TM-AuNPs were expected to be very stable in solution, while the other five samples that had zeta potentials less than  $-30$  mV might be prone to aggregation. These samples include  ${}_M$ TMSB-AuNPs synthesized at  $25$  °C,  ${}_W$ TMR-AuNPs synthesized at  $25$  °C,  ${}_M$ TMR-AuNPs synthesized at  $70$  °C and  ${}_W$ TML-AuNPs synthesized at both  $25$  °C and  $70$  °C.

The study shows that temperature greatly influenced the hydrodynamic size, charge and size distribution of the AuNPs. Using the same extract at two different temperatures produced AuNPs with very different physicochemical properties. This is further proof that the phytochemicals involved in the synthesis process vary between the different TM-AuNPs. The  ${}_W$ TMR-AuNPs had a Pdi of 0.8, indicating that these nanoparticles might aggregate over time. However, an increase in the temperature at which synthesis was done for  ${}_M$ TMR-AuNPs not only change size but resulted in polydispersed nanoparticles as reflected by a change in Pdi from 0.4 at  $25$  °C to 0.5 at  $70$  °C. Nanoparticles with low Pdi value are likely to be monodispersed [46], thus, TM-AuNPs that gave the lowest Pdi values may be of uniform size, shape and stable in its colloidal form.

### 2.2.3. HRTEM, SAED and EDX Analyses

HRTEM analysis showed that the TM-AuNPs display a variety of geometrical shapes, as shown in Figure S1. Most of the TM-AuNPs were spherical in shape with some triangular, hexagonal and pentagonal shapes. Obtaining AuNPs with a variety of geometrical shapes is very common for NPs produced through plant-mediated synthesis [46]. This is speculated to be due to the presence of different phytochemicals in the extracts that might act in synergy to reduce the gold ions and form AuNPs [51]. Polyphenols have been reported to produce NPs with different shapes [5]. Biomolecules that contains highly polar groups (e.g.,  $-\text{OH}$ ) on their surface may increase the rate of nucleation and induce AuNP formation. The TM-AuNPs had well-defined edges and most of them were well dispersed. Based on the HRTEM analysis, the  ${}_M$ TML-AuNPs,  ${}_W$ TML-AuNPs and  ${}_W$ TMR-AuNPs appears to be agglomerated. However, HRTEM analysis is not the best test to use to determine NP aggregation. Further analysis of the stability of the TM-AuNPs over time is needed.

The size distribution of TM-AuNPs was calculated from the HRTEM micrographs, the representative histograms (Figure 3) demonstrate that  ${}_M$ TMSB-AuNPs synthesized at  $25$  °C and  $70$  °C had a core size of 25.5 nm and 28.3 nm, respectively. The TM-AuNPs had a core size ranging from 21.5 to 43 nm as shown in Table 4. The  ${}_W$ TML-AuNPs produced at  $70$  °C had a smaller core size (21.5 nm) when compared to others. This might suggest that TML might be richer in reducing and capping agents. These results were comparable to those reported by Ankamwar on AuNPs synthesized from leaf extract obtained from *T. Catappa*. The NPs were also spherical in morphology, with an average core size of 21.9 nm [5]. The core sizes of  ${}_W$ TMSB and  ${}_W$ TMR-AuNPs were bigger when compared to the sizes of the other TM-AuNPs.

To highlight the crystalline nature of nanoparticles, SAED analysis was performed. The fringe lattice values ranged from 0.167 to 0.257 nm and the SAED pattern (Figure S2, Supplementary data), which confirmed the crystalline nature of the TM-AuNPs varied between AuNPs synthesized at  $25$  °C and  $70$  °C.  ${}_M$ TMSB-AuNPs synthesized at  $70$  °C for example had a typical HRTEM image with

clear lattice fringes. Furthermore, a d-spacing or interplanar distance of 0.233 nm was obtained for TM-AuNPs, which was comparable with 0.2355 nm, corresponding to the (111) planes of face-centered cubic (fcc) gold single crystals. The clear lattice fringes in HRTEM images and the typical SAED pattern with bright circular rings corresponding to the (111), (200), (220) and (311) planes were obtained in most TM-AuNPs. This was an indication that the nanoparticles obtained were highly crystalline, confirming the fcc crystalline geometry of AuNPs (JCPDS file no. 4-0783) [52]. The diffraction patterns of TM-AuNPs were also comparable to the AuNPs synthesized from *T. catappa* leaf extracts, which showed the Bragg reflections corresponding to the (111), (200), (220), (311) and (222) sets of lattice planes [5,18]. This may be indexed based on the fcc structure of gold. However, the lattice plane was predominantly (111)-oriented. The amorphous effect (diffuse rings) was observed with  $W$ TMSB and  $M$ TMR AuNPs at 70 °C, and the Bragg reflections were weak and considerably broadened relative to the intense (111) and (200) reflections. Finally, the crystallinity was more pronounced for AuNPs synthesized at 25 °C compared to the ones produced at 70 °C.

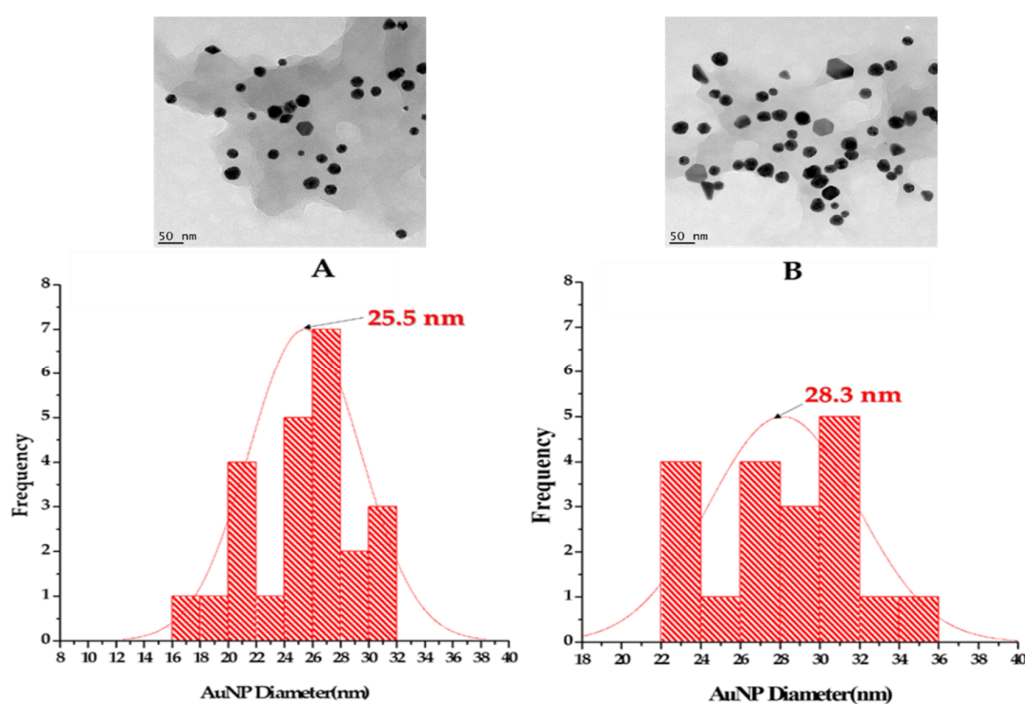


**Figure 3.** HRTEM analysis of shape and size distribution of  $M$ TMSB-AuNPs synthesized (A) at 25 °C and (B) 70 °C.

**Table 4.** Core sizes of TM-AuNPs were analyzed by HRTEM.

AuNPs	AuNP Core Size (nm)	
	25 °C	70 °C
$W$ TMSB-AuNPs	35.5	43.0
$M$ TMSB-AuNPs	25.5	28.3
$W$ TML-AuNPs	26.5	21.5
$M$ TML-AuNPs	23.5	25.0
$W$ TMR-AuNPs	32.0	33.5
$M$ TMR-AuNPs	26.0	29.5

The EDX spectra of TM-AuNPs confirmed the presence of gold ions in all the AuNPs (Figure S2, Supplementary data). The Au peaks were acquired around 2.3 keV, 9.7 keV and 11.3 keV. In some AuNPs, the EDX spectrum showed the presence of silicone (Si), which might be due to a high degree of crystallinity. These results further confirmed the SAED patterns in Figure S3 (Supplementary data).

Moreover, the presence of elements such as calcium and potassium can be due to the micronutrients in the TM extracts used in the synthesis. The weak signals for oxygen in the spectra may have originated from the biomolecules bound to the surface of the NPs [52], Cu from the support HRTEM grid and film and Co from the lenses of the microscope [16].

#### 2.2.4. FTIR Analysis of TM-AuNPs

FTIR analysis was carried out to identify the possible functional chemical bonds from the phytochemicals in the TM extracts that are responsible for reduction, capping and stabilization of AuNPs [53]. The representative FTIR spectra of TMR and TMR-AuNPs are shown in Figure S4 (Supplementary data), highlighting some of the chemical bonds involved in NP synthesis. Generally, the chemical bonds identified in the TM extracts and AuNPs included C-O, C-H,  $\text{-C=C-}$ ,  $\text{H-C=O}$ ,  $\text{-C}\equiv\text{C-}$  and O-H (Table S1). Some of the peaks were absent in the AuNPs depending on the temperature (25 °C and 70 °C). For example, the FTIR spectra of  ${}_w\text{TMSB}$ ,  ${}_w\text{TMSB-AuNPs}$  synthesized at 25 °C and at 70 °C showed prominent absorption bands at (1108  $\text{cm}^{-1}$ , 1347  $\text{cm}^{-1}$ , 1627  $\text{cm}^{-1}$ , 2106  $\text{cm}^{-1}$ , 2939  $\text{cm}^{-1}$  and 3409  $\text{cm}^{-1}$ ), (1048  $\text{cm}^{-1}$ , 1384  $\text{cm}^{-1}$ , 1639  $\text{cm}^{-1}$ , 2016  $\text{cm}^{-1}$ , 2920  $\text{cm}^{-1}$  and 3717  $\text{cm}^{-1}$ ) and (1123  $\text{cm}^{-1}$ , 1636  $\text{cm}^{-1}$ , 2106  $\text{cm}^{-1}$ , 2939  $\text{cm}^{-1}$  and 3452  $\text{cm}^{-1}$ ), respectively. The shoulder at 1048  $\text{cm}^{-1}$ , 1108  $\text{cm}^{-1}$  and 1123  $\text{cm}^{-1}$  was characteristic of C=O vibrations, while the stretch at 1347  $\text{cm}^{-1}$  and 1384  $\text{cm}^{-1}$  arose from the C-H methyl rock alkanes stretching but was absent on  ${}_w\text{TMSB-AuNPs}$  at 70 °C. The recorded peaks at 1639  $\text{cm}^{-1}$ , 1627  $\text{cm}^{-1}$  and 1638  $\text{cm}^{-1}$  were due to the vibration of  $\text{-C=C-}$  stretch alkenes. In addition, the band at 2016  $\text{cm}^{-1}$  could be attributed to the  $\text{-C}\equiv\text{C-}$  stretch alkynes. The broad stretching at 2920  $\text{cm}^{-1}$  and 2939  $\text{cm}^{-1}$  arose from the vibrations of  $\text{H-C=O}$ : C-H stretch aldehydes. Moreover, the presence of the shifted band at 3717  $\text{cm}^{-1}$ , 3409  $\text{cm}^{-1}$  and 3452  $\text{cm}^{-1}$ , in the FTIR spectrum of  ${}_w\text{TMSB}$  and  ${}_w\text{TMSB-AuNPs}$  at 25 °C and  ${}_w\text{TMSB-AuNPs}$  at 70 °C respectively, could be attributed to the OH groups in the alcohol or phenols groups. Moreover, the FTIR analysis showed the presence of OH and COOH chemical bonds in the TM extracts and AuNPs, which could be the most dominant in the synthesis of AuNPs [53]. These are the most commonly used groups ( $\text{-OH}$ ,  $\text{-COOH}$  and long alkyl chains) for the functionalization of metal NPs, especially gold. This is due to the fact that they can ensure compatibility and stability within the environment of the NPs and can be used as a base for further chemical reactions once attached to the particle surface. The recorded FTIR spectra confirms that the chemical functional groups in the TM active metabolites acted as reducing and stabilizing agents in the synthesis of TM-AuNPs [23,54].

#### 2.3. Effects of TM Extracts and AuNPs on Cancer Cells

The cytotoxicity of the TM extracts and AuNPs was evaluated on Caco-2 (human colon cancer cell line), MCF-7 (human breast cancer cell line), HepG2 (human liver cancer cell line) and KMST-6 (human skin fibroblasts) cells using the MTT assay. The results revealed that most of the TM extracts, and TM-AuNPs exerted significant cytotoxicity on the cancer cells in a dose-dependent manner. The  $\text{IC}_{50}$  values, summarized in Table 5, ranged from 0.18 to 93.73  $\mu\text{g/mL}$ . This study found for the first time that methanol extracts of TM root and stem/bark were particularly toxic to the human breast cancer (MCF-7) cell line.

In general, the  $\text{IC}_{50}$  values of the TM-AuNPs were lower than that of the TM extracts, suggesting that the TM-AuNPs were more cytotoxic than the TM extracts (Table 5). The  ${}_M\text{TMR}$  and  ${}_M\text{TMSB}$  extracts were more toxic than the other four extracts. However, MCF-7 cells in particular were highly susceptible to the effects of  ${}_M\text{TMR}$  and  ${}_M\text{TMSB}$  extracts, with  $\text{IC}_{50}$  values 2.73 and 19.73  $\mu\text{g/mL}$ , respectively. The cytotoxic profile of the TM extracts and TM-AuNPs did not display any particular pattern that could be related to the type of extract, the method of NP synthesis (i.e., synthesis at 25 or 70 °C) or the cell type. For example, while the  $\text{IC}_{50}$  values for  ${}_w\text{TML-AuNPs-25 }^\circ\text{C}$  and  ${}_w\text{TML-AuNPs-70 }^\circ\text{C}$  was only 5.71  $\mu\text{g/mL}$  in the Caco-2 cell line, the cytotoxicity of these NPs was very different in the MCF-7 and HepG2 cell lines. The  $\text{IC}_{50}$  value for  ${}_w\text{TML-AuNPs-25 }^\circ\text{C}$  in the MCF-7 cell line was 6.56  $\mu\text{g/mL}$ , while the  $\text{IC}_{50}$  value for  ${}_w\text{TML-AuNPs-70 }^\circ\text{C}$  at 32.59  $\mu\text{g/mL}$  was much higher. Similarly,  ${}_M\text{TMR-AuNPs-25}$

$^{\circ}\text{C}$  and  $_{\text{M}}\text{TMR-AuNPs-70 }^{\circ}\text{C}$  displayed very different cytotoxicity in HepG2 cells. With an  $\text{IC}_{50}$  value of  $0.18 \mu\text{g/mL}$ ,  $_{\text{M}}\text{TMR-AuNPs-25 }^{\circ}\text{C}$  was highly toxic to HepG2 cells, but  $_{\text{M}}\text{TMR-AuNPs-70 }^{\circ}\text{C}$  was less toxic to these cells with an  $\text{IC}_{50}$  value of  $90.85 \mu\text{g/mL}$ . The cytotoxicity of the TM-AuNPs was thus highly selective. This selectivity may be as a result of the cell type and the characteristics of the AuNPs. These characteristics were greatly influenced by the type of extract and the method of synthesis. This selective cytotoxicity is a highly desirable characteristic that can be explored for the selective destruction of specific cancer cells. Interestingly, the  $\text{IC}_{50}$  values of some of the AuNPs were significantly lower than the dose used for the positive controls. Dimethyl sulfoxide (DMSO) at 10% reduced the cell viability to 17–55%, while cisplatin reduced viability to 2–39%. DMSO was selected as a positive control as it is well known to induce cell death at high doses [55]. The proven toxicity of the solvent has led to its use as a positive control [56], while cisplatin is a clinically used chemotherapeutic antitumor drug [57].

**Table 5.**  $\text{IC}_{50}$  values of TM extracts and AuNPs against Caco-2, MCF-7 and HepG2 cells.

Treatments	$\text{IC}_{50}$ Values ( $\mu\text{g/mL}$ )		
	HepG2	Caco-2	MCF-7
$_{\text{W}}\text{TML}$	$61.19 \pm 0.00$	$90.19 \pm 0.12$	$66.84 \pm 0.01$
$_{\text{M}}\text{TML}$	$75.07 \pm 0.01$	$87.34 \pm 0.00$	$72.44 \pm 0.00$
$_{\text{W}}\text{TMSB}$	$93.73 \pm 0.00$	$62.66 \pm 0.01$	$49.23 \pm 0.00$
$_{\text{M}}\text{TMSB}$	$41.28 \pm 0.02$	$76.37 \pm 0.01$	$19.73 \pm 0.02$
$_{\text{W}}\text{TMR}$	$90.47 \pm 0.01$	$73.03 \pm 0.00$	$43.30 \pm 0.00$
$_{\text{M}}\text{TMR}$	$43.24 \pm 0.13$	$89.02 \pm 0.00$	$2.73 \pm 0.01$
$_{\text{W}}\text{TML-AuNPs (25 }^{\circ}\text{C)}$	$63.09 \pm 0.00$	$5.71 \pm 0.03$	$6.56 \pm 0.01$
$_{\text{W}}\text{TML-AuNPs (70 }^{\circ}\text{C)}$	$41.74 \pm 0.06$	$5.71 \pm 0.31$	$32.59 \pm 0.10$
$_{\text{M}}\text{TML-AuNPs (25 }^{\circ}\text{C)}$	$38.75 \pm 0.01$	$41.20 \pm 0.03$	$15.37 \pm 0.06$
$_{\text{M}}\text{TML-AuNPs (70 }^{\circ}\text{C)}$	$85.07 \pm 0.05$	$18.37 \pm 0.41$	$54.56 \pm 0.02$
$_{\text{W}}\text{TMSB-AuNPs (25 }^{\circ}\text{C)}$	$66.29 \pm 0.01$	$20.34 \pm 0.05$	$65.15 \pm 0.02$
$_{\text{W}}\text{TMSB-AuNPs (70 }^{\circ}\text{C)}$	$63.09 \pm 0.21$	$7.04 \pm 0.01$	$1.77 \pm 0.01$
$_{\text{M}}\text{TMSB-AuNPs (25 }^{\circ}\text{C)}$	$30.56 \pm 0.10$	$75.83 \pm 0.01$	$54.46 \pm 0.01$
$_{\text{M}}\text{TMSB-AuNPs (70 }^{\circ}\text{C)}$	$36.26 \pm 0.07$	$6.56 \pm 0.05$	$1.24 \pm 0.00$
$_{\text{M}}\text{TMR-AuNPs (25 }^{\circ}\text{C)}$	$0.18 \pm 0.01$	$23.58 \pm 0.02$	$3.36 \pm 0.20$
$_{\text{M}}\text{TMR-AuNPs (70 }^{\circ}\text{C)}$	$90.85 \pm 0.08$	$31.51 \pm 0.03$	$6.23 \pm 0.01$
$_{\text{W}}\text{TMR-AuNPs (25 }^{\circ}\text{C)}$	$88.59 \pm 0.11$	$4.74 \pm 0.01$	$1.24 \pm 0.01$
$_{\text{W}}\text{TMR-AuNPs (70 }^{\circ}\text{C)}$	$58.03 \pm 0.41$	$40.42 \pm 0.04$	$6.29 \pm 0.01$
<b>% Cell Viability</b>			
10% DMSO	$17.04 \pm 0.06$	$34.24 \pm 0.22$	$55.23 \pm 0.14$
100 $\mu\text{g/mL}$ Cisplatin	$20.6 \pm 0.34$	$39.2 \pm 1.67$	$1.9 \pm 0.04$

Note: The  $\text{IC}_{50}$  values were determined using GraphPad Prism. The temperatures in brackets indicate the temperature at which synthesis was carried out. Samples were compared using a one-way ANOVA and Turkey post-hoc test.

The antitumor activity of *Terminalia* species is well known [58]. *T. ferdinandiana* fruit and leaf extracts exhibited cytotoxicity against human carcinoma cell lines including Caco-2 cells ( $\text{IC}_{50} = 102 \mu\text{g/mL}$ ). Nandagopal et al. [58] demonstrated the cytotoxicity of *T. cheduba* seed extracts against HepG2 cells ( $\text{IC}_{50} = 40 \mu\text{g/mL}$ ). Likewise, acetone extracts of *T. bellerica* and *T. chebula* exhibited differential cytotoxic activities in several cancer cell lines, with the breast cancer cell line, MCF-7 being highly susceptible to the effects of this extract [59]. Saleem et al. [60] reported that methanol extracts of the *T. chebula* fruit reduced cell viability and inhibited cell proliferation in several malignant cell lines including MCF-7 cells. Phytochemical analysis of TM has revealed the presence of alkaloids, flavonoids, glucosides and total phenols (Table 1), these secondary metabolites were reported to have antitumor activities.

It has been demonstrated before that AuNPs exert in vitro cytotoxicity on several human cancer cells including HepG2 and triple negative breast cancer cells (MDA-MB-231) [61–63]. Green-synthesized



AuNPs from *Cassia tora* leaf extracts demonstrated the cytotoxic efficacy against colon cancer (Col320) cell lines and not in the normal (Vero) cell lines [64]. AuNPs from *Gymnema sylvestre* leaf extracts were also investigated for their antitumor effects against HT-29 cells. The study revealed that these AuNPs exerted significant cytotoxic effects against HT-29 cancer cells at a maximal concentration of 95 µg/mL [65].

It has been reported that spherical and rod-shaped AuNPs are more efficient in reducing cell proliferation of cancer cells than AuNPs with other shapes [66]. TM-AuNPs studied here were mostly spherical, which possibly contributes to the high cytotoxicity of these AuNPs. The capping agents (phytochemicals) that play a role in the synthesis of biogenic AuNPs can also affect the cytotoxicity of AuNPs [3,5,20]. Phytochemical analysis showed that chemical composition of the various extracts was very different. This may account for the differences in the physical characteristics of the TM-AuNP as well as the differences in cytotoxicity.

The AuNPs that demonstrated higher cytotoxicity ( $M_{TMR}$ -AuNPs at 25 °C and  $M_{TMSB}$ -AuNPs at 70 °C) with  $IC_{50} \leq 40$  µg/mL on at least two cancer cell lines were selected for evaluating the cytotoxicity with non-cancerous fibroblast KMST-6 cells. The  $CC_{50}$  values (cytotoxic concentration of the AuNPs that inhibited 50% cell viability in normal cells) and the selectivity index of the selected TM-AuNPs are summarized in Table 6. The  $CC_{50}$  values of  $M_{TMR}$ -AuNPs at 25 °C and  $M_{TMSB}$ -AuNPs at 70 °C were 275.7 and 334.5 µg/mL, respectively. The selectivity of  $M_{TMR}$ -AuNPs (25 °C) and  $M_{TMSB}$ -AuNPs (70 °C) on the three cancer (MCF, HepG2 and Caco-2) cells was within the selectivity index range from 6.5 to 82.2. The results corroborate with the finding of [53] that showed that biogenic AuNPs synthesized from the South African *Galenia africana* and *Hypoxis hemerocallidea* plants extracts showed that there was no significant reduction in viability of KMST-6 cell after 24 h treatment with AuNPs with concentrations up to 32 nM [16]. The same finding has been demonstrated by Patra [67], showing that AuNPs were non-toxic towards Hek293T cells. These findings suggested that AuNPs-assisted thermotherapy could cause targeted cancer cell ablation while avoiding damage to surrounding noncancerous cells [11,67] and used in humans for drug delivery and bioimaging applications.

**Table 6.** Cytotoxicity of selected TM-AuNPs on KMST-6 cells and their selectivity index.

AuNPs	Selectivity Index ( $CC_{50}/IC_{50}$ )			
	CC <sub>50</sub> (µg/mL) KMST-6	MCF-7	HepG2	Caco-2
$M_{TMR}$ -AuNPs (25 °C)	275.7 ± 0.010	82.05 ± 0.010	1531.66 ± 0.100	11.69 ± 0.500
$M_{TMSB}$ -AuNPs (70 °C)	334.5 ± 0.020	269.75 ± 0.100	9.23 ± 0.110	50.99 ± 0.100

Note: The  $CC_{50}$  values were determined using GraphPad Prism. Samples were compared using a one-way ANOVA and Turkey post-hoc test.

### 3. Materials and Methods

#### 3.1. Collection and Processing of Plant Material

Mature TM leaves (TML), root (TMR) and the stem/bark (TMSB) were collected from Yaoundé (Cameroon, East Africa). The plant species was identified at the National Herbarium of Cameroon in Yaoundé, Reference number 64212/HNC. The TML, TMR and TMSB samples were washed using sterile distilled water and air dried at room temperature ( $25 \pm 2$  °C) for 3 weeks. The dried plant materials were ground into fine powders using a high-speed electrical blender and stored in a desiccator at room temperature until further analysis.

#### 3.2. Plant Extraction and Phytochemical Analysis

##### 3.2.1. Preparation of Crude Extracts

The plant material was extracted using water (denoted as  $w$ ) and methanol (denoted as  $M$ ). Six different extracts, denoted as  $w_{TMSB}$ ,  $w_{TMR}$ ,  $w_{TML}$ ,  $M_{TMSB}$ ,  $M_{TMR}$  and  $M_{TML}$ , were prepared.

The samples were prepared according to the following protocol: 100 g of plant material was added into 500 mL of either methanol or distilled water and incubated at room temperature (25 °C) for 48–72 h. The samples were filtered using Whatman N°1 filter paper, the residues were re-extracted under the same conditions and added to the first filtrates. The methanolic extracts were evaporated using a rotary evaporator (Büchi 011, Flawil, Switzerland) at 40 °C, the water extracts were lyophilized using a Martin Christ Beta 2-8 lyophilizer (Osterode am Harz, Germany). The dried residues were kept at 4 °C until further experiments.

### 3.2.2. Qualitative Phytochemical Analysis

The presence of the following classes of compounds, i.e., alkaloids, flavonoids, glycosides, saponins, tannins and terpenoids, in the TM extracts was performed according to previously described standard procedures [68,69]. Briefly, 50 mg/mL of  $W_{TM}$  and  $M_{TM}$  were subjected to various chemicals to determine the presence of various phytochemicals. The assays or chemicals used include Mayer's reagent (alkaloids), Shinoda test (flavonoids), Ferhling solution (glycosides), froth test (saponins), tannins (ferric chloride test), phenolic content (ferric chloride test), anthraquinones (Borntrager's reaction test), sterols and terpenoids (Liebermann–Burchard test). The assays are qualitative and based on color change, frothing or precipitation between the active groups in the extracts and specific chemical reagents.

### 3.3. Biosynthesis of AuNPs and Characterization

#### 3.3.1. Green Synthesis of AuNPs

AuNPs were synthesized following a protocol described by Elbagory et al. [70] with slight modifications. In a 96 well polystyrene microplates, 250  $\mu$ L of 1 mM of sodium tetrachloroaurate(III) dihydrate (Sigma-Aldrich, St Louis, USA) was added to 50  $\mu$ L of plant extract stock solutions at varying concentrations (0.78–50 mg/mL) to a final volume of 300  $\mu$ L. The solutions were incubated at 25 °C and 70 °C with orbital shaking at 40 rpm for 5 h. AuNP formation was assessed by measuring the SPR within the UV–Vis range (450–700 nm) using a POLARstar Omega microtitre plate reader (BMG Labtech, Germany). AuNP synthesis was scaled up to 2 mL following the optimum conditions.

#### 3.3.2. Characterization of TM-AuNPs

The TM-AuNPs were characterized by UV–visible spectroscopy, dynamic light scattering (DLS), high-resolution transmission electron microscopy (HRTEM), energy-dispersive X-ray spectroscopy (EDX) and the selected area electron diffraction (SAED) analyses.

##### UV–Visible Spectroscopy

Formation of TM-AuNPs was preliminarily confirmed by visual observation for color change to red wine, further by UV–visible spectra after 5 h synthesis. Sharp peak obtained from the UV–visible spectrum confirmed the presence of AuNP at the absorption range between 450 and 700 nm using a POLAR star Omega microplate reader (BMG labtech, Offenburg, Germany).

##### DLS Analysis

The TM-AuNPs were washed 3 times with distilled H<sub>2</sub>O and centrifuged at 10,000 rpm for 10 min, the NPs were resuspended in double distilled H<sub>2</sub>O. The AuNPs were analyzed by DLS to measure their hydrodynamic size, zeta potential and Pdi using a Zetasizer (Malvern Instruments Ltd., Malvern, UK).

##### TM-AuNPs HRTEM, EDX and SAED Pattern Analysis

The structure, size distribution, composition, presence of reducing Au<sup>3+</sup> ions and crystallinity form of TM-AuNPs were analyzed by the HRTEM using a FEI Tecnai G2 20 field-emission HRTEM (Oregon, OR, USA). Additionally, the HRTEM was also used for EDX and SAED analyses. The samples were

prepared by drop-coating one drop of each sample onto a carbon-coated copper grid. The AuNPs were dried under a Xenon lamp for 10 min and analyzed by HRTEM. Transmission electron micrographs were captured in the bright field mode at an accelerating voltage of 200 KeV. EDX spectra were collected using an EDX liquid nitrogen cooled lithium doped silicon detector. The TEM micrographs were analyzed using origin 8.5 and Image J Software (50b version 1.8.0\_60, <http://imagej.175nih.gov/ij>).

#### FTIR Spectroscopy Measurements

The FTIR spectra were obtained from JASCO 460 plus spectrophotometer (Perkin Elmer, Massachusetts, MA, USA) with KBr at a frequency ranging from 4000 to 400  $\text{cm}^{-1}$  in a KBr matrix. The TM-AuNPs were centrifuged at 10,000 rpm for 10 min and dried at 70 °C using an oven for 2 min. The TM extracts and AuNPs powders were individually mixed with KBr powder and pressed into a pellet for measurement. Background correction was made using a reference blank KBr pellet. The baseline corrections were performed for all spectra.

#### 3.4. Cell Viability Using MTT Assay

The viability of the MCF 7, Caco-2, HePG2 and KMST-6 cells treated with TM crude extracts and AuNPs was evaluated using the MTT assay as described previously with some modifications [71]. The cells were maintained in DMEM containing 10% fetal bovine serum and 1% penicillin–streptomycin cocktail in a 37 °C humidified incubator with 5%  $\text{CO}_2$  saturation. The cells were seeded in 96-well microtitre plates at a density of  $5 \times 10^5$  cells/100  $\mu\text{L}$ /well. After 24 h, the culture medium was replaced with fresh medium containing the TM extracts and AuNPs at increasing concentrations. The stock solutions of TM-AuNPs were prepared in ddH<sub>2</sub>O at 1 mg/mL, and for the TM-extracts (10 mg/mL) were prepared in 10% DMSO. Two-fold dilutions of the samples from 7.8125–1000  $\mu\text{g}/\text{mL}$  were added to the 96-well plate containing various cell lines. Untreated cells were used as a negative control, and cells were treated with 10% DMSO and 100  $\mu\text{g}/\text{mL}$  of cisplatin (Sigma-Aldrich) as positive controls. For the AuNP interference test, cells treated with increasing concentrations of TM-AuNPs were left without the MTT dye. All treatments were done in triplicate. After 24 h, the media were removed in all wells. Thereafter, 100  $\mu\text{L}$  of the MTT reagent (prepared from 5.0 mg/mL stock solution) was added to each well. The cells were incubated at 37 °C for 4 h then the MTT reagent was replaced with 100  $\mu\text{L}$  of DMSO to dissolve the purple formazan crystals and incubated for a further 30 min. The absorbance of the formazan product formed was measured at a 570 nm wavelength ( $\lambda$ ), with background subtracted at the  $\lambda$  of 700 nm using a PolarSTAR Omega plate reader. The percentage of cell viability was calculated by comparing the absorbance of the test samples with the absorbance of the control (untreated) samples, multiplied by 100%. The data represent the average means of triplicate measurement from three independent experiments. The IC<sub>50</sub> for cancer cells and CC<sub>50</sub> for non-cancer cells values were determined using GraphPad Prism version 8.0.0, GraphPad Software, San Diego, California USA. The degree of selective toxicity of the active TM-AuNPs towards cancer cell lines relative to the non-cancer cell line (KMST-6) was expressed as the selectivity index (SI) and calculated as follows:

$$\text{Selectivity Index (SI)} = \frac{\text{CC}_{50} \text{ in non - cancer cells (KMST - 6 cells)}}{\text{IC}_{50} \text{ in cancer cells}}$$

#### 3.5. Statistical Analysis

The data were from at least three independent experiments and analyzed using a one-way ANOVA and Turkey post-hoc test using Graph Pad Prism. Data are expressed as mean  $\pm$  SD of experiments performed in triplicate.

## 4. Conclusions

The reported synthesis is not only cost-effective but also ecofriendly and has the ability to produce stable and monodispersed AuNPs. The metabolites in the TM extracts played a key biochemical role

in the synthesis, size and morphology of the AuNPs. To the best of our knowledge, this is the first report describing the potential of biomolecules from TM extracts to produce highly stable AuNPs with a small diameter range from 22.5 to 43 nm. The study also demonstrated the enhanced and selective cytotoxic properties of TM-AuNPs. The study clearly shows the potential of TM-AuNPs as antitumor agents. Further studies will be performed to isolate and characterize the phytochemicals responsible for AuNP synthesis in order to produce uniform shapes, to evaluate the possible cell death mechanism and to further explore the selective cytotoxic effects in other cancer cells.

**Supplementary Materials:** The following are available online, Figure S1: HRTEM images of TM-AuNPs synthesized at 25 °C (A) and 70 °C (B). The arrows points at different NP shapes. Scale bar at 10 and 20 nm, Figure S2: EDX spectra of TM-AuNPs synthesized at 25 and 75 °C. The green arrows show Au ions peaks, Figure S3: SAED patterns of TM-AuNPs showing single facets of NPs in TEM micrographs. The HRTEM images shows a fringe spacing of TM-AuNPs synthesized at 25 °C and 70 °C, Figure S4: FTIR spectra of TMR extracts and AuNPs synthesized at 25 °C and 70 °C, Table S1: FTIR analysis of chemicals groups in the TM extracts and AuNPs synthesized at 25 °C and 70 °C

**Author Contributions:** M.S.M., F.F.B., and M.M. conceived and designed the experiments; M.S.M., J.R.S., N.R.S.S., and M.B.T. performed the experiments. M.S.M. drafted the paper; M.S.M., M.B.T., N.R.S.S., M.M., and F.F.B. coordinated the data analysis and writing of the paper. All authors significantly contributed to this manuscript. All authors have read and agreed to the published version of the manuscript.

**Funding:** Michele S. Majoumouo's PhD research was funded by Organization for Women in Science for the Developing World (OWSD) grant number 3240287277. The APC was funded by the UWC.

**Acknowledgments:** This study was financially supported by the OWSD and the DSI/Mintek Nanotechnology Innovation Centre (NIC)—Biolabels Node.

**Conflicts of Interest:** There is no conflict of interest regarding the publication of this paper.

## References

1. Shalom, J.; Cock, I.E. *Terminalia ferdinandiana* Exell. Fruit and leaf extracts inhibit proliferation and induce apoptosis in selected human cancer cell lines. *Nutr. Cancer* **2018**, *70*, 579–593. [[CrossRef](#)] [[PubMed](#)]
2. Ngouana, K.T.; Mbouna, J.C.D.; Kuipou, T.R.M.; Tchuenmogne, M.A.T.; Zeuko'o, M.E.; Ngouana, V.; Mallié, M.; Bertout, S.; Boyom, F.F. Potent and synergistic extract combinations from *Terminalia catappa*, *Terminalia mantaly* and *Monodora tenuifolia* against pathogenic yeasts. *Medicines* **2015**, *2*, 220–235. [[CrossRef](#)] [[PubMed](#)]
3. Majoumouo, M.S.; Dube, A.; Tincho, M.B.; Mbekou, M.; Boyom, F.F.; Meyer, M. Enhanced anti-bacterial activity of biogenic silver nanoparticles synthesized from *Terminalia mantaly* Extracts. *Int. J. Nanomed.* **2019**, *14*, 9031–9046. [[CrossRef](#)]
4. Elbagory, A.M.; Hussein, A.A.; Meyer, M. The In Vitro Immunomodulatory Effects of Gold Nanoparticles synthesized from *Hypoxis hemerocallidea* aqueous extract and hypoxoside on macrophage and natural killer cells. *Int. J. Nanomed.* **2019**, *14*, 9007–9018. [[CrossRef](#)] [[PubMed](#)]
5. Ankamwar, B. Biosynthesis of gold nanoparticles (Green-gold) using leaf extract of *Terminalia Catappa*. *J. Chem.* **2010**, *7*, 1334–1339. [[CrossRef](#)]
6. Dudhane, A.A.; Waghmode, S.R.; Dama, L.B.; Mhaindarkar, V.P.; Sonawane, A.; Katariya, S. Synthesis and Characterization of gold nanoparticles using plant extract of *Terminalia arjuna* with antibacterial activity. *J. Nanosci. Nanotechnol.* **2019**, *15*, 75–82.
7. Mitra, M.; Bandyopadhyay, A.; Datta, G.; Nandi, D.K. Protective Role of Green synthesized gold nanoparticles using *Terminalia arjuna* against acetaminophen induced hematological alterations in male Wistar rats. *J. Nanomed. Nanotechnol.* **2019**, *10*, 2. [[CrossRef](#)]
8. Annavaram, V.; Posa, V.R.; Lakshmi, D.V.; Sumalatha, J.; Somala, A.R. *Terminalia bellirica* fruit extract mediated synthesis of gold nanoparticles (AuNPs) and studies on antimicrobial and antioxidant activity. *Inorg. Nano-Metal Chem.* **2016**, *47*, 681–687. [[CrossRef](#)]
9. Lee, S.Y.; Krishnamurthy, S.; Cho, C.-W.; Yun, Y.-S. Biosynthesis of gold nanoparticles using *Ocimum sanctum* extracts by solvents with different polarity. *ACS Sustain. Chem. Eng.* **2016**, *4*, 2651–2659. [[CrossRef](#)]

10. Balasooriya, E.R.; Jayasinghe, C.D.; Jayawardena, U.; Ruwanthika, R.W.D.; De Silva, R.M.; Udagama, P. honey mediated green synthesis of nanoparticles: New era of safe nanotechnology. *J. Nanomater.* **2017**, *2017*, 1–10. [[CrossRef](#)]
11. Adil, S.F.; Assal, M.E.; Khan, M.; Al-Warthan, A.; Siddiqui, M.R.H.; Liz-Marzán, L.M. Biogenic synthesis of metallic nanoparticles and prospects toward green chemistry. *Dalton Trans.* **2015**, *44*, 9709–9717. [[CrossRef](#)] [[PubMed](#)]
12. Jafarizad, A.; Safaee, K.; Gharibian, S.; Omid, Y.; Ekinci, D. Biosynthesis and *in-vitro* study of gold nanoparticles using Mentha and Pelargonium extracts. *Procedia Mater. Sci.* **2015**, *11*, 224–230. [[CrossRef](#)]
13. Khan, M.; Al-Marri, A.H.; Khan, M.; Shaik, M.R.; Mohri, N.; Adil, S.F.; Kuniyil, M.; Alkathlan, H.Z.; Al-Warthan, A.; Tremel, W.; et al. Green approach for the effective reduction of graphene oxide using *Salvadora persica* L. root (Miswak) extract. *Nanoscale Res. Lett.* **2015**, *10*, 1–9. [[CrossRef](#)] [[PubMed](#)]
14. Pavlin, M.; Vladimir, B. Stability of nanoparticles suspensions in different biologically relevant media. *Dig. J. Nanomater. Biostruct.* **2012**, *7*, 1389–1400.
15. Aromal, S.A.; Philip, D. Green synthesis of gold nanoparticles using *Trigonella foenum-graecum* and its size-dependent catalytic activity. *Spectrochim. Acta Part A Mol. Biomol. Spectrosc.* **2012**, *97*, 1–5. [[CrossRef](#)]
16. Elbagory, A.M.; Meyer, M.; Cupido, C.N.; Hussein, A.A. Inhibition of bacteria associated with wound infection by biocompatible green synthesized gold nanoparticles from south african plant extracts. *Nanomaterials* **2017**, *7*, 417. [[CrossRef](#)]
17. Mahmoudi, M.; Simchi, A.; Imani, M. Cytotoxicity of uncoated and polyvinyl alcohol coated superparamagnetic iron oxide nanoparticles. *J. Phys. Chem. C* **2009**, *113*, 9573–9580. [[CrossRef](#)]
18. De Aberasturi, D.J.; Serrano-Montes, A.B.; Liz-Marzán, L.M. modern applications of plasmonic nanoparticles: From energy to health. *Adv. Opt. Mater.* **2015**, *3*, 602–617. [[CrossRef](#)]
19. Suvarna, S.; Das, U.; Kc, S.; Mishra, S.; Sudarshan, M.; Das Saha, K.; Dey, S.; Chakraborty, A.; Yerol, N. Synthesis of a novel glucose capped gold nanoparticle as a better theranostic candidate. *PLoS ONE* **2017**, *12*, e0178202. [[CrossRef](#)]
20. Peeyush, K.; Sapna, M.; Malik, A.; Santosh, S. Insecticidal properties of Mentha species: A review. *Ind. Crops. Prod.* **2011**, *34*, 802–817.
21. Singh, D.; Rathod, V.; Ninganagouda, S.; Hiremath, J.; Singh, A.K.; Mathew, J. Optimization and Characterization of silver nanoparticle by endophytic fungi *Penicillium* sp. isolated from *Curcuma longa* (Turmeric) and application studies against MDR E. coli and S. aureus. *Bioinorg. Chem. Appl.* **2014**, *2014*, 1–8. [[CrossRef](#)]
22. Gräfe, C.; Weidner, A.; Lühe, M.V.; Bergemann, C.; Schacher, F.H.; Clement, J.H.; Dutz, S. Intentional formation of a protein corona on nanoparticles: Serum concentration affects protein corona mass, surface charge, and nanoparticle–cell interaction. *Int. J. Biochem. Cell Biol.* **2016**, *75*, 196–202. [[CrossRef](#)] [[PubMed](#)]
23. Zhang, X.; Tan, Z.; Jia, K.; Zhang, W.; Dang, M. *Rabdosia rubescens* Linn: Green synthesis of gold nanoparticles and their anticancer effects against human lung cancer cells A549. *Artif. Cells Nanomed. Biotechnol.* **2019**, *47*, 2171–2178. [[CrossRef](#)] [[PubMed](#)]
24. Khatoon, N.; Yasin, H.M.; Younus, M.; Ahmed, W.; Rehman, N.U.; Zakauallah, M.; Iqbal, M.Z. Synthesis and spectroscopic characterization of gold nanoparticles via plasma-liquid interaction technique. *AIP Adv.* **2018**, *8*, 015130. [[CrossRef](#)]
25. Naz, F.; Koul, V.; Srivastava, A.; Gupta, Y.K.; Dinda, A.K. Biokinetics of ultrafine gold nanoparticles (AuNPs) relating to redistribution and urinary excretion: A long-term in vivo study. *J. Drug Target.* **2016**, *24*, 720–729. [[CrossRef](#)] [[PubMed](#)]
26. Kesarla, M.K.; Mandal, B.K.; Bandapalli, P.R. Gold nanoparticles by *Terminalia bellirica* aqueous extract—a rapid green method. *J. Exp. Nanosci.* **2014**, *9*, 825–830. [[CrossRef](#)]
27. Ajdari, Z.; Rahman, H.S.; Shameli, K.; Abdullah, R.; Ghani, M.A.; Yeap, S.K.; Abbasiliasi, S.; Ajdari, D.; Ariff, A.B. Novel Gold Nanoparticles Reduced by *Sargassum glaucescens*: Preparation, Characterization and Anticancer Activity. *Molecules* **2016**, *21*, 123. [[CrossRef](#)] [[PubMed](#)]
28. Panahi, Y.; Mohammadhosseini, M.; Nejati-Koshki, K.; Abadi, A.J.N.; Moafi, H.F.; Akbarzadeh, A.; Farshbaf, M. Preparation, surface properties, and therapeutic applications of gold nanoparticles in biomedicine. *Drug Res.* **2017**, *67*, 77–87. [[CrossRef](#)]
29. Zhang, J.; Wang, M.; Webster, T.J. Growth process and anticancer properties of gold nanorods. *J. Biomed. Mater. Res. Part A* **2017**, *105*, 2616–2621. [[CrossRef](#)]

30. Banu, H.; Renuka, N.; Faheem, S.; Ismail, R.; Singh, V.; Saadatmand, Z.; Khan, S.S.; Narayanan, K.; Raheem, A.; Premkumar, K.; et al. Gold and silver nanoparticles biomimetically synthesized using Date Palm pollen extract-induce apoptosis and regulate p53 and Bcl-2 expression in human breast adenocarcinoma cells. *Boil. Trace Element Res.* **2018**, *186*, 122–134. [[CrossRef](#)]
31. Makarov, V.V.; Love, A.J.; Sinitsyna, O.V.; Makarova, S.S.; Yaminsky, I.V.; Taliansky, M.E.; Kalinina, N.O. “Green” Nanotechnologies: Synthesis of metal nanoparticles using plants. *Acta Nat.* **2014**, *6*, 35. [[CrossRef](#)] [[PubMed](#)]
32. Thiye, V.C.; Panjtan Amiri, K.; Bloebaum, P.; Raphael Karikachery, A.; Khoobchandani, M.; Katti, K.K.; Jurisson, S.S.; Katti, K.V. Development of resveratrol-conjugated gold nanoparticles: Interrelationship of increased resveratrol corona on anti-tumor efficacy against breast, pancreatic and prostate cancers. *Int. J. Nanomed.* **2019**, *14*, 4413–4428. [[CrossRef](#)] [[PubMed](#)]
33. Edison, T.J.I.; Sethuraman, M. Instant green synthesis of silver nanoparticles using Terminalia chebula fruit extract and evaluation of their catalytic activity on reduction of methylene blue. *Process. Biochem.* **2012**, *47*, 1351–1357. [[CrossRef](#)]
34. Singh, C. Biocompatible synthesis of silver and gold nanoparticles using leaf extract of *Dalbergia sissoo*. *Adv. Mater. Lett.* **2012**, *3*, 279–285. [[CrossRef](#)]
35. Cai, W.; Gao, T.; Hong, H.; Sun, J. Applications of gold nanoparticles in cancer nanotechnology. *Nanotechnol. Sci. Appl.* **2008**, *1*, 17–32. [[CrossRef](#)]
36. Dehghanizade, S.; Arasteh, J.; Mirzaie, A. Green synthesis of silver nanoparticles using *Anthemis atropatana* extract: Characterization and in vitro biological activities. *Artif. Cells Nanomed. Biotechnol.* **2017**, *46*, 160–168. [[CrossRef](#)] [[PubMed](#)]
37. Zeiri, Y.; Elia, P.; Zach, R.; Hazan, S.; Kolusheva, S.; Porat, Z. Green synthesis of gold nanoparticles using plant extracts as reducing agents. *Int. J. Nanomed.* **2014**, *9*, 4007. [[CrossRef](#)]
38. Shankar, S.S.; Rai, A.; Ahmad, A.; Sastry, M. Rapid synthesis of Au, Ag, and bimetallic Au core-Ag shell nanoparticles using Neem. *J. Colloid Interface Sci.* **2004**, *275*, 496–502. [[CrossRef](#)]
39. Rao, Y.; Inwati, G.K.; Singh, M. Green synthesis of capped gold nanoparticles and their effect on Gram-positive and Gram-negative bacteria. *Futur. Sci. OA* **2017**, *3*, FSO239. [[CrossRef](#)]
40. Liu, Y.; Kim, S.Y.; Kim, J.Y.; Perumalsamy, H.; Lee, S.; Hwang, E.; Yi, T.-H. Green synthesis of gold nanoparticles using *Euphrasia officinalis* leaf extract to inhibit lipopolysaccharide-induced inflammation through NF- $\kappa$ B and JAK/STAT pathways in RAW 264.7 macrophages. *Int. J. Nanomed.* **2019**, *14*, 2945. [[CrossRef](#)]
41. Rastogi, L.; Arunachalam, J. Microwave-Assisted green synthesis of small gold nanoparticles using aqueous Garlic (*Allium sativum*) extract: Their application as antibiotic carriers. *Int. J. Green Nanotechnol.* **2012**, *4*, 163–173. [[CrossRef](#)]
42. Wang, C.; Mathiyalagan, R.; Kim, Y.J. Rapid green synthesis of silver and gold nanoparticles using *Dendropanax morbifera* leaf extract and their anticancer activities. *Int. J. Nanomed.* **2016**, *11*, 3691. [[CrossRef](#)]
43. Zhang, P.; Wang, P.; Yan, L.; Liu, L. Synthesis of gold nanoparticles with *Solanum xanthocarpum* extract and their in vitro anticancer potential on nasopharyngeal carcinoma cells. *Int. J. Nanomed.* **2018**, *13*, 7047–7059. [[CrossRef](#)] [[PubMed](#)]
44. Danaei, M.; Dehghanhold, M.; Ataei, S.; Davarani, F.H.; Javanmard, R.; Dokhani, A.; Khorasani, S.; Mozafari, M.R. Impact of particle size and polydispersity index on the clinical applications of lipidic nanocarrier systems. *Pharmaceutics* **2018**, *10*, 57. [[CrossRef](#)]
45. Mittal, J.; Batra, A.; Singh, A.; Sharma, M.M. Phytofabrication of nanoparticles through plant as nanofactories. *Adv. Nat. Sci. Nanosci. Nanotechnol.* **2014**, *5*, 043002. [[CrossRef](#)]
46. Dwivedi, A.D.; Gopal, K. Biosynthesis of silver and gold nanoparticles using *Chenopodium album* leaf extract. *Colloids Surf. A Physicochem. Eng. Asp.* **2010**, *369*, 27–33. [[CrossRef](#)]
47. Clayton, K.N.; Salameh, J.W.; Wereley, S.T.; Kinzer-Ursem, T.L. Physical characterization of nanoparticle size and surface modification using particle scattering diffusometry. *Biomicrofluidics* **2016**, *10*, 054107. [[CrossRef](#)]
48. Grabinski, C.M. Nanoparticle Deposition and Dosimetry for In Vitro Toxicology. Ph.D. Thesis, Doctor of Philosophy. Case Western Reserve University, Cleveland, OH, USA, May 2015; 134p.

49. Chanda, N.; Shukla, R.; Zambre, A.; Mekapothula, S.; Kulkarni, R.R.; Katti, K.; Bhattacharyya, K.; Fent, G.M.; Casteel, S.W.; Boote, E.J.; et al. An effective strategy for the synthesis of biocompatible gold nanoparticles using cinnamon phytochemicals for phantom ct imaging and photoacoustic detection of cancerous cells. *Pharm. Res.* **2010**, *28*, 279–291. [[CrossRef](#)]
50. Moraes, C.M.; De Paula, E.; Rosa, A.H.; Fraceto, L.F. Physicochemical stability of poly(lactide-co-glycolide) nanocapsules containing the local anesthetic Bupivacaine. *J. Braz. Chem. Soc.* **2010**, *21*, 995–1000. [[CrossRef](#)]
51. Lyklema, J.; Leeuwen, V.H.P.; Minor, M. DLVO-theory, a dynamic re-interpretation. *Adv. Colloid Interface Sci.* **1999**, *83*, 33–69. [[CrossRef](#)]
52. Agrawal, Y.K.; Patel, V.R. Nanosuspension: An approach to enhance solubility of drugs. *J. Adv. Pharm. Technol. Res.* **2011**, *2*, 81–87. [[CrossRef](#)] [[PubMed](#)]
53. Kumar, K.M.; Mandal, B.K.; Sinha, M.; Krishnakumar, V. *Terminalia chebula* mediated green and rapid synthesis of gold nanoparticles. *Spectrochim. Acta Part A Mol. Biomol. Spectrosc.* **2012**, *86*, 490–494. [[CrossRef](#)] [[PubMed](#)]
54. Arumugam, A.; Gopinath, K. Green synthesis, characterization of silver, gold and bimetallic nanoparticles using bark extract of *Terminalia arjuna* and their larvicidal activity against malaria vector, *Anopheles stephensi*. *Int. J. Recent Sci. Res.* **2013**, *4*, 904–910.
55. Singh, M.; McKenzie, K.; Ma, X. Effect of dimethyl sulfoxide on in vitro proliferation of skin fibroblast cells. *J. Biotech Res.* **2017**, *8*, 78–82.
56. Ali-Boucetta, H.; Al-Jamal, K.T.; Kostarelos, K. Cytotoxic Assessment of Carbon Nanotube Interaction with Cell Cultures. *Biomed. Nanotechnol. Hum. Press.* **2011**, *726*, 299–312. [[CrossRef](#)]
57. Mirmalek, S.A.; Jangholi, E.; Jafari, M.; Yadollah-Damavandi, S.; Javidi, M.A.; Parsa, Y.; Parsa, T.; Salimi-Tabatabaee, S.A.; Kolagar, H.G.; Jalil, S.K.; et al. Comparison of In Vitro Cytotoxicity and Apoptogenic Activity of Magnesium Chloride and Cisplatin as Conventional Chemotherapeutic Agents in the MCF-7 Cell Line. *Asian Pac. J. Cancer Prev.* **2016**, *17*, 131–134. [[CrossRef](#)]
58. Nandagopal, S.; Kumar, G.A.; Dhanalakshmi, D.P.; Prakash, P. Bioprospecting the antibacterial and anticancer activities of silver nanoparticles synthesized using *Terminalia chebula* seed extract. *Int. J. Pharm. Pharm. Sci.* **2014**, *6*, 36837.
59. Kaur, S.; Michael, H.; Arora, S.; Härkönen, P.L.; Kumar, S. The in vitro cytotoxic and apoptotic activity of Triphala—An Indian herbal drug. *J. Ethnopharmacol.* **2005**, *97*, 15–20. [[CrossRef](#)]
60. Saleem, A.; Husheem, M.; Härkönen, P.; Pihlaja, K. Inhibition of cancer cell growth by crude extract and the phenolics of *Terminalia chebula* retz. Fruit. *J. Ethnopharmacol.* **2002**, *81*, 327–336. [[CrossRef](#)]
61. Arnida; Malugin, A.; Ghandehari, H. Cellular uptake and toxicity of gold nanoparticles in prostate cancer cells: A comparative study of rods and spheres. *J. Appl. Toxicol.* **2010**, *30*, 212–217. [[CrossRef](#)]
62. Paino, I.M.M.; Marangoni, V.S.; de Oliveira, R.C.S.; Antunes, L.M.G.; Zucolotto, V. Cytotoxicity and genotoxicity of gold nanoparticles in human hepatocellular carcinoma and peripheral blood mononuclear cells. *Toxicol. Lett.* **2012**, *215*, 119–125. [[CrossRef](#)] [[PubMed](#)]
63. Moses, S.L.; Edwards, V.M.; Brantley, E. Cytotoxicity in MCF-7 and MDA-MB-231 Breast Cancer Cells, without Harming MCF-10A Healthy Cells. *J. Nanomed. Nanotechnol.* **2016**, *7*, 369. [[CrossRef](#)]
64. Abel, E.E.; Poonga, P.R.J.; Panicker, S.G. Characterization and in vitro studies on anticancer, antioxidant activity against colon cancer cell line of gold nanoparticles capped with *Cassia tora* SM leaf extract. *Appl. Nanosci.* **2016**, *6*, 121–129. [[CrossRef](#)]
65. Arunachalam, K.D.; Arun, L.B.; Annamalai, S.K.; Arunachalam, A.M. Biofunctionalized gold nanoparticles synthesis from *Gymnema sylvestre* and its preliminary anticancer activity. *Int. J. Pharm. Pharm. Sci.* **2014**, *6*, 423–430.
66. Woźniak, A.; Malankowska, A.; Nowaczyk, G.; Grześkowiak, B.F.; Tuśnio, K.; Słomski, R.; Zaleska-Medynska, A.; Jurga, S. Size and shape-dependent cytotoxicity profile of gold nanoparticles for biomedical applications. *J. Mater. Sci. Mater. Electron.* **2017**, *28*, 92. [[CrossRef](#)] [[PubMed](#)]
67. Patra, B.; Gautam, R.; Priyadarsini, E.; Rajamani, P.; Pradhan, S.N.; Saravanan, M.; Meena, R. Piper betle: Augmented Synthesis of Gold Nanoparticles and Its In-vitro Cytotoxicity Assessment on HeLa and HEK293 Cells. *J. Clust. Sci.* **2019**, *31*, 133–145. [[CrossRef](#)]
68. Harborne, J.B. *Phytochemical Methods. A Guide of Modern Techniques of Plants Analysis*; Chapman and Hall: London, UK, 1976; p. 150.

69. Sofowora, A.; Odebeyi. *Medicinal Plants and Traditional Medicinal in Africa*, 2nd ed.; Spectrum Book Ltd.: Ibadan, Nigeria, 1993; pp. 20–70.
70. Elbagory, A.M.; Cupido, C.N.; Meyer, M.; Hussein, A.A. Large Scale Screening of Southern African Plant Extracts for the Green Synthesis of Gold Nanoparticles Using Microtitre-Plate Method. *Molecules* **2016**, *21*, 1498. [[CrossRef](#)]
71. Mmola, M.; Le Roes-Hill, M.; Durrell, K.; Bolton, J.J.; Sibuyi, N.; Meyer, M.; Beukes, D.R.; Antunes, E.; Roes-Hill, M. Enhanced Antimicrobial and Anticancer Activity of Silver and Gold Nanoparticles Synthesised Using *Sargassum incisifolium* Aqueous Extracts. *Molecules* **2016**, *21*, 1633. [[CrossRef](#)]

**Sample Availability:** Samples of the TM-extracts are available on request from the authors.



© 2020 by the authors. Licensee MDPI, Basel, Switzerland. This article is an open access article distributed under the terms and conditions of the Creative Commons Attribution (CC BY) license (<http://creativecommons.org/licenses/by/4.0/>).